Kinetic Schemes for the Relativistic Hydrodynamics

Shamsul Qamar

Fakultät für Mathematik

Otto-von-Guericke Universität Magdeburg

Kinetic Schemes for the Relativistic Hydrodynamics

Dissertation
zur Erlangung des akademischen Grades

doctor rerum naturalium
(Dr. rer. nat.)

genehmigt durch die Fakultät für Mathematik
der Otto-von-Guericke-Universität Magdeburg

von **M.Phil Math. Shamsul Qamar**
geb. am 12. März 1972 in Mardan, Pakistan

Gutachter:
Prof. Dr. Mária Lukáčová
Prof. Dr. Thomas Sonar
Prof. Dr. Gerald Warnecke

Eingereicht am: 5. Mai 2003
Verteidigung am: 26. September 2003

Betreuer:
Dr. Matthias Kunik
Prof. Dr. Gerald Warnecke

Abstract

Kinetic schemes for the relativistic Euler equations are presented, which describe the flow of a perfect gas in terms of the particle density n, the spatial part of the four-velocity $\mathbf{u}$ and the pressure p. The physical frame in the whole study will be exclusively special relativity. We consider both, the ultra-relativistic Euler equations, and a more general form of the relativistic Euler equations. The general form of relativistic Euler equations covers the whole range from the non-relativistic to the ultra-relativistic limit. We also consider as a special case the non-relativistic theory. The basic ingredients of the kinetic schemes are the phase density in equilibrium and the free-flight. The phase density generalizes the non-relativistic Maxwellian for a gas in local equilibrium. The free-flight is given by solutions of a collision free kinetic transport equation. The kinetic schemes presented here are discrete in time but continuous in space. The schemes are explicit and unconditionally stable, i.e., no Courant-Friedrichs-Levy (CFL) condition is needed. Also the schemes are truly multi-dimensional as they cover all the directions of wave propagation in the gas evolution stage. These kinetic schemes preserve the positivity of particle density and pressure for all times and hence are L^1-stable. The schemes satisfy the weak form of conservation laws for mass, momentum, and energy, as well as an entropy inequality in any arbitrary domain. The schemes also satisfy the total variation diminishing (TVD) property for the distribution function through a suitable choice of the interpolation strategy. We also extend the schemes to account for the boundary conditions. The kinetic schemes described above are first order in time and space. We also extend the schemes to second order for the one- and two-dimensional ultra-relativistic Euler equations.

In addition, we develop another type of kinetic schemes for the ultra-relativistic Euler equations which are discrete both in time and space. These are an upwind conservative form of the kinetic schemes in which the fluxes are the moments of the relativistic free-flight phase density. We use flux vector splitting in order to calculate the free-flight moment integrals under a natural CFL condition due to the structure of light cone, since every signal speed is bounded by the velocity of light. The schemes are then called kinetic flux vector splitting (KFVS) schemes. Since KFVS schemes are based on the free particle transport at the cells interface in the gas evolution stage, they give smeared solutions especially at the contact discontinuity. To overcome this problem "particle" collisions are included in the transport process. Consequently, the artificial dissipation in the schemes are much reduced in comparison with the usual KFVS schemes. These new upwind schemes are called BGK-type KFVS schemes. For the ultra-relativistic Euler equations we have to evaluate the free-flight moment integrals over the compact unit sphere due to the finite domain of dependence in the relativistic kinetic theory. But in the classical kinetic schemes the free-flight moment integrals have infinite integration limits, therefore they need some error-functions which have to be cutoff at their tails. Our schemes are extended to the two-dimensional case in a usual dimensionally split manner. We use a MUSCL-type initial reconstruction for the second order accuracy.

For the comparison of the numerical results, we give the results of exact Riemann solver and Godunov scheme for the one-dimensional ultra-relativistic Euler equations. We also present the central schemes and apply them to both non-relativistic and relativistic Euler equations. The main advantages of the central schemes are compactness and simplicity. We have carried out several one- and two-dimensional numerical test case computations. It was found that kinetic schemes have a comparable accuracy with the upwind and central schemes.

Zusammenfassung

Wir stellen kinetische Verfahren für die relativistischen Euler-Gleichungen vor, die die Strömung eines perfekten Gases anhand der Teilchendichte n, des räumlichen Anteils der Vierergeschwindigkeit $\mathbf{u}$ und des Druckes p beschreiben. Wir betrachten im folgenden ausschließlich den physikalischen Rahmen der speziellen Relativitätstheorie, mit Ausnahme einiger klassischer Grenzfälle. Wir untersuchen sowohl die ultra-relativistischen Euler-Gleichungen als auch eine allgemeinere Form der relativistischen Euler-Gleichungen. Die allgemeine Form der relativistischen Euler-Gleichungen deckt den gesamten Bereich vom nicht-relativistischen bis zum ultra-relativistischen Grenzfall ab. Die Grundbestandtteile der kinetischen Schemata sind die Phasendichte im Gleichgewicht und der freie Flug. Die Phasendichte verallgemeinert die klassische Maxwellsche Phasendichte für ein Gas im lokalen Gleichgewicht. Der freie Flug ist durch die Lösungen einer kollisionsfreien kinetischen Transportgleichung gegeben. Die hier dargestellten kinetischen Schemata sind diskret in der Zeit, aber kontinuierlich bezüglich des Ortes. Die Verfahren sind explizit und unbedingt stabil, d.h. es wird keine Courant-Friedrichs-Levy- (CFL) Bedingung benötigt. Außerdem sind die Verfahren echt mehrdimensional, da sie alle Richtungen der Wellen-Bewegung gleichwertig behandeln. Die kinetischen Schemata erhalten die Positivität von Teilchendichte und Druck für alle Zeiten und sind deshalb L^1-stabil. Die Verfahren erfüllen die schwache Form der Erhaltungsgesetze für Masse, Impuls und Energie sowie eine Entropie-Ungleichung in einem beliebigen Gebiet. Außerdem haben die Schemata die Eigenschaft der Reduktion der totalen Variation für die Verteilungsfunktion bei geeigneter Wahl der Interpolationsstrategie. Wir führen weiterhin Randbedingungen in die Verfahren ein. Die oben beschriebenen kinetischen Schemata sind erster Ordnung in Zeit und Raum. Wir erweitern diese Verfahren auf zweite Ordnung für ein- und zweidimensionale ultra-relativistische Euler-Gleichungen.

Desweiteren entwickeln wir einen anderen Typ kinetischer Schemata für die ultra-relativistischen Euler-Gleichungen. Diese Verfahren sind diskret in Zeit und Raum. Sie stellen eine Upwind-Form der konservativen kinetischen Schemata dar, bei der die Flüsse die Momente der relativistischen Phasendichte beim freien Flug sind. Wir benutzen Fluss-Vektor-Splitting, um die Integrale der Momente beim freien Flug mit einer natürlichen CFL-Bedingung, die sich aus der Struktur des Lichtkegels ergibt, zu berechnen, denn die Geschwindigkeit eines jeden Signals ist durch die Lichtgeschwindigkeit begrenzt. Diese Verfahren werden als kinetische Fluss-Vektor-Splitting (KFVS) Schemata bezeichnet. Da KFVS-Schemata auf dem freien Teilchentransport basieren, ergeben sich zu dissipative Lösungen insbesondere an einer Kontaktunstetigkeit. Um diesem Problem entgegenzuwirken, werden Teilchenkollisionen in den Transportprozess eingeführt. Das hat zur Folge, dass die numerische Dissipation in diesen Verfahren, im Vergleich zu gewöhnlichen KFVS-Schemata, stark reduziert wird. Diese neuen Upwind-Schemata werden KFVS-Schemata vom BGK-Typ genannt. Für die ultra-relativistischen Euler-Gleichungen müssen wir, wegen des endlichen Abhängigkeitsbereichs in der relativistischen Theorie, die Momenten-Integrale des freien Flugs nur über der kompakten Einheitssphäre auswerten. Bei den klassischen kinetischen Schemata haben die Momenten-Integrale des freien Flugs unendliche Integrationsgrenzen. Deshalb brauchen diese Schemata gewisse Fehlerfunktionen, die an den Enden abgeschnitten werden müssen. Wir erweitern unsere Schemata in der gewöhnlichen Weise durch Dimensions-Splitting auf den zweidimensionalen Fall. Dabei benutzen wir eine Anfangs-Rekonstruktion vom MUSCL-Typ für die Genauigkeit zweiter Ordnung.

Zum numerischen Vergleich geben wir die Ergebnisse des exakten Riemann-Lösers und des Godunov-Verfahrens für die eindimensionalen ultra-relativistischen Euler-Gleichungen an. Wir präsentieren außerdem das hochauflösende zentrale Schema und wenden es sowohl auf die nicht-relativistischen als auch auf die relativistischen Euler-Gleichungen an. Die wesentlichen Vorteile zentraler Schemata sind deren Einfachheit. Wir haben eine Reihe von ein- und zeidimensionalen numerischen Beispielrechnungen ausgeführt. Es stellt sich heraus, dass kinetische Schemata eine vergleichbare Genauigkeit gegenüber Upwind- und zentralen Schemata besitzen.

Acknowledgements

I wish to acknowledge high indebtedness and my deep gratitude to my good natured and devoted supervisor Prof. Dr. Gerald Warnecke for constant encouragement, remarkable suggestions and invaluable supervision during my studies. He introduced me to the interesting field of conservation laws. His generosity to share his insight and ideas with me, was the starting point for the work of my research project. Due to financial support out of his grants, I was able to participate in conferences. During my stay, I found Gerald Warnecke and his family very hospitable and helpful.

I am highly indebted to my affectionate co-supervisor Dr. Matthias Kunik for giving me an initiative to this research. His inspiring guidance, remarkable suggestions, constructive criticism and friendly discussions enabled me to complete the research work and this thesis efficiently. He spared a lot of his precious time in advising and helping me throughout the research work.

I would like to express my sincere gratitude to Dr. Wolfgang Dreyer (WIAS Berlin) for his useful discussion and valuable remarks. Due to partial financial support out of his grants, I was able to complete this thesis project. I found him very kind, friendly and helpful person.

I am grateful to Prof. Dr. Mária Lukáčová and Prof. Dr. Thomas Sonar for their valuable remarks.

I am also very grateful to Prof. Dr. Jürgen Sprekels (director WIAS Berlin) for providing me a good research environment to complete this thesis project.

I wish to express my deep obligation to my parents for their sacrifices during the pursuance of my education. It is indeed of the prayers of my parents and well wishers that I have been able to complete my Ph.D. studies. Their encouragement and inspiration have always been with me.

I am grateful to my colleagues Wolfram Heineken, Rüdiger Müller, Dr. Nikolai Andrianov, Dr. Yousef Zahaykah and Qurrat-ul-Ain for their good cooperation and useful discussions.

This work is partially supported by the projects

"Long-time behaviour of nonlinear hyperbolic systems of conservation laws and their numerical approximation", contract # DFG WA 633/7-2.

"Kinetic methods for selected initial and boundary value problems", contract # DFG DR 401/2-2.

Contents

Chapter 1

Introduction

1.1 Historical Background

In modeling flow at speeds where relativistic effects become important, space and time become intrinsically coupled and the Euler equations of gas dynamics become more complicated. However, it is still possible to write the relativistic Euler equations as a first order hyperbolic system that can be advanced forward in time in some fixed reference frame. We call the reference frame a laboratory frame since this is typically the frame from which we are observing. Relativistic gas dynamics plays an important role in areas of astrophysics, high energy particle beams, high energy nuclear collisions, and free-electron laser technology. We consider exclusively special relativity including some non-relativistic limits.

Kinetic approaches in order to solve the non-relativistic Euler equations of gas dynamics were successfully applied to several initial and boundary value problems, see for example Deshpande and Raul [12], Deshpande [13, 16, 15], Perthame [72, 73], Tang and Xu [83], Xu [91, 92, 93], as well as Dreyer, Kunik and Herrmann [18, 19, 21]. Some interesting links between the Euler system and the so called kinetic BGK-model, which was introduced by Bhatnagar, Gross and Krook [3], are discussed in the textbooks by Cercignani [5], Cercignani, Illner and Pulvirenti [6] as well as by Godlewski and Raviart [33].

The hyperbolic systems that can be treated by the kinetic method are those which may be generated from kinetic transport equation and from the *Maximum Entropy Principle*. Since these systems lead to a convex entropy function, they enable several rigorous mathematical results, see for example Friedrichs and Lax [29] as well as Dafermos [11]. In the case of *thermodynamical equilibrium* the Maximum Entropy Principle constitutes a successful method in order to obtain the Maxwellian phase density for the Boltzmann gas as well as the corresponding phase densities for the Fermi- and Bose gas in equilibrium from the corresponding kinetic entropy definitions.

A few years after Einstein's famous paper "Zur Elektrodynamik bewegter Körper", Jüttner [41] extended the kinetic theory of gases which was developed by D. Bernoulli, Clausius, Maxwell and Boltzmann, to the domain of relativity. He succeeded in deriving the relativistic generalization of the Maxwellian equilibrium phase density. Later on this phase density and the whole relativistic kinetic theory was structured in a well organized Lorentz-invariant form,

see Chernikov [7], [8], Israel [38], Müller [63] and the textbook of deGroot, van Leeuven and van Weert [32]. Jüttner [42] also established the relativistic form of equilibrium phase densities and the corresponding equations of state for the systems of bosons and fermions. In the textbook of Weinberg [87] one can find a short introduction to special relativity and relativistic hydrodynamics with further literature also for the imperfect fluid (gas), see for example the papers of Eckart [23, 24, 25].

There are two approaches to solve the Euler equations numerically. One is based on the Euler equations, for example Godunov-type schemes and central schemes. While the other approach is based on the transport equations, for example kinetic schemes. In the kinetic schemes the moments of the Maxwellian phase density are used in order to derive the constitutive relations. Using the conservation laws these constitutive relations lead to the Euler equations. This distinction in the solution approaches was first made by Harten, Lax and van Leer [36]. No matter how a numerical scheme for the Euler equations is derived we expect it to have certain properties apart from being consistent with the equations. Due to the presence of discontinuities and weak solutions *convergence* is very difficult to prove. Some convergence results are available for scalar hyperbolic equations and for special 2×2 systems, however, no such result exist for the Euler equations. Other properties are needed to ascertain good quality of the numerical solution: the numerical scheme should be robust in handling discontinuities, and it should show no grid dependencies in multi-dimensions. In addition, it should retain properties specific to the Euler equations: conservation of mass, momentum, and energy, positivity of density and pressure, and entropy inequalities. We will show in this study that kinetic schemes preserve all these properties.

Zimmermann [95] in her Ph.D. thesis showed the connection between the method of transport (MoT) and kinetic schemes for the classical Euler equations. She first considered the goup of kinetic scheme for which Perthame [74] has already proved the positivity of density and pressure. She showed that the standard first order method of transport presented by Fey [27, 28] can be written as such a scheme: where decomposition and advection are then "kinetic". She however showed that second order extensions do not fit to the framework, let alone computationally less expensive extensions, for example extensions developed by Maurer[62] and Noelle [66]. In order to prove the positivity property for more general decompositions and advection solvers she generalized the concept of kinetic schemes. As a results she obtained general, physically sensible, conditions on the decomposition and advection solver, which were also satisfied by the second order extensions. In her numerical calculations she saw that these conditions were in fact necessary. Recently Noelle, Kröger and Zimmermann [44] have extended these results to the Evolution Galerkin (EG) schemes showing the connection among kinetic schemes, MoT and EG schemes.

Several numerical methods for solving relativistic gas dynamics have been reported, see Martí and Müller [61] and references therein. All these methods are mostly developed out of the existing reliable methods for solving the Euler equations of non-relativistic or Newtonian gas dynamics. It is noted that all these methods developed for the relativistic Euler equations are based on a macroscopic continuum description. The reason is, that they solved a phenomenological form of the relativistic Euler equations, see Martí et al. [59, 60, 61]. These are the relativistic Euler equation which can be obtained by using the classical constitutive relation for the internal energy density and gamma-gas law. Since these equations are in Lorentz

invariant form, they are still relativistic Euler equations. The disadvantage is, it seems that there is no consistent kinetic phase density which can recover all the constitutive relations for these Euler equations.

On the other hand we use kinetic schemes to solve the fully relativistic Euler equations. All the constitutive relations for these Euler equations can be obtained directly from the moments of the relativistic kinetic phase density, and hence is fully consistent with the kinetic theory. Also this is the first time that kinetic theory based methods have been developed for the solution of the relativistic Euler equations. We will formulate two types of kinetic schemes in order to solve the initial and boundary value problems of the *relativistic Euler equations*, i.e., unconditionally and conditionally stable kinetic schemes. Both types of kinetic schemes are explained in the following paragraphs.

Our unconditionally stable kinetic schemes presented in Chapters 4 and 6 are discrete in time but continuous in space. These schemes are explicit and unconditionally stable. Also the schemes are truly multi-dimensional as they cover all the directions of wave propagation at the gas evolution stage. We derive these kinetic schemes for both general form of relativistic Euler equations as well as its limiting case, i.e., ultra-relativistic Euler equations. There are three basic ingredients of the kinetic schemes. The first one is the relativistic phase density developed by Jüttner. The second one is the solution of a collision free kinetic transport equation, which can be given explicitly in terms of a known initial phase density. For the formulation of such type of kinetic schemes we prescribe a time step $\tau_M > 0$ and define the equidistant times $t_n = n\,\tau_M$, $n = 0, 1, 2, ...$, called maximization times. We solve a collisionless kinetic transport equation on each time interval $t_n < t < t_{n+1}$, with a relativistic Maxwellian as the initial phase density at each maximization time t_n. The third component of our schemes consist of continuity conditions, which guarantee that the conservation laws are also satisfied across the maximization times. They also determine the new initial data for the next free-flight period. Finally, it is also possible to incorporate the out-flow and adiabatic boundary conditions into these kinetic schemes in a quite natural way, which we will explain after deriving the schemes. By taking moments of the corresponding phase densities one can obtain every macroscopic quantity like particle density, energy density, pressure and velocity four-vector. These macroscopic quantities will solve the relativistic Euler equations in the limit $\tau_M \to 0$. These kinetic schemes preserve the properties like conservations laws, entropy inequality, positivity, and L_1- stability. In order to calculate the relativistic phase density in free-flight, a suitable interpolation polynomial is needed which should satisfy TVD property, see [13]. The schemes are first order accurate in space and time with numerical dissipation of the order of time step. We extend these schemes to second order by using the approach of Deshpande [13] which he used in order to extend the non-relativistic kinetic schemes to second order. We will extend our schemes to second order for the one- and two-dimensional ultra-relativistic Euler equations. Despite of the above several advantages the schemes have a disadvantage that they are numerically expensive. These schemes are about five to six times slower than the other schemes like, Godunov, central and KFVS schemes.

The conditionally stable kinetic schemes presented in Chapter 5 are discrete in time and space. These are an upwind conservative schemes called kinetic flux vector splitting (KFVS) schemes. The schemes are stable under a CFL condition, that is, the fluid movement is restricted only to the neighbouring cells. In the classical case the CFL condition for the nu-

merical schemes of the Euler equations depends on the initial data, whereas in the relativistic theory there is a natural CFL conditions which is independent of the initial data due to the light cone structure. In these schemes the flux moment integrals are calculated using the idea of flux vector splitting under the CFL condition. Since KFVS schemes are based on the free particle transport at the cell interface in the gas evolution stage, therefore we get smeared solutions especially at the contact discontinuity. In order to overcome this problem we include "particle" collisions in the gas evolution stage, see Xu [92, 93]. Consequently, the artificial numerical dissipation in the new schemes are much reduced in comparison with the usual kinetic flux vector splitting (KFVS) schemes. These new upwind schemes are named as BGK-type KFVS schemes. The BGK-type KFVS schemes give robust and reliable solutions as well as good resolution at the contact discontinuity. The schemes are extended to the two-dimensional case in a usual dimensionally split manner, that is, the formulae for the fluxes can be used along each coordinate direction. The second order accuracy of the schemes are achieved by using a MUSCL-type initial reconstruction. For the ultra-relativistic Euler equations we have to evaluate the free-flight moment integrals over the compact unit sphere due to the finite domain of dependence in the relativistic kinetic theory. While, in the classical kinetic schemes the free-flight moment integrals have infinite integration limits, therefore they need some error-functions which have to be cutoff at their tails. The main difference between the Godunov schemes and the present schemes are the calculation of fluxes. In the Godunov schemes fluxes are calculated using the exact or approximate Riemann solvers. While in the present schemes fluxes are calculated from the moments of the phase density. Since in the relativistic case the solution lies inside a light-cone, therefore the natural CFL condition is $\Delta t = 0.5 * \min(\Delta x, \Delta y)$, as we solve one Riemann problem in each cell. Here Δt is the time step and Δx and Δy are the mesh widths in x- and y-directions. We have developed the above KFVS and BGK-type KFVS schemes for the one- and two-dimensional ultra-relativistic Euler equations.

For the comparison of the results, we develop an exact Riemann solver as well as first and second order Godunov upwind schemes for the ultra-relativistic Euler equations, however it seems impossible to get such schemes for the general form of special relativistic Euler equations due to the presence of modified Bessel functions of second kind in the relativistic Maxwellian. Apart from these, we also present one- and two-dimensional high order non-oscillatory central schemes of Nessyahu and Tadmor [64] as well as Jiang and Tadmor [39] for both ultra-relativistic Euler equations and general form of relativistic Euler equations. Furthermore, we also use the central schemes in order to solve the phenomenological form of the relativistic Euler equations as well as the non-relativistic Euler equations. We use a MUSCL-type reconstruction to achieve second order accuracy.

Some of the work reported in this thesis has been submitted for publication in Journals. Five preprints were completed during this work. In these five preprints the first four preprints have co-authors M. Kunik and G. Warnecke, while the last article has G. Warnecke as co-author. Our first article [45] has been accepted in the Journal of *Computational Physics*. This was on the first order kinetic schemes for the ultra-relativistic Euler equations presented here in Chapter 4. The work on the second order kinetic schemes for the ultra-relativistic Euler equations appearing in Chapter 4 will be submitted soon for publication. Our second preprint [47] on the BGK-type KFVS schemes appearing in Chapter 5, our third article [46] appearing in Chapter 6 as well as our fourth article [48] have been submitted. The latter article is on

the solution of Boltzmann-Peierls equation which uses a similar idea as presented in Chapters 4 and 5, however has not been included in this thesis. Our fifth submitted article [75] is on the application of central schemes to multi-component flows which are not considered in the thesis.

1.2 A Short Overview of the Work

In Chapter 2, we introduce kinetic schemes for the non-relativistic Euler equations. The Euler equations are written in differential form as well as in a weak integral form. Also the weak form of the entropy inequality is given, see [13, 18]. We explain the unconditionally stable (continuous in space) kinetic schemes in order to solve these equations, see [13, 17, 18]. The proofs of conservation laws, entropy inequality, positivity and L_1 stability are given for these kinetic schemes, see [18] and [74]. We explain the numerical implementation of the kinetic schemes for the solution of both one- and two-dimensional Euler equations, see [13] and [17]. We also give the proof of TVD property for the one-dimensional kinetic scheme which was first proved in [13]. We also give a brief introduction to the KFVS (discrete in space) schemes for the one- and two-dimensional non-relativistic Euler equations, see [15, 16, 91]. The results obtained from the kinetic schemes and KFVS schemes are compared with exact solutions, the Godunov scheme, and central schemes.

In Chapter 3, we present the basic definitions of the relativistic kinetic theory, namely Lorentz-transformations, vectors and tensors, the light cone, Einstein's velocity addition, as well as the relativistic phase density and its macroscopic moments. Moreover the two limiting cases of the relativistic phase density are introduced, one is the classical Maxwellian for a cool non-relativistic gas and the other is ultra-relativistic phase density. We also introduce some limiting inequalities for the modified Bessel functions, see the hand book of Jeffrey [40]. These relations will be used in Chapter 6 in order to write the general form of relativistic kinetic theory in a more convenient form.

In Chapter 4, we calculate the macroscopic moments of the relativistic Maxwellian in order to formulate the ultra-relativistic Euler equations as conservation laws for the particle number, momentum, and energy. The Euler equations are written in differential form as well as in a weak integral form. An entropy inequality is given in weak integral form with an entropy function which satisfies the Gibbs equation. The Rankine-Hugoniot jump conditions and the entropy inequality were used in order to derive a simple parameter representation for the admissible shocks. Also parametrization for the rarefaction fan has been derived here. We use these shock and rarefaction parametrizations in order to derive an exact Riemann solver for the one-dimensional ultra-relativistic Euler equations. We first formulate the kinetic scheme in order to solve the three-dimensional ultra-relativistic Euler equations. We prove that this kinetic scheme strictly preserves the positivity of particle density and pressure for all later times. In contrast to the kinetic scheme for the non-relativistic Euler equations, we show that the three-fold moment integrals for the particle-density four-vector and energy-momentum tensor reduces simply to a surface integrals where the integration is performed with respect to the unit sphere. A similar idea was used by [21] and Kunik, Qamar and Warnecke [48] in order to solve the Boltzmann-Peierls equation and its moment system for a phonon Bose-gas. We derive the continuity conditions for the zero components of the macroscopic moments

which play a crucial role in the proof of conservation laws and entropy inequality. These continuity conditions are also used in order to initialize the kinetic schemes for the next time step. The proof of conservation laws and entropy inequality for the kinetic schemes are given for any arbitrary domain. We also derive the kinetic schemes for the spatially one and two-dimensional ultra-relativistic Euler equations. Furthermore, using special coordinates in a spatially one-dimensional case, we have further reduced the surface integrals of the three-dimensional kinetic scheme to single integrals which ranges from -1 to $+1$. We explain the numerical implementation of the kinetic scheme for the one-dimensional case. The procedure for implementation of the reflected boundary conditions conditions in the scheme is also given here. In order to compute the free-flight phase density inside the moment integrals we need a linear interpolation polynomial, because we only know the initial data at the nodal points. We are using the linear polynomial proposed by Deshpande [13] for which he has proved the TVD property. Both one and two-dimensional solutions indicate the finite domain of dependence on the preceding initial data, which is covered by the backward light-cones. This property does not hold for non-relativistic kinetic schemes. We also discuss the Eulerian limit $\tau_M \to 0$ of the kinetic schemes where weak solutions are obtained from the initial value problems including arbitrary shock interactions. The kinetic schemes described above are first order in space and time. The second order accuracy in time is achieved by adding correction terms to the moment integrals of the kinetic schemes which were obtained from the comparison of the exact and numerical solutions. To get second order accuracy in space we use second order interpolation polynomials in order to calculate the free-flight phase density inside the moments integrals.

In Chapter 5, we derive conditionally stable kinetic schemes which we call BGK-type KFVS schemes. This type of kinetic schemes are discrete in time and space. We start with a one-dimensional ultra-relativistic Euler equations and derive the BGK-tpe KFVS scheme for it. Since the scheme is first order accurate in time and space, therefore we also extend it to second order by using a MUSCL-type reconstruction. The second order accuracy is simple in ultra-relativistic case and the idea is similar to that of second order accuracy of the upwind schemes using a MUSCL-type reconstruction. We have also derived the similar scheme for the two-dimensional ultra-relativistic Euler equations in a dimensionally split manner. The scheme is then extended to second order analogously to the one-dimensional case. Apart from the above schemes we also derive the one-dimensional Godunov scheme for the ultra-relativistic Euler equations, see Toro [85]. In order to calculate the fluxes we use the exact Riemann solver derived in Chapter 4. The results obtained from the BGK-type KFVS schemes are compared with exact solutions, the KFVS schemes, the Godunov scheme, and the central schemes.

In Chapter 6, we first determine the macroscopic moments of the general form of the relativistic Maxwellian, which gives the so called constitutive relations. The conservation laws and these constitutive relations then gives the *general form special relativistic Euler equations*. The Euler equations are written in differential form as well as in a weak integral form, which takes care for the evolution of shock waves. There holds an entropy inequality in terms of a specific entropy function which satisfies the Gibbs equation. We also derive the Rankine conditions for these Euler equations. The kinetic schemes for these Euler equations is an extension of the theory presented in Chapter 4. We formulate the schemes in such a way that the whole range from the classical Eulerian limit to the ultra-relativistic limit is covered. The schemes derivation procedures are analogous to that in Chapter 4. But are more complicated

due to the presence of modified Bessel functions of second kind in the relativistic Maxwellian. The limiting relations for these Bessel functions which are given in Chapter 3 can be used in order to get the limiting values for the non-relativistic or ultra-relativistic kinetic theory of gases. Another very interesting theory in this chapter is the proof of the Maximum Entropy Principle. Before coming to the proof of the Maximum Entropy Principle, we have first proved four lemmas which were needed for this purpose. After that we have formulated and proved the Maximum Entropy Principle. At the end of this chapter we extend the scheme in order to solve initial and boundary value problems. Apart from these, we also introduce the three-dimensional phenomenological form of the relativistic Euler equations and then reduce them to one space dimension. As discussed before in the introduction, these Euler equations cannot be solved by using kinetic schemes. We solve these phenomenological relativistic Euler equations using second order central schemes.

In Chapter 7, we formulate the Lax-Friedrichs (LxF) central schemes for one- and two-dimensional hyperbolic systems. We extend these schemes to the second order non-oscillatory central schemes of Nessyahu and Tadmor [64] as well as Jiang and Tadmor [39]. The main advantage of these schemes is that unlike upwind schemes, no Riemann solver is needed for the calculation of fluxes. Central schemes are important in cases when there is no Riemann solver or it is difficult to obtain. The central schemes are also very important in the case of general form of relativistic Euler equations because it is looking impossible to get an exact Riemann solver for these equations. The central schemes are compact and easy to implement. In the previous chapters we have used the central schemes in order to solve the non-relativistic and relativistic Euler equations in one and two space dimensions.

Chapter 2

Kinetic Schemes for the Non-relativistic Euler Equations

In this chapter we introduce first order conditionally and unconditionally stable kinetic schemes for the non-relativistic Euler equations. These kinetic schemes were introduced by Reitz [77], Deshpande and Raul [12], Deshpande [13, 16], Dreyer et al. [18, 17], Tang and Xu [83], as well as Xu [91, 93]. This chapter is a background study for the better understanding of the relativistic kinetic theory presented in the coming chapters.

As explained in the introduction the unconditionally stable kinetic schemes are discrete in time but continuous in space. This type of kinetic schemes are explicit and does not need any CFL condition. These kinetic schemes are truly multi-dimensional as they cover all directions of wave propagation. The schemes are very useful and interesting for analysis. Furthermore they allows the particle movement from a cell to any other cell. This is particularly important in high speed flows. We prove the positivity, conservation laws and entropy inequality for the three-dimensional kinetic scheme, see [18]. We explain the numerical implementation of both the one- and two-dimensional kinetic schemes, [13, 17]. We generalize the schemes in order to include the boundary conditions in one space dimension, however the procedure for multi-dimensions is analogous.

On the other hand the conditionally stable kinetic schemes are an upwind conservative schemes which are discrete both in time and space. The scheme are stable under a CFL condition, that is, the fluid movement is restricted only to the neighbouring cells. In order to calculate fluxes the idea of flux vector splitting technique of Harten, Lax and von Leer [36] is used. This type of schemes are then called kinetic flux vector splitting (KFVS) schemes, see [15, 91, 93]. Harten et al. [36] drew a distinction between two numerical approaches to the solution of the Euler equations, namely, the Godunov and KFVS schemes. Broadly speaking, the Godunov schemes are based on the Riemann solution in the gas evolution stage, and the KFVS schemes uses the microscopic particle distribution function as the basis to construct the fluxes. While the construction methodology is different between the Godunov and kinetic schemes, both first order schemes can be written in the framework of the three-point conservative methods. As compared to the unconditionally stable kinetic schemes, KFVS schemes are computationally more efficient and easy to implement. Therefore this type of schemes are highly desirable from the computational point of view. Lui and Xu [57] have proved the entropy inequality

for the KFVS schemes, while Tang and Xu [83] have proved the positivity of the schemes.

In coming sections the name *kinetic schemes* will be used for the unconditionally stable kinetic schemes (continuous in space), while the name *KFVS schemes* will be used for the conditionally stable kinetic schemes (discrete in space).

2.1 Non-relativistic Euler Equations

In this section we consider the time-dependent non-relativistic Euler equations. These are a system of non-linear hyperbolic conservation laws that govern the dynamics of a compressible material, such as gases or liquids at high pressures, for which the effects of body forces, viscous stresses and heat flux are neglected.

There is some freedom in choosing a set of variables to describe the flow under consideration. A possible choice is the so called *primitive variables* or *physical variables,* namely $\rho(t,x,y,z)$ = density or mass density, $p(t,x,y,z)$ = pressure, $v_1(t,x,y,z)$ = x-component of velocity, $v_2(t,x,y,z)$ = y-component of velocity, $v_3(t,x,y,z)$ = z-component of velocity. The velocity vector is $\mathbf{v} = (v_1, v_2, v_3)$. An alternative choice is provided by the so called *conserved variables*. These are the mass-density ρ, the x-momentum component ρv_1, the y-momentum component ρv_2, the z-momentum component ρv_3 and the total energy E. Physically, these conserved quantities result naturally from the application of the fundamental laws of conservation of mass, Newton's second law and conservation of energy. Computationally, there are some advantages in expressing the governing equations in terms of the conserved variables. This gives rise to a large class of numerical methods called conservative methods.

At regular points where the solution is continuously differentiable in space and time, the three-dimensional non-relativistic Euler equations for a perfect gas are

$$\frac{\partial}{\partial t}\,\rho + \nabla\cdot(\rho\,\mathbf{v}) = 0\,, \tag{2.1.1}$$

$$\frac{\partial}{\partial t}(\rho\,v_i) + \sum_{k=1}^{3}\frac{\partial}{\partial x^k}\,(p\,\delta_{ik} + \rho\,v_i\,v_k) = 0\,, \tag{2.1.2}$$

$$\frac{\partial E}{\partial t} + \sum_{k=1}^{3}\frac{\partial}{\partial x^k}\,\left[\mathbf{v}\,(E+p)\right] = 0\,, \tag{2.1.3}$$

where $i = 1,2,3$. The total energy E is given by

$$E = \frac{p}{(\gamma-1)} + \frac{\rho\mathbf{v}^2}{2}\,, \qquad 1 \le \gamma \le 3\,,$$

here γ is the ratio of specific heats. The relation between the pressure p and temperature T for a thermally ideal gas is given by $p = \rho RT$, where R is the gas constant. Also due to the γ-gas law the specific internal energy e and pressure p are related as $p = (\gamma-1)\rho e$.

We consider initial data of bounded variation for ρ, $\mathbf{v}$ and p, which may have jumps:

$$\rho(0,\mathbf{x}) = \rho_0(\mathbf{x})\,, \qquad \mathbf{v}(0,\mathbf{x}) = v_0(\mathbf{x})\,, \qquad p(0,\mathbf{x}) = p_0(\mathbf{x})\,.$$

Now we are looking for special solutions of the three-dimensional Euler equations, which will not depend on x^2, x^3 but only depend on $x = x^1$. Therefore we restrict to one-dimensional flow field $\mathbf{v} = (v(t,x), 0, 0)^T$

$$\begin{aligned} \rho_t + (\rho v)_x &= 0\,, \\ (\rho v)_t + (\rho v^2 + p)_x &= 0\,, \\ E_t + (v(E+p))_x &= 0\,. \end{aligned} \tag{2.1.4}$$

where $E = \dfrac{p}{(\gamma-1)} + \dfrac{\rho v^2}{2}$ and $p = \rho RT = (\gamma-1)\rho e$. These differential equations constitute a strictly hyperbolic system with the characteristic velocities

$$\lambda_1 = -\sqrt{\gamma\frac{p}{\rho}}\,, \qquad \lambda_2 = v\,, \qquad \lambda_3 = \sqrt{\gamma\frac{p}{\rho}}\,. \tag{2.1.5}$$

The differential equations (2.1.4) are not sufficient if we take into account shock discontinuities. Therefore we choose a weak integral formulation which is given due to Oleinik [68] by curve integrals in time and space, namely

$$\begin{aligned} \int_{\partial\Omega} \rho dx - (\rho v) dt &= 0\,, \\ \int_{\partial\Omega} (\rho v) dx - (\rho v^2 + p) dt &= 0\,, \\ \int_{\partial\Omega} E dx - v\,(E+p)\,dt &= 0\,. \end{aligned} \tag{2.1.6}$$

Here $\Omega \subset \mathbb{R}_0^+ \times \mathbb{R}$ is a convex set in space-time with piecewise smooth, positive oriented boundary, where $\mathbb{R}^+ \in]0,\infty[$ and $\mathbb{R} \in]-\infty,\infty[$. Note that this weak formulation takes discontinuities into account, since there are no derivatives of the field involved. If we apply the Gaussian divergence theorem to the weak formulation (2.1.6) in space-time regions where the solution is regular we come back to the differential form of the Euler equations (2.1.4).

Furthermore we require that the weak solution (2.1.6) must also satisfy the *entropy-inequality*

$$\int_{\partial\Omega} h dx - \Phi dt \geq 0\,, \tag{2.1.7}$$

with positive oriented $\partial\Omega$. Where the entropy density h and the entropy flux Φ are given by

$$h(\rho,p) = \frac{\rho}{\gamma-1}\ln\left(\frac{p}{\rho^\gamma}\right) + \frac{\rho}{\gamma-1}(1+\ln 2\pi)\,, \qquad \Phi(\rho,v,p) = v\cdot h(\rho,p)\,. \tag{2.1.8}$$

2.2 Kinetic Scheme in Three Space Dimensions

The kinetic schemes uses the well-known fact that Euler equations (2.1.1) are the first moments of the Boltzmann equation when the distribution function is Maxwellian [5]. The basic

unknown in the Boltzmann equation is the velocity distribution function $f(t, \mathbf{x}, \mathbf{c}, I)$, where t is time, $\mathbf{x}$ is the position vector, $\mathbf{c}$ is the molecular velocity vector, and I is the independent internal-energy variable corresponding to nontranslational degrees of freedom. The Boltzmann transport equation in its three-dimensional form, see Cercignani [5, Chapters II and IV] as well as Cercignani, Illner and Pulvirenti [6, Sections 3.2, 3.3, 11.1], is given by

$$\frac{\partial f}{\partial t} + \sum_{k=1}^{3} c_k \frac{\partial f}{\partial x^k} = Q(f)\,. \tag{2.2.1}$$

The left hand side of the above equation is the free-flight or convective term, while the right hand side is the collision term. The field variables ρ, $\mathbf{v}$, and E are related to f through moment equations given by

$$\begin{aligned}
\rho(t, \mathbf{x}) &= \int_{\mathbb{R}^3 \times \mathbb{R}^+} f(t, \mathbf{x}, \mathbf{c}, I)\, d^3\mathbf{c}\, dI\,, \\
\rho\mathbf{v}(t, \mathbf{x}) &= \int_{\mathbb{R}^3 \times \mathbb{R}^+} \mathbf{c} f(t, \mathbf{x}, \mathbf{c}, I)\, d^3\mathbf{c}\, dI\,, \\
E(t, \mathbf{x}) &= \int_{\mathbb{R}^3 \times \mathbb{R}^+} \left(I + \frac{\mathbf{c}^2}{2}\right) f(t, \mathbf{x}, \mathbf{c}, I)\, d^3\mathbf{c}\, dI\,,
\end{aligned} \tag{2.2.2}$$

here, $\mathbb{R} \in]-\infty, +\infty[$ and $R^+ \in]0, \infty[$. The free-flight term gives the rate of change of f per unit volume in $(\mathbf{x}, \mathbf{c}, I)$ space because of movement of molecules, and the collision term gives the rate of change of f because of intermolecular collisions.

Note that the collision term $Q(f)$ has the property

$$\int_{\mathbb{R}^3 \times \mathbb{R}^+} \psi(\mathbf{c}, I) Q(f)\, d^3\mathbf{c}\, dI = 0\,, \tag{2.2.3}$$

where $\psi = \left(1, \mathbf{c}, I + \dfrac{\mathbf{c}^2}{2}\right)^T$. This is a direct consequence of the conservation of mass, momentum, and energy during the collisions, see [6, Sections 3.2, 3.3, 11.1].

In the Euler limit $Q(f) = 0$ and the distribution function f is then the Maxwellian distribution:

$$f(\mathbf{x}, \mathbf{c}, I) = w_M(\mathbf{x}, \mathbf{c}, I) = \frac{\rho}{(2\pi RT)^{3/2}} \exp\left[-\frac{(\mathbf{c} - \mathbf{v})^2}{2RT}\right] \frac{\exp\left(-I/I_0\right)}{I_0}\,. \tag{2.2.4}$$

The variable I corresponds to the nontranslational degrees of freedom and

$$I_0 = \frac{(2 + D_f) - \gamma D_f}{2(\gamma - 1)} RT\,, \tag{2.2.5}$$

where D_f is the degree of freedom of molecules, and γ is the ratio of specific heats.

Now we formulate the iterated scheme for the mass density ρ, the velocity $\mathbf{v}$ and temperature T. To initialize the scheme we start with

- Bounded and integrable initial data for $\mathbf{x} \in \mathbb{R}^3$:
  $\rho(0,\mathbf{x}) = \rho_0(\mathbf{x}) \geq \epsilon > 0, \quad \mathbf{v}(0,\mathbf{x}) = \mathbf{v}_0(\mathbf{x}), \quad p(0,\mathbf{x}) = p_0(\mathbf{x}) \geq \delta > 0.$
- A fixed time $\tau_M > 0$ of free-flight, so that at equidistant times $t_n = n \cdot \tau_M$, $(n = 0, 1, 2, ...)$, the maximization of entropy takes place.

By substituting $Q(f) = 0$ in the Boltzmann equation (2.2.1), we get a collisionless transport equation

$$\frac{\partial f}{\partial t} + \sum_{k=1}^{3} c_k \frac{\partial f}{\partial x^k} = 0\,. \tag{2.2.6}$$

The exact solution of this equation with initial distribution function at time level n denoted by $f_n(\mathbf{x}, \mathbf{c}, I)$ is

$$f(t_n + \tau, \mathbf{x}, \mathbf{c}, I) = f_n(\mathbf{x} - \tau\mathbf{c}, \mathbf{c}, I)\,, \quad 0 \leq \tau \leq \tau_M\,. \tag{2.2.7}$$

The vanishing of $Q(f)$ is due to large number of collisions because $Q(f) = 0$ if and only if f is a Maxwellian distribution (2.2.4).

By substituting (2.2.7) in (2.2.2), we get an iterated scheme for the variables density ρ, velocity $\mathbf{v}$ and temperature T within the time interval $0 < \tau < \tau_M$:

$$\begin{aligned}
\rho(t_n + \tau, \mathbf{x}) &= \int_{\mathbb{R}^3 \times \mathbb{R}^+} f_n(\mathbf{x} - \tau\mathbf{c}, \mathbf{c}, I)\, d^3\mathbf{c}\, dI\,, \\
\rho\mathbf{v}(t_n + \tau, \mathbf{x}) &= \int_{\mathbb{R}^3 \times \mathbb{R}^+} \mathbf{c} f_n(\mathbf{x} - \tau\mathbf{c}, \mathbf{c}, I)\, d^3\mathbf{c}\, dI\,, \\
E(t_n + \tau, \mathbf{x}) &= \int_{\mathbb{R}^3 \times \mathbb{R}^+} \left(I + \frac{\mathbf{c}^2}{2}\right) f_n(\mathbf{x} - \tau\mathbf{c}, \mathbf{c}, I)\, d^3\mathbf{c}\, dI\,.
\end{aligned} \tag{2.2.8}$$

Here $f_n(\mathbf{y}, \mathbf{c}, I) = w_M(\rho(t_n, \mathbf{y}), \mathbf{v}(t_n, \mathbf{y}), T(t_n, \mathbf{y}), \mathbf{c}, I)$ is the Maxwellian phase density (2.2.4).

In the following we will consider the dimensionless quantities, therefore we take the gas constant $R = 1$. Now the integration with respect to the variable I in (2.2.8) yields

$$\begin{aligned}
\rho(t_n + \tau, \mathbf{x}) &= \int_{\mathbb{R}^3} f_n(\mathbf{x} - \tau\mathbf{c}, \mathbf{c})\; d^3\mathbf{c}\,, \\
(\rho v_i)(t_n + \tau, \mathbf{x}) &= \int_{\mathbb{R}^3} c_i f_n(\mathbf{x} - \tau\mathbf{c}, \mathbf{c})\; d^3\mathbf{c}\,, \\
E(t_n + \tau, \mathbf{x}) &= \int_{\mathbb{R}^3} \left(I_0 + \frac{\mathbf{c}^2}{2}\right) f_n(\mathbf{x} - \tau\mathbf{c}, \mathbf{c})\; d^3\mathbf{c}\,,
\end{aligned} \tag{2.2.9}$$

where f_n is the contracted local Maxwellian distribution defined by

$$f_n(\mathbf{y}, \mathbf{c}) = w_M(\mathbf{y}, \mathbf{c}) = \frac{\rho(t_n, \mathbf{y})}{(2\pi T(t_n, \mathbf{y}))^{3/2}} \exp\left[-\frac{(\mathbf{c} - \mathbf{v})^2}{2T(t_n, \mathbf{y})}\right]\,, \tag{2.2.10}$$

and (2.2.5) implies $I_0 = \dfrac{5 - 3\gamma}{2(\gamma - 1)} T$, for $D_f = 3$.

This scheme can be brought into compact generic form, if we introduce the abbreviations

$$\mathbf{c_A} = \begin{cases} 1 & , \quad A = 0\,, \\ c_i & , \quad A = i = 1,2,3\,, \\ \left(I_0 + \frac{\mathbf{c}^2}{2}\right) & , \quad A = 4\,. \end{cases} \tag{2.2.11}$$

Then the variables u_A and fluxes F_{Ak} read

$$\begin{aligned} u_A(t_n + \tau, \mathbf{x}) &= \int_{\mathbb{R}^3} \mathbf{c_A} f_n(\mathbf{x} - \tau\mathbf{c}, \mathbf{c})\; d^3\mathbf{c}\,, \\ F_{Ak}(t_n + \tau, \mathbf{x}) &= \int_{\mathbb{R}^3} \mathbf{c_A} c_k f_n(\mathbf{x} - \tau\mathbf{c}, \mathbf{c})\; d^3\mathbf{c}\,. \end{aligned} \tag{2.2.12}$$

Note that $u_0 = \rho$, $u_i = \rho v_i\,(i = 1,2,3)$ and $u_4 = E = \dfrac{p}{(\gamma - 1)} + \dfrac{\rho \mathbf{v}^2}{2}$.

The entropy density h and entropy flux Φ_k are

$$\begin{aligned} h(t_n + \tau, \mathbf{x}) &= -\int_{\mathbb{R}^3} (f_n \ln f_n)(\mathbf{x} - \tau\mathbf{c}, \mathbf{c})\; d^3\mathbf{c}\,, \\ \Phi_k(t_n + \tau, \mathbf{x}) &= -\int_{\mathbb{R}^3} c_k (f_n \ln f_n)(\mathbf{x} - \tau\mathbf{c}, \mathbf{c})\; d^3\mathbf{c}\,. \end{aligned} \tag{2.2.13}$$

For $\tau = 0$, f_n is the phase density (2.2.10) that can obtained by maximizing the entropy at time t_n for given constraints $u_A(t_n, \mathbf{x})$. Within the range $0 < \tau < \tau_M$ the phase density solves the collision free Boltzmann equation. When the time $t_{n+1} = t_n + \tau_M$ is reached f_{n+1} will be the phase density (2.2.10) that can obtained by the maximization of entropy under the new constraints $u_A(t_{n+1}, \mathbf{x})$.

In order to initialize the kinetic scheme for the next time step, we require the following continuity conditions for the conservative variables u_A across the maximization time t_n, $n \geq 1$

$$u_A(t_n^+, \mathbf{x}) = u_A(t_n^-, \mathbf{x})\,. \tag{2.2.14}$$

These continuity conditions are the direct consequence of (2.2.3). Since we are implementing the computation in these variables, these conditions are automatically enforced. Here we have used the following abbreviation for the one-sided limits across the maximization time t_n, $n \geq 1$, where for a positive number ε

$$u_A(t_n^{\pm}, \mathbf{x}) = \lim_{\varepsilon \to 0} u_A(t_n \pm \varepsilon, \mathbf{x})\,.$$

Later on we see that these conditions are necessary in order to guarantee the conservation laws for the mass momentum and energy across the maximization time t_n.

2.2.1 Proof of Conservation Laws and Entropy Inequality

Now we present the proof of conservation laws and entropy inequality for the kinetic schemes, see [18].

Proposition 2.1: *Let $0 < \tau < \tau_M$ and $n = 0, 1, 2, ...$ The fields $u_A(t_n + \tau, \mathbf{x})$, $F_{Ak}(t_n + \tau, \mathbf{x})$ and all of their derivatives in space and time are smooth, i.e. arbitrarily often continuously diffrentiable, and they satisfy the conservation laws*

$$\frac{\partial u_A}{\partial \tau}(t_n + \tau, \mathbf{x}) + \frac{\partial F_{Ak}}{\partial x_k}(t_n + \tau, \mathbf{x}) = 0.$$

Remark: Note that these equations do not constitute a *local* quasi linear hyperbolic system for the variables u_A, because the fluxes F_{Ak} at time $t_n + \tau$ and position $\mathbf{x}$ depend on the whole field $u_A(\cdot, t_n)$ at time t_n.

Proof: If we substitute $\mathbf{c}$ by $\mathbf{y} = \mathbf{x} - \tau\mathbf{c}$ in (2.2.12) and regard $f_n(\mathbf{y}, \mathbf{c}) = w_M(u_A(t_n, \mathbf{y}), \mathbf{c})$ we obtain

$$\begin{aligned} u_A(t_n + \tau, \mathbf{x}) &= \frac{1}{\tau^3} \int_{\mathbb{R}^3} c_A w_M \left(u_A(t_n, \mathbf{y}), \frac{\mathbf{x} - \mathbf{y}}{\tau} \right) d^3\mathbf{y}\,, \\ F_{Ak}(t_n + \tau, \mathbf{x}) &= \frac{1}{\tau^3} \int_{\mathbb{R}^3} c_A \frac{x_k - y_k}{\tau} w_M \left(u_A(t_n, \mathbf{y}), \frac{\mathbf{x} - \mathbf{y}}{\tau} \right) d^3\mathbf{y}\,, \end{aligned}$$

with

$$c_A = \left(1,\ \frac{x_i - y_i}{\tau},\ I_0 + \frac{(\mathbf{x} - \mathbf{y})^2}{2\tau^2} \right).$$

In these integrals the u_A's do not depend on $\mathbf{x}$ and τ. We have thus shown the smoothness of u_A, F_{Ak} and of all its derivatives with respect to τ and $\mathbf{x}$.

In order to prove the conservation form for these variables and fluxes we rely again on the expressions (2.2.12). There holds due to the chain rule:

$$\begin{aligned} \partial_\tau u_A(t_n + \tau, \mathbf{x}) &= \int_{\mathbb{R}^3} \mathbf{c_A} \partial_\tau f_n(\mathbf{x} - \tau\mathbf{c}, \mathbf{c})\ d^3\mathbf{c} \\ &= -\int_{\mathbb{R}^3} \mathbf{c_A} c_k \partial_{x_k} f_n(\mathbf{x} - \tau\mathbf{c}, \mathbf{c})\ d^3\mathbf{c} \\ &= -\partial_{x_k} \int_{\mathbb{R}^3} \mathbf{c_A} c_k f_n(\mathbf{x} - \tau\mathbf{c}, \mathbf{c})\ d^3\mathbf{c} \\ &= -\partial_{x_k} F_{Ak}(t_n + \tau, \mathbf{x}). \end{aligned}$$

Proposition 2.2: *Let $\Omega \subset \mathbb{R}_0^+ \times \mathbb{R}^3$ be any bounded convex region in space and time. By $d\vec{o}$ we denote a positively oriented boundary element of $\partial\Omega$. The representations (2.2.12) have the following properties:*

(i) *In the limit $\tau_M \to 0$ the volume densities u_A, fluxes F_{Ak}, the entropy density h and entropy flux Φ_k become local functions of the variables ρ, v_i and T, viz.*

$$u_A = \begin{pmatrix} \rho \\ \rho v_i \\ \rho \frac{v^2}{2} + \frac{3}{2}\rho T \end{pmatrix}, \qquad F_{Ak} = \begin{pmatrix} \rho v_k \\ \rho v_i v_k + \rho T \delta^{ik} \\ \rho \left(\frac{v^2}{2} + \frac{5}{2} T \right) v_k \end{pmatrix},$$

$$h = \frac{\rho}{\gamma - 1} \ln \left(\frac{p}{\rho^\gamma} \right) + \frac{\rho}{\gamma - 1} (1 + \ln 2\pi)\,, \quad \Phi_k = h v_k.$$

(ii) *For $\tau_M > 0$ as well as in the Eulerian limit $\tau_M \to 0$ we obtain the following weak formulation, which takes discontinuities into account:*

$$\int_{\partial\Omega} (u_A, F_{Ak})\, d\vec{o} = 0. \tag{2.2.15}$$

(iii) *In regular points where the solution is continuously differentiable, the differential form of the Euler equations is satisfied for $\tau_M \to 0$.*

(iv) *The following entropy inequality is satisfied for $\tau_M > 0$ as well as in the Eulerian limit $\tau_M \to 0$:*

$$\int_{\partial\Omega} (h, \Phi_k) d\vec{o} \geq 0. \tag{2.2.16}$$

The brackets (u_A, F_{Ak}) and (h, Φ_k) denote four-vectors in time (first position) and space (last three positions).

Remarks:

(1) The limit $\tau_M \to 0$ means that a thermodynamic process is realized by an infinite number of maximizations within a time interval Δt.

(2) Each maximization increases the entropy, and for this reason the maximization of entropy simulates the interaction of the microscopic particles of the gas.

(3) In singular points of a shock curve with velocity v_s, which may appear in the limit $\tau_M \to 0$, the Rankine-Hugoniot equations

$$-v_s [\![u_A]\!] + [\![F_{Ak}]\!] N_k = 0$$

hold. In addition, there is a positiv entropy production according to

$$\sigma_s = -v_s [\![h]\!] + [\![\Phi_k]\!] N_k \geq 0.$$

Proof:
(i): In the limit $\tau_M \to 0$ the fields ρ and T in (2.2.10) an therefore in the integrals (2.2.12) do not depend on $\mathbf{c}$ anymore, i.e. they are constants regarding the $\mathbf{c}$-integrations. Since in this limit the free-flight phase density reduces to the Maxwellian phase density, we obtain from (2.2.12), (2.2.13) the representations given in (i). The convergence should be proved in the L_1-norm. This is an open point until now.

Regarding the propositions (ii) + (iii) it is sufficient to prove $\int_{\partial\Omega}(u_A, F_{Ak})d\vec{o} = 0$ for $\tau_M > 0$. The Eulerian limit $\tau_M \to 0$ can be obtained by means of (i).

Let be $\tau_M > 0$. The time axis is divided by the maximization times $0 = t_0 < t_1 < t_2 < \cdots$, so that the convex domain Ω can be decomposed into the subdomains

$$\begin{cases} \Omega_0 &= \left\{(\delta, \mathbf{x}) \in \Omega \middle| \, 0 \leq \delta \leq \frac{t_0+t_1}{2}\right\}, \\ \Omega_n &= \left\{(\delta, \mathbf{x}) \in \Omega \middle| \, \frac{t_{n-1}+t_n}{2} \leq \delta \leq \frac{t_n+t_{n+1}}{2}\right\} (n = 1, 2, 3, \dots). \end{cases} \tag{2.2.17}$$

Since $\int_{\partial\Omega}(u_A, F_{Ak})d\vec{o} = \sum_{n\geq 0}\int_{\partial\Omega_n}(u_A, F_{Ak})d\vec{o}$, it is sufficient to assume without loss of generality that the time range

$$\Theta_\Omega = \left\{t \geq 0 \middle|\ \text{there exists } x \in \mathbb{R}^3 : (t, \mathbf{x}) \in \Omega\right\}$$

of Ω contains at most one maximization time t. Then for ε out of the range $0 < \varepsilon < \frac{1}{2}\tau_M$ we define a further decomposition of each $\Omega_n, n \geq 1$, into three parts:

$$\begin{cases} \Omega^\varepsilon_{n,L} &= \left\{(\delta, \mathbf{x}) \in \Omega_n \middle|\ \delta \leq t_n - \varepsilon\right\}, \\ \Omega^\varepsilon_{n,M} &= \left\{(\delta, \mathbf{x}) \in \Omega_n \middle|\ t_n - \varepsilon \leq \delta \leq t_n + \varepsilon\right\}, \\ \Omega^\varepsilon_{n,R} &= \left\{(\delta, \mathbf{x}) \in \Omega_n \middle|\ \delta \geq t_n + \varepsilon\right\}. \end{cases} \tag{2.2.18}$$

These decompositions are visualized in the following two graphs:

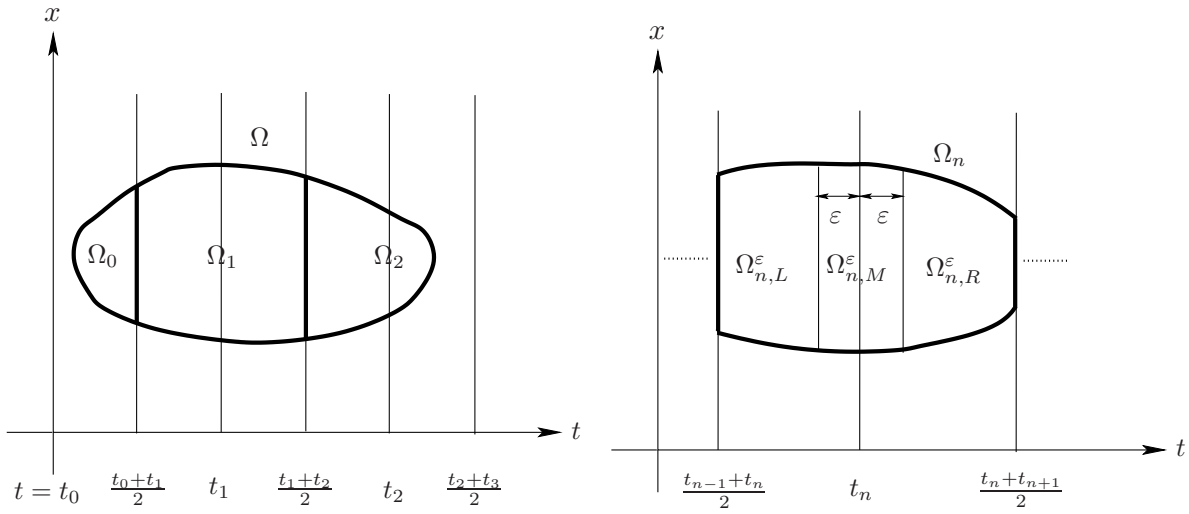

Figure 2.1: The decompositions of Ω and Ω_n.

We obtain

$$\int\limits_{\partial\Omega_n}(u_A, F_{Ak})d\vec{o} = \int\limits_{\partial\Omega^\varepsilon_{n,L}}(u_A, F_{Ak})d\vec{o} + \int\limits_{\partial\Omega^\varepsilon_{n,R}}(u_A, F_{Ak})d\vec{o} + \int\limits_{\partial\Omega^\varepsilon_{n,M}}(u_A, F_{Ak})d\vec{o}, \tag{2.2.19}$$

and proceed to show that the first two integrals on the right-hand side must vanish:

The fields $u_A(t, \mathbf{x})$ and $F_{Ak}(t, \mathbf{x})$ are smooth in the domains $\Omega^\varepsilon_{n,L}$, $\Omega^\varepsilon_{n,R}$. For both domains we thus can apply the Gaussian Divergence Theorem to the conservation law $\partial_t u_A + \partial_{x_k} F_{Ak} = 0$ resulting from the Proposition 2.1 in order to get

$$\int\limits_{\partial\Omega^\varepsilon_{n,L}}(u_A, F_{Ak})d\vec{o} = \int\limits_{\partial\Omega^\varepsilon_{n,R}}(u_A, F_{Ak})d\vec{o} = 0.$$

A similar proof in the one-dimensional case is given in Appendix A for the relativistic case. However one can use that proof for the non-relativistic case with little modification. This

implies

$$\begin{aligned}\int\limits_{\partial\Omega_n}(u_A,F_{Ak})d\vec{o} &= \int\limits_{\partial\Omega^\varepsilon_{n,M}}(u_A,F_{Ak})d\vec{o} = \lim_{\varepsilon\to 0}\int\limits_{\partial\Omega^\varepsilon_{n,M}}(u_A,F_{Ak})d\vec{o}\\ &= \int_{\Omega_n^*}\left\{\int_{\mathbb{R}^3} c_A\left[f_n(\mathbf{x},\mathbf{c})-f_{n-1}(\mathbf{x}-\tau_M\mathbf{c},\mathbf{c})\right]d^3\mathbf{c}\right\}d^3\mathbf{x},\end{aligned}$$

where $\Omega_n^*=\{\mathbf{x}\in\mathbb{R}^3|(t_n,\mathbf{x})\in\Omega\}$. The time t_{n-1} is the maximization time that preceeds the maximization time t_n. The Maxwellian f_n has to be read off from (2.2.10).

The last integral expression vanishes due to continuity conditions (2.2.14), i.e.,

$$u_A(t_n^-,\mathbf{x})=u_A(t_n^+,\mathbf{x})\,.$$

We have thus established that the weak form (2.2.15) for a general convex domain Ω is implied by the representations (2.2.12). In particular (2.2.15) holds also in the Eulerian limit $\tau_M\to 0$.

In each regular point $(t,\mathbf{x})$ we can now apply the Gaussian Divergence Theorem to (2.2.15) in the Eulerian limit in order to get the proposition (iii).

Regarding the proposition (iv) which states the existence of the entropy inequality (2.2.16), we start the again with the decompositions (2.2.17) and (2.2.18) of Ω. Since $\int_{\partial\Omega}(h,\Phi_k)d\vec{o}=\sum_{n\geq 0}\int_{\partial\Omega_n}(h,\Phi_k)d\vec{o}$, it is sufficient to prove $\int_{\partial\Omega_n}(h,\Phi_k)d\vec{o}\geq 0$ for each n. We obtain

$$\int_{\partial\Omega_n}(h,\Phi_k)d\vec{o}=\int_{\partial\Omega^\varepsilon_{n,L}}(h,\Phi_k)d\vec{o}+\int_{\partial\Omega^\varepsilon_{n,R}}(h,\Phi_k)d\vec{o}+\int_{\partial\Omega^\varepsilon_{n,M}}(h,\Phi_k)d\vec{o}. \tag{2.2.20}$$

We will now show that the first two integrals on the right hand side vanishes. The entropy-function $h(t,\mathbf{x})$ and the entropy-flux $\Phi_k(t,\mathbf{x})$ are smooth fields in the domain $\Omega^\varepsilon_{n,R}$, because according to (2.2.13) we have for $(t,\mathbf{x})\in\Omega^\varepsilon_{n,R}$

$$\begin{aligned}h(t,\mathbf{x}) &= -\int_{\mathbb{R}^3}(f_n\ln f_n)(\mathbf{x}-(t-t_n)\mathbf{c},\mathbf{c})\,d^3\mathbf{c}\,,\\ \Phi_k(t,\mathbf{x}) &= -\int_{\mathbb{R}^3}c_k(f_n\ln f_n)(\mathbf{x}-(t-t_n)\mathbf{c},\mathbf{c})\,d^3\mathbf{c}\,.\end{aligned}$$

In this domain we obtain due to the chain rule:

$$\partial_t h(t,\mathbf{x})=-\partial_{x_k}\Phi_k(t,\mathbf{x}). \tag{2.2.21}$$

This implies $\int_{\partial\Omega^\varepsilon_{n,R}}(h,\Phi_k)d\vec{o}=0$, and $\int_{\partial\Omega^\varepsilon_{n,L}}(h,\Phi_k)d\vec{o}=0$ can likewise be obtained. For every sufficiently small $\varepsilon>0$ there holds

$$\begin{aligned}\int\limits_{\partial\Omega_n}(h,\Phi_k)d\vec{o} &= \lim_{\varepsilon\to 0}\int\limits_{\partial\Omega^\varepsilon_{n,M}}(h,\Phi_k)d\vec{o} \qquad (2.2.22)\\ &= \int\limits_{\Omega_n^*}\left\{\int_{\mathbb{R}^3}\left[-(f_n\ln f_n)(\mathbf{x},\mathbf{c})+(f_{n-1}\ln f_{n-1})(\mathbf{x}-\tau_M\mathbf{c},\mathbf{c})\right]d^3\mathbf{c}\right\}d^3\mathbf{x},\end{aligned}$$

where $\Omega_n^* = \{\mathbf{x} \in \mathbb{R}^3 | (t_n, \mathbf{x}) \in \Omega\}$, and $t_{n-1} < t_n$ is the maximization time that preceeds t_n. Next we shall show that the integral (2.2.22) is non-negative. To this we need the following

Lemma 2.3: *For $u, v > 0$ we have*

$$v \ln v - u \ln u = [\ln u + 1](v - u) + S(u, v)\,, \tag{2.2.23}$$

with a function $S(u, v) \geq 0$.

Proof of Lemma 2.3: Due to Taylor's formula there is a $\xi > 0$ between $u, v > 0$ such that

$$v \ln v = u \ln u + (\ln u + 1)(v - u) + \frac{1}{2\xi}(v - u)^2. \tag{2.2.24}$$

We conclude $S(u, v) \geq 0$. ■

Now we apply Lemma 2.3 to $u = f_n(\mathbf{x}, \mathbf{c})$, $v = f_{n-1}(\mathbf{x} - \tau_M \mathbf{c}, \mathbf{c})$:

$$\begin{aligned} & \int_{\mathbb{R}^3} [-(f_n \ln f_n)(\mathbf{x}, \mathbf{c}) + (f_{n-1} \ln f_{n-1})(\mathbf{x} - \tau_M \mathbf{c}, \mathbf{c})]\, d^3\mathbf{c} \qquad (2.2.25) \\ = \; & -\int_{\mathbb{R}^3} [1 + \ln f_n(\mathbf{x}, \mathbf{c})]\, [f_n(\mathbf{x}, \mathbf{c}) - f_{n-1}(\mathbf{x} - \tau_M \mathbf{c}, \mathbf{c})]\, d^3\mathbf{c} \\ & + \int_{\mathbb{R}^3} S(f_n(\mathbf{x}, \mathbf{c}), f_{n-1}(\mathbf{x} - \tau_M \mathbf{c}, \mathbf{c})) d^3\mathbf{c}. \end{aligned}$$

The second integral is non-negative and the first one vanishes because $[1 + \ln f_n(\mathbf{x}, \mathbf{c})]$ is a quadratic polynomial in $\mathbf{c}$, containing only c_i and $\mathbf{c}^2$, and for $c_A = \left(1, c_i, I_0 + \frac{\mathbf{c}^2}{2}\right)$ there follows due to (2.2.14)

$$0 = \int_{\mathbb{R}^3} c_A\, [f_n(\mathbf{x}, \mathbf{c}) - f_{n-1}(\mathbf{x} - \tau_M \mathbf{c}, \mathbf{c})]\, d^3\mathbf{c}. \tag{2.2.26}$$

For $\tau_M > 0$ we have thus established the entropy inequality (2.2.16). It is due to proposition 2.2 (i) that this inequality is also valid in the Eulerian limit, where shocks may appear. ■

2.2.2 Positivity and L^1-Stability of the Kinetic Scheme

One advantage of kinetic schemes is that it is straightforward to show that they preserve positivity of the density and pressure. A similar theorem was proved by Perthame [74] in case of KFVS scheme.

Theorem 2.4: *Assume that the initial distribution function $f_n(\mathbf{y}, \mathbf{c}) \geq 0$, additionally $f_n(\mathbf{y}, \mathbf{c})$ does not vanish almost everywhere for all microscopic velocities $\mathbf{c}$, macroscopic velocities $\mathbf{v}$ and positive density and pressure. Then the numerical solution obtained by the resulting kinetic scheme has the following property: its density, total energy and pressure remain positive for all times. This mean that the numerical scheme defined by* (2.2.8) *is stable in L^1:*

$$\rho(t_n + \tau, \mathbf{x}) > 0\,, \qquad E(t_n + \tau, \mathbf{x}) > 0\,, \qquad p(t_n + \tau, \mathbf{x}) > 0\,. \tag{2.2.27}$$

Proof: Since we have assumed that initial phase-density is positive, therefore (2.2.8) implies

$$\rho(t_n+\tau,\mathbf{x}) = \int_{\mathbb{R}^3} f_n(\mathbf{x}-\tau\mathbf{c},\mathbf{c})\; d^3\mathbf{c} > 0\,. \tag{2.2.28}$$

Simlarly

$$E(t_n+\tau,\mathbf{x}) = \int_{\mathbb{R}^3} \left(I_0+\frac{\mathbf{c}^2}{2}\right) f_n(\mathbf{x}-\tau\mathbf{c},\mathbf{c})\; d^3\mathbf{c} > 0\,. \tag{2.2.29}$$

According to the Cauchy-Schwarz inequality, if we have two functions f and g then

$$\left(\int_a^b f\cdot g\,dx\right)^2 \le \left(\int_a^b f^2\,dx\right)\cdot\left(\int_a^b g^2\,dx\right)\,, \tag{2.2.30}$$

where equality holds iff the functions f and g are linearly dependent.

Let us define for abbreviation $\mathbf{y}=\mathbf{x}-\tau\mathbf{c}$. Using (2.2.8) and Cauchy-Schwarz inequality, we get

$$\begin{aligned}
(\rho v_1)^2(t_n+\tau,\mathbf{x}) &= \left(\int_{\mathbb{R}^3} c_1\, f_n(\mathbf{y},\mathbf{c})\, d^3\mathbf{c}\right)^2 \\
&= \left(\int_{\mathbb{R}^3} \left(\left(c_1\sqrt{f_n}\right)\cdot\left(\sqrt{f_n}\right)\right)(\mathbf{y},\mathbf{c})\, d^3\mathbf{c}\;\right)^2 \\
&< \left(\int_{\mathbb{R}^3} \left(c_1\sqrt{f_n}\right)^2(\mathbf{y},\mathbf{c})\, d^3\mathbf{c}\right)\cdot\left(\int_{\mathbb{R}^3} \left(\sqrt{f_n}\right)^2(\mathbf{y},\mathbf{c})\, d^3\mathbf{c}\right) \\
&= \rho(t_n+\tau,\mathbf{x})\left(\int_{\mathbb{R}^3} c_1^2 f_n(\mathbf{y},\mathbf{c})\, d^3\mathbf{c}\right)\,.
\end{aligned} \tag{2.2.31}$$

In Cauchy-Schwarz inequality we have not taken the equality sign because the functions $c_1\sqrt{f_n(\mathbf{y},\mathbf{c})}$ and $\sqrt{f_n(\mathbf{y},\mathbf{c})}$ are linearly independent. Similarly

$$\begin{aligned}
(\rho v_2)^2(t_n+\tau,\mathbf{x}) &< \rho(t_n+\tau,\mathbf{x})\left(\int_{\mathbb{R}^3} c_2^2 f_n(\mathbf{y},\mathbf{c})\, d^3\mathbf{c}\;\right)\,, \\
(\rho v_3)^2(t_n+\tau,\mathbf{x}) &< \rho(t_n+\tau,\mathbf{x})\left(\int_{\mathbb{R}^3} c_3^2 f_n(\mathbf{y},\mathbf{c})\, d^3\mathbf{c}\;\right)\,.
\end{aligned} \tag{2.2.32}$$

Now adding (2.2.31), (2.2.32), and using the fact that $\mathbf{v}^2=v_1^2+v_2^2+v_3^2$, $\mathbf{c}^2=c_1^2+c_2^2+c_3^2$, we finally get

$$\begin{aligned}
\frac{1}{2}\rho\mathbf{v}^2(t_n+\tau,\mathbf{x}) &< \int_{\mathbb{R}^3} \frac{\mathbf{c}^2}{2} f_n(\mathbf{y},\mathbf{c})\, d^3\mathbf{c}\,. \\
&\le \int_{\mathbb{R}^3} \left(I_0+\frac{\mathbf{c}^2}{2}\right) f_n(\mathbf{y},\mathbf{c})\, d^3\mathbf{c}\,. \\
&= E(t_n+\tau,\mathbf{x})\,.
\end{aligned}$$

Thus we have proved that $E(t_n+\tau,\mathbf{x}) > \frac{1}{2}\rho\mathbf{v}^2(t_n+\tau,\mathbf{x})$. This implies that

$$p(t_n+\tau,\mathbf{x}) = (\gamma-1)\left(E-\frac{1}{2}\rho\mathbf{v}^2\right)(t_n+\tau,\mathbf{x}) > 0\,.$$

■

Now we prove the L_1-stability of the scheme. We have already proved that the kinetic scheme is conservative and give positive values of particle density ρ and total energy E . Therefore using $(2.2.8)_1$ we get

$$\begin{aligned}
||\rho(t_n+\tau,.)||_{L^1(R)} &= \int_{\mathbb{R}^3} |\rho(t_n+\tau,\mathbf{x})| d^3\mathbf{x} = \int_{\mathbb{R}^3} \rho(t_n+\tau,\mathbf{x}) d^3\mathbf{x} \\
&= \int_{\mathbb{R}^3} \rho(t_n,\mathbf{x}) dx = \int_{\mathbb{R}^3} |\rho(t_n,\mathbf{x})| d^3\mathbf{x} \\
&= ||\rho(t_n,.)||_{L^1(R)}\,.
\end{aligned}$$

Similarly $||E(t_n+\tau,.)||_{L^1(R)} = ||E(t_n,.)||_{L^1(R)}$. Now using (2.2.8) with $\mathbf{y} = \mathbf{x}-\tau\mathbf{c}$ and Cauchy-schwarz inequality (2.2.30) we get

$$\begin{aligned}
||\rho v_i(t_n+\tau,.)||_{L^1(R)} &= \int_{\mathbb{R}^3} \left| \int_{\mathbb{R}^3} c_i f_n(\mathbf{y},\mathbf{c}) d^3\mathbf{c} \right| d^3\mathbf{x} \\
&= \int_{\mathbb{R}^3} \left| \int_{\mathbb{R}^3} \left(\sqrt{f_n}\right)\left(c_i\sqrt{f_n}\right)(\mathbf{y},\mathbf{c}) d^3\mathbf{c} \right| d^3\mathbf{x} \\
&< \left[\int_{\mathbb{R}^3} \left| \int_{\mathbb{R}^3} f_n(\mathbf{y},\mathbf{c}) d^3\mathbf{c} \right| d^3\mathbf{x} \cdot 2 \int_{\mathbb{R}^3} \left| \int_{\mathbb{R}^3} \left(I_0 + \frac{\mathbf{c}^2}{2}\right) f_n(\mathbf{y},\mathbf{c}) d^3\mathbf{c} \right| d^3\mathbf{x} \right]^{\frac{1}{2}} \\
&= \left(2\,||\rho(t_n,.)||_{L^1(R)}\,||E(t_n,.)||_{L^1(R)}\right)^{\frac{1}{2}}.
\end{aligned}$$

This proves the L^1 stability of the scheme. ■

2.3 Kinetic Scheme in One Space Dimension

In the following we are looking for spatially one-dimensional solutions, which are nevertheless solutions to the full three dimensional equations. We only consider solutions which depend on t and $x = x_1$ and satisfy $\rho = \rho(t,x)$, $\mathbf{v} = (v(t,x),0,0)$, $p = p(t,x)$.

We choose a fixed $\tau = \tau_M > 0$ and define the equidistant times $t_n = n\tau_M$ $(n = 0,1,2,\dots)$. For given fields $\rho_n(x) = \rho(t_n,x)$, $v_n(x) = v(t_n,x)$, $T_n(x) = T(t_n,x)$ at time t_n, starting with the initial data ρ_0, v_0, T_0 given at time $t = 0$, these fields are obtained at time t_{n+1} according

to the scheme

$$\begin{aligned}\rho(t_{n+1},x) &= \int_{-\infty}^{+\infty} f_n(x-c\tau,c)\,dc\,,\\ (\rho v)(t_{n+1},x) &= \int_{-\infty}^{+\infty} c f_n(x-c\tau,c)\,dc\,,\\ E(t_{n+1},x) &= \int_{-\infty}^{+\infty} (I_0+\frac{c^2}{2}) f_n(x-c\tau,c)\,dc.\end{aligned} \tag{2.3.1}$$

Here the phase density $f_n(y,c)$ is given by

$$f_n(y,c) = w_M(y,c) = \frac{\rho_n(y)}{\sqrt{2\pi T_n(y)}} \exp\left[-\frac{(c-v_n(y))^2}{2T_n(y)}\right], \tag{2.3.2}$$

and (2.2.5) implies $I_0 = \dfrac{3-\gamma}{2(\gamma-1)}T$, for $D_f = 1$. This scheme can be obtained from the representations (2.2.9) by integrating over c_2 and c_3.

2.3.1 Numerical Implementation of the Scheme in 1D

Here we explain the numerical implementation of the one-dimensional kinetic scheme. However the procedure is similar for the two-dimensional case.

- We start with the values of initial data $\rho(t_n,x)$, $v(t_n,x)$ and $T(t_n,x)$ at equidistant grid points.
- We specify the length L of the spatial domain, the number N_x of elements (intervals) in the spatial domain $0 \le x \le L$, the final time t_f of output and the number E_m of maximization times. For $i = 0,...,N_x$, we introduce the nodes $x_i = i \cdot \frac{L}{N_x}$.
- The time step Δt is calculated by $\Delta t = \frac{t_f}{E_M}$. The step in the spatial domain is $\Delta x = L/N_x$.
- Our aim is to calculate the moments (2.3.1). These moments are then used to update the fields ρ, v and T.

In order to perform the integration with respect to variable c, we need to cut the integration limits which are ranging from $-\infty$ to ∞. For this purpose we need a sufficiently large domain

$$R = [c_{\min}, c_{\max}]\,, \tag{2.3.3}$$

so that the Maxwellian $f_n(y,c)$ is sufficiently small outside of R. In order to construct R, we use the knowledge of dynamic fields at the preceding time step t_n. Thus at the actual time t_{n+1}, the size of R is determined as follows:

We choose R and a positive constant $\eta \geq 3$, for example $\eta = 4$, so that each c which is outside of R must satisfy the following inequality for all $y \in \mathbb{R}$:

$$\exp\left[-\frac{(c - v(t_n, y))^2}{2T(t_n, y)}\right] < \exp\left(-\eta^2\right) = \exp\left(-16\right) = 1.125 \times 10^{-7}\,, \tag{2.3.4}$$

this implies that the contribution is only coming from

$$|c - v| \leq \eta\sqrt{2T}\,.$$

We are able to control the following extreme values of the fields $v(t_n, .)$ and $T(t_n, .)$ at the previous time step t_n:

$$c_{\min} = v_{\min} - \eta\sqrt{2T_{max}}\,, \quad c_{\max} = v_{\max} + \eta\sqrt{2T_{max}}\,, \tag{2.3.5}$$

for

$$\begin{aligned} v_{\min} &= \min_{y\in\mathbb{R}} v(t_n, y), \quad v_{\max} = \max_{y\in\mathbb{R}} v(t_n, y)\,, \\ T_{\min} &= \min_{y\in\mathbb{R}} T(t_n, y), \quad T_{\max} = \max_{y\in\mathbb{R}} T(t_n, y)\,. \end{aligned}$$

In above all the fields variables $\rho(t_n, x),\ v(t_n, x)$ and $T(t_n, x)$ are stored at mesh points only, and therefore $f_n(x_i - c\tau, c)$ has to be determined by linear interpolation. One choice of interpolation is

$$f_n(x_j - c\tau, c) = f_n(x_i, c) + \delta\ [f_n(x_{i+1}, c) - f_n(x_i, c)]\ , \tag{2.3.6}$$

where $x_j - c\tau = x_i + \delta\,(x_{i+1} - x_i)$ for $0 \leq \delta \leq 1$. Here $f_n(x_j - \tau c)$ and $f_n(x_i, c) = w_M(x_i, c)$ are the one-dimensional free-flight and Maxwellian phase phase densities, respectively. The relations between x_i, x_j and δ are shown in Figure 2.2. The linear interpolation of the previous fields corresponds to the application of the trapezoidal integration rule in (2.3.1).

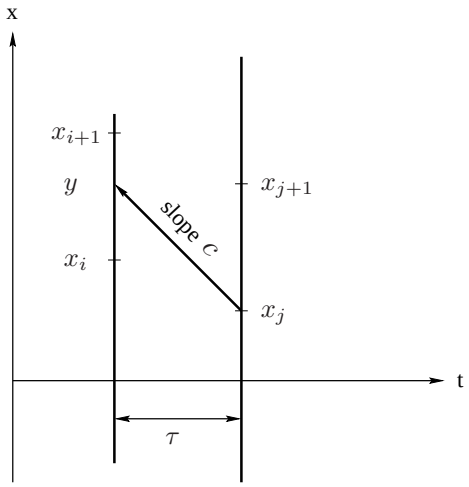

Figure 2.2: Interpolation of $y = x_j - c\tau$ at the grid points x_i and x_{i+1}.

2.3.2 Application of Boundary Conditions

Here we generalize the above numerical kinetic scheme in order to include boundaries. We are restricting ourselves to the one space dimension, however the procedure is analogous for the two and three space dimensions.

It is possible that a point $y = x - c\tau$ is outside the computational domain $0 \leq x \leq L$, i.e., the fluid particle has then crossed the domain boundaries during free-flight. Consequently, a boundary strategy is required to find $f_n(y, c)$ so that physically meaningful desired boundary conditions are satisfied.

Reflecting boundary conditions:

In Figure 2.3 a single gas particle trajectory is shown. We consider the lower boundary as a solid wall, therefore the particles having negative velocity will reach the wall. The particle starts from a position x_* with negative microscopic velocity and reach the lower boundary in time τ_1. The particle then reflects with positive velocity and reaches the position x in time τ_2. Since the reflection from the lower adiabatic wall is elastic, therefore particle incident and reflected angles are the same. Now using Figure 2.3 we get the following relations

$$x = \tau_2\, c\,, \qquad x_* = -\tau_1\, c\,, \qquad \tau_1 + \tau_2 = \tau\,. \tag{2.3.7}$$

Subtracting $(2.3.7)_{1,2}$ and using $(2.3.7)_3$ we get $x_* = |x - \tau c| \geq 0$.

Therefore in case of lower adiabatic boundary we replace $f_n(x - \tau c, c)$ in the kinetic scheme (2.3.1) by $f_n(|x - \tau c|, c_*)$ for $c_* = -c$.

Similarly if we consider the boundary $x = L$ as adiabatic wall then only those particles will reach to the boundary which have positive microscopic velocity c. Let $\Delta = y - L$ then the reflecting boundary conditions will be $x_* = L - \Delta$ and $c_* = -c$. Thus we will replace $f_n(x - \tau c, c)$ in the kinetic scheme (2.3.1) by $f_n(x_*, c_*)$.

Absorbing boundary conditions:

When the fluid particle crosses the lower boundary as shown by the dashed line in Figure 2.3, i.e., $y = x - c\tau < 0$, then we replace $f_n(x - \tau c, c)$ in the kinetic scheme (2.3.1) by $f_n(|x - \tau c|, c)$. Similarly if $y = x - c\tau > L$, i.e., fluid particles have acrossed the upper boundary then we take $x_* = L - \Delta$ where $\Delta = y - L$ and replace $f_n(x - \tau c, c)$ in the kinetic scheme (2.3.1) by $f_n(x_*, c)$.

2.3.3 Total Variation Diminishing (TVD) Property

The validity of the TVD property for the kinetic scheme was proved by Deshpande [13]. Here we present his proof. Let us define for abbreviation $y_j = x_j - \tau c$, then we can rewrite (2.3.6) for $0 < \tau < \tau_M$ as

$$f(t_n + \tau, x_j, c) = f_n(y_j, c) = (1 - \eta)\, f_n(x_i, c) + \eta\, f_n(x_{i+1}, c)\,, \quad (0 \leq \eta \leq 1)\,. \tag{2.3.8}$$

Here i is the mesh point such that $x_j - c\tau$ lies between x_i and x_{i+1}. The phase densities $f_n(x_i, c)$ and $f_n(x_{i+1}, c)$ are the Maxwellian at time t_n. The total variation of f_n at time t_n

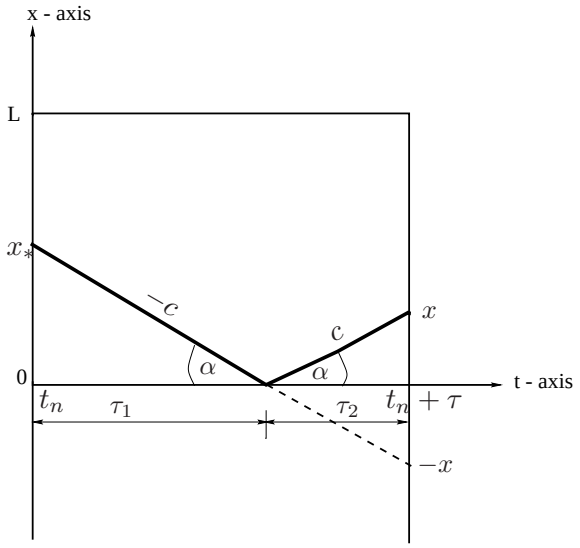

Figure 2.3: Trajectory of a single gas particle.

is defined by

$$TV\left(f_n(c)\right) = \sum_{j\in\mathbb{Z}} \left|f_n(x_{j+1}, c) - f_n(x_j, c)\right|. \tag{2.3.9}$$

Due to the constraints (2.2.14) and (2.2.3), the density, fluid velocity, and temperature does not change during the maximization time. Hence

$$TV(\rho(t_n^-)) = TV(\rho(t_n^+))\,, \quad TV(v(t_n^-)) = TV(v(t_n^+))\,, \qquad TV(T(t_n^-)) = TV(T(t_n^+))\,.$$

Therefore, it is sufficient to deal with the change of total variation during free-flight $t_n < t_n + \tau < t_{n+1}$, $0 < \tau < \tau_M$. Using (2.3.8) the total variation is given by

$$\begin{aligned} TV\left(f(t_n+\tau, c)\right) &= \sum_{j\in\mathbb{Z}} \left|f_n(y_{j+1}, c) - f_n(y_j, c)\right| \\ &\le \sum_{i\in\mathbb{Z}} (1-\eta)\left|f_n(x_{i+1}, c) - f_n(x_i, c)\right| + \sum_{i\in\mathbb{Z}} \eta\left|f_n(x_{i+2}, c) - f_n(x_{i+1}, c)\right|. \end{aligned} \tag{2.3.10}$$

Evidently,

$$\sum_{i\in\mathbb{Z}} \eta\left|f_n(x_{i+2}, c) - f_n(x_{i+1}, c)\right| = \sum_{i\in\mathbb{Z}} \eta\left|f_n(x_{i+1}, c) - f_n(x_i, c)\right|,$$

and hence with the use of (2.3.9), the inequality (2.3.10) becomes

$$TV\left(f(t_n+\tau, c)\right) \le \sum_{i\in\mathbb{Z}} \left|f_n(x_{i+1}, c) - f_n(x_i, c)\right| \le TV\left(f_n(c)\right)\,.$$

Thus, for every value of η, the total variation of the velocity distribution function is non-increasing during the free-flight phase. There are some advantages to considering the total

variation (TV) of the phase density f instead of the TV of the fields ρ, v, T. The conservation laws of the Euler type are moments of a single scalar equation for phase density f. This equation being linear and hyperbolic admits the exact solution $f_n(x - \tau c, c)$, which is TV-preserving. It is therefore quite consistent to demand that numerical solution for f be TV-preserving. The present approach connects the TVD property of the linear, hyperbolic equation with the vector conservation laws by use of the fact that the laws are moments of the equation. From the above analysis the TVD property of the kinetic scheme hinges upon the interpolation strategy adopted in calculating $f_n(x - c\tau, c)$.

2.4 Kinetic Scheme in Two Space Dimensions

We are looking for the solutions $u_A(t, x_1, x_2, x_3)$ which do not depend on x_3. In this case we can carry out the c_3-integration in (2.2.9) and obtain the two-dimensional scheme for ρ, $\mathbf{v} = (v_1, v_2)$ and T:

$$\begin{aligned} \rho(t_{n+1}, \mathbf{x}) &= \int_{\mathbb{R}^2} f_n(\mathbf{x} - \mathbf{c}\tau, \mathbf{c})\, d^2c\,, \\ (\rho v_i)(t_{n+1}, \mathbf{x}) &= \int_{\mathbb{R}^2} c_i f_n(\mathbf{x} - \mathbf{c}\tau, \mathbf{c})\, d^2c\,, \\ E(t_{n+1}, \mathbf{x}) &= \int_{\mathbb{R}^2} \left(I_0 + \frac{\mathbf{c}^2}{2} \right) f_n(\mathbf{x} - \mathbf{c}\tau, \mathbf{c})\, d^2c\,. \end{aligned} \tag{2.4.1}$$

Here $\mathbf{x}$, $\mathbf{c}$, $\mathbf{v} \in \mathbb{R}^2$, $i = 1, 2$, and the phase density $f_n(\mathbf{y}, \mathbf{c})$ is given by

$$f_n(\mathbf{y}, \mathbf{c}) = \frac{\rho_n(\mathbf{y})}{\sqrt{2\pi T_n(\mathbf{y})}} \exp\left[-\frac{(\mathbf{c} - \mathbf{v}_n(\mathbf{y}))^2}{2T_n(\mathbf{y})} \right], \tag{2.4.2}$$

and (2.2.5) implies $I_0 = \dfrac{2 - \gamma}{(\gamma - 1)} T$, for $D_f = 2$.

We choose a fixed $\tau = \tau_M > 0$ and define the equidistant times $t_n = n\tau_M$ $(n = 0, 1, 2, \dots)$. For given fields $\rho_n(\mathbf{x}) = \rho(t_n, \mathbf{x})$, $\mathbf{v}_n(\mathbf{x}) = \mathbf{v}(t_n, \mathbf{x})$, $T_n(\mathbf{x}) = T(t_n, \mathbf{x})$ at time t_n, starting with the initial data $\rho_0(\mathbf{x}), v_0(\mathbf{x}), T_0(\mathbf{x})$ given at time $t = 0$, these fields are obtained at time t_{n+1} by evaluating the integrals (2.4.1).

2.4.1 Numerical Implementation of the Scheme in 2D

This is a two-dimensional extension of the procedure given in Subsection 2.3.1 for the one-dimensional case, see [17]. We start with the values of initial data $\rho(t_n, \mathbf{x})$, $\mathbf{v}(t_n, \mathbf{x})$ and $T(t_n, \mathbf{x})$ at equidistant grid points.

In order to perform the integration with respect to variable $\mathbf{c}$, we again need to cut the integration limits which are ranging from $-\infty$ to ∞. For this purpose we need a sufficiently large rectangular domain

$$R = \left[c_1^{\min}, c_1^{\max}\right] \times \left[c_2^{\min}, c_2^{\max}\right], \tag{2.4.3}$$

so that the Maxwellian $f_n(\mathbf{y},\mathbf{c})$ in (2.4.2) is sufficiently small outside of R. In order to construct R, we use the knowledge of dynamic fields at the preceding time step t_n. Thus at the actual time t_{n+1}, the size of R is determined as follows:

We choose R and a positive constant $\eta \geq 3$, for example $\eta = 4$, so that each $\mathbf{c}$ which is outside of R must satisfy the following inequality for all $\mathbf{y} \in R^2$:

$$\exp\left[-\frac{(\mathbf{c}-\mathbf{v}(t_n,\mathbf{y}))^2}{2T(t_n,\mathbf{y})}\right] < \exp\left(-\eta^2\right) = \exp\left(-16\right) = 1.125 \times 10^{-7}\,, \tag{2.4.4}$$

this implies the contribution is only coming from

$$|\mathbf{c}-\mathbf{v}| \leq \eta\sqrt{2T}\,,$$

which is a circle of radius $\eta\sqrt{2T}$ and center at $\mathbf{v}$. We are able to control the following extreme values of the fields $\mathbf{v}(t_n,.)$ and $T(t_n,.)$ at the previous time step t_n:

$$v_1^{\min} = \min_{y\in\mathbb{R}^2} v_1(t_n,\mathbf{y}), \quad v_1^{\max} = \max_{y\in\mathbb{R}^2} v_1(t_n,\mathbf{y}), \tag{2.4.5}$$

$$v_2^{\min} = \min_{y\in\mathbb{R}^2} v_2(t_n,\mathbf{y}), \quad v_2^{\max} = \max_{y\in\mathbb{R}^2} v_2(t_n,\mathbf{y}), \tag{2.4.6}$$

$$T^{\min} = \min_{y\in\mathbb{R}^2} T(t_n,\mathbf{y}), \quad T^{\max} = \max_{y\in\mathbb{R}^2} T(t_n,\mathbf{y})\,. \tag{2.4.7}$$

Consequently it is an easy matter to determine that an appropriate choice of integration domain R is given by the following square with the side length r:

$$\begin{aligned} r &= \frac{1}{2}\left[\left(v_1^{\min}-v_1^{\max}\right)^2 + \left(v_2^{\min}-v_2^{\max}\right)^2\right]^{1/2} + \eta\sqrt{2T^{\max}}\,,\\ c_1^{\min} &= \frac{1}{2}(v_1^{\min}+v_1^{\max}) - r\,,\ c_1^{\max} = \frac{1}{2}(v_1^{\min}+v_1^{\max}) + r\,,\\ c_2^{\min} &= \frac{1}{2}(v_2^{\min}+v_2^{\max}) - r\,,\ c_2^{\max} = \frac{1}{2}(v_2^{\min}+v_2^{\max}) + r\,. \end{aligned} \tag{2.4.8}$$

Finally we have to solve the problem of space-discretization. To this end we choose a rectangular computational domain $\Omega \subset \mathbb{R}^2$. For initial value problems we take the domain Ω large enough to avoid the boundary effects, while for the boundary value problems we have to follow the same procedure as given in Subsection 2.3.2 for the one-dimensional case. Next we cover the resulting domain

$$\Omega = \left[x_1^{\min}, x_1^{\max}\right] \times \left[x_2^{\min}, x_2^{\max}\right]\,, \tag{2.4.9}$$

with a rectangular mesh with mesh points

$$x_1^{(i)} = x_1^{\min} + \frac{x_1^{\max}-x_1^{\min}}{n_1-1}\,,\quad x_2^{(i)} = x_2^{\min} + \frac{x_2^{\max}-x_2^{\min}}{n_2-1}\,,$$

where $0 \leq i \leq n_1,\ 0 \leq j \leq n_2$ and $n_1,\, n_2 \geq 2$ are the numbers of grid points in the x_1 and x_2 directions, respectively. Then we decompose each rectangle $\left[x_1^{(i)}, x_1^{(i+1)}\right] \times \left[x_2^{(j)}, x_2^{(j+1)}\right]$ into two triangles so that the final decomposition of Ω is as given in Figure 2.4.

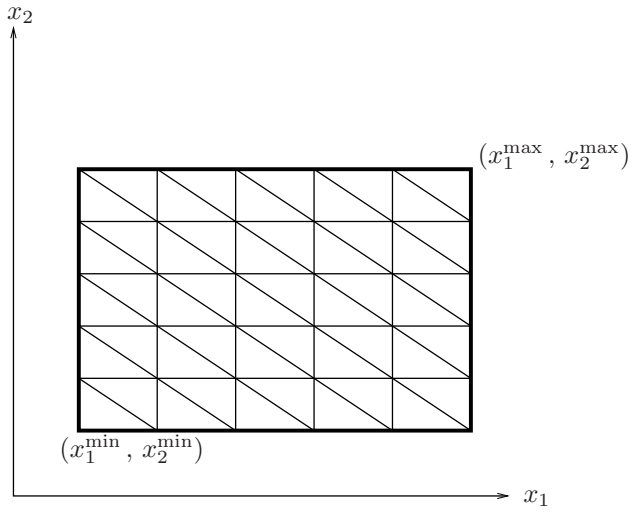

Figure 2.4: Decomposition of Ω

The new fields $\rho(t_{n+1}, .)$, $\mathbf{v}(t_{n+1}, .)$, $T(t_{n+1}, .)$ are computed at the grid points $x_1^{(i)}$, $x_1^{(j)}$ relying on the knowledge of the previous fields, which are interpolated linearly to each triangle. The linear interpolation of the previous fields corresponds to the application of the trapezoidal integration rule in (2.4.1) to each triangle.

We choose a triangulation in order to use linear interpolation. On quadrilaterals one would have to use piecewise bilinear functions.

2.5 Kinetic Flux Vector Splitting (KFVS) Schemes

The kinetic schemes described above are discrete in time but continuous in space. Now we come to another type of kinetic schemes which are discrete both in time and space. These schemes are called KFVS schemes. The KFVS schemes are stable under CFL condition and the fluid flow is limited to the neighbouring cells only.

Flux vector splitting is a technique for achieving upwinding bias in numerical flux functions, which is a natural consequence of regarding a fluid as an ensemble of particles. Since particles can move forward or backward through an interface, this automatically splits the fluxes of mass, momentum and energy into forward and backward fluxes through the cell interface, i.e,

$$F_{i+\frac{1}{2}} = F^+(W_i) + F^-(W_{i+1})\,,$$

where W_i represents mass, momentum and energy densities inside the cell i. The equivalence between the above splitting mechanism and the collisionless Boltzmann equation was first realized by Harten, Lax and van Leer [36]. Numerically it is observed that the explicit flux formulation of the kinetic flux vector splitting (KFVS) schemes, by solving the collisionless transport equation, are identical to the flux function of van Leer [58].

Kinetic flux splitting schemes (KFVS) have been widely used in solving multi-dimensional non-relativistic Euler equations. Mandal and Deshpande [58] have applied KFVS to solve the

bump in a channel problem with structured meshes. Numerically, it has been observed in [58] that the explicit flux function of the KFVS scheme, by using the collisionless Boltzmann equation, is identical to the flux function of van Leer [54] which was first realized by [36]. Weatherill et al. [86] have applied the first order and high order resolution KFVS scheme to several 2-D problems with structured and unstructured meshes. Deshpande et al. [14] have developed 3-D time marching Euler code called BHEEMA using KFVS method for aerodynamic design and analysis of practical configurations. Perthame [74] has derived a second order KFVS scheme using the Maxwellian phase density which is second order accurate in time. This second order phase density was first obtained by Deshpande [13] to get second order kinetic scheme and is based on Chapman Enskog analysis for the solution of Boltzmann equation. Tang and Xu [83] proved the positivity of the KFVS scheme, while Lui and Xu [57] proved the entropy inequality for the scheme. Deshpande and Kulkarni [16] also applied the idea of KFVS scheme on moving grids.

2.5.1 One-Dimensional KFVS Scheme

Here we want to solve the one-dimensional Euler equations (2.1.4) written in abbreviated form

$$\frac{\partial W}{\partial t} + \frac{\partial F(W)}{\partial x} = 0\,, \tag{2.5.1}$$

where

$$W = \begin{pmatrix} \rho \\ \rho v \\ E \end{pmatrix}\,,\; F(W) = \begin{pmatrix} \rho v \\ p + \rho v^2 \\ v(E+p) \end{pmatrix}\,, \tag{2.5.2}$$

where $E = \frac{p}{(\gamma-1)} + \frac{1}{2}\rho\left(v^2\right)$.

We start with a piecewise constant initial data $\overline{W}_i^n$ at time t_n over the cells $[x_{i-\frac{1}{2}}, x_{i+\frac{1}{2}}]$ of a given mesh size $\Delta x = x_{i+\frac{1}{2}} - x_{i-\frac{1}{2}}$. We have to compute $\overline{W}_i^{n+1}$ over the same cells at time t_{n+1}. This is performed easily by assuming the CFL condition

$$\Delta t \leq \Delta x \left(\frac{1}{\max|v_i| + \lambda_i}\right)\,, \tag{2.5.3}$$

where the speed of sound is $\lambda_i = \sqrt{\gamma T_i}$. Then we can write the kinetic scheme (2.3.1) in compact form for $\tau = \Delta t$ as follows

$$W(t_{n+1}, x) = \int_{-\infty}^{+\infty} \psi_\alpha\, f_n(x - c\tau, c)\, dc, \quad \psi_\alpha = \left(1\,,\, c\,,\, I_0 + \frac{c^2}{2}\right)\,. \tag{2.5.4}$$

Again we take Maxwellian distribution (2.3.2) as an initial phase density with $I_0 = \dfrac{3-\gamma}{2(\gamma-1)}T$.

The one-dimensional weak form of conservation laws

$$\oint_{\partial\Omega} W(t,x)\, dx - F(W(t,x))\, dt = 0\,, \tag{2.5.5}$$

over the domain $[t_n, t_{n+1}] \times [x_{i-\frac{1}{2}}, x_{i+\frac{1}{2}}]$ gives

$$\int_{x_{i-\frac{1}{2}}}^{x_{i+\frac{1}{2}}} [W(t_{n+1}, x) - W(t_n, x)]\, dx + \int_{t_n}^{t_{n+1}} \left[F(\tau, x_{i+\frac{1}{2}}) - F(\tau, x_{i-\frac{1}{2}})\right] d\tau = 0\,.$$

Let us define the integral mean values by

$$\overline{W}_i(t) = \frac{1}{\Delta x} \int_{x_{i-\frac{1}{2}}}^{x_{i+\frac{1}{2}}} W(t, x) dx\,.$$

Dividing the above balance equation by Δx, we get the following conservative formula

$$\overline{W}_i(t_{n+1}) = \overline{W}_i(t_n) - \frac{1}{\Delta x} \int_{t_n}^{t_{n+1}} \left[F(\tau, x_{i+\frac{1}{2}}) - F(\tau, x_{i-\frac{1}{2}})\right] d\tau\,, \tag{2.5.6}$$

where equation (2.2.12) for the one-dimensional case gives

$$F(\tau, x) = \int_{-\infty}^{+\infty} c\psi_\alpha\, f_n(x - c\tau, c)\, dc\,. \tag{2.5.7}$$

Let use define

$$F_n\left(W_{i+\frac{1}{2}}\right) = \frac{1}{\Delta t} \int_{t_n}^{t_{n+1}} \int_{-\infty}^{+\infty} c\psi_\alpha\, f_n(x_{i+\frac{1}{2}} - c\tau, c)\, dc\, d\tau\,, \tag{2.5.8}$$

then (2.5.6) can be rewritten as

$$\overline{W}_i^{n+1} = \overline{W}_i^n - \frac{\Delta t}{\Delta x}\left[F_n(W_{i+\frac{1}{2}}) - F_n(W_{i-\frac{1}{2}})\right]\,. \tag{2.5.9}$$

If the CFL condition (2.5.3) is satisfied then $x_{i\pm\frac{1}{2}} - c\tau$ is confined to the direct neighbouring cells of $x_{i\pm\frac{1}{2}}$. This implies that the field variables ρ, v, T in the split flux integrals will not depend on the $c-$integration. Furthermore, the integrand in (2.5.8) will be also independent of the $\tau-$integration. Therefore (2.5.8) after flux vector splitting implies

$$\begin{aligned} F_n(W_{i+\frac{1}{2}}) &= F_n^-(W_{i+1}) + F_n^+(W_i) \\ &= \int_{-\infty}^{0} c\,\psi_\alpha\, f_n(W_{i+1})\, dc + \int_{0}^{\infty} c\,\psi_\alpha\, f_n(W_i)\, dc\,. \end{aligned} \tag{2.5.10}$$

After integration of the fluxes we get the following KFVS scheme from (2.5.9)

$$\overline{W}_i^{n+1} = \overline{W}_i^n - \frac{\Delta t}{\Delta x}\left[F_n^+(W_i) + F_n^-(W_{i+1}) - F_n^+(W_{i-1}) - F_n^-(W_i)\right]\,, \tag{2.5.11}$$

where if for abbreviation $\xi = \frac{v}{\sqrt{2T}}$, then

$$F_n^{\pm}(W_i) = \pm\sqrt{\frac{T_i}{2\pi}}\exp(-\xi^2)\begin{pmatrix}\rho_i\\ \rho v_i\\ E_i+\frac{1}{2}p_i\end{pmatrix} + \frac{1}{2}(1\pm erf(\xi))\begin{pmatrix}\rho_i v_i\\ \rho_i v_i^2+p_i\\ E_i v_i + p_i v_i\end{pmatrix}, \qquad (2.5.12)$$

where the fields ρ_i, v_i and p_i are defined at time t_n. The complementary error function is given by

$$erf(z) = \frac{2}{\sqrt{\pi}}\int_o^z \exp(-\vartheta^2)\,d\vartheta\,.$$

In the above derivations we saw that the splitting of flux vector F_n into F_n^+ and F_n^- is based on the sign of the molecular velocity c.

2.5.2 Two-Dimensional KFVS Scheme

Here we want to solve the two-dimensional Euler equations

$$\frac{\partial W}{\partial t} + \frac{\partial F(W)}{\partial x} + \frac{\partial G(W)}{\partial y} = 0\,, \qquad (2.5.13)$$

where

$$W = \begin{pmatrix}\rho\\ \rho v_1\\ \rho v_2\\ E\end{pmatrix},\ F(W) = \begin{pmatrix}\rho v_1\\ p+\rho v_1^2\\ \rho v_1 v_2\\ v_1(E+p)\end{pmatrix},\ G(W) = \begin{pmatrix}\rho v_2\\ \rho v_1 v_2\\ p+\rho v_2^2\\ v_2(E+p)\end{pmatrix}, \qquad (2.5.14)$$

where $E = \frac{p}{(\gamma-1)} + \frac{1}{2}\rho\left(v_1^2+v_2^2\right)$. Now we can write the kinetic scheme (2.4.1) in compact form for $\tau = \Delta t$ and $t_{n+1} = t_n + \Delta t$ as follow

$$W(t_{n+1},\mathbf{x}) = \int_{\mathbb{R}^2}\psi_\alpha\, f_n(\mathbf{x}-\mathbf{c}\tau,\mathbf{c})\,d^2\mathbf{c}, \quad \psi_\alpha = \left(1\,,\,\mathbf{c}\,,\,I_0+\frac{\mathbf{c}^2}{2}\right), \qquad (2.5.15)$$

where $I_0 = \dfrac{2-\gamma}{\gamma-1}T$, $\mathbf{x} = (x,y)$, $\mathbf{c} = (c_1,c_2)$, and f_n is initially Maxwellian distribution function (2.4.2).

We start with a piecewise constant initial data $\overline{W}_{i,j}^n$ at time t_n. Integrating (2.5.15) over the control volume $[t_n,t_{n+1}]\times[x_{i-\frac{1}{2}},x_{i+\frac{1}{2}}]\times[y_{j-\frac{1}{2}},y_{j+\frac{1}{2}}]$, we get analogously to the one-dimensional case

$$\begin{aligned}\overline{W}_{ij}^{n+1} =& \overline{W}_{ij}^n\\ &-\frac{1}{\Delta x}\int_{t_n}^{t_{n+1}}\int_{\mathbb{R}^2}\mathbf{c}\,\psi_\alpha\left[f_n(x_{i+\frac{1}{2}}-c_1\tau,y_j-c_2\tau,\mathbf{c}) - f_n(x_{i-\frac{1}{2}}-c_1\tau,y_j-c_2\tau,\mathbf{c})\right]d^2\mathbf{c}\,dt\\ &-\frac{1}{\Delta y}\int_{t_n}^{t_{n+1}}\int_{\mathbb{R}^2}\mathbf{c}\,\psi_\alpha\left[f_n(x_i-c_1\tau,y_{j+\frac{1}{2}}-c_2\tau,\mathbf{c}) - f_n(x_i-c_1\tau,y_{j-\frac{1}{2}}-c_2\tau,\mathbf{c})\right]d^2\mathbf{c}\,dt\,.\end{aligned}$$

If the CFL condition

$$\Delta t \leq \min\left(\frac{\Delta x}{\max|(v_1)_i| + \lambda_{ij}}, \frac{\Delta y}{\max|(v_2)_j| + \lambda_{ij}}\right), \quad \lambda_{ij} = \sqrt{\gamma T_{ij}}, \tag{2.5.16}$$

is satisfied then $(x_{i\pm\frac{1}{2}} - c_1\tau, y_j - c_2\tau)$ will remains in the direct neighbouring cells to $(x_{i\pm\frac{1}{2}}, y_j)$ and $(x_i - c_1\tau, y_{j\pm\frac{1}{2}} - c_2\tau)$ will remains in the neighbouring cells to $(x_i, y_{j\pm\frac{1}{2}})$, therefore we get

$$\begin{aligned}\overline{W}_{i,j}^{n+1} = \overline{W}_{i,j}^{n} &- \frac{\Delta t}{\Delta x}\left[F_n(W_{i+\frac{1}{2},j}) - F_n(W_{i-\frac{1}{2},j})\right] \\ &- \frac{\Delta t}{\Delta y}\left[G_n(W_{i,j+\frac{1}{2}}) - G_n(W_{i,j-\frac{1}{2}})\right],\end{aligned} \tag{2.5.17}$$

with

$$\begin{aligned}F_n(W_{i+\frac{1}{2},j}) &= F_n^+(W_{i,j}) + F_n^-(W_{i+1,j}), \\ G_n(W_{i,j+\frac{1}{2}}) &= G_n^+(W_{i,j}) + F_n^-(W_{i,j+1}),\end{aligned} \tag{2.5.18}$$

where for $S_1 = \frac{v_1}{\sqrt{2T}}$ and $S_2 = \frac{v_2}{\sqrt{2T}}$ we have

$$F_n^{\pm}(W_{i,j}) = \pm\sqrt{\frac{T_i}{2\pi}}\exp(-S_1^2)\begin{pmatrix}\rho\\ \rho v_1\\ \rho v_2\\ E + \frac{1}{2}p\end{pmatrix}_{i,j} + \frac{1}{2}(1 \pm erf(S_1))\begin{pmatrix}\rho v_1\\ p + \rho v_1^2\\ \rho v_1 v_2\\ E v_1 + p v_1\end{pmatrix}_{i,j}, \tag{2.5.19}$$

$$G_n^{\pm}(W_{i,j}) = \pm\sqrt{\frac{T_i}{2\pi}}\exp(-S_2^2)\begin{pmatrix}\rho\\ \rho v_1\\ \rho v_2\\ E + \frac{1}{2}p\end{pmatrix}_{i,j} + \frac{1}{2}(1 \pm erf(S_2))\begin{pmatrix}\rho v_2\\ \rho v_1 v_2\\ p + \rho v_2^2\\ E v_2 + p v_2\end{pmatrix}_{i,j}. \tag{2.5.20}$$

2.6 Numerical Case Studies

In order to validate the theory discussed above we give the results of some numerical case studies for the solution of the one- and two-dimensional non-relativistic Euler equations. For the comparison of the results we use Godunov and central schemes which are discussed in Chapters 5 and 7, respectively.

2.6.1 One-Dimensional Test Problems

Here we present one-dimensional test problems. In all the these problems we take the ratio of specific heats $\gamma = \frac{5}{3}$. The results obtained from kinetic scheme are compared with exact solution, KFVS scheme and Godunov scheme results. We take 500 mesh points in the spatial domain. Also we take 100 maximization times for the kinetic scheme. In KFVS and Godunov schemes we take CFL number equal to 0.4.

Problem 1: From free flight to the Eulerian limit

We consider a density distribution $\rho_0(x)$ at zero velocity and uniform temperature:

$$\rho(0,x) = \rho_0(x) = \begin{cases} 1 & |x| > 1 \\ \\ 1.1 & |x| \leq 1 \end{cases}, \quad v(0,x) = v_0 = 0,\ T(0,x) = T_0 = 1.$$

This problem was studied in [18]. We are interested in the solution within the range $x \in [-5,5]$ at time $t = 1.5$ for different maximizing entropy times τ_M. Figure 2.5 depicts the density, velocity and pressure distributions at $t = 1.5$. The diffusion like distributions result from pure free-flight with only one maximization at the beginning. The distributions that show already the formation of moving fronts are obtained when we choose $\tau_M = 0.15$, i.e. there are 10 maximizations within the time interval $[0, 1.5]$. When we decrease τ_M further, the fronts become steeper, and this is exhibited by the the distributions that are obtained for $\tau_M = 0,015$. This is almost the Eulerian limit. The physical content of the Eulerian limit is the overwhelming importance of collisions against free-flight. A chosen $\tau_M > 0$ thus determines which of both mechanisms has more influence on a thermodynamic process. The exact Euler solution was obtained by using second order central scheme on very fine mesh.

Problem 2: This Riemann problem was proposed by Sod [82]. The initial data are

$$(\rho, u, p) = \begin{cases} (1.0, 0.0, 1.0) & \text{if } x < 0.5\,, \\ (0.125, 0.0, 0.1) & \text{if } x \geq 0.5\,. \end{cases}$$

Where the spatial domain is $0 \leq x \leq 1$ and the final time is $t = 0.25$. The results are shown in Figure 2.6.

Problem 3: This problem given in [85] is concerned with collision of two shocks. The initial data are

$$(\rho, u, p) = \begin{cases} (5.99924, 19.5975, 460.94) & \text{if } x < 0.4\,, \\ (5.99242, -6.19633, 46.0950) & \text{if } x \geq 0.4\,. \end{cases}$$

Where the spatial domain is $0 \leq x \leq 1$ and the final time is $t = 0.035$. The results are shown in Figure 2.7.

Problem 4: A single shock reflection

This problem was studied by Dreyer et al. [19]. We consider a single shock which is reflected by an adiabatic wall at $x = 0$. The initial data are

$$(\rho, u, p) = \begin{cases} (2.0/3.0, 0.0, 0.5) & \text{if } x < 1.5\,, \\ (1.0, -0.5, 1.0) & \text{if } x \geq 1.5\,, \end{cases}$$

where the spatial domain is $0 \leq x \leq 2$. This initial data creates a 1-shock that propagates with the speed $-\frac{3}{2}$. The shock reaches the wall at $t = 1$, which leads to a reflection. After reflection a 3-shock arises which propagates with the speed $\frac{7}{6}$. We take the total time $t_f = \frac{13}{7}$. We have solved this problem with unconditionally stable kinetic scheme (continuous in space)

for 1000 mesh point and 200 maximizations times. The results are shown in Figure 2.8.

Problem 5: Blast wave problem

In this example, we test the schemes on the blast wave problem which was carefully studied by Woodward and Colella [88]. The initial data are taken as

$$(\rho, u, p) = \begin{cases} (1.0, 0.0, 1000.0) & \text{if } x < 0.1\,, \\ (1.0, 0.0, 0.01) & \text{if } 0.1 \leq x < 0.9\,, \\ (1.0, 0.0, 100.0) & \text{if } 0.9 \leq x \leq 1.0\,. \end{cases}$$

The reflective boundary conditions are applied at both $x = 0$ and $x = 1$. The results are shown in Figure 5.13 at time is $t = 0.038$. The exact solution is a second order Godunov scheme solution on very fine grid.

2.6.2 Two-Dimensional Test Problems

Here we present two-dimensional test problems for both the kinetic scheme and the KFVS scheme. We also compare these results with the first order Lax-Friedrichs (LxF) scheme and exact solution. Here the exact solution is a second order central scheme solution on a very fine mesh. The results are obtained by using 500×500 mesh points. We take 100 maximization times in the kinetic scheme.

Problem 6: A two-dimensional quadratic pulse

This initial value problem was studied by Dreyer et al. [17]. Here we consider a two-dimensional initial value problem inside a square box (1×1 units). Initially the velocities are zero. Both particle density and pressure are equal 4 in a square box $0.4 \leq x \leq 0.6$, $0.4 \leq y \leq 0.6$ and equal 1 elsewhere. We are interested in the solution at time $t = 0.1$. Figure 2.10 shows the results obtained from the kinetic scheme, first order Lax-Friedrichs (LxF) scheme and KFVS scheme at $y = 0.5$. The exact solution is obtained by using second order central scheme at fine mesh. We found that kinetic scheme has comparable accuracy to LxF and KFVS schemes. Figure 2.11 shows the global solution using kinetic scheme. The initial data has only symmetry at an angle of 90^o, the same effect we can see in Figure 2.11.

Problem 7: Interaction of two spherically symmetric fields

This example was also studied by Dreyer et al. [17]. Here we consider the interaction of two spherically symmetric fields with initial data: $\rho_0(x_1, x_2) = 4$, $p_0(x_1, x_2) = 4$ for $(x_1 - 0.4)^2 + (x_2 - 0.4)^2 \leq 0.015$ and for $(x_1 - 0.6)^2 + (x_2 - 0.6)^2 \leq 0.015$. Otherwise $\rho(x_1, x_2) = 1$, $p_0(x_1, x_2) = 1$. Where velocities are zero everywhere, i.e. $u = v = 0$. Our computational domain is $(x, y) \in [0, 1] \times [0, 1]$. We are interested in the solution at time $t = 0.15$. Figure 2.12 shows the comparison of the kinetic scheme with other methods at $y = 0.5$. Figure 2.13 shows the global solution using the kinetic scheme.

Problem 8: 2-D Riemann problem with four shocks

This problem was studied by Schulz-Rinne et al. [81]. Here we choose the initial data of the form

$$(\rho, u, v, p) = \begin{cases} (1.1, 0.0, 0.0, 1.1) & \text{if } x > 0.5, \quad y > 0.5\,, \\ (0.5065, 0.8939, 0.0, 0.35) & \text{if } x < 0.5, \quad y > 0.5\,, \\ (1.1, 0.8939, 0.8939, 1.1) & \text{if } x < 0.5, \quad y < 0.5\,, \\ (0.5065, 0.0, 0.8939, 0.35) & \text{if } x > 0.5, \quad y < 0.5\,, \end{cases}$$

which correspond to the case of left forward shock, right backward shock, upper backward shock, and a lower forward shock. The problem is solved on the square $(x, y) \in [0, 1] \times [0, 1]$ and time $t = 0.25$. We take the ratio of specific heats $\gamma = 1.4$. Figure 2.14 shows the results from kinetic scheme, KFVS scheme and Lax-Friedrichs (LxF) scheme. We can see from the results that all the three schemes do not produce any noise in the solution.

2.7 Summary

In this chapter we have presented the first order kinetic schemes and KFVS schemes for the non-relativistic Euler equations. The purpose of this chapter was to give an introduction to the kinetic schemes and KFVS schemes for the non-relativistic Euler equations. This chapter is a useful background to understand the relativistic kinetic theory coming in the next chapters. We have numerically implemented the one- and two-dimensional kinetic schemes and KFVS schemes. The numerical results from both type of schemes were compared with the first order Godunov and Lax-Friedrichs (LxF) schemes. The programing codes for the KFVS and central schemes are compact and simpler compared to the Godunov schemes. The boundary conditions implementation for the KFVS schemes are analogous to the Godunov schemes. The programing codes for the kinetic schemes are also simple. As explained in the theory the boundary condition implementations strategies for the kinetic schemes are different from the KFVS, Godunov and LxF schemes. It was found that both kinetic and KFVS schemes give a better resolution of the contact discontinuity as compared to the LxF schemes. However Godunov scheme has a slightly better resolution than all the other three schemes at the contact. The computational time for the KFVS schemes are comparable to both central and Godunov schemes. However kinetic schemes were found to be computationally expensive and five to six times slower than than other schemes due to the inside loop for the $\mathbf{c}$ integration in each computational cell. However, as discussed in the introduction the kinetic schemes have other advantages like, they need no CFL condition and are truly multi-dimensional. On the other hand like Godunov and LxF schemes, KFVS schemes are also stable under CFL condition, therefore the flow is only restricted to the neighbouring cells only. Secondly they are not truly multidimensional. Thus we conclude that both KFVS and kinetic schemes have their own advantages and disadvantages and the selection of one from the two schemes will depend on the purpose for which they are intended to be used.

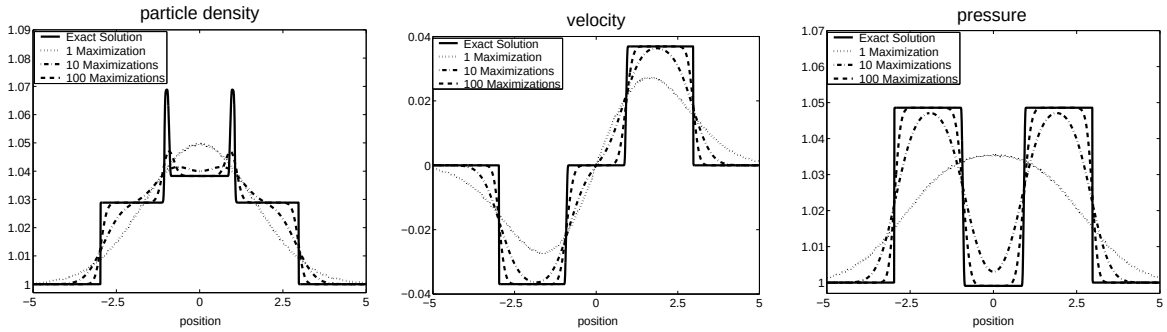

Figure 2.5: Density, velocity and pressure distributions for $1, 10, 100$ maximizations.

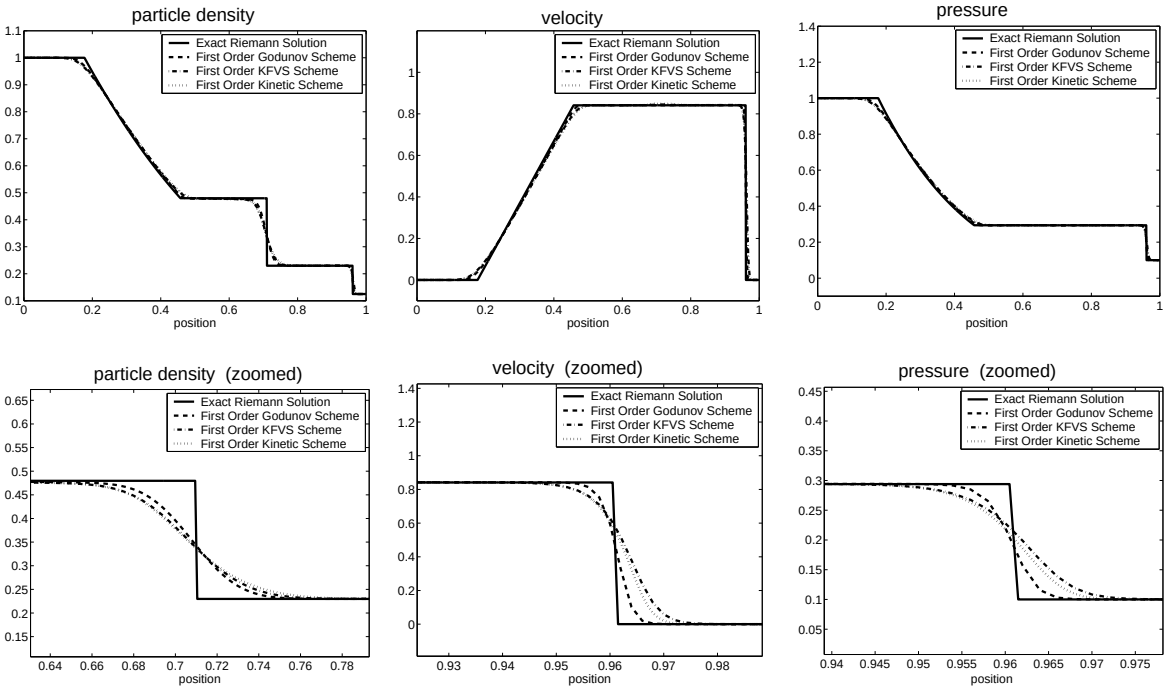

Figure 2.6: Sod problem at $t = 0.25$.

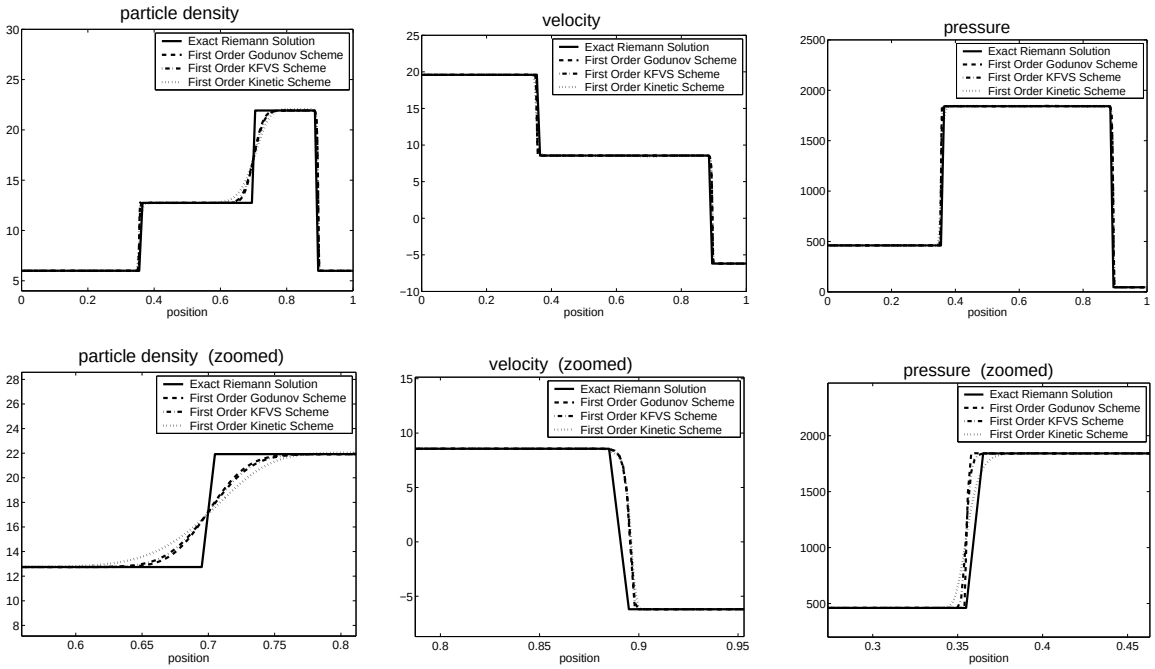

Figure 2.7: Collision of two shocks at $t = 0.035$.

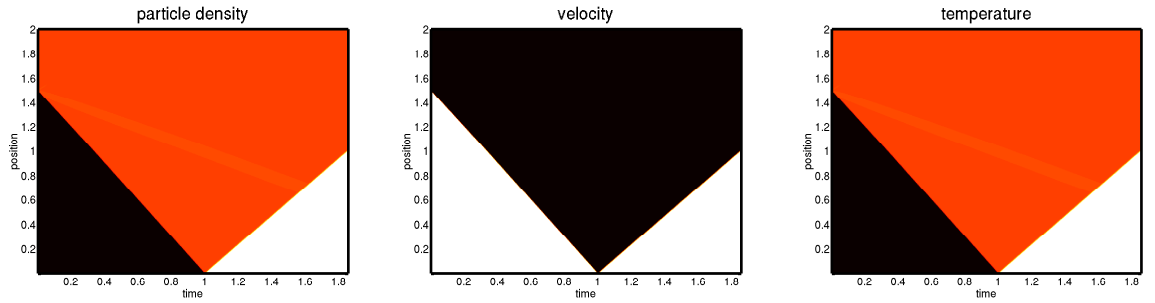

Figure 2.8: Reflection of a shock wave on an adiabatic wall.

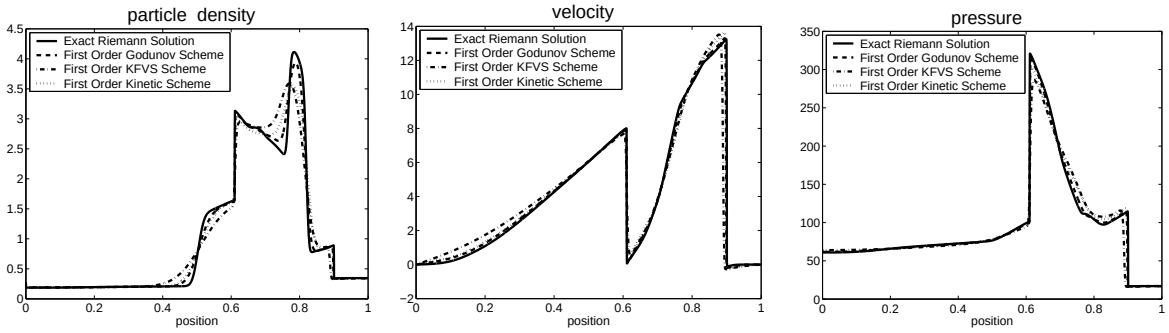

Figure 2.9: Blast wave problem at $t = 0.038$.

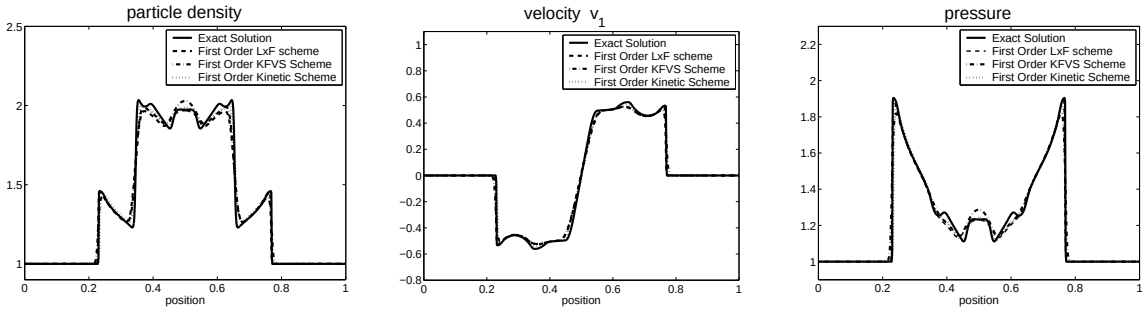

Figure 2.10: Quadratic pulse problem at $y = 0.5$ and time $t = 0.1$.

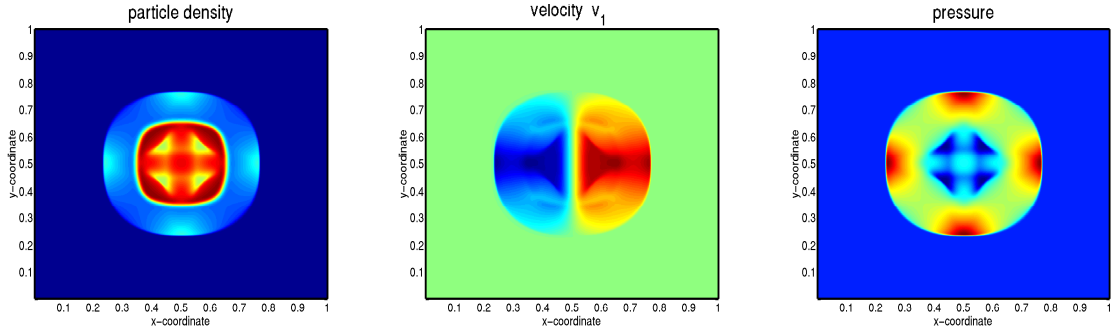

Figure 2.11: Quadratic pulse problem at time $t = 0.1$ by using kinetic scheme.

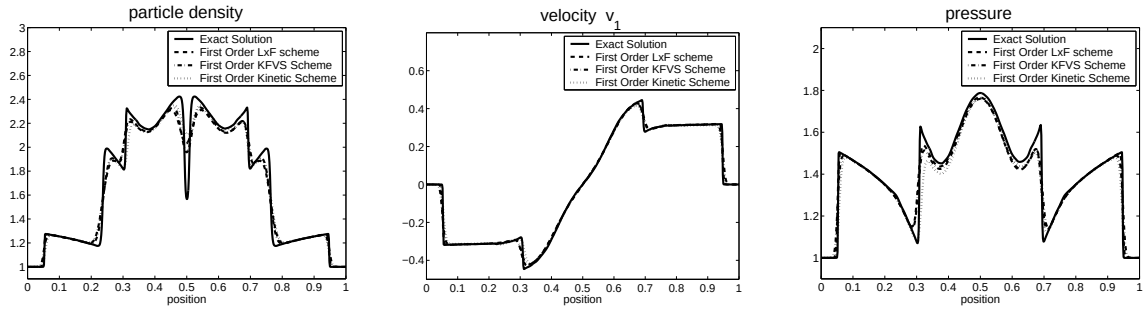

Figure 2.12: Two interacting spherical waves at $y = 0.5$ and time $t = 0.15$.

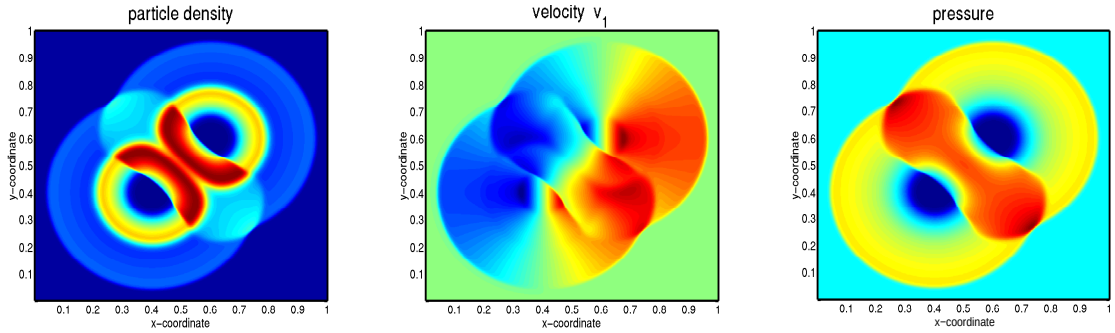

Figure 2.13: Two interacting spherical waves at time $t = 0.15$ by using kinetic scheme.

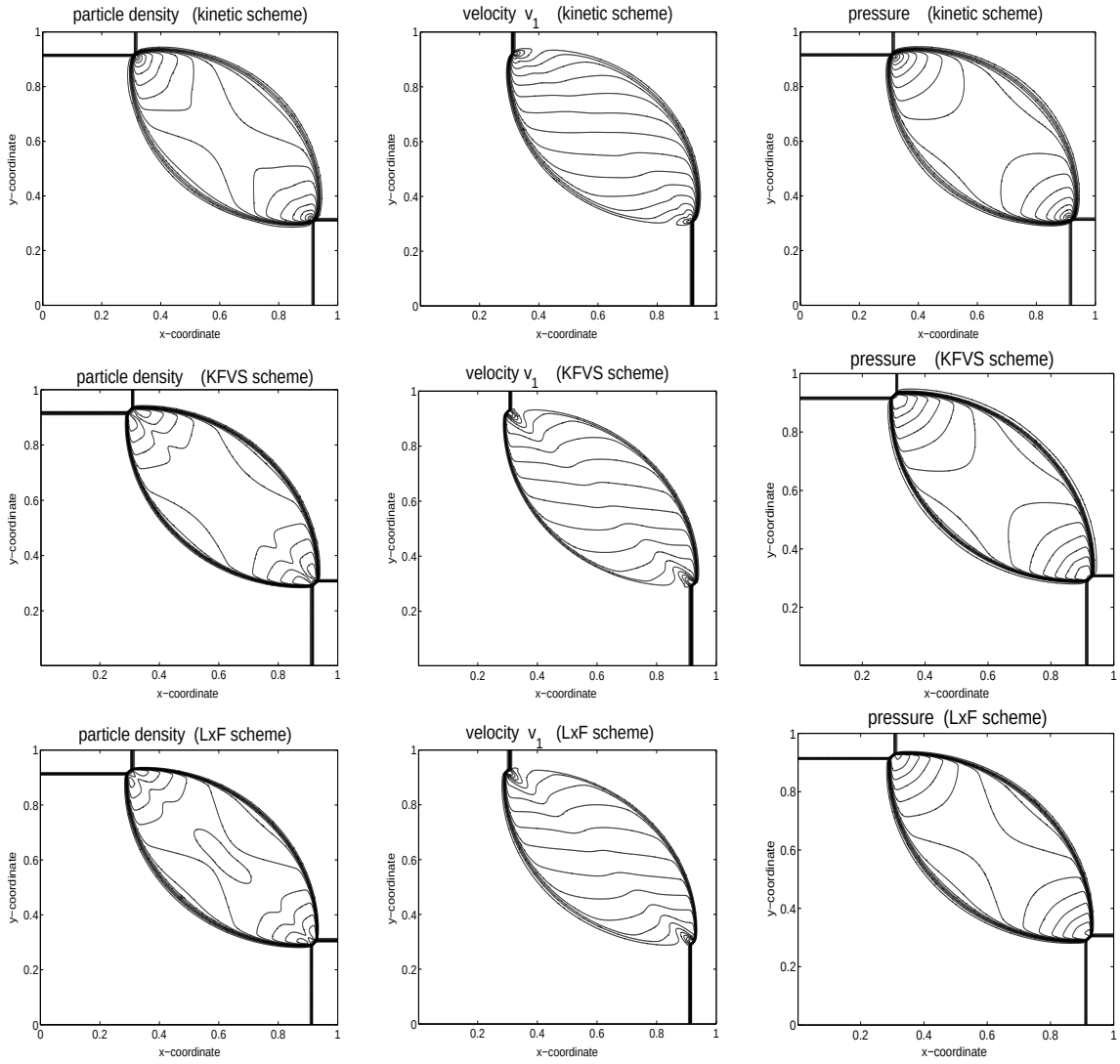

Figure 2.14: Riemann problem with 4 shocks at $t = 0.25$.

Chapter 3

Relativistic Kinetic Theory

3.1 Lorentz-Transformations

In special relativity the laws of nature are invariant under a particular group of space-time coordinate transformations, called Lorentz-transformations. In order to formulate our theory in a Lorentz-invariant form, we make use of the notations for the tensor calculus used in the textbook of Weinberg [87], with only slight modifications:

A) **The space-time coordinates** are x^μ, $\mu = 0, 1, 2, 3$, with $x^0 := ct$ for the time, x^1, x^2, x^3 for the position.

B) **The metric tensor** is

$$g_{\mu\nu} = g^{\mu\nu} = \begin{cases} +1 & , \quad \mu = \nu = 0\,, \\ -1 & , \quad \mu = \nu = 1, 2, 3\,, \\ 0 & , \quad \mu \neq \nu\,. \end{cases} \tag{3.1.1}$$

In Matrix-form it can be written as

$$G = (g_{\mu\nu})_{\mu,\nu=0,1,2,3} = \begin{pmatrix} +1 & 0 & 0 & 0 \\ 0 & -1 & 0 & 0 \\ 0 & 0 & -1 & 0 \\ 0 & 0 & 0 & -1 \end{pmatrix}. \tag{3.1.2}$$

C) **The proper Lorentz-transformations** are linear transformations $\Lambda^\alpha{}_\beta$ from one system of space-time with coordinates x^α to another system x'^α. They must satisfy

$$x'^\alpha = \Lambda^\alpha{}_\beta\, x^\beta,\ g_{\mu\nu} = \Lambda^\alpha{}_\mu\, \Lambda^\beta{}_\nu\, g_{\alpha\beta},\ \Lambda^0{}_0 \geq 1,\ \det\Lambda = +1\,. \tag{3.1.3}$$

The conditions $\Lambda^0{}_0 \geq 1$ and $\det\Lambda = +1$ are necessary in order to exclude inversion in time and space. Then the following quantity forms a tensor with respect to proper Lorentz-transformations, the so called Levi-Civita tensor:

$$\epsilon_{\alpha\beta\gamma\delta} = \begin{cases} +1, & \alpha\beta\gamma\delta \text{ even permutation of } 0123, \\ -1, & \alpha\beta\gamma\delta \text{ odd permutation of } 0123\,, \\ 0, & \text{otherwise.} \end{cases}$$

Note that in the textbook of Weinberg [87] this tensor as well as the metric tensor both take the sign opposite to the notation used here.

D) **Einstein's summation convention:**
Any Greek index like α, β, that appears twice, once as a subscript and once as a superscript, is understood to be summed over 0,1,2,3 if not noted otherwise. For spatial indices, which are denoted by Latin indices like i, j, k, we will not apply this summation convention.

Proposition 3.1: *Given a matric tesor G as in* (3.1.2)*, the following statements are equivalent for any matrix $\Lambda = (\Lambda^{\alpha}_{\beta}) \in \mathbb{R}^{4\times 4}$, $\alpha, \beta = 0, 1, 2, 3$.*

(i) The Lorentz-matrix Λ leaves the Einstein-Minkowski metric $Q(x) = x^T G x$ invariant.

(ii) The matrix Λ is regular and has the inverse matrix $\Lambda^{-1} = G\Lambda^T G$.

(iii) We have $G = \Lambda^T G \Lambda$, i.e. the Matrix Λ leaves the wave operator $\Box$ invariant.

Proof: Let $\mathbf{I}$ be the unit matrix in $\mathbb{R}^4$. Regarding statement (ii) and (iii) we have:

$$\begin{aligned}
G =& \Lambda^T G \Lambda & \Leftrightarrow \\
\mathbf{I} =& G^2 = (G\,\Lambda^T G)\Lambda & \Leftrightarrow \\
\Lambda^{-1} =& \, G\,\Lambda^T\, G & \Leftrightarrow \\
\mathbf{I} =& \Lambda\,\Lambda^{-1} = (\Lambda G\,\Lambda^T)\, G & \Leftrightarrow \\
G^2 =& (\Lambda\, G\,\Lambda^T)\, G & \Leftrightarrow \\
G =& \Lambda G\,\Lambda^T .
\end{aligned}$$

The first relation shows the invariance of the metric G in space-time, while the last relation shows the invariance of the d'Alembertian wave-operator. We define the d'Alembertian wave-operator by

$$\Box := \frac{1}{c^2}\frac{\partial^2}{\partial t^2} - \Delta = g_{\mu\nu}\frac{\partial^2}{\partial x^\mu \partial x^\nu}.$$

The invariance of d'Alembertian wave-operator means that

$$\psi'(x') := \psi(x) = \psi(\Lambda^{-1}x') \quad \Rightarrow \quad (\Box'\psi')(x') = (\Box\psi)(x).$$

Also according to the statement (i) we have:

$$\begin{aligned}
Q(x) &= x^T G x = g_{\mu\nu} x^\mu x^\nu \,. \\
Q(\Lambda x) &= x^T(\Lambda^T G \Lambda)x = x^T G x = Q(x).
\end{aligned}$$

The invariance of $Q(x)$ and d'Alembertian wave-operator are equivalent.

Remark: The invariance of the d'Alembertian wave-operator is useful in order to write the Maxwell equations in Lorentz invariant form.

Definition: A constant matrix $\Lambda \in \mathbb{R}^{4\times 4}$ which satisfies the equivalent conditions (i), (ii) and (iii) in above Proposition 3.1 is called a **Lorentz-matrix**.

A Lorentz-matrix Λ and a constant four-quantity $a \in \mathbb{R}^4$ describe a Lorentz-transformation

$$x \Rightarrow x' = \Lambda x + a\,, \tag{3.1.4}$$

of the four space-time coordinates. The Lorentz-transformation is called homogeneous if $a = 0$. An important example of the homogeneous Lorentz-transformation is

$$t' = \frac{t - \frac{vx}{c^2}}{\sqrt{1 - \frac{v^2}{c^2}}}\,, \qquad x' = \frac{x - vt}{\sqrt{1 - \frac{v^2}{c^2}}}\,, \qquad y' = y\,, \qquad z' = z\,, \tag{3.1.5}$$

with velocity $v = v_x$ along the x-axis, which reduces for $|\mathbf{v}| << c$ to the classical Gallilean transformation

$$t' = t\,, \qquad x' = x - vt\,. \tag{3.1.6}$$

3.2 Vectors and Tensors

Any quantity that transforms like $f'^{\alpha} = \Lambda^{\alpha}{}_{\beta} f^{\beta}$ is called four-vector.

Contravariant four-vector: is a vector with single upper index having the following Lorentz-transformation property

$$V^{\alpha}(x) \to V'^{\alpha}(x') = \Lambda^{\alpha}{}_{\beta} V^{\beta}(x)\,. \tag{3.2.1}$$

Covariant four-vector: is a quantity with a single lower index having transformation

$$U_{\alpha}(x) \to U'{}_{\alpha}(x') = \Lambda_{\alpha}{}^{\beta} U_{\beta}(x)\,, \tag{3.2.2}$$

where

$$\Lambda_{\beta}{}^{\alpha} = g_{\beta\gamma} g^{\alpha\delta} \Lambda^{\gamma}{}_{\delta}\,. \tag{3.2.3}$$

The matrix $g^{\alpha\delta}$ introduced here is numerically the same as $g_{\alpha\delta}$, that is

$$g^{\alpha\delta} = g_{\alpha\delta}. \tag{3.2.4}$$

Also note that

$$g^{\alpha\delta} g_{\delta\beta} = \begin{cases} +1 & , \quad \alpha = \beta\,, \\ 0 & , \quad \alpha \neq \beta\,. \end{cases} \tag{3.2.5}$$

This means that $\Lambda_{\alpha}{}^{\beta}$ is the inverse of the matrix $\Lambda^{\beta}{}_{\alpha}$, that is using (3.2.3) and (3.1.3)

$$\Lambda_{\alpha}{}^{\gamma} \Lambda^{\alpha}{}_{\beta} = g_{\alpha\delta} g^{\gamma\eta} \Lambda^{\delta}{}_{\eta} \Lambda^{\alpha}{}_{\beta} = g_{\eta\beta} g^{\gamma\eta} = \delta^{\gamma}{}_{\beta}\,. \tag{3.2.6}$$

It follows that the scalar product of a contravariant with a covariant four-vector is invariant with respect to Lorentz-transformation (3.1.3), that is,

$$U'_{\alpha} V'^{\alpha} = \Lambda_{\alpha}{}^{\gamma} \Lambda^{\alpha}{}_{\beta} U_{\gamma} V^{\beta} = U_{\beta} V^{\beta}\,. \tag{3.2.7}$$

To every contravariant four-vector V^α there corresponds a covariant four-vector

$$V_\alpha = g_{\alpha\beta} V^\beta \,, \tag{3.2.8}$$

and to every covariant U_α there corresponds a contravariant

$$U^\alpha = g^{\alpha\beta} U_\beta \,. \tag{3.2.9}$$

A co- or contravariant vector is a tensor with one index, and scalar (invariant expression) is a tensor without indices.

Note that raising the index on V_α simply gives back V^α, and lowering the index on U^α simply gives back U_α,

$$g^{\alpha\beta} V_\beta = g^{\alpha\beta} g_{\beta\gamma} V^\gamma = V^\alpha \,, \tag{3.2.10}$$

$$g_{\alpha\beta} U^\beta = g_{\alpha\beta} g^{\beta\gamma} U_\gamma = U_\alpha \,. \tag{3.2.11}$$

Derivatives: Although any vector can be written in a contravariant or a covariant form, there are some vectors, such as dx^α, that appear more naturally contravariant and others that appear more naturally covariant. An example of the latter is the gradient $\partial/\partial x^\alpha$, which obeys the transformation rule

$$\frac{\partial}{\partial x^\alpha} \;\rightarrow\; \frac{\partial}{\partial x'^\alpha} \;=\; \frac{\partial x^\beta}{\partial x'^\alpha} \frac{\partial}{\partial x^\beta} \,. \tag{3.2.12}$$

We also know the coordinate transformation

$$x^\alpha \;\rightarrow\; x'^\alpha \;=\; \Lambda^\alpha{}_\beta x^\beta \,. \tag{3.2.13}$$

Multiplying (3.2.13) by $\Lambda_\alpha{}^\gamma$ gives

$$x^\gamma \;=\; \Lambda_\alpha{}^\gamma x'^\alpha \,, \tag{3.2.14}$$

so

$$\frac{\partial x^\beta}{\partial x'^\alpha} \;=\; \Lambda_\alpha{}^\beta \,. \tag{3.2.15}$$

One consequence is that the divergence of a covariant vector $\frac{\partial V^\alpha}{\partial x^\alpha}$ is invariant. Another is that the scalar product of $\frac{\partial}{\partial x^\alpha}$ with itself, the d'Alembertian operator

$$\Box := \frac{1}{c^2}\frac{\partial^2}{\partial t^2} - \Delta = g_{\alpha\beta} \frac{\partial^2}{\partial x^\alpha \partial x^\beta},$$

is also invariant.

Many physical quantities are not scalars or vectors, but more complicated objects called tensors. A tensor has several contravariant and/or covariant indices with corresponding Lorentz-transformation properties, for example

$$T^\gamma{}_{\alpha\beta}(x) \;\rightarrow\; T'^\gamma{}_{\alpha\beta} = \Lambda^\gamma{}_\delta \Lambda_\alpha{}^\varepsilon \Lambda_\beta{}^\xi T^\delta{}_{\varepsilon\xi} \,. \tag{3.2.16}$$

A contravariant or covariant vector can be regarded as a tensor with one index, and a scalar is a tensor with no indices.

3.2.1 Four Rules for Constructing New Tensors From the Old Ones

In the following we are looking for simple rules which enables us to construct new tensors from the old ones. These rules may be combined with each others under certain constraints to obtain every possible tensor. These rules will also enable us to tell at a glance that an equation is Lorentz-invariant.

Rule I: Linear combinations:
A linear combination of tensors with same upper and lower indices is a tensor with these indices.

$$T^{\alpha}_{\ \beta} \equiv aR^{\alpha}_{\ \beta} + bS^{\alpha}_{\ \beta}\,, \tag{3.2.17}$$

where $R^{\alpha}_{\ \beta}$ and $S^{\alpha}_{\ \beta}$ are tensors, and a and b are scalars. Then $T^{\alpha}_{\ \beta}$ is also a tensor, that is,

$$\begin{aligned} T'^{\alpha}_{\ \ \beta} &= a\,R'^{\alpha}_{\ \ \beta} + b\,S'^{\alpha}_{\ \ \beta} \\ &= a\,\Lambda^{\alpha}_{\ \kappa}\,\Lambda_{\beta}^{\ \mu}\,R^{\kappa}_{\ \mu} + b\,\Lambda^{\alpha}_{\ \kappa}\,\Lambda_{\beta}^{\ \mu}\,S^{\kappa}_{\ \mu} \\ &= \Lambda^{\alpha}_{\ \kappa}\,\Lambda_{\beta}^{\ \mu}\,T^{\kappa}_{\ \mu}\,. \end{aligned}$$

Rule II: Direct product:
The product of the components of two tensors is a tensor whose upper and lower indices consist of all upper and lower indices of the two original tensors. For instance, if $A^{\alpha}_{\ \beta}$ and B^{γ} are tensors, and

$$T^{\alpha\ \gamma}_{\ \beta} = A^{\alpha}_{\ \beta}\,B^{\gamma}\,, \tag{3.2.18}$$

then $T^{\alpha\ \gamma}_{\ \beta}$ is a tensor, that is,

$$\begin{aligned} T'^{\alpha\ \gamma}_{\ \ \beta} &= A'^{\alpha}_{\ \ \beta}\,B'^{\gamma} \\ &= \Lambda^{\alpha}_{\ \kappa}\,\Lambda_{\beta}^{\ \lambda}\,\Lambda^{\gamma}_{\ \mu}\,T^{\kappa\ \mu}_{\ \lambda}\,. \end{aligned}$$

Rule III: **Contractions:**
Setting an upper and lower index equal and summing it over its values 0,1,2,3, yields a tensor with these two indices absent. For example if $T^{\alpha\ \gamma\delta}_{\ \ \beta}$ is a tensor and

$$T^{\alpha\gamma} = T^{\alpha\ \gamma\beta}_{\ \ \beta}, \tag{3.2.19}$$

then $T^{\alpha\gamma}$ is a tensor, that is,

$$\begin{aligned} T'^{\alpha\gamma} &= T'^{\alpha\ \ \gamma\beta}_{\ \ \beta} \\ &= \Lambda^{\alpha}_{\ \delta}\,\Lambda_{\beta}^{\ \varepsilon}\,\Lambda^{\gamma}_{\ \xi}\,\Lambda^{\beta}_{\ \kappa}\,T^{\delta\ \ \xi\kappa}_{\ \ \varepsilon} \\ &= \Lambda^{\alpha}_{\ \delta}\,\Lambda^{\gamma}_{\ \xi}\,\delta^{\varepsilon}_{\ \kappa}\,T^{\delta\ \ \xi\kappa}_{\ \ \varepsilon} \\ &= \Lambda^{\alpha}_{\ \delta}\,\Lambda^{\gamma}_{\ \xi}\,T^{\delta\xi}\,. \end{aligned}$$

Rul IV: Differentiation:
The derivative $\partial/\partial x^{\alpha}$ of any tensor is a tensor with one additional lower index α. For instance, if $T^{\beta\gamma}$ is a tensor and

$$T_{\alpha}^{\ \beta\gamma} \equiv \frac{\partial}{\partial x^{\alpha}} T^{\beta\gamma}\,. \tag{3.2.20}$$

then $T_\alpha{}^{\beta\gamma}$ is a tensor, that is,

$$\begin{aligned} T'_\alpha{}^{\beta\gamma} &\equiv \frac{\partial}{\partial x'^\alpha} T'^{\beta\gamma} \\ &= \Lambda_\alpha{}^\delta \frac{\partial}{\partial x^\delta} \Lambda^\beta{}_\varepsilon \Lambda^\gamma{}_\xi T^{\varepsilon\xi} \\ &= \Lambda_\alpha{}^\delta \Lambda^\beta{}_\varepsilon \Lambda^\gamma{}_\xi T_\delta{}^{\varepsilon\xi} . \end{aligned}$$

Note that the order of indices matters, even as between upper and lower indices. For instance, $T_\alpha{}^{\beta\gamma}$ may or may not be the same as $T^\beta{}_\alpha{}^\gamma$.

3.2.2 Special Tensors

Aside from the scalars, there are three special tensors whose components are the same in all coordinates systems:

- *The zero tensor*, whose components are zero in any reference frame for an arbitrary but fixed combination of upper and lower indices.
- *The metric tensor*, which transforms according to ($G = \Lambda G \Lambda^T$) as

$$g'^{\alpha\beta} = g^{\alpha\beta} = \Lambda^\alpha{}_\mu \Lambda^\beta{}_\nu g^{\nu\mu} . \tag{3.2.21}$$

- *The Kronecker tensor*

$$\delta'^\alpha{}_\beta = \delta^\alpha{}_\beta = \Lambda^\alpha{}_\mu \Lambda_\beta{}^\nu \delta^\mu{}_\nu = \begin{cases} +1 & , \quad \mu = \nu , \\ 0 & , \quad \text{otherwise.} \end{cases}$$

- *The Levi-Civita tensor*, is a quantity $\epsilon_{\alpha\beta\gamma\delta}$ defined by

$$\epsilon_{\alpha\beta\gamma\delta} = \begin{cases} +1 & , \quad \alpha\beta\gamma\delta \text{ even permutation of } 0123, \\ -1 & , \quad \alpha\beta\gamma\delta \text{ odd permutation of } 0123 , \\ 0 & , \quad \text{otherwise.} \end{cases} \tag{3.2.22}$$

Note that

$$\epsilon_{\alpha\beta\gamma\delta} = \Lambda_\alpha{}^\kappa \Lambda_\beta{}^\lambda \Lambda_\gamma{}^\mu \Lambda_\delta{}^\nu \, \epsilon_{\kappa\lambda\mu\nu} .$$

Since $g^{\alpha\beta}$ and $g_{\alpha\beta}$ are tensors, we can use them to raise or lower indices on an arbitrary tensor; rule II and rule III tell us that this gives a new tensor with one more upper or lower index and one less lower or upper index. For instance $T_{\alpha\beta\gamma}$ is a tensor, then so is

$$T_\alpha{}^\delta{}_\gamma \equiv g^{\delta\beta} T_{\alpha\beta\gamma} . \tag{3.2.23}$$

In particular, we can lower some or all of the indices on the Levi-Civita tensor $\epsilon_{\alpha\beta\gamma\delta}$. Lowering all the indices gives back the same numerical quantity except for a minus sign.

$$\epsilon_{\alpha\beta\gamma\delta} = -\epsilon^{\alpha\beta\gamma\delta} .$$

The fundamental theorem for any Lorentz invariant theory is that *if two tensors with the same upper and lower indices are equal in one coordinate frame, then they are equal in any other coordinate system related to the first by a Lorentz-transformation*, for instance, if $T^{\alpha}{}_{\beta} = S^{\alpha}{}_{\beta}$, then

$$\begin{aligned} T'^{\alpha}{}_{\beta} &= \Lambda^{\alpha}{}_{\kappa}\Lambda_{\beta}{}^{\mu}T^{\kappa}{}_{\mu} = \Lambda^{\alpha}{}_{\kappa}\Lambda_{\beta}{}^{\mu}S^{\kappa}{}_{\mu} \\ &= S'^{\alpha}{}_{\beta}\,. \end{aligned} \tag{3.2.24}$$

In particular, *the statement that a tensor vanishes is Lorentz-invariant.*

3.3 Light Cone

Definitions: ***Space-time*** *is the set of all (possible) events in a universe; it represents the history of an entire universe. An* ***event*** *is a "point" in the space-time.* ***Worldlines*** *represent the histories of objects in space-time. Hence a worldline is a continuous sequence of events.*

It has become conventional to use plots such as that shown in the Figure 3.1 to represent space-time events. They are called Minkowski or space-time diagrams. Since we cannot plot four dimensions, space-time is reduced to three dimensions with two spatial components and one time component. It is usual to call the zeroth component the time component, and 1, 2, 3 the spatial components. It is also usual to use superscripts, rather than subscripts, for the components (this just has to do with conventions which became established in the early relativity papers, and also with the notation of tensor operations). Remember that real space-time would have another spatial dimension.

Each event in space-time has a double-cone attached to it. The present is represented by the point where the two cones meet, i.e., the tip of the cone. By the conventional choice of units used in relativity, the sides of cone are sloped at 45 degrees. This corresponds to choosing units where time is measured in seconds and distance in light-seconds. A light-second is the distance light travels in one seconds.

- The right-cone (called the *future light-cone*) represents the future history of a light-flash emitted at that event.

- The left-cone (called the *past light-cone*) represents all directions from which light-flashes can be received at that event.

The light cone represents the idea that "*the direction of the light-flash does not depend on the motion of source, but just on the event at which the light-flash is emitted*". In addition, by the Einstein Principle of Relativity, all observers, regardless of their motions, must (because of Maxwell's Laws) measure the speed of light to be the same constant, in all directions. That is to say, "*all observers will universally agree on the light cones at each event*". This means that each observer drawing a space-time diagram in which he is at rest must have the worldlines of light-flashes at the same angle of 45 degrees from his worldline (in time axis), and 45 degrees from his plane of simultaneity (his space axis). Understanding of the light cone is an important first step towards understanding the theory of relativity.

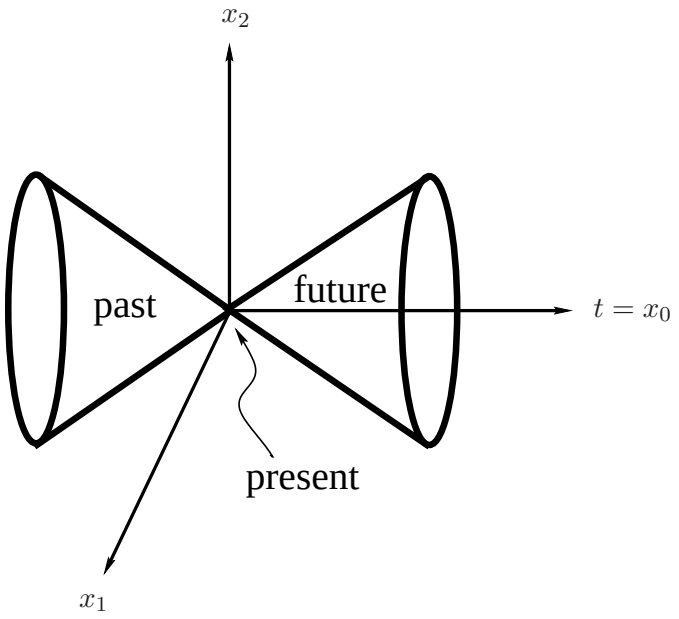

Figure 3.1: Light cone

3.3.1 Einstein Velocity Addition

Einstein abandoned absolute time and fixed space so that the speed of light could be the same for everybody observing it, as Maxwell's Laws said it would be. According to Einstein's postulates the relative velocity of any two objects never exceeds the velocity of light. Applying the Lorentz transformation to the velocities, expressions are obtained for the relative velocities as seen by the different observers. They are called the Einstein velocity addition relationships. Let us consider an observer "B" that fires a bullet from a gun at velocity u measured in a rest frame of "B", while both observer "B" and the gun are moving with velocity w in the bullet direction with respect to the rest frame of an observer "A", see Figure 3.2. A stationary observer "A" standing behind measures the bullet velocity by

$$v = \frac{u + w}{1 + \frac{uw}{c^2}} \,. \tag{3.3.1}$$

On the other hand the the velocity measured by observer "B" is

$$u = \frac{v - w}{1 - \frac{vw}{c^2}} \,. \tag{3.3.2}$$

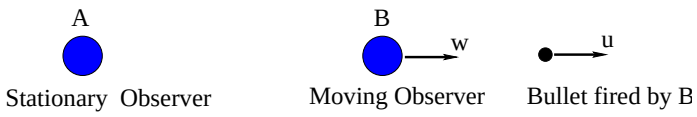

Figure 3.2: Einstein velocity addition

3.4 Relativistic Phase Density and its Moments

In this section we describe a relativistic gas consisting of many microscopic structureless particles in terms of the relativistic kinetic phase density. From this fundamental phase density we calculate the moments in tensor form which give the local macroscopic physical quantities of the gas like the particle density, the velocity, the pressure, the temperature, and so on.

First we take a microscopic look at the gas and start with the kinematics of a representative gas atom with particle trajectory $\mathbf{x} = \mathbf{x}(t)$, where the time coordinate t and the space coordinate $\mathbf{x}$ are related to an arbitrary Lorentz-frame. The invariant mass of all structureless particles is assumed to be the same and is denoted by m_0. The microscopic velocity of the gas atom is $\frac{d\,\mathbf{x}(t)}{dt}$, and its microscopic velocity four-vector is given by $c\,q^\mu$, where the *dimensionless microscopic velocity four-vector* q^μ is defined by

$$\big(q^0, \mathbf{q}\big)^T\,, \qquad q^0 = q_0 = \sqrt{1+\mathbf{q}^2}\,, \qquad \mathbf{q} = \frac{\frac{1}{c}\frac{d\,\mathbf{x}}{dt}}{\sqrt{1-\big(\frac{1}{c}\frac{d\,\mathbf{x}}{dt}\big)^2}}\,. \tag{3.4.1}$$

The *relativistic phase density* $f(t, \mathbf{x}, \mathbf{q}) \geq 0$ is the basic quantity of the kinetic theory. This function may be interpreted as giving the average number of particles with certain momentum at each space-time point. A physical interpretation of the phase density will be discussed when we derive the basic quantities like particle density, velocity four-vector and pressure from its moments defined below. These basic quantities describes the state of a gas at Macroscopic level and are functions of space-time coordinates. We make use of the fact that the so called *proper volume element* d^3q/q_0 is invariant with respect to Lorentz-transformations, for the proof see Appendix B.

3.4.1 Macroscopic Moments and Entropy Four-Vector

(i) *Particle-density four-vector*:
In relativistic theory the two local quantities, the particle density and the particle flow, constitute a four-vector field, which is defined as

$$N^\mu = N^\mu(t, \mathbf{x}) = \int_{\mathbb{R}^3} q^\mu\, f(t, \mathbf{x}, \mathbf{q})\, \frac{d^3q}{q^0}\,. \tag{3.4.2}$$

The index μ takes the four values 0,1,2,3, while $x^\mu = (ct, \mathbf{x})$ denotes a space-time point.

(ii) *Energy-momentum tensor*:
The energy-momentum tensor is a second moment of the distribution function, and thus a symmetric quantity. It is defined as

$$T^{\mu\nu} = T^{\mu\nu}(t, \mathbf{x}) = m_0 c^2 \int_{\mathbb{R}^3} q^\mu q^\nu\, f(t, \mathbf{x}, \mathbf{q})\, \frac{d^3q}{q^0}\,, \tag{3.4.3}$$

with $\mu, \nu = 0, 1, 2, 3$, i.e., these are in total sixteen quantities of which ten are distinct. The energy-momentum tensor only takes the rest energy and the kinetic energy into account.

(iii) *Entropy four-vector*:
The *H-function*, introduced by Boltzmann, implies that the local entropy density and entropy flow is combined to give the entropy four-vector of the form

$$S^\mu = S^\mu(t,\mathbf{x}) = -k_B \int_{\mathbb{R}^3} q^\mu \, f(t,\mathbf{x},\mathbf{q}) \, \ln\left(\frac{f(t,\mathbf{x},\mathbf{q})}{\chi}\right) \frac{d^3q}{q^0} \,. \tag{3.4.4}$$

Here $k_B = 1.38062 \times 10^{-23} J/K$ is Boltzmann's constant and $\chi = (\frac{m_0 c}{\hbar})^3$ with Planck's constant $\hbar = 1.05459 \times 10^{-34} Jsec.$ Note that χ has the same dimension as f, namely 1/volume. We also state here that the entropy formula (3.4.4) can be generalized easily in such a way, that the well known case of a Fermi- or Bose gas is also included in this kinetic framework. Then formula (3.4.4) reads in the general case

$$S^\mu = -k_B \int_{\mathbb{R}^3} q^\mu \, \left[f \ln \frac{f}{\chi} - \eta\chi \left(1 + \eta\frac{f}{\chi}\right) \ln\left(1 + \eta\frac{f}{\chi}\right)\right] \frac{d^3q}{q^0} \,. \tag{3.4.5}$$

Here $\eta = 0$ we get (3.4.4), which is valid for the relativistic generalization of Boltzmann's statistic, whereas $\eta = +1$ is required for the Bose-Einstein statistic and $\eta = -1$ for the Fermi statistic.

Note that the spatial part $\mathbf{q} \in \mathbb{R}^3$ of the dimensionless microscopic velocity four-vector is used as an integration variable in the relativistic kinetic theory.

Now we may use the macroscopic moments N^μ, $T^{\mu\nu}$ and S^μ of the relativistic phase density f in order to calculate the other macroscopic quantities of the gas, which are

Tensor algebraic combinations of these moments:

(i) *The proper particle density*

$$n = \sqrt{N^\mu N_\mu} \,. \tag{3.4.6}$$

(ii) *The dimensionless velocity four-vector*

$$u^\mu = \frac{1}{n} N^\mu \,, \tag{3.4.7}$$

u^μ is also time-like vector with length c in each space-time point i.e. $u^\mu u_\mu = c^2$.

(iii) *The proper energy density*

$$e = u_\mu u_\nu \, T^{\mu\nu} \,. \tag{3.4.8}$$

(iv) *The proper pressure and temperature*

$$p = \frac{1}{3} \left(u_\mu u_\nu - g_{\mu\nu}\right) T^{\mu\nu} = k_B \, nT \,. \tag{3.4.9}$$

(v) *The proper entropy density*

$$\sigma = S^\mu u_\mu \,. \tag{3.4.10}$$

Remarks:

(i) Since $f \geq 0$, it can be shown that N^μ is a time-like vector, $N^\mu N_\mu > 0$, if f does not vanish almost everywhere for any fixed t, $\mathbf{x}$, which will be assumed in the following. It follows that the particle density n is well defined and positive. In order to see that the energy density is always positive we write it in the form

$$e = m_0 c^2 \int_{\mathbb{R}^3} (u_\mu q^\mu)^2 \, f(t, \mathbf{x}, \mathbf{q}) \, \frac{d^3 q}{q^0} \, . \tag{3.4.11}$$

(ii) The *macroscopic velocity* $\mathbf{v}$ of the gas can be obtained easily from the spatial part $\mathbf{u} = (u^1, u^2, u^3)^T$ of the dimensionless velocity four-vector by

$$\mathbf{v} = c \, \frac{\mathbf{u}}{\sqrt{1 + \mathbf{u}^2}} \, . \tag{3.4.12}$$

From this formula we can immediately read off that $|\mathbf{v}| < c$, i.e. the absolute value of the velocity is bounded by the speed of light. Note also that $u^0 = \sqrt{1 + \mathbf{u}^2}$.

Let be $\mathbf{u} = (u^1, u^2, u^3)^T \in \mathbb{R}^3$ fixed. In order to present a short derivation of the relativistic Euler equations, we will later use the following relations for the so called **Lorentz boost** $\Lambda^\alpha{}_\beta = \Lambda^\alpha{}_\beta(\mathbf{u})$,

$$\Lambda^0{}_0 = \sqrt{1 + \mathbf{u}^2} \, , \;\; \Lambda^0{}_j = \Lambda^j{}_0 = -u^j \, , \;\; \Lambda^j{}_k = \delta^j{}_k + \frac{u^j u^k}{1 + \sqrt{1 + \mathbf{u}^2}} \, , \tag{3.4.13}$$

where $j, \, k \in \{1, 2, 3\}$ are spatial indices. Using the above relations (3.4.13) we can find that

(a) $G = \Lambda(\mathbf{u}) \, G \, \Lambda(\mathbf{u})^T$, $\Lambda^0{}_0(\mathbf{u}) \geq 1$ and $\det(\Lambda(\mathbf{u})) = 1$, i.e. $\Lambda(\mathbf{u})$ is a proper Lorentz-matrix.

(b) $\Lambda^{-1}(\mathbf{u}) = \Lambda(-\mathbf{u})$.

The attribute 'proper' denotes a Lorentz-invariant quantity, which takes its simplest form with respect to a Lorentz-frame where the gas is locally at rest. Since all quantities under consideration are written down in Lorentz-invariant form, we may omit the word 'proper' in the following.

These definitions are valid for any relativistic phase-density $f = f(t, \mathbf{x}, \mathbf{q})$, which has to be determined from a kinetic equation of the following form

$$q^\mu \frac{\partial f}{\partial x^\mu} = Q(f) \, , \qquad \mu = 0, 1, 2, 3 \, . \tag{3.4.14}$$

As in the non-relativistic kinetic theory we have a corresponding transport part on the left-hand side and a collision part $Q(f)$ on the right-hand side. In the simplest case $Q(f)$ is determined in such a way that the following five conservation laws hold for the particle number, the energy and the momentum

$$\frac{\partial N^\mu}{\partial x^\mu} = 0 \, , \qquad \frac{\partial T^{\mu\nu}}{\partial x^\nu} = 0 \, . \tag{3.4.15}$$

This simple case holds if the particles interact only during elastic collisions without other forces and radiation, but will nevertheless lead to an interesting and self-consistent relativistic thermodynamics, even if it is physically not realizable. Also note that $Q(f) = 0$ in Euler limit, therefore equation (3.4.14) reduces to a free-flight equation

$$q^\mu \frac{\partial f}{\partial x^\mu} = 0\,, \qquad \mu = 0, 1, 2, 3. \tag{3.4.16}$$

3.5 Relativistic Jüttner Phase Density

Jüttner [41, 42] extended the non-relativistic velocity distribution of Maxwell for a gas in equilibrium to the relativistic case. The resulting *Jüttner distribution* $f_J(n, T, \mathbf{u}, \mathbf{q})$ depends on five constant parameters, which describe the state of the gas in equilibrium, namely the particle density n, the absolute temperature T and the spatial part $\mathbf{u} \in \mathbb{R}^3$ of the dimensionless four-velocity. It is given by

$$\begin{aligned} f_J(n, T, \mathbf{u}, \mathbf{q}) &= \frac{n}{M(\beta)} \exp\left(-\beta\, u_\mu q^\mu\right) \\ &= \frac{n}{M(\beta)} \exp\left(-\beta \left(\sqrt{(1+\mathbf{u}^2)(1+\mathbf{q}^2)} - \mathbf{u}\cdot\mathbf{q}\right)\right), \end{aligned} \tag{3.5.1}$$

where $\beta = \frac{m_0 c^2}{k_B T}$ and

$$M(\beta) = \int_{\mathbb{R}^3} \exp(-\beta\sqrt{1+\mathbf{q}^2}) d^3q = 4\pi \int_0^\infty \vartheta^2 \exp(-\beta\sqrt{1+\vartheta^2})\, d\vartheta\,. \tag{3.5.2}$$

The function $M(\beta)$ is chosen in such a way that

$$n\, u^\mu = \int\limits_{\mathbb{R}^3} q^\mu\, f_J(n, T, \mathbf{u}, \mathbf{q})\, \frac{d^3q}{q^0}\,, \tag{3.5.3}$$

holds for the spatial part $\mathbf{u} = (u^1, u^2, u^3)^T$ of the dimensionless macroscopic velocity four-vector. This is equation (3.4.7), where $\mathbf{u}$ and n are in addition parameters of Jüttner's relativistic phase density.

Using the Bessel functions

$$K_m(\beta) = \int\limits_0^\infty \cosh(ms)\, \exp(-\beta\, \cosh(s))\, ds\,, \tag{3.5.4}$$

and applying the integral substitution $\vartheta = \sinh(s)$ we may also write $M(\beta)$ in the form

$$M(\beta) = \frac{4\pi}{\beta}\, K_2(\beta)\,. \tag{3.5.5}$$

We have in addition recursion relations for the modified Bessel functions, which can be found in the hand book of Jeffrey [40],

$$K_{m+1}(\beta) = \frac{2m}{\beta}\, K_m(\beta) + K_{m-1}(\beta)\,, \tag{3.5.6}$$

where m is the integer order of the modified Bessel functions. Using (3.5.4), (3.5.5) and (3.5.6) we can write

$$M'(\beta) = -4\pi \left(\frac{K_1(\beta)}{\beta} + \frac{3K_2(\beta)}{\beta^2} \right) ,$$
$$\eta(\beta) = 4\pi \int_0^\infty \frac{\vartheta^2}{\sqrt{1+\vartheta^2}} \exp(-\beta\sqrt{1+\theta^2}) d\vartheta = \frac{4\pi}{\beta} K_1(\beta) . \tag{3.5.7}$$

Note that

$$\eta'(\beta) = M(\beta) . \tag{3.5.8}$$

The equations (3.5.5) and (3.5.7) will be used in Chapter 6 in order to find the constitutive relations for e, p, σ in more general form.

In order to formulate the Euler equations and other relations coming in Chapter 6 in a friendly form, we introduce the function

$$\Psi(\beta) = \frac{3}{\beta} + \frac{K_1(\beta)}{K_2(\beta)} . \tag{3.5.9}$$

It turns out later in Chapter 6 that $\Psi(\beta)$ is just the specific energy $\frac{e}{n}$ for the gas in equilibrium.

3.5.1 Limiting Cases of Relativistic Jüttner Phase Density

Here we discuss two important special cases for this phase density, namely the non-relativistic limit for a cool gas and the ultra-relativistic limit $m_0 \to 0$.

Case 1: The non-relativistic limit (small temperatures, small velocities)

For the first case we rewrite (3.5.1) in the form

$$f_J(n, T, \mathbf{u}, \mathbf{q}) = \frac{n}{M_1(\beta)} \exp \left(-\beta \frac{(\mathbf{q}-\mathbf{u})^2 + \mathbf{u}^2\mathbf{q}^2 - (\mathbf{u}\cdot\mathbf{q})^2}{1 + \sqrt{(1+\mathbf{u}^2)(1+\mathbf{q}^2)} + \mathbf{u}\cdot\mathbf{q}} \right) , \tag{3.5.10}$$

where

$$M_1(\beta) = M(\beta) \exp(\beta) . \tag{3.5.11}$$

If we apply for $\vartheta > 0$ the integral substitution

$$\xi = \sqrt{2\beta(\sqrt{1+\vartheta^2} - 1)} , \tag{3.5.12}$$

then we can rewrite $M_1(\beta)$ in the form

$$M_1(\beta) = \left(\frac{2\pi}{\beta} \right)^{\frac{3}{2}} \cdot 2 \int_0^\infty \left(1 + \frac{\xi^2}{2\beta} \right) \sqrt{1 + \frac{\xi^2}{4\beta}} \, \frac{\exp(-\frac{\xi^2}{2})}{\sqrt{2\pi}} \, d\xi . \tag{3.5.13}$$

For β very large compared to 1, i.e. for small temperature, we can conclude from (3.5.13) that

$$M_1(\beta) = (\frac{2\pi}{\beta})^{\frac{3}{2}} + O(\beta^{-\frac{5}{2}}) = \left(\frac{2\pi K_B T}{m_0 c^2}\right)^{\frac{3}{2}} + O(T^{\frac{5}{2}}),$$

and the representation (3.5.10) shows that the Jüttner phase density reduces to the non-relativistic Maxwellian for $|\mathbf{u}|$, $|\mathbf{q}|$ very small, namely

$$f_c(n, T, \mathbf{u}, \mathbf{q}) = n \left(\frac{m_0 c^2}{2\pi K_B T}\right)^{\frac{3}{2}} \exp\left[-\frac{m_0 c^2 (\mathbf{q}-\mathbf{u})^2}{2K_B T}\right]. \tag{3.5.14}$$

Furthermore, in order to get the non-relativistic limit (i.e. $\beta \gg 1$) from the formulations coming in Chapter 6, we will need the following asymptotic relations for $\beta \to \infty$,

$$\begin{aligned} K_1(\beta) &= \sqrt{\frac{\pi}{2\beta}} \exp(-\beta) \left(1 + \frac{3}{8\beta}\right) + O\left(\frac{\exp(-\beta)}{\beta^{\frac{5}{2}}}\right), \\ K_2(\beta) &= \sqrt{\frac{\pi}{2\beta}} \exp(-\beta) \left(1 + \frac{15}{8\beta}\right) + O\left(\frac{\exp(-\beta)}{\beta^{\frac{5}{2}}}\right), \\ \Psi(\beta) &= 1 + \frac{3}{2\beta} + O\left(\frac{\exp(-\beta)}{\beta^{\frac{5}{2}}}\right). \end{aligned} \tag{3.5.15}$$

Case 2: The ultra-relativistic limit (zero rest mass of the particles)

For the ultra-relativistic limit $m_0 \to 0$ with fixed temperature we apply the substitution $\mathbf{q}' = m_0.\mathbf{q}$ in order to write (3.5.1) in the form

$$f_J(n, T, \mathbf{u}, \mathbf{q}) = m_0^3 \frac{n}{M_2(\tilde{\beta})} \exp\left(-\tilde{\beta}\left(\sqrt{(1+\mathbf{u}^2)(m_0^2 + \mathbf{q}'^2)} - \mathbf{u}\cdot\mathbf{q}'\right)\right), \tag{3.5.16}$$

where

$$\tilde{\beta} = \frac{\beta}{m_0} = \frac{c^2}{k_B T}, \quad M_2(\tilde{\beta}) = \frac{8\pi}{\tilde{\beta}^3} \int_0^\infty \frac{\xi^2}{2} \exp\left(-\sqrt{m_0^2 \tilde{\beta}^2 + \xi^2}\right) d\xi. \tag{3.5.17}$$

In the following we do not use primes for the new integration variable $\mathbf{q}$.

Now we are able to pass to the ultra-relativistic limit $m_0 \to 0$. In order to do this we first have to replace the four-vector q^μ defined in (3.4.1) by the light vector

$$\left(q^0, \mathbf{q}\right)^T, \qquad q^0 = q_0 = |\mathbf{q}|. \tag{3.5.18}$$

Also to get the ultra-relativistic limit (i.e. $\beta \ll 1$) from the formulations coming in Chapter 6, we have the following asymptotic relations for $\beta \to 0$

$$K_1(\beta) = \frac{1}{\beta} + O(\beta \ln \beta), \; K_2(\beta) = \frac{2}{\beta^2} + O(1), \; \Psi(\beta) = \frac{3}{\beta} + O(\beta). \tag{3.5.19}$$

3.6 Moments in Dimensionless Form

Next we will introduce dimensionless quantities by setting $m_0 = c = k_B = \hbar = 1$. Then the relativistic moments and the entropy four-vector given in (3.4.2), (3.4.3) and (3.4.4) simply reduces to

$$N^\mu = N^\mu(t, \mathbf{x}) = \int_{\mathbb{R}^3} q^\mu \, f(t, \mathbf{x}, \mathbf{q}) \, \frac{d^3q}{q^0} \,, \tag{3.6.1}$$

$$T^{\mu\nu} = T^{\mu\nu}(t, \mathbf{x}) = \int_{\mathbb{R}^3} q^\mu q^\nu \, f(t, \mathbf{x}, \mathbf{q}) \, \frac{d^3q}{q^0} \,, \tag{3.6.2}$$

$$S^\mu = S^\mu(t, \mathbf{x}) = -\int_{\mathbb{R}^3} q^\mu \, f(t, \mathbf{x}, \mathbf{q}) \, \ln f(t, \mathbf{x}, \mathbf{q}) \, \frac{d^3q}{q^0} \,, \tag{3.6.3}$$

where f is first taken as Jüttner phase density as given in (3.5.1) in its dimensionless form.

But the equations (3.6.1), (3.6.2) and (3.6.3) are more general definitions and can be used for any phase density. For that reason we have used the general symbol f in the moments definitions instead of f_J. These more general definitions will be important for the formulation of kinetic schemes in order to solve the fluid dynamic equations in relativistic case.

Also note that all the definitions given for the particle density n, velocity four-vector u^μ, energy density e and for the pressure p, which are tensor invariant algebraic combinations of the basic moments N^μ and $T^{\mu\nu}$, are still valid for an arbitrary phase density f.

The ultra-relativistic moments and entropy four-vector take a similar form as given in (3.6.1), (3.6.2) and (3.6.3) by just replacing q^0 by $|\mathbf{q}|$, and are given below

$$N^\mu = N^\mu(t, \mathbf{x}) = \int_{\mathbb{R}^3} q^\mu \, f(t, \mathbf{x}, \mathbf{q}) \, \frac{d^3q}{|\mathbf{q}|} \,, \tag{3.6.4}$$

$$T^{\mu\nu} = T^{\mu\nu}(t, \mathbf{x}) = \int_{\mathbb{R}^3} q^\mu q^\nu \, f(t, \mathbf{x}, \mathbf{q}) \, \frac{d^3q}{|\mathbf{q}|} \,, \tag{3.6.5}$$

and the macroscopic *entropy four-vector*

$$S^\mu = S^\mu(t, \mathbf{x}) = -\int_{\mathbb{R}^3} q^\mu \, f(t, \mathbf{x}, \mathbf{q}) \, \ln f(t, \mathbf{x}, \mathbf{q}) \, \frac{d^3q}{|\mathbf{q}|} \,. \tag{3.6.6}$$

Here f is the ultra-relativistic Jüttner phase density (3.5.16) in dimensionless form

$$\begin{aligned} f_J^*(n, T, \mathbf{u}, \mathbf{q}) &= \frac{n}{8\pi T^3} \, \exp\left(-\frac{u_\mu q^\mu}{T}\right) \\ &= \frac{n}{8\pi T^3} \, \exp\left(-\frac{|\mathbf{q}|}{T}\left(\sqrt{1+\mathbf{u}^2} - \mathbf{u}\cdot\frac{\mathbf{q}}{|\mathbf{q}|}\right)\right) \,. \end{aligned} \tag{3.6.7}$$

In ultra-relativistic limit the generally valid formula (3.4.9) for the pressure simplifies to

$$\begin{aligned} p &= \frac{1}{3}\, u_\mu u_\nu T^{\mu\nu} - \frac{1}{3}\, g_{\mu\nu} T^{\mu\nu} \\ &= \frac{1}{3}\, u_\mu u_\nu T^{\mu\nu} - \int_{\mathbb{R}^3} g_{\mu\nu} q^\mu q^\nu \, f \, \frac{d^3 q}{q^0}\,. \end{aligned} \tag{3.6.8}$$

Also in ultra-relativistic case $g_{\mu\nu} q^\mu q^\nu = q_\nu q^\nu = 0$ due to (3.5.18), therefore we get

$$p = \frac{e}{3} = \frac{1}{3}\, T^{\mu\nu} u_\mu u_\nu = nT\,. \tag{3.6.9}$$

Chapter 4

Ultra-relativistic Euler Equations

In this chapter we discuss the ultra-relativistic Euler equations of gas dynamic. We derive a single shock parametrization by using the Rankine-Hugoniot jump conditions and a parametrization of rarefaction wave for the one-dimensional ultra-relativistic Euler equations. We use these parametrizations in order to develop an exact Riemann solver.

We derive the unconditionally stable kinetic schemes in order to solve the ultra-relativistic Euler equations. As mentioned before these schemes are discrete in time but continuous in space. We prove the conservation laws, entropy inequality, positivity and L_1-stability for the three-dimensional kinetic scheme. We also explain the numerical implementation of the kinetic schemes. In order to extend the schemes to second order we follow the approach of Deshpande [13]. For second order accuracy we have restricted ourselves to one and two space dimensions. We calculate the L_1-error and experimental order of convergence by considering numerical examples for smooth initial data.

4.1 Derivation of Ultra-relativistic Euler Equations

Using the ultra-relativistic Jüttner distribution (3.6.7) in the moment integrals (3.6.4), (3.6.5) and (3.6.6) we get

$$N^\mu = n\,u^\mu, \qquad T^{\mu\nu} = -p\,g^{\mu\nu} + 4pu^\mu u^\nu\,, \tag{4.1.1}$$

$$S^\mu = -N^\mu \ln\frac{n^4}{p^3} + \gamma N^\mu, \qquad \sigma = -n\ln\frac{n^4}{p^3} + \gamma n\,, \tag{4.1.2}$$

where γ is any real constant. The divergence of S^μ give rise to the H-theorem, and will be formulated later. Also note that due to the mass conservation $(3.4.15)_1$ this divergence of S^μ will not change when we add some multiple of N^μ to S^μ. The above formulas can be easily checked for a special Lorentz frame where $u^0 = 1$, $u^1 = u^2 = u^3 = 0$, i.e. where the gas is locally at rest. Since the ultra-relativistic moments (4.1.1) and (4.1.2) are valid in a special Lorentz frame and since these equations are written in tensor invariant form, they are generally valid in every Lorentz frame.

Lemma 4.1: *Let σ, given by* (4.1.2) *for $\gamma = 0$, be the entropy density corresponding to the Jüttner phase density $f_J(n, T, \mathbf{u}, \mathbf{q})$. This is equivalent to the Gibbs equation*

$$d\hat{\sigma} = \frac{p}{T} d\left(\frac{1}{n}\right) + \frac{1}{T} d\left(\frac{e}{n}\right), \tag{4.1.3}$$

i.e. (4.1.2) *and* (4.1.3) *are equivalent. Here $\hat{\sigma}$ is a specific entropy density i.e., $\hat{\sigma} = \dfrac{\sigma}{n}$.*

Proof: For the ultra-relativistic limit we know from (3.6.9) that $e = 3p = 3nT$. Thus we can write $\frac{p}{T} = n$ and $\dfrac{e}{n} = 3T$. Now (4.1.3) can be rewritten as

$$\begin{aligned} d\hat{\sigma} &= n\, d\left(\frac{1}{n}\right) + \frac{3}{T} dT \\ &= \frac{1}{\left(\frac{1}{n}\right)} d\left(\frac{1}{n}\right) + \frac{3}{T} d(T). \end{aligned} \tag{4.1.4}$$

From (4.1.4) it is clear that $\hat{\sigma} = \hat{\sigma}(\frac{1}{n}, T)$. Using the chain rule we have

$$d\hat{\sigma} = \frac{\partial \hat{\sigma}}{\partial\left(\frac{1}{n}\right)} d\left(\frac{1}{n}\right) + \frac{\partial \hat{\sigma}}{\partial T} dT\,. \tag{4.1.5}$$

Comparing (4.1.4) and (4.1.5) we whave

$$\frac{\partial \hat{\sigma}}{\partial\left(\frac{1}{n}\right)} = \frac{1}{\left(\frac{1}{n}\right)}, \qquad \frac{\partial \hat{\sigma}}{\partial T} = \frac{3}{T}\,. \tag{4.1.6}$$

Integrating $(4.1.6)_1$ with respect to $\frac{1}{n}$ we get

$$\hat{\sigma}\left(\frac{1}{n}, T\right) = \ln\left(\frac{1}{n}\right) + \alpha(T)\,. \tag{4.1.7}$$

Now differentiating (4.1.7) with respect to T and using $(4.1.6)_2$ we get

$$\alpha'(T) = \frac{\partial \hat{\sigma}}{\partial T} = \frac{3}{T}\,. \tag{4.1.8}$$

Integrating (4.1.8) with respect to T we get

$$\alpha(T) = 3 \ln T = \ln T^3\,. \tag{4.1.9}$$

Using (4.1.9) in (4.1.7) we get

$$\begin{aligned} \hat{\sigma}\left(\frac{1}{n}, T\right) &= \ln\left(\frac{1}{n}\right) + \ln T^3 \\ &= -\ln \frac{n}{T^3}\,. \end{aligned} \tag{4.1.10}$$

Since $\hat{\sigma}$ is the specific entropy density i.e. $\sigma = n \cdot \hat{\sigma}$ so we can write

$$\sigma = n \cdot \hat{\sigma} = -n \ln \frac{n}{T^3} = -n \ln \frac{n^4}{p^3}\,. \tag{4.1.11}$$

Conversely, using (4.1.11) in (4.1.5) one can easily get back the Gibbs equation (4.1.3). Thus both equations (4.1.11) and (4.1.3) are equivalent. ■

Using the moments (4.1.1) and the conservation laws (3.4.15), we get at regular points, where the solution is continuously differentiable, the three-dimensional ultra-relativistic Euler equations in differential form

$$\frac{\partial}{\partial t}\,(n\,\sqrt{1+\mathbf{u}^2}) + \nabla\cdot(n\,\mathbf{u}) = 0\,, \tag{4.1.12}$$

$$\frac{\partial}{\partial t}(4pu^i\sqrt{1+\mathbf{u}^2}) + \sum_{k=1}^{3}\frac{\partial}{\partial x^k}\,(p\,\delta^{ik} + 4pu^iu^k) = 0\,, \tag{4.1.13}$$

$$\frac{\partial}{\partial t}\,(3p + 4p\mathbf{u}^2) + \sum_{k=1}^{3}\frac{\partial}{\partial x^k}\,(4pu^k\sqrt{1+\mathbf{u}^2}) = 0\,, \tag{4.1.14}$$

where $i = 1, 2, 3$. Note that the equations (4.1.13), (4.1.14) are a closed 4×4 system for p and $\mathbf{u}$. The relativistic continuity equation (4.1.12) decouples from the system. For given $\mathbf{u}$ it is a scalar equation for n.

Now we are looking for special solutions of the three-dimensional Euler equations, which will not depend on x^2, x^3 but only on $x = x^1$. Moreover, we restrict to a one-dimensional flow field $\mathbf{u} = (u(t,x), 0, 0)^T$

$$\begin{aligned}(n\sqrt{1+u^2})_t + (nu)_x &= 0\,,\\ (4pu\sqrt{1+u^2})_t + (p(1+4u^2))_x &= 0\,,\\ (p(3+4u^2))_t + (4pu\sqrt{1+u^2})_x &= 0\,.\end{aligned} \tag{4.1.15}$$

Note that these differential equations constitute a strictly hyperbolic system with the characteristic velocities

$$\lambda_1 = \frac{2u\sqrt{1+u^2}-\sqrt{3}}{3+2u^2}\,,\ \lambda_2 = \frac{u}{\sqrt{1+u^2}}\,,\ \lambda_3 = \frac{2u\sqrt{1+u^2}+\sqrt{3}}{3+2u^2}\,. \tag{4.1.16}$$

These eigenvalues may first be obtained in the Lorentz rest frame where $u = 0$. Then using the Einstein's velocity addition (3.3.1), we can easily obtain (4.1.16) in the general Lorentz frame. In the Lorentz rest frame the positive speed of sound is $\lambda = \frac{1}{\sqrt{3}}$, which is independent of the spatial direction.

The differential equations (4.1.15) are not sufficient if the shock discontinuities are taken into account. Therefore we need a weak integral formulation which is given due to Oleinik [68] by curve integrals in time and space, namely

$$\begin{aligned}\oint_{\partial\Omega} n\sqrt{1+u^2}dx - nudt &= 0\,,\\ \oint_{\partial\Omega} 4pu\sqrt{1+u^2}dx - p(1+4u^2)dt &= 0\,,\\ \oint_{\partial\Omega} p(3+4u^2)dx - 4pu\sqrt{1+u^2}dt &= 0\,.\end{aligned} \tag{4.1.17}$$

Here $\Omega \subset \mathbb{R}_0^+ \times \mathbb{R}$ is a normal region in space-time with a piecewise smooth positively oriented boundary. Note that this weak formulation takes discontinuities into account, since there are no derivatives of the fields involved. If we apply the Gaussian divergence theorem to the weak formulation (4.1.17) in arbitrary space-time regions where the solution is regular we come back to the differential equation form of the Euler equations (4.1.15).

Furthermore, we require that the weak solution (4.1.17) must also satisfy the *entropy-inequality*

$$\oint_{\partial\Omega} S^0 dx - S^1 dt \geq 0\,, \tag{4.1.18}$$

where

$$S^0 = -n\sqrt{1+u^2}\,\ln\frac{n^4}{p^3}\,, \qquad S^1 = -nu\,\ln\frac{n^4}{p^3}\,. \tag{4.1.19}$$

4.1.1 Rankine Hugoniot Jump Conditions

Now we consider bounded and integrable *initial data* for a positive particle density n, transformed velocity u and absolute temperature T, which may have jumps

$$n(0,x) = n_0(x) > 0, \qquad u(0,x) = u_0(x), \qquad T(0,x) = T_0(x) > 0. \tag{4.1.20}$$

If $x = x(t)$ is a shock-discontinuity of the weak solution (4.1.17) with speed $v_s = \dot{x}(t)$, $W_- = (n_-, u_-, p_-)$ the state left to the shock and $W_+ = (n_+, u_+, p_+)$ the state to the right, then (4.1.17) leads to the *Rankine-Hugoniot jump conditions*

$$\begin{aligned}
v_s\left[n_+\sqrt{1+u_+^2} - n_-\sqrt{1+u_-^2}\right] &= n_+u_+ - n_-u_-\,,\\
v_s\left[4p_+u_+\sqrt{1+u_+^2} - 4p_-u_-\sqrt{1+u_-^2}\right] &= (p_+ + 4p_+u_+^2) - (p_- + 4p_-u_-^2)\,,\\
v_s\left[(3p_+ + 4p_+u_+^2) - (3p_- + 4p_-u_-^2)\right] &= 4p_+u_+\sqrt{1+u_+^2} - 4p_-u_-\sqrt{1+u_-^2}\,.
\end{aligned} \tag{4.1.21}$$

Also in singular points the local form of (4.1.18) reads

$$-v_s(S_+^0 - S_-^0) + (S_+^1 - S_-^1) \geq 0, \tag{4.1.22}$$

which must be satisfied on each shock curve of (4.1.17). A shock that satisfies (4.1.21) and (4.1.22) is called an *entropy shock*.

Now we give parameter representations for single entropy shocks. For this purpose we choose the initial data as follows:

Let be $(n_*, u_*, T_*) \in \mathbb{R}^+ \times \mathbb{R} \times \mathbb{R}^+$ and define $p_* = n_*T_*$. We use the pressure p as a parameter which determines the strength of an entropy shock. Equations (4.1.21) and (4.1.22) are solved by

$$n(p) = n_* \sqrt{\frac{p}{p_*}\left(\frac{3p+p_*}{p+3p_*}\right)}, \tag{4.1.23}$$

$$u(p) = \frac{u_*\sqrt{p_*+3p}\sqrt{p+3p_*} \pm \sqrt{3}(p-p_*)\sqrt{1+u_*^2}}{4\sqrt{pp_*}}, \tag{4.1.24}$$

$$T(p) = \frac{p}{n(p)}, \tag{4.1.25}$$

$$u_s(p) = \frac{u_*\sqrt{3(p+3p_*)} \pm \sqrt{p_*+3p}\sqrt{1+u_*^2}}{\sqrt{8p_*}}, \tag{4.1.26}$$

$$v_s = \frac{u_s}{\sqrt{1+u_s^2}}, \quad v = \frac{u}{\sqrt{1+u^2}}, \quad v_* = \frac{u_*}{\sqrt{1+u_*^2}}, \tag{4.1.27}$$

in the following way:

- The "+" sign in (4.1.24), (4.1.26) and $p > p_*$ gives the so called *3-shocks* with the constant state (n_*, u_*, T_*) on the right

  $$(n_-, u_-, T_-) = (n(p), u(p), T(p)), \quad (n_+, u_+, T_+) = (n_*, u_*, T_*).$$

  These 3-shocks satisfy both the Rankine-Hugoniot conditions (4.1.21) as well as the entropy condition (4.1.22).

- The "−" sign in (4.1.24), (4.1.26) and $p > p_*$ gives the so called *1-shocks* with the constant state (n_*, u_*, T_*) on the left:

  $$(n_-, u_-, T_-) = (n_*, u_*, T_*), \quad (n_+, u_+, T_+) = (n(p), u(p), T(p)).$$

  These 1-shocks satisfy both the Rankine-Hugoniot conditions (4.1.21) as well as the entropy condition (4.1.22).

Now we define the *2-contacts*, that are *contact-discontinuities without entropy-production*. Only for these we choose $n > 0$ instead of p as a parameter and set

$$(n_-, u_-, T_-) = (n_*, u_*, T_*), \quad (n_+, u_+, T_+) = \left(n, u_*, \frac{n_* T_*}{n}\right).$$

These waves satisfy the Rankine-Hugoniot and entropy conditions. Also note that velocity and pressure are constant across a 2-contact. Here the wave-speed is $v_s = v_* = \frac{u_*}{\sqrt{1+u_*^2}}$.

Remark. One can prove that the only discontinuities satisfying (4.1.21) and (4.1.22) are 1- and 3-shocks as well as 2-contacts, see Courant and Friedrichs [9].

4.1.2 Rarefaction Wave

Rarefaction waves in the ultra-relativistic Euler equations are associated with the eigenvalues $(4.1.16)_1$ and $(4.1.16)_3$. These waves have a fan-type shape that is enclosed by two bounding characteristics corresponding to the head and the tail of the wave.

Let $(n_*, u_*, T_*) \in \mathbb{R}^+ \times \mathbb{R} \times \mathbb{R}^+$ be the initial data on one side and let $p_* = n_* T_*$. Then we can find the initial state on the other side by the following procedure.

Let $s = \dfrac{x}{t}$ be the characteristic speed, then we can write from (4.1.17)

$$s\frac{d}{ds}[n(s)\sqrt{1+u^2(s)}] = \frac{d}{ds}[n(s)u(s)]\,, \tag{4.1.28}$$

$$s\frac{d}{ds}[4p(s)u(s)\sqrt{1+u^2(s)}] = \frac{d}{ds}[p(s)(1+4u^2(s)]\,, \tag{4.1.29}$$

$$s\frac{d}{ds}[p(s)(3+4u^2(s))] = \frac{d}{ds}[4p(s)u(s)\sqrt{1+u^2(s)}]\,. \tag{4.1.30}$$

The last two equations (4.1.29), (4.1.30) are decoupled from the first equation (4.1.28), and are two equations for the two unknowns $u(s)$ and $p(s)$. We first solve them for $u(s)$ in term of s. Secondly we solve these equations for $p(s)$ in term of $u(s)$, where we use the right eigenvalues $(4.1.16)_1$, $(4.1.16)_3$ as values of s, i.e. $s = \frac{2u\sqrt{1+u^2}\pm\sqrt{3}}{3+2u^2}$. At last we solve (4.1.28) for $n(s)$. These values of $u(s)$, $p(s)$ and $n(s)$ are given as

$$u(s) = \sqrt{\frac{3}{2}}\left(\frac{s \pm \frac{1}{\sqrt{3}}}{\sqrt{1-s^2}}\right)\,, \tag{4.1.31}$$

$$p(s) = \delta_*\left(\sqrt{1+u^2(s)} \pm u(s)\right)^{\frac{4}{\sqrt{3}}}\,, \tag{4.1.32}$$

$$n(s) = \gamma_*(\sqrt{1+u^2(s)} \pm u(s))^{\sqrt{3}}\,, \tag{4.1.33}$$

where δ_* and γ_* are integration constants that can be found from the initial data (n_*, u_*, T_*). δ_* and γ_* are used for adjusting the broadness of the rarefaction fan. In the above equations the "+" sign corresponds to three wave and the "−" sign corresponds to one wave.

One can rewrite the above equations by using the pressure p as a parameter. We get

$$u(p) = \pm\frac{\left(\frac{p}{\delta_*}\right)^{\frac{\sqrt{3}}{2}} - 1}{2\left(\frac{p}{\delta_*}\right)^{\frac{\sqrt{3}}{4}}}\,, \tag{4.1.34}$$

$$n(p) = \left(\frac{\gamma_* p}{\delta_*}\right)^{\frac{3}{4}}\,, \tag{4.1.35}$$

$$s(p) = \pm\frac{\left(\frac{p}{\delta_*}\right)^{\sqrt{3}} + 2\sqrt{3}\left(\frac{p}{\delta_*}\right)^{\frac{\sqrt{3}}{2}} - 1}{\left(\frac{p}{\delta_*}\right)^{\sqrt{3}} + 4\left(\frac{p}{\delta_*}\right)^{\frac{\sqrt{3}}{2}} + 1}\,. \tag{4.1.36}$$

4.2 Exact Riemann Solution

The Riemann problem for the one-dimensional time-dependent ultra-relativistic Euler Equations (4.1.15) is the initial value problem (IVP) for the conservation laws

$$W_t + F(W)_x = 0\,, \tag{4.2.1}$$

$$W = \begin{bmatrix} n\sqrt{1+u^2} \\ 4pu\sqrt{1+u^2} \\ p(3+4u^2) \end{bmatrix}, \qquad F = \begin{bmatrix} nu \\ p(1+4u^2) \\ 4pu\sqrt{1+u^2} \end{bmatrix},$$

with initial conditions

$$W(0,x) = W^{(0)}(x) = \begin{cases} W_L & \text{if } x < 0 \\ W_R & \text{if } x > 0 \end{cases} . \tag{4.2.2}$$

The domain of interest in the t, x plane are points (t, x) with $t > 0$ and $-\infty < x < \infty$. In practice one lets x vary in a finite interval $[x_L, x_R]$ around the point $x = 0$. A typical Riemann problem is shown in Figure 4.1. In this figure we can see that the Riemann solution lies inside the light cone of slope $s = \pm 1$. There is an advantage in the relativistic case with dimensionless variables $c = 1$ because it gives a natural CFL condition $\Delta t = \Delta x$.

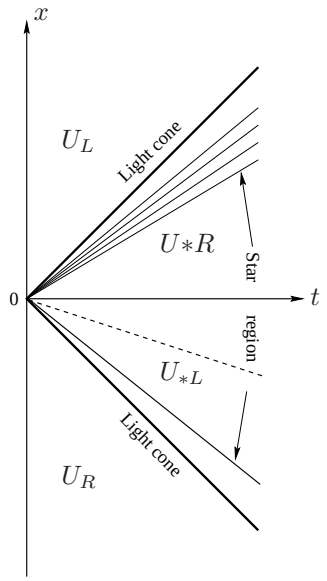

Figure 4.1: A typical Riemann problem in the t, x plane.

The main idea behind the solution of a Riemann problem is to solve the initial value problem (4.2.1) and (4.2.2) for two constant states, which in terms of primitive variables are $U_L = (n_L, u_L, p_L)$ to the left of $x = 0$ and $U_R = (n_R, u_R, p_R)$ to the right of $x = 0$, separated by a discontinuity at $x = 0$. For classical hydrodynamics the solution can be found, e.g., in Toro [85].

The solution to this problem is self-similar, because it only depends on the two constant states defining the discontinuity U_L and U_R, as well as on the ratio x/t. Both in relativistic and classical hydrodynamics the discontinuity decays into two elementary nonlinear waves (shocks or rarefactions) which move in opposite directions towards the initial left and right states. Between these waves two new constant states U_{*L} and U_{*R} appear, which are separated from each other through a contact discontinuity moving with the fluid. Across the contact discontinuity the density exhibits a jump, whereas pressure and velocity are continuous. As in the classical case, the self-similar character of the flow through rarefaction waves and

the Rankine-Hugoniot conditions across shocks provide the relations to link the intermediate states U_{*S} $(S = L, R)$ with the corresponding initial states U_S. They also allow one to express the fluid flow velocity in the intermediate states u_{*S} as a function of the pressure p_{*S} in these states. Finally, the steadiness of pressure and velocity across the contact discontinuity implies

$$u_L(p_*) = u_R(p_*)\,, \tag{4.2.3}$$

where $p_* = P_{*L} = P_{*R}$, which closes the system. The functions $u_{*S}(p)$ are defined by

$$u_{*S}(p) = \begin{cases} R^S(p) \text{ if } p \le p_S \\ S^S(p) \text{ if } p > p_S \end{cases}\,, \tag{4.2.4}$$

where $R^S(p)\,/\,S^S(p)$ denotes the family of all states which can be connected through a rarefaction / shock with a given state U_S ahead of the wave. Here $S^S(p)$ is given by (4.1.24) and $R^S(p)$ is given by (4.1.34). We solve the implicit relation (4.2.3) for p_* using a root finding method, for example the Newton-Raphson method. Once we get the value of p_* then the value of u_* can be obtained explicitly from either the left or right wave equations. Similarly n_{*L} and n_{*R} can be calculated from the left and right waves across the contact discontinuity (middle wave), respectively.

4.3 Kinetic Scheme in Three Space Dimensions

We first formulate the scheme for the three-dimensional Euler equations. After that we solve the one-dimensional Euler equations, using a special integration technique. Recalling the ultra-relativistic Jüttner phase density (3.6.7), we start with the given initial data $n_I(\mathbf{x}) = n(0,\mathbf{x})$, $T_I(\mathbf{x}) = T(0,\mathbf{x})$, $u_I(\mathbf{x}) = u(0,\mathbf{x})$. We prescribe a time step $\tau_M > 0$ and let $t_n = n\,\tau_M$ for $n = 0, 1, 2, 3...$ be the maximization times. Then we define the moments and the entropy four-vector in the free-flight for $0 < \tau < \tau_M$ as

$$\begin{aligned} N^\mu(t_n + \tau, \mathbf{x}) &= \int_{\mathbb{R}^3} q^\mu\, f_n(\mathbf{x} - \tau\frac{\mathbf{q}}{|\mathbf{q}|}, \mathbf{q})\frac{d^3q}{|\mathbf{q}|}\,, \\ T^{\mu\nu}(t_n + \tau, \mathbf{x}) &= \int_{\mathbb{R}^3} q^\mu q^\nu\, f_n(\mathbf{x} - \tau\frac{\mathbf{q}}{|\mathbf{q}|}, \mathbf{q})\frac{d^3q}{|\mathbf{q}|}\,, \end{aligned} \tag{4.3.1}$$

$$S^\mu(t_n + \tau, \mathbf{x}) = -\int_{\mathbb{R}^3} q^\mu\,(f_n \ln f_n)(\mathbf{x} - \tau\frac{\mathbf{q}}{|\mathbf{q}|}, \mathbf{q})\frac{d^3q}{|\mathbf{q}|}\,, \tag{4.3.2}$$

with the ultra-relativistic initial phase density (3.6.7) at the maximizaton time t_n is given as

$$f_n(\mathbf{y}, \mathbf{q}) = f_J^*(n(t_n, \mathbf{y}), T(t_n, \mathbf{y}), \mathbf{u}(t_n, \mathbf{y}), \mathbf{q})\,. \tag{4.3.3}$$

Moreover n, T, u^μ are calculated from N^μ and $T^{\mu\nu}$ for the next time step from the following generally valid definitions

$$n = \sqrt{N^\mu N_\mu}, \qquad u^\mu = \frac{1}{n}N^\mu\,, \qquad T = \frac{1}{3n}u_\mu u_\nu\, T^{\mu\nu}\,. \tag{4.3.4}$$

In order to initialize the kinetic scheme for the next time step, we first require the following continuity conditions for the zero-components of the moments across the maximization time t_n, $n \geq 1$

$$\begin{aligned} N^0(t_n^+, \mathbf{x}) &= N^0(t_n^-, \mathbf{x})\,, \\ T^{0k}(t_n^+, \mathbf{x}) &= T^{0k}(t_n^-, \mathbf{x}),\ k = 1, 2, 3\,, \\ T^{00}(t_n^+, \mathbf{x}) &= T^{00}(t_n^-, \mathbf{x})\,. \end{aligned} \tag{4.3.5}$$

Since we are implementing the computation in these variables, these conditions are automatically enforced. Here we have used the following abbreviations for the one-sided limits across the maximization time t_n, $n \geq 1$, where ε is a positive real number

$$\begin{aligned} N^\mu(t_n^\pm, \mathbf{x}) &= \lim_{\varepsilon \to 0} N^\mu(t_n \pm \varepsilon, \mathbf{x})\,, \\ T^{\mu\nu}(t_n^\pm, \mathbf{x}) &= \lim_{\varepsilon \to 0} T^{\mu\nu}(t_n \pm \varepsilon, \mathbf{x})\,. \end{aligned}$$

Later on we will see in Proposition 4.3 that these conditions are necessary in order to guarantee the conservation laws for mass, momentum and energy across the maximization time t_n. Moreover we start again with a ultra-relativistic Jüttner distribution for the next time step. Then we obtain, using the constitutive relations (4.1.1), for the three-dimensional Euler equations which are valid for the t_n^+ side of the maximization time

$$\begin{aligned} N^0(t_n^+, \mathbf{x}) &= n(t_n^+, \mathbf{x}) \sqrt{1 + \mathbf{u}^2(t_n^+, \mathbf{x})}\,, \\ T^{0k}(t_n^+, \mathbf{x}) &= 4\, p(t_n^+, \mathbf{x})\, u^k(t_n^+, \mathbf{x}) \sqrt{1 + \mathbf{u}^2(t_n^+, \mathbf{x})}\,, \\ T^{00}(t_n^+, \mathbf{x}) &= p(t_n^+, \mathbf{x}) \left[3 + 4\, \mathbf{u}^2(t_n^+, \mathbf{x})\right]\,. \end{aligned} \tag{4.3.6}$$

Here $k = 1, 2, 3$ again denote a spatial indices. Since these components of the moments are continuous across the maximization time t_n, we can replace them by the free-flight moments for t_n^- and solve the equations (4.3.6) for $p, \mathbf{u}, n$ in order to initialize the kinetic scheme for the next time step by the following relations

$$p(t_n^+, \mathbf{x}) = \frac{1}{3} \left[-T^{00} + \sqrt{4(T^{00})^2 - 3 \sum_{k=1}^{3} (T^{0k})^2} \right]\,, \tag{4.3.7}$$

$$u^k(t_n^+, \mathbf{x}) = \frac{T^{0k}}{\sqrt{4p(t_n^+, \mathbf{x})[p(t_n^+, \mathbf{x}) + T^{00}]}}\,, \tag{4.3.8}$$

$$n(t_n^+, \mathbf{x}) = \frac{N^0}{\sqrt{1 + \sum_{k=1}^{3} [u^k(t_n^+, \mathbf{x})]^2}}\,. \tag{4.3.9}$$

In these formulas N^0, T^{00} and T^{0k} are abbreviations for the free-flight moments $N^0(t_n^-, \mathbf{x})$, $T^{00}(t_n^-, \mathbf{x})$ and $T^{0k}(t_n^-, \mathbf{x})$, respectively.

Note that the quantities on the left hand side have to be calculated in the prescribed order from the free-flight moments N^0, T^{00} and T^{0k}. Since they initialize the scheme for the next time step they conclude the formulation of the kinetic scheme.

4.3.1 Reduction of the Volume Integrals to Surface Integrals

Here we apply an important simplification to the volume integrals (4.3.1) and (4.3.2) for the free-flight moments. We can see in (4.3.3) that the fields $n(t,\mathbf{y})$, $T(t,\mathbf{y})$ and $\mathbf{u}(t,\mathbf{y})$ are not depending on $|\mathbf{q}|$ but only on the unit vector $\mathbf{w} = (w^1, w^2, w^3)^T = \frac{\mathbf{q}}{|\mathbf{q}|}$. This fact enables us to reduce the three-fold volume integrals to two-fold surface integrals by applying polar coordinates. Now integration with respect to $|\mathbf{q}|$ can be carried out explicitly, and we obtain the reduced surface integrals for the moments. For abbreviation we introduce

$$\phi(\mathbf{y},\mathbf{w}) = \frac{1}{4\pi}\frac{n(\mathbf{y})}{(\sqrt{1+\mathbf{u}^2(\mathbf{y})} - \mathbf{w}\cdot\mathbf{u}(\mathbf{y}))^3}\,, \quad \psi(\mathbf{y},\mathbf{w}) = \frac{3}{4\pi}\frac{(nT)(\mathbf{y})}{(\sqrt{1+\mathbf{u}^2(\mathbf{y})} - \mathbf{w}\cdot\mathbf{u}(\mathbf{y}))^4}\,, \tag{4.3.10}$$

then the reduced surface integrals for the moments can be written as

$$\begin{aligned}
N^0(t_n+\tau,\mathbf{x}) &= \oint\limits_{\partial B(0,1)} \phi(\mathbf{x}-\tau\mathbf{w},\mathbf{w})\,dS(\mathbf{w})\,,\\
N^k(t_n+\tau,\mathbf{x}) &= \oint\limits_{\partial B(0,1)} w^k\phi(\mathbf{x}-\tau\mathbf{w},\mathbf{w})\,dS(\mathbf{w})\,,\\
T^{00}(t_n+\tau,\mathbf{x}) &= \oint\limits_{\partial B(0,1)} \psi(\mathbf{x}-\tau\mathbf{w},\mathbf{w})\,dS(\mathbf{w})\,,\\
T^{0k}(t_n+\tau,\mathbf{x}) &= \oint\limits_{\partial B(0,1)} w^k\psi(\mathbf{x}-\tau\mathbf{w},\mathbf{w})\,dS(\mathbf{w})\,,\\
T^{km}(t_n+\tau,\mathbf{x}) &= \oint\limits_{\partial B(0,1)} w^kw^m\psi(\mathbf{x}-\tau\mathbf{w},\mathbf{w})\,dS(\mathbf{w})\,,
\end{aligned} \tag{4.3.11}$$

$$S^0(t_n+\tau,\mathbf{x}) = -\oint\limits_{\partial B(0,1)} \left[\ln\left(\frac{n(\mathbf{x}-\tau\mathbf{w})}{8\pi T^3(\mathbf{x}-\tau\mathbf{w})}\right) - 3\,n(\mathbf{x}-\tau\mathbf{w})\right]\phi(\mathbf{x}-\tau\mathbf{w},\mathbf{w})\,dS(\mathbf{w})\,, \tag{4.3.12}$$

$$S^k(t_n+\tau,\mathbf{x}) = -\oint\limits_{\partial B(0,1)} w^k\left[\ln\left(\frac{n(\mathbf{x}-\tau\mathbf{w})}{8\pi T^3(\mathbf{x}-\tau\mathbf{w})}\right) - 3\,n(\mathbf{x}-\tau\mathbf{w})\right]\phi(\mathbf{x}-\tau\mathbf{w},\mathbf{w})\,dS(\mathbf{w})\,.$$

Here $\mathbf{w} = \frac{\mathbf{q}}{|\mathbf{q}|}$ is the unit vector in direction of $\mathbf{q}$ and $B(\mathbf{x}_0, r)$ is the ball with radius r and center $\mathbf{x}_0$. Its boundary is the sphere $\partial B(\mathbf{x}_0, r)$. These surface integrals reflect the fact that in the ultra-relativistic case the particles are moving on the surface of the light cone. Using the Cauchy-Schwarz inequality one can prove that n, p, e resulting from the moment integrals (4.3.11) are well defined and positive quantities for all times and positions.

4.3.2 Proof of Conservation Laws and Entropy Inequality

In the following propositions we prove the conservation laws and entropy inequality for the kinetic scheme.

Proposition 4.2: *Let $0 < \tau < \tau_M$ and $n = 0, 1, 2, ...$ We consider the moments in the free-flight between the two maximization times t_n and t_{n+1}. Within this free-flight zone the moments $N^\mu(t_n + \tau, \mathbf{x})$, $T^{\mu\nu}(t_n + \tau, \mathbf{x})$ and the entropy four-vector $S^\mu(t_n + \tau, \mathbf{x})$ satisfy the following conservation laws in weak integral form*

$$\oint\limits_{\partial\Omega} N^\nu(t_n + \tau, \mathbf{x}) do_\nu = 0, \ \oint\limits_{\partial\Omega} T^{\mu\nu}(t_n + \tau, \mathbf{x}) do_\nu = 0, \ \oint\limits_{\partial\Omega} S^\nu(t_n + \tau, \mathbf{x}) do_\nu = 0\,. \tag{4.3.13}$$

Here $\Omega \subset \mathbb{R}^+_0 \times \mathbb{R}^3$ is a normal region in space-time with a piecewise smooth positively oriented boundary. The covariant vector do_ν is a positively oriented surface element to the boundary $\partial\Omega$. It can be written in covariant form as

$$do_\kappa = \varepsilon_{\kappa\lambda\mu\nu} \sum_{i,j,m=1}^{3} \frac{\partial x^\lambda}{\partial u^i} \frac{\partial x^\mu}{\partial u^j} \frac{\partial x^\nu}{\partial u^m} du^i\, du^j\, du^m\,,$$

where $x^\alpha = x^\alpha(u^1, u^2, u^3)$ is a positively oriented parametrization of the boundary $\partial\Omega$.

Remark. Note that these weak formulations correspond to the differential equations

$$\frac{\partial N^\nu}{\partial x^\nu}(t_n + \tau, \mathbf{x}) = 0, \quad \frac{\partial T^{\mu\nu}}{\partial x^\nu}(t_n + \tau, \mathbf{x}) = 0, \quad \frac{\partial S^\nu}{\partial x^\nu}(t_n + \tau, \mathbf{x}) = 0. \tag{4.3.14}$$

Proof: For $0 < \tau < \tau_M$ let be $t_n < t = t_n + \tau < t_{n+1} = t_n + \tau_M$. If we start with the relativistic Maxwellian (4.3.3) as the initial phase density at the time t_n we then obtain within the time-region $0 < t_n < t < t_n + \tau_M$ the free-flight density $f(t, \mathbf{x}, \mathbf{q}) = f(\mathbf{x} - \tau \frac{\mathbf{q}}{|\mathbf{q}|}, \mathbf{q})$. It satisfies the weak integral form of the free-flight transport equation (3.4.16). Therefore we get

$$\oint\limits_{\partial\Omega} q^\nu\, f(t, \mathbf{x}, \mathbf{q}) do_\nu = q^\nu \oint\limits_{\partial\Omega} f(t, \mathbf{x}, \mathbf{q}) do_\nu = 0\,. \tag{4.3.15}$$

The proof of (4.3.15) is given in Appendix A for the spatially one-dimensional case. The equation (4.3.15) and its multiplication with q^μ leads after integration with respect to $\mathbf{q}$ to the following equations

$$\begin{aligned} \int\limits_{\mathbb{R}^3} \left(\oint\limits_{\partial\Omega} q^\nu\, f(t, \mathbf{x}, \mathbf{q}) do_\nu \right) \frac{d^3q}{|\mathbf{q}|} = 0\,, \\ \int\limits_{\mathbb{R}^3} \left(\oint\limits_{\partial\Omega} q^\mu\, q^\nu\, f(t, \mathbf{x}, \mathbf{q}) do_\nu \right) \frac{d^3q}{|\mathbf{q}|} = 0\,. \end{aligned} \tag{4.3.16}$$

Since the volume integral with respect to $\mathbf{q}$ and the surface integral with respect to t and $\mathbf{x}$ are interchangeable, we can rewrite equations (4.3.16) in order to get the conservation laws

$$\oint\limits_{\partial\Omega}\left(\int\limits_{\mathbb{R}^3} q^\nu\, f(t,\mathbf{x},\mathbf{q})\frac{d^3q}{|\mathbf{q}|}\right)do_\nu = \oint\limits_{\partial\Omega} N^\nu(t_n+\tau\mathbf{x},\mathbf{q})do_\nu = 0\,,$$
$$\oint\limits_{\partial\Omega}\left(\int\limits_{\mathbb{R}^3} q^\mu\, q^\nu\, f(t,\mathbf{x},\mathbf{q})\frac{d^3q}{|\mathbf{q}|}\right)do_\nu = \oint\limits_{\partial\Omega} T^{\mu\nu}(t_n+\tau\mathbf{x},\mathbf{q})do_\nu = 0\,. \tag{4.3.17}$$

Let us use the fact that if $f(t,\mathbf{x},\mathbf{q}) = f(\mathbf{x}-\tau\frac{\mathbf{q}}{|\mathbf{q}|},\mathbf{q})$ is a solution of the free-flight equation (3.4.16), then $\ln f(t,\mathbf{x},\mathbf{q}) = \ln f(\mathbf{x}-\tau\frac{\mathbf{q}}{|\mathbf{q}|},\mathbf{q})$ will be the solution of

$$q^\mu\frac{\partial \ln f}{\partial x^\mu} = 0\,, \qquad \mu = 0,1,2,3. \tag{4.3.18}$$

Now we define

$$\psi(t,\mathbf{x},\mathbf{q}) = -(f_n\ln f_n)(\mathbf{x}-\tau\frac{\mathbf{q}}{|\mathbf{q}|},\mathbf{q})\,. \tag{4.3.19}$$

Using the product rule and equations (3.4.16), (4.3.18) we conclude that ψ also satisfies the free-flight equation, namely

$$q^\mu\frac{\partial \psi}{\partial x^\mu} = 0\,, \qquad \mu = 0,1,2,3\,, \tag{4.3.20}$$

which in Oleinik'e weak integral form gives

$$\oint\limits_{\partial\Omega} q^\nu\,\psi(t,\mathbf{x},\mathbf{q})do_\nu = 0\,. \tag{4.3.21}$$

This is coming from the Gauss Divergence Theorem.

Integrating equation (4.3.21) with respect to $\mathbf{q}$ and interchanging the volume and surface integrals, we finally get, using equation (4.3.2)

$$\oint\limits_{\partial\Omega}\left(\int\limits_{\mathbb{R}^3} q^\nu\,\psi(t,\mathbf{x},\mathbf{q})\frac{d^3q}{|\mathbf{q}|}\right)do_\nu = \oint\limits_{\partial\Omega} S^\nu(t_n+\tau\mathbf{x},\mathbf{q})do_\nu = 0\,. \tag{4.3.22}$$

■

Proposition 4.3: *Let $\Omega\subset\mathbb{R}_0^+\times\mathbb{R}^3$ be any bounded convex region in time and space. By do_ν we denote the positively oriented surface element of $\partial\Omega$. Let $\tau_M>0$ be a fixed time step. The moment representations* (4.3.1) *and* (4.3.2) *calculated by the iterated scheme defined above have the following properties:*

(i) *The conservation laws for the particle number, the momentum and energy hold, i.e.*

$$\oint\limits_{\partial\Omega} N^\nu do_\nu = 0, \quad \oint\limits_{\partial\Omega} T^{\mu\nu}do_\nu = 0. \tag{4.3.23}$$

(ii) *The following entropy inequality is satisfied*

$$\oint_{\partial\Omega} S^\nu do_\nu \geq 0. \tag{4.3.24}$$

Proof: Let be $\tau_M > 0$. We first prove part (i) of the proposition. The time axis is divided by the maximization times $0 = t_0 < t_1 < t_2 < \cdots$, so that the convex domain Ω can be decomposed into the subdomains

$$\begin{cases} \Omega_0 &= \left\{(\delta, \mathbf{x}) \in \Omega \middle| \, 0 \leq \delta \leq \frac{t_0+t_1}{2}\right\}, \\ \Omega_n &= \left\{(\delta, \mathbf{x}) \in \Omega \middle| \, \frac{t_{n-1}+t_n}{2} \leq \delta \leq \frac{t_n+t_{n+1}}{2}\right\} (n = 1, 2, 3, \dots). \end{cases} \tag{4.3.25}$$

Since $\oint_{\partial\Omega} N^\nu do_\nu = \sum_{n\geq 0} \oint_{\partial\Omega_n} N^\nu do_\nu$ and $\oint_{\partial\Omega} T^{\mu\nu} do_\nu = \sum_{n\geq 0} \oint_{\partial\Omega_n} T^{\mu\nu} do_\nu$, it is sufficient to assume without loss of generality that the time range

$$\Theta_\Omega = \left\{t \geq 0 \middle| \text{ there exists an } \mathbf{x} \in \mathbb{R}^3 \text{ such that } (t, \mathbf{x}) \in \Omega\right\}$$

of Ω contains at most one maximization time t.
Then for ε in the range $0 < \varepsilon < \frac{1}{2}\tau_M$ we define a further decomposition of each $\Omega_n, n \geq 1$, into three parts

$$\begin{cases} \Omega^\varepsilon_{n,L} &= \left\{(\delta, \mathbf{x}) \in \Omega_n \middle| \, \delta \leq t_n - \varepsilon\right\}, \\ \Omega^\varepsilon_{n,M} &= \left\{(\delta, \mathbf{x}) \in \Omega_n \middle| \, t_n - \varepsilon \leq \delta \leq t_n + \varepsilon\right\}, \\ \Omega^\varepsilon_{n,R} &= \left\{(\delta, \mathbf{x}) \in \Omega_n \middle| \, \delta \geq t_n + \varepsilon\right\}. \end{cases} \tag{4.3.26}$$

The decompositions which are illustrated in the following figure, were also applied in order to prove the conservation laws and the entropy inequality for the classical Euler equations, see [18] and Subsection 2.2.1.

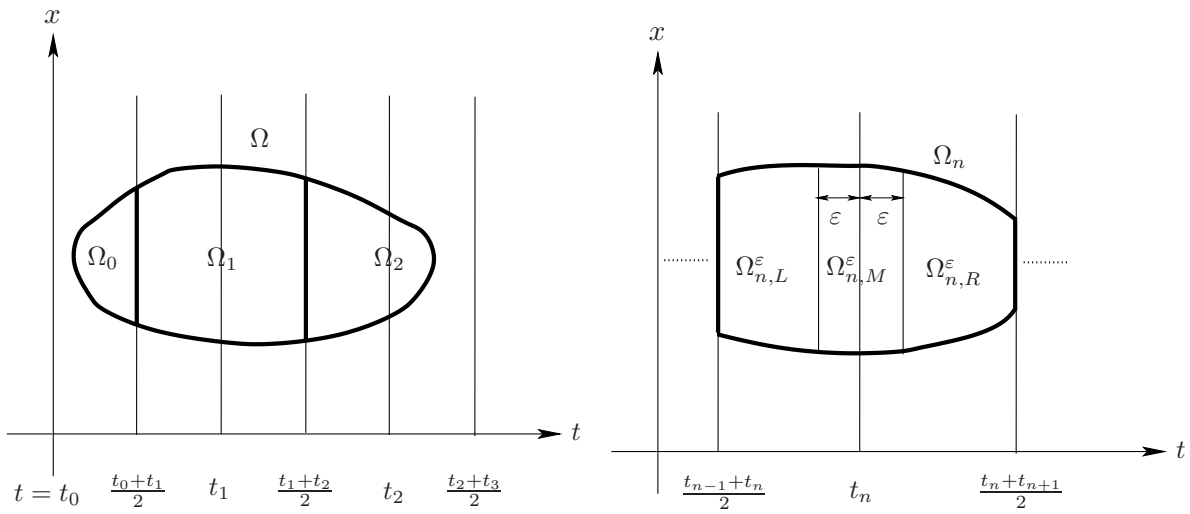

Figure 4.2: The decompositions of Ω and Ω_n.

We obtain

$$\oint\limits_{\partial\Omega_n} N^\nu do_\nu = \oint\limits_{\partial\Omega^\varepsilon_{n,L}} N^\nu do_\nu + \oint\limits_{\partial\Omega^\varepsilon_{n,R}} N^\nu do_\nu + \oint\limits_{\partial\Omega^\varepsilon_{n,M}} N^\nu do_\nu,$$

$$\oint\limits_{\partial\Omega_n} T^{\mu\nu} do_\nu = \oint\limits_{\partial\Omega^\varepsilon_{n,L}} T^{\mu\nu} do_\nu + \oint\limits_{\partial\Omega^\varepsilon_{n,R}} T^{\mu\nu} do_\nu + \oint\limits_{\partial\Omega^\varepsilon_{n,M}} T^{\mu\nu} do_\nu\,.$$

Since the first two integrals on the right hand side are in the free-flight zone, so we conclude from equation (4.3.17) that these integrals vanish, i.e.,

$$\oint\limits_{\partial\Omega^\varepsilon_{n,L}} N^\nu do_\nu = \oint\limits_{\partial\Omega^\varepsilon_{n,R}} N^\nu do_\nu = 0, \qquad \oint\limits_{\partial\Omega^\varepsilon_{n,L}} T^{\mu\nu} do_\nu = \oint\limits_{\partial\Omega^\varepsilon_{n,R}} T^{\mu\nu} do_\nu = 0.$$

This implies that using the domain $\Omega^*_n = \{\mathbf{x} \in \mathbb{R}^3 | (t_n, \mathbf{x}) \in \Omega\}$

$$\begin{aligned}\oint\limits_{\partial\Omega_n} N^\nu do_\nu &= \oint\limits_{\partial\Omega^\varepsilon_{n,M}} N^\nu do_\nu = \lim_{\varepsilon\to 0} \oint\limits_{\partial\Omega^\varepsilon_{n,M}} N^\nu do_\nu\,,\\ &= \int_{\Omega^*_n} \left\{ \int q^0 \left[f_n(\mathbf{x},\mathbf{q}) - f_{n-1}(\mathbf{x} - \tau_M \frac{\mathbf{q}}{|\mathbf{q}|}) \right] \frac{d^3q}{|\mathbf{q}|} \right\} d^3\mathbf{x}\,,\end{aligned}$$

and

$$\begin{aligned}\oint\limits_{\partial\Omega_n} T^{\mu\nu} do_\nu &= \oint\limits_{\partial\Omega^\varepsilon_{n,M}} T^{\mu\nu} do_\nu = \lim_{\varepsilon\to 0} \oint\limits_{\partial\Omega^\varepsilon_{n,M}} T^{\mu\nu} do_\nu\,,\\ &= \int_{\Omega^*_n} \left\{ \int q^0 q^\mu \left[f_n(\mathbf{x},\mathbf{q}) - f_{n-1}(\mathbf{x} - \tau_M \frac{\mathbf{q}}{|\mathbf{q}|}) \right] \frac{d^3q}{|\mathbf{q}|} \right\} d^3\mathbf{x},\end{aligned}$$

where t_{n-1} is the maximization time that preceedes the maximization time t_n. The phase density f_n has to be taken to be the ultra-relativistic Jüttner phase density (3.6.7).

The last integral expression in these equations vanishes due to the continuity conditions (4.3.5) across the maximization time t_n, i.e.,

$$\begin{aligned} N^0(t_n^+, \mathbf{x}) &= N^0(t_n^-, \mathbf{x})\,,\\ T^{0\mu}(t_n^+, \mathbf{x}) &= T^{0\mu}(t_n^-, \mathbf{x}),\ \mu = 0,1,2,3\,,\end{aligned} \tag{4.3.27}$$

which yields

$$\begin{aligned}\int_{\mathbb{R}^3} q^0 f_n(\mathbf{x},\mathbf{q}) \frac{d^3q}{|\mathbf{q}|} &= \int_{\mathbb{R}^3} q^0 f_{n-1}(\mathbf{x} - \tau_M \frac{\mathbf{q}}{|\mathbf{q}|}, \mathbf{q}) \frac{d^3q}{|\mathbf{q}|}\,,\\ \int_{\mathbb{R}^3} q^0 q^\mu f_n(\mathbf{x},\mathbf{q}) \frac{d^3q}{|\mathbf{q}|} &= \int_{\mathbb{R}^3} q^0 q^\mu f_{n-1}(\mathbf{x} - \tau_M \frac{\mathbf{q}}{|\mathbf{q}|}, \mathbf{q}) \frac{d^3q}{|\mathbf{q}|}\,.\end{aligned} \tag{4.3.28}$$

This expresses the constraints that were used for the maximization procedure. We have thus established that the weak form (4.3.23) for an arbitrary convex domain Ω is implied by the

representations (4.3.1).

Regarding the second part (ii) which states the existence of the entropy inequality (4.3.24), we start the proof again with the decompositions (4.3.25) and (4.3.26) of Ω. Since $\int_{\partial\Omega} S^\nu do_\nu = \sum_{n\geq 0}\int_{\partial\Omega_n} S^\nu do_\nu$, it is sufficient to prove $\int_{\partial\Omega_n} S^\nu do_\nu \geq 0$ for each n. We obtain

$$\oint_{\partial\Omega_n} S^\nu do_\nu = \oint_{\partial\Omega^\varepsilon_{n,L}} S^\nu do_\nu + \oint_{\partial\Omega^\varepsilon_{n,R}} S^\nu do_\nu + \oint_{\partial\Omega^\varepsilon_{n,M}} S^\nu do_\nu \,. \tag{4.3.29}$$

Again the first two integrals lie in the free-flight zone. We can see from equation (4.3.22) that these integrals vanish i.e., $\oint_{\partial\Omega^\varepsilon_{n,R}} S^\nu do_\nu = 0$, and $\oint_{\partial\Omega^\varepsilon_{n,L}} S^\nu do_\nu = 0$.
For every sufficiently small $\varepsilon > 0$ the following holds

$$\begin{aligned}\oint\limits_{\partial\Omega_n} S^\nu do_\nu &= \lim_{\varepsilon\to 0} \oint\limits_{\partial\Omega^\varepsilon_{n,M}} S^\nu do_\nu \qquad (4.3.30)\\ &= \int\limits_{\Omega^*_n} \left\{ \int_{\mathbb{R}^3} q^0 \left[-(f_n \ln f_n)(\mathbf{x},\mathbf{q}) + (f_{n-1}\ln f_{n-1})(\mathbf{x} - \tau_M \frac{\mathbf{q}}{|\mathbf{q}|}, \mathbf{q}) \right] \frac{d^3q}{|\mathbf{q}|} \right\} d^3\mathbf{x},\end{aligned}$$

where $\Omega^*_n = \{\mathbf{x}\in\mathbb{R}^3 | (t_n,\mathbf{x})\in\Omega\}$, and $t_{n-1} < t_n$ is the maximization time that preceeds t_n. Next we shall show that the integral (4.3.30) is non-negative. Applying Lemma 2.3 for $u = f_n(\mathbf{x},\mathbf{q})$ and $v = f_{n-1}(\mathbf{x} - \tau_M \frac{\mathbf{q}}{|\mathbf{q}|}, \mathbf{q})$ we get

$$\begin{aligned}&\int_{\mathbb{R}^3} q^0 \left[-(f_n \ln f_n)(\mathbf{x},\mathbf{q}) + (f_{n-1}\ln f_{n-1})(\mathbf{x} - \tau_M \frac{\mathbf{q}}{|\mathbf{q}|}, \mathbf{q}) \right] \frac{d^3q}{|\mathbf{q}|}\\ &\qquad = -\int_{\mathbb{R}^3} q^0 \left[1 + \ln f_n(\mathbf{x},\mathbf{q})\right] \left[f_n(\mathbf{x},\mathbf{q}) - f_{n-1}(\mathbf{x} - \tau_M \frac{\mathbf{q}}{|\mathbf{q}|}, \mathbf{q}) \right] \frac{d^3q}{|\mathbf{q}|}\\ &\qquad\qquad + \int_{\mathbb{R}^3} R\left(f_n(\mathbf{x},\mathbf{q}), f_{n-1}(\mathbf{x} - \tau_M \frac{\mathbf{q}}{|\mathbf{q}|}, \mathbf{q}) \right) \frac{d^3q}{|\mathbf{q}|}. \qquad (4.3.31)\end{aligned}$$

The second integral is non-negative and the first one vanishes due to the following reasons. Using Jüttner's phase density for $f_n(\mathbf{x},\mathbf{q})$ we have

$$\ln f_n(\mathbf{x},\mathbf{q}) = \ln\left[\frac{n(\mathbf{x})}{8\pi T^3(\mathbf{x})} \exp\left(\frac{-u_\nu q^\nu}{T(\mathbf{x})} \right) \right] = A(x) - B(x) u_\nu q^\nu \,, \tag{4.3.32}$$

where $A(\mathbf{x}) = \ln \frac{n(\mathbf{x})}{8\pi T^3(\mathbf{x})}$ and $B(\mathbf{x}) = \frac{1}{T(\mathbf{x})}$. We use the value (4.3.32) of $\ln f_n(\mathbf{x},\mathbf{q})$ in (4.3.31). Using the definitions (4.3.1) for N^μ, $T^{\mu\nu}$ and the continuity conditions (4.3.5) for the zero components N^0, $T^{0\nu}$, we can see that the first integral in (4.3.31) is zero. We have thus established the entropy inequality (4.3.24). ∎

4.3.3 Positivity and L^1-Stability of the Kinetic Scheme

Here we show that our kinetic scheme preserve positivity of the density and pressure. A similar theorem has been proved in Chapter 2 for the classical kinetic scheme.

Theorem 4.4: *Assume that the initial distribution function satisfies $f_n(\mathbf{y},\mathbf{q}) \geq 0$, additionally $f_n(\mathbf{y},\mathbf{q})$ does not vanish almost everywhere for all microscopic velocities $\mathbf{q}$, macroscopic velocities $\mathbf{u}$, positive densities n and pressures p. Then the numerical solution obtained by the resulting kinetic scheme has the following property: Its density, pressure and total energy remain positive for all times:*

$$n(t_n+\tau,\mathbf{x}) > 0\,, \quad p(t_n+\tau,\mathbf{x}) = \frac{1}{3}e(t_n+\tau,\mathbf{x}) > 0\,, \quad E(t_n+\tau,\mathbf{x}) > 0\,. \tag{4.3.33}$$

This also mean that the numerical scheme defined by (4.3.1) *and* (4.3.2) *is stable in* L^1.

Proof. The particle density is defined as $n = \sqrt{N^\mu N_\mu}$. Therefore we have to prove that

$$N^\mu\, N_\mu(t_n+\tau,\mathbf{x}) = \left((N^0)^2 - (N^1)^2 - (N^2)^2 - (N^3)^2\right)(t_n+\tau,\mathbf{x}) > 0. \tag{4.3.34}$$

According to the Cauchy-Schwarz inequality, if we have two functions f and g then

$$\left(\int_a^b f\cdot g\,dx\right)^2 \leq \left(\int_a^b f^2\,dx\right)\cdot\left(\int_a^b g^2\,dx\right)\,, \tag{4.3.35}$$

where equality holds iff the functions f and g are linearly dependent.

From the moments $(4.3.1)_1$, we have

$$N^0(t_n+\tau,\mathbf{x}) = \int_{\mathbb{R}^3} f_n(\mathbf{x}-\tau\frac{\mathbf{q}}{|\mathbf{q}|},\mathbf{q})\,d^3q > 0\,. \tag{4.3.36}$$

Using again the free-flight moments $(4.3.1)_1$ and the Cauchy Schwarz inequality, we get

$$\begin{aligned}
(N^1)^2(t_n+\tau,\mathbf{x}) &= \left(\int_{\mathbb{R}^3} q^1\, f_n(\mathbf{x}-\tau\frac{\mathbf{q}}{|\mathbf{q}|},\mathbf{q})\,\frac{d^3q}{|\mathbf{q}|}\right)^2 \\
&= \left(\int_{\mathbb{R}^3}\left(\left(\frac{q^1}{|\mathbf{q}|}\sqrt{f_n}\right)\cdot\left(\sqrt{f_n}\right)\right)(\mathbf{x}-\tau\frac{\mathbf{q}}{|\mathbf{q}|},\mathbf{q})\,d^3q\right)^2 \\
&< \left(\int_{\mathbb{R}^3}\left(\frac{q^1}{|\mathbf{q}|}\sqrt{f_n}\right)^2(\mathbf{x}-\tau\frac{\mathbf{q}}{|\mathbf{q}|},\mathbf{q})\,d^3q\right)\cdot\left(\int_{\mathbb{R}^3}\left(\sqrt{f_n}\right)^2(\mathbf{x}-\tau\frac{\mathbf{q}}{|\mathbf{q}|},\mathbf{q})\,d^3q\right) \\
&= N^0(t_n+\tau,\mathbf{x})\left(\int_{\mathbb{R}^3}\left(\frac{q^1}{|\mathbf{q}|}\right)^2 f_n(\mathbf{x}-\tau\frac{\mathbf{q}}{|\mathbf{q}|},\mathbf{q})\,d^3q\right).
\end{aligned} \tag{4.3.37}$$

In Cauchy-Schwarz inequality we have not taken the equality sign, because the functions $\frac{q^1}{|\mathbf{q}|}\sqrt{f_n(\mathbf{y},\mathbf{q})}$ and $\sqrt{f_n(\mathbf{y},\mathbf{q})}$ are linearly independent. Similarly

$$\begin{aligned}
(N^2)^2(t_n+\tau,\mathbf{x}) &< N^0(t_n+\tau,\mathbf{x})\left(\int_{\mathbb{R}^3}\left(\frac{q^2}{|\mathbf{q}|}\right)^2 f_n(\mathbf{x}-\tau\frac{\mathbf{q}}{|\mathbf{q}|},\mathbf{q})\,d^3q\right), \\
(N^3)^2(t_n+\tau,\mathbf{x}) &< N^0(t_n+\tau,\mathbf{x})\left(\int_{\mathbb{R}^3}\left(\frac{q^3}{|\mathbf{q}|}\right)^2 f_n(\mathbf{x}-\tau\frac{\mathbf{q}}{|\mathbf{q}|},\mathbf{q})\,d^3q\right).
\end{aligned} \tag{4.3.38}$$

Now we use (4.3.37) and (4.3.38) in (4.3.34). Also in ultra-relativistic case

$$|\mathbf{q}| = \sqrt{(q^1)^2 + (q^2)^2 + (q^3)^2}\,,$$

therefore we get

$$\begin{aligned} N^\mu\, N_\mu(t_n+\tau,\mathbf{x}) &= \left((N^0)^2 - (N^1)^2 - (N^2)^2 - (N^3)^2\right)(t_n+\tau,\mathbf{x}) \\ &> N^0(t_n+\tau,\mathbf{x}) \left(N^0(t_n+\tau,\mathbf{x}) - \int_{\mathbb{R}^3} \frac{\sum_{k=1}^{3}(q^k)^2}{|\mathbf{q}|^2} f_n(\mathbf{x}-\tau\frac{\mathbf{q}}{|\mathbf{q}|},\mathbf{q})\, d^3q \right) \\ &= N^0(t_n+\tau,\mathbf{x}) \left[N^0(t_n+\tau,\mathbf{x}) - \int_{\mathbb{R}^3} f_n(\mathbf{x}-\tau\frac{\mathbf{q}}{|\mathbf{q}|},\mathbf{q})\, d^3q \right]. \\ &= 0\,. \end{aligned}$$

Thus we have proved that $n(t_n+\tau,\mathbf{x}) = \sqrt{N^\mu\, N_\mu(t_n+\tau,\mathbf{x})} > 0$.

Now using the kinetic scheme $(4.3.1)_2$ and relation (3.6.9), we get

$$\begin{aligned} p(t_n+\tau,\mathbf{x}) = \frac{1}{3}e(t_n+\tau,\mathbf{x}) &= \frac{1}{3}u_\mu u_\nu T^{\mu\nu}(t_n+\tau,\mathbf{x}) \\ &= \frac{1}{3}\int_{\mathbb{R}^3} q^\mu q^\nu\, f_n(\mathbf{x}-\tau\frac{\mathbf{q}}{|\mathbf{q}|},\mathbf{q})\frac{d^3q}{|\mathbf{q}|}\, u_\mu u_\nu \\ &= \frac{1}{3}\int_{\mathbb{R}^3} (q^\mu u_\mu)^2\, f_n(\mathbf{x}-\tau\frac{\mathbf{q}}{|\mathbf{q}|},\mathbf{q})\frac{d^3q}{|\mathbf{q}|} \\ &> 0\,. \end{aligned}$$

Thus we conclude that $p(t_n+\tau,\mathbf{x}) > 0$. Also we know from $(4.3.1)_2$ that

$$T^{00}(t_n+\tau,\mathbf{x}) = \int_{\mathbb{R}^3} |\mathbf{q}| f_n(\mathbf{x}-\tau\frac{\mathbf{q}}{|\mathbf{q}|},\mathbf{q})\, d^3q > 0\,. \tag{4.3.39}$$

Now since our scheme is conservative, using (4.3.36), (4.3.39) and $|\mathbf{q}| = \sqrt{\sum_{k=1}^{3}(q^k)^2}$, we have

$$\begin{aligned} ||N^0(t_n+\tau,.)||_{L^1(R)} &= \int_{\mathbb{R}^3} |N^0(t_n+\tau,\mathbf{x})| d^3\mathbf{x} = \int_{\mathbb{R}^3} N^0(t_n+\tau,\mathbf{x}) d^3\mathbf{x} \\ &= \int_{\mathbb{R}^3} N^0(t_n,\mathbf{x}) d^3\mathbf{x} = \int_{\mathbb{R}^3} |N^0(t_n,\mathbf{x})| d^3\mathbf{x} \\ &= ||N^0(t_n,.)||_{L^1(R)}\,. \end{aligned}$$

Similarly $||T^{00}(t_n+\tau,.)||_{L^1(R)} = \|T^{00}(t_n,.)\|_{L^1(R)}$. Now using (4.3.1) with $\mathbf{y} = \mathbf{x} - \tau\frac{\mathbf{q}}{|\mathbf{q}|}$ and

Cauchy-schwarz inequality (4.3.35) we get

$$\begin{aligned}
||T^{0k}(t_n+\tau,.)||_{L^1(R)} &= \int_{\mathbb{R}^3}\left|\int_{\mathbb{R}^3} q^k f_n(\mathbf{y},\mathbf{q})\,\frac{d^3q}{|\mathbf{q}|}\right| d^3\mathbf{x} \\
&= \int_{\mathbb{R}^3}\left|\int_{\mathbb{R}^3}\left(\sqrt{f_n}\right)\left(q^k\sqrt{f_n}\right)(\mathbf{y},\mathbf{q})\frac{d^3q}{|\mathbf{q}|}\right| d^3\mathbf{x} \\
&< \left[\int_{\mathbb{R}^3}\left|\int_{\mathbb{R}^3} f_n(\mathbf{y},\mathbf{q})\frac{d^3q}{|\mathbf{q}|}\right| d^3\mathbf{x}\cdot\int_{\mathbb{R}^3}\left|\int_{\mathbb{R}^3}|\mathbf{q}|^2 f_n(\mathbf{y},\mathbf{q})\frac{d^3q}{|\mathbf{q}|}\right| d^3\mathbf{x}\right]^{\frac{1}{2}} \\
&= \left(||n(t_n,.)||_{L^1(R)}\,||T^{00}(t_n,.)||_{L^1(R)}\right)^{\frac{1}{2}}.
\end{aligned}$$

This proves the L^1 stability of the scheme. ■

4.3.4 From the Kinetic Scheme to the Eulerian Limit ($\tau_M \to 0$)

In the previous sections we have shown how to calculate the solution of the kinetic schemes. This was done for the prescribed initial data of n, u and p for a given free-flight time step $\tau_M > 0$. If we calculate these solutions for $\tau_M \to 0$ then we get the Eulerian limit

$$N^\mu \to n\,u^\mu, \qquad T^{\mu\nu} \to -p\,g^{\mu\nu} + 4pu^\mu u^\nu, \qquad S^\mu \to n\,u^\mu \ln\frac{n^4}{p^3}\,. \tag{4.3.40}$$

First we pass to the Eulerian limit (4.3.40) at the points of smoothness in the following way using (3.4.16)

$$\begin{aligned}
\lim_{\tau\to 0}\frac{\partial}{\partial\tau}N^0(t_n+\tau,\mathbf{x}) &= \lim_{\tau\to 0}\frac{\partial}{\partial\tau}(n(t_n+\tau,\mathbf{x})\sqrt{1+u^2(t_n+\tau,\mathbf{x})}\,) \\
&= \lim_{\tau\to 0}\frac{\partial}{\partial\tau}\int_{\mathbb{R}^3}|\mathbf{q}|f_n(\mathbf{x}-\tau\frac{\mathbf{q}}{|\mathbf{q}|},\mathbf{q})\frac{d^3q}{|\mathbf{q}|} \\
&= -\lim_{\tau\to 0}\int_{\mathbb{R}^3}|\mathbf{q}|\sum_{k=1}^3\frac{q^k}{|\mathbf{q}|}\frac{\partial}{\partial x^k}f_n(\mathbf{x}-\tau\frac{\mathbf{q}}{|\mathbf{q}|},\mathbf{q})\frac{d^3q}{|\mathbf{q}|} \\
&= -\int_{\mathbb{R}^3}\sum_{k=1}^3 q^k\frac{\partial}{\partial x^k}f_n(\mathbf{x},\mathbf{q})\frac{d^3q}{|\mathbf{q}|} \\
&= -\sum_{k=1}^3\frac{\partial}{\partial x^k}(u^k(t_n^+,\mathbf{x})n(t_n^+,\mathbf{x})) \\
&= -\nabla\cdot(\mathbf{u}(t_n^+,\mathbf{x})n(t_n^+,\mathbf{x}))\,.
\end{aligned}$$

This implies

$$\frac{\partial}{\partial t}(n(t_n^+,\mathbf{x})\sqrt{1+u^2(t_n^+,\mathbf{x})}\,) + \nabla\cdot(\mathbf{u}(t_n^+,\mathbf{x})n(t_n^+,\mathbf{x})) = 0\,, \tag{4.3.41}$$

which is the first Euler equation (4.1.12). Similarly we get the other two Euler equations if we differentiate $T^{00}(t_n+\tau,\mathbf{x})$ and $T^{0k}(t_n+\tau,\mathbf{x})$ with respect to τ and pass to the limit $\tau\to 0$.

Secondly, on the left hand sides of (4.3.40) there are the moments N^μ, $T^{\mu\nu}$ and S^μ as calculated by the kinetic scheme see (4.3.1) and (4.3.2). Since we have already established the conservation laws and the entropy inequality for the solution of the kinetic scheme in Proposition 4.3, we conclude from (4.3.40) that this also results for the weak entropy solution in the Eulerian limit $\tau_M \to 0$. The weak entropy solution in the Eulerian limit in one space dimension is given by (4.1.17), (4.1.18) and (4.1.19).

4.4 Non-relativistic Versus Relativistic Kinetic Schemes

Here we compare the kinetic scheme for the ultra-relativistic Euler equations with the corresponding kinetic scheme for the non-relativistic Euler equations.

Common properties:

The basic ingredients of the kinetic scheme are the same in both cases, as given below.

a) There are given initial data for the mass-density, denoted by ρ in the classical case, the velocity $\mathbf{v}$ and the pressure p, which can be chosen as the five basic variables in the Euler equations.

b) There is a phase density f_n, usually called the **Maxwellian**, which describes the velocity distribution for the atoms of a gas in local equilibrium in terms of the five basic variables.

c) There is a time step $\tau_M > 0$ and a corresponding sequence of equidistant time steps $t_n = n\,\tau_M$ with $n \geq 0$, also called the maximization times, see Chapter 2.

d) At each maximization time $t = t_n$ we take the Maxwellian phase density, starting initially from the given initial data for $n = 0$. This Maxwellian is used as an initial phase density in order to solve the **collision free** kinetic phase density within the time range $t_n < t_n + \tau < t_{n+1}$, which will be called a free-flight interval. All thermodynamic quantities are algebraic combinations of moment integrals from this free-flight phase density f, and therefore they are defined everywhere in the free-flight interval under consideration.

It is very important to note here that the free-flight phase density is in general not a Maxwellian. Therefore in the free-flight intervals of the kinetic scheme the gas is usually neither in equilibrium nor does it satisfy the isotropic constitutive relations for the Euler equations !

e) In the free-flight intervals it can be seen very easily that the conservation laws for mass, momentum, energy and even for the entropy hold. The requirements that the kinetic schemes must satisfy the conservation laws and the entropy inequality across each maximization time t_{n+1} turns out to be equivalent to the five **continuity conditions**, which state that the "densities" written under the time-derivatives in the conservation laws must be continuous across t_{n+1}.

In turn, the continuity conditions must be used in order to **initialize** the kinetic schemes for

the next time step t_{n+1}, after the free-flight was performed in the time interval $t_n < t < t_{n+1}$.

Differences in the two schemes:

Now there comes an interesting difference.

A) In the **non-relativistic case** the densities for mass, momentum and energy are given by ρ, $\rho\,\mathbf{v}$ and $\frac{1}{2}\,\rho\,\mathbf{v}^2 + \frac{p}{\gamma-1}$, and hence they are algebraic functions of the primitive variables ρ, $\mathbf{v}$, p. Here it is crucial to note that this is even true in the free-flight phase, where the gas is not in local equilibrium. Due to the continuity conditions these densities and hence the five basic variables are continuous across the maximization time.

In contrast, the non-relativistic fluxes of momentum and energy, which are moment integrals of the classical phase densities, are in general discontinuous across t_{n+1}, since the gas is not isotropic in the free-flight domain immediately to the left of t_{n+1}.

B) In the **relativistic case** the densities under the time derivatives in the conservation laws are given by N^0 and $T^{0\mu}$, and in the free-flight intervals they cannot be written as functions of the basic variables n, $\mathbf{v} = \frac{\mathbf{u}}{\sqrt{1+\mathbf{u}^2}}$ and p. This is a consequence of the generally valid equations $n = \sqrt{N^\mu N_\mu}$, $u^\mu = \frac{1}{n}\,N^\mu$ and and $p = \frac{1}{3}\,(u_\mu u_\nu - g_{\mu\nu})\,T^{\mu\nu}$, which depend on **all** components of the tensors N^μ, $T^{\mu\nu}$.

Immediately before the maximization time t_{n+1} we have a non-isotropic tensor $T^{\mu\nu}_-$ in the free-flight regime, whereas at t_{n+1} we have the isotropic tensor $T^{\mu\nu}_+$ which satisfies the constitutive Euler-relations (4.1.1) in local equilibrium. Combining this with the argumentation above and comparing with the evaluation (4.3.7)-(4.3.9) of the continuity conditions we finally conclude that the basic fields calculated from the relativistic kinetic scheme may in general lead to jumps across the maximization times.

Finally we note that this would not be the case if we choose the zero-components N^0 and $T^{0\mu}$ as the basic variables of the relativistic Euler system. These are usually called "conservative variables" in the upwind and central conservative schemes.

4.5 A Kinetic Scheme for the One-Dimensional Case

In the following we are looking for spatially one-dimensional solutions, which are nevertheless solutions to the full three dimensional equations. We only consider solutions which depend on t and $x = x^1$ and satisfy $n = n(t,x)$, $\mathbf{u} = (u(t,x), 0, 0)$, $p = p(t,x)$. We will use the generally valid equation $p = nT$ and go back to the full three-dimensional scheme.

In order to calculate the surface integrals (4.3.11) and (4.3.12) again we introduce instead of the unit vector $\mathbf{w}$ the new variables $-1 \le \xi \le 1$ and $0 \leqq \varphi \leqq 2\pi$ by

$$w^1 = \xi\,, \qquad w^2 = \sqrt{1-\xi^2}\sin\varphi\,, \qquad w^3 = \sqrt{1-\xi^2}\cos\varphi\,, \tag{4.5.1}$$

with the surface element $dS(\mathbf{w}) = d\xi d\varphi$.

Note that the quantities n, T, u in the integrals (4.3.11) and (4.3.12) do not depend on the variable φ. This fact enables us to carry out the integration with respect to φ directly. Thus the two-fold surface integral reduces to a simple $\xi-$integral. For abbreviation we introduce

$$\phi(y,\xi) = \frac{1}{2}\frac{n(y)}{(\sqrt{1+u^2(y)} - \xi u(y))^3}\,, \quad \psi(y,\xi) = \frac{3}{2}\frac{p(y)}{(\sqrt{1+u^2(y)} - \xi u(y))^4}\,, \tag{4.5.2}$$

then the reduced integrals for the moments can be written as

$$N^0(t_n+\tau,x) = \int_{-1}^{1} \phi(x-\tau\xi,\xi)\,d\xi\,, \quad N^1(t_n+\tau,x) = \int_{-1}^{1} \xi\phi(x-\tau\xi,\xi)\,d\xi\,, \tag{4.5.3}$$

$$\begin{aligned} T^{00}(t_n+\tau,x) &= \int_{-1}^{1} \psi(x-\tau\xi,\xi)\,d\xi\,,\\ T^{01}(t_n+\tau,x) &= \int_{-1}^{1} \xi\psi(x-\tau\xi)\,d\xi\,,\\ T^{11}(t_n+\tau,x) &= \int_{-1}^{1} \xi^2\psi(x-\tau\xi)\,d\xi\,, \end{aligned} \tag{4.5.4}$$

$$\begin{aligned} S^0(t_n+\tau,x) &= -\int_{-1}^{1} \left[\ln\left(\frac{n^4(x-\tau\xi)}{8\pi p^3(x-\tau\xi)}\right) - 3\,n(x-\tau\xi)\right]\phi(x-\tau\xi,\xi)\,d\xi\,,\\ S^1(t_n+\tau,x) &= -\int_{-1}^{1} \xi\left[\ln\left(\frac{n^4(x-\tau\xi)}{8\pi p^3(x-\tau\xi)}\right) - 3\,n(x-\tau\xi)\right]\phi(x-\tau\xi,\xi)\,d\xi\,. \end{aligned} \tag{4.5.5}$$

Again the integrals reflect the fact that in the ultra-relativistic case the particles are moving on the surface of the light cone, see (4.3.11), (4.3.12). Moreover we obtain

$$\begin{aligned} N^2(t_n+\tau,x) &= N^3(t_n+\tau,x) = 0\,,\\ T^{10}(t_n+\tau,x) &= T^{01}(t_n+\tau,x)\,,\\ T^{22}(t_n+\tau,x) &= T^{33}(t_n+\tau,x) = \frac{1}{2}[T^{00}(t_n+\tau,x) - T^{11}(t_n+\tau,x)]\,, \end{aligned}$$

where all the other components of $T^{\mu\nu}$ are zero. So in the one-dimensional case n, u and T

can be found from the generally valid relations given in (4.3.4) as follows

$$\begin{aligned} n(t_n+\tau,x) &= \sqrt{(N^0(t_n+\tau,x))^2-(N^1(t_n+\tau,x))^2}\,, \\ u(t_n+\tau,x) &= \frac{1}{n}N^1(t_n+\tau,x)\,, \\ p(t_n+\tau,x) &= \frac{1}{3}[\{1+u^2(t_n+\tau,x)\}T^{00}(t_n+\tau,x)-2u\sqrt{1+u^2(t_n+\tau,x)} \\ &\quad \cdot T^{01}(t_n+\tau,x)+u^2(t_n+\tau,x)T^{11}(t_n+\tau,x)]\,. \end{aligned} \tag{4.5.6}$$

We can now simplify the equations (4.3.7)-(4.3.9), which are used in order to initialize the general three-dimensional scheme, and obtain for the one-dimensional case

$$\begin{aligned} p(t_n^+,\mathbf{x}) &= \frac{1}{3}\left[-T^{00}+\sqrt{4(T^{00})^2-3(T^{01})^2}\,\right]\,, \\ u(t_n^+,\mathbf{x}) &= \frac{T^{01}}{\sqrt{4p(t_n^+,\mathbf{x})[p(t_n^+,\mathbf{x})+T^{00}]}}\,, \\ n(t_n^+,\mathbf{x}) &= \frac{N^0}{\sqrt{1+u(t_n^+,\mathbf{x})^2}}\,. \end{aligned} \tag{4.5.7}$$

Here again $N^0 = N^0(t_n^-,\mathbf{x})$, $T^{00} = T^{00}(t_n^-,\mathbf{x})$ and $T^{01} = T^{01}(t_n^-,\mathbf{x})$ are given by the free-flight moments.

4.5.1 Numerical Implementation of the Scheme in 1D

Here we explain the numerical implementation of the one-dimensional kinetic scheme. However the procedure is similar for the two-dimensional case.

- We start with the values of initial data $n(t_n,x)$, $u(t_n,x)$ and $T(t_n,x)$ at equidistant grid points.
- We specify the length L of the spatial cells, the number N_x of elements (intervals) in the spatial domain $0 \le x \le L$, the final time t_f of output and the number E_m of maximization times. For $i = 0,...,N_x$, we introduce the nodes $x_i = i \cdot \frac{L}{N_x}$.
- The time step Δt is calculated by $\Delta t = \frac{t_f}{E_m}$. The step in the spatial domain is $\Delta x = L/N_x$.
- Our aim is to calculate the moments (4.5.3) and (4.5.4). These moments are then used to update the fields n, u and T.
- Since we only know the values of the fields at the nodal points, the free-flight fields in the integrands of (4.5.3) and (4.5.4) must be calculated from the knowledge of the nodal values at the points x_i. Here we use linear interpolation between two subsequent nodal points x_i and x_{i+1}. We use the following interpolation formula

  $$f_n(x_j-\xi\tau,\xi) = (1-\eta)\,f_J(x_i,\xi)+\eta\,f_J(x_{i+1},\xi)\,,$$

  where $x_j - \xi\tau = x_i + \eta\,(x_{i+1}-x_i)$ for $0 \le \eta \le 1$. Here f_n and f_J are free-flight and Jüttner phase densities, respectively. The relation between x_i, x_j and η is shown in Figure 4.3.

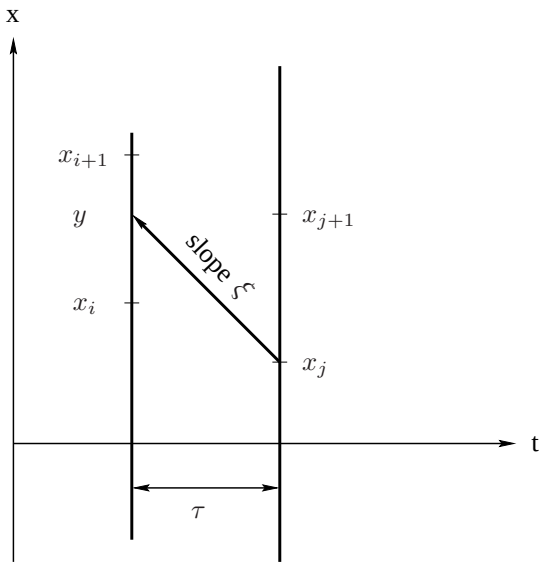

Figure 4.3: Interpolation of $y = x_j - \xi\tau$ at the grid points x_i and x_{i+1}.

- The $\xi-$ integration is performed with the composite trapezoidal rule.
- When we are in the free-flight the values of the fields n, u and T are calculated by using the generally valid algebraic relations (4.5.6), while at the maximization time, i.e. after the end of free-flight loop, the fields are updated by using the continuity relations (4.5.7) in order to initialize the scheme for next time step.

Remark: The difference in above procedure and one given in Subsection 2.3.1 is that, we do not need the error function to cutoff the $\xi-$integration limits in the kinetic scheme for the ultra-relativistic Euler equations, while it was required in the kinetic scheme for the non-relativistic Euler equations in order to cutoff the $c-$integration limits. The rest procedure is the same for both cases. Similarly the two-dimensional numerical implementation procedure given in Subsection 2.4.1 can be applied to the kinetic scheme for the two-dimensional ultra-relativistic Euler equations by just eliminating the portions which calculates the error function to cutoff the integration limits. The procedure for the application of boundary conditions is exactly the same as given in Section 2.3.2 by only replacing c by ξ. The TVD property proved in Section 2.3.3 is still valid because we are using exactly the same polynomial in the ultra-relativistic kinetic scheme as was used in non-relativistic kinetic scheme of Section 2.3.

4.5.2 Second Order Extension of the One-Dimensional Kinetic Scheme

Here we intend to extend our kinetic scheme to second order. We will use the approach of Deshpande [13] which he has used in order to obtain second order accuracy in one-dimensional kinetic scheme for the non-relativistic Euler equations. There are two steps in order to get second order accuracy. In the first step we will proceed to achieve second order accuracy in time, while the second step is to achieve second order accuracy in space. There are two approaches to achieve second order accuracy in time and both approaches lead to the same result. We will present both approaches in our study.

The first order kinetic schemes described in the previous sections suffer from the major disadvantage that the numerical diffusion is proportional to the time step. From the physical point of view, such a result is only to be expected because the fluid particles in the above kinetic schemes are allowed to move over the time step $\tau_M = \Delta t$ before they undergo collisions. The distance traveled between collisions is thus proportional to Δt. From the kinetic theory it then follows that the mean free path, and hence the viscosity, will be of the order Δt. This is a very large amount of viscosity, as the results shown later will verify. Therefore, a modifications in the above kinetic schemes is required that will ensure that the method has a high order accuracy. The analysis given below will show that how this is possible to achieve the second order accuracy.

The one-dimensional ultra-relativistic Euler equations (4.1.15) are

$$\begin{aligned} (n\sqrt{1+u^2})_t + (nu)_x &= 0\,, \\ (4pu\sqrt{1+u^2})_t + (p(1+4u^2))_x &= 0\,, \\ (p(3+4u^2))_t + (4pu\sqrt{1+u^2})_x &= 0\,. \end{aligned} \tag{4.5.8}$$

In one-dimensional case we know from the constitutive relations (4.1.1) that

$$W = \begin{pmatrix} N^0 \\ T^{01} \\ T^{00} \end{pmatrix} = \begin{pmatrix} n\sqrt{1+u^2} \\ 4pu\sqrt{1+u^2} \\ p(3+4u^2) \end{pmatrix}, \quad F = \begin{pmatrix} N^1 \\ T^{11} \\ T^{01} \end{pmatrix} = \begin{pmatrix} nu \\ p(1+4u^2) \\ 4pu\sqrt{1+u^2} \end{pmatrix}. \tag{4.5.9}$$

First approach: Second order accuracy in time

First we aim for second order accuracy in time. For this purpose it will be sufficient to consider the zero components N^0, T^{01} and T^{00}. In the following theory we will use the symbol Δt for the time step τ_M used in the first order kinetic scheme. The second order accurate Taylor expansions of $N^0(t_n + \Delta t, x)$, $T^{01}(t_n + \Delta t, x)$, and $T^{00}(t_n + \Delta t, x)$ are

$$\begin{aligned} N^0(t_n+\Delta t,x) &= N^0(t_n,x) + \Delta t\frac{\partial N^0}{\partial t}(t_n,x) + \frac{1}{2}\Delta t^2\frac{\partial^2 N^0}{\partial t^2}(t_n,x) + O(\Delta t^3)\,, \\ T^{01}(t_n+\Delta t,x) &= T^{01}(t_n,x) + \Delta t\frac{\partial T^{01}}{\partial t}(t_n,x) + \frac{1}{2}\Delta t^2\frac{\partial^2 T^{01}}{\partial t^2}(t_n,x) + O(\Delta t^3)\,, \\ T^{00}(t_n+\Delta t,x) &= T^{00}(t_n,x) + \Delta t\frac{\partial T^{00}}{\partial t}(t_n,x) + \frac{1}{2}\Delta t^2\frac{\partial^2 T^{00}}{\partial t^2}(t_n,x) + O(\Delta t^3)\,. \end{aligned} \tag{4.5.10}$$

These expansions contain the first and second-order time derivatives of N^0, T^{01} and T^{00}. The first order time derivatives can be replaced in terms of the first order space derivatives by using the Euler equations (4.5.8). To replace the second order time derivatives in terms of space derivatives requires detailed manipulations. Using equations (4.5.8) and (4.5.9) in

(4.5.10) we get

$$
\begin{aligned}
N^0(t_n+\Delta t,x) &= N^0(t_n,x) - \Delta t\frac{\partial N^1}{\partial x}(t_n,x) - \frac{1}{2}\Delta t^2\frac{\partial}{\partial x}\left(\frac{\partial N^1}{\partial t}(t_n,x)\right) + O(\Delta t^3)\,,\\
T^{01}(t_n+\Delta t,x) &= T^{01}(t_n,x) - \Delta t\frac{\partial T^{11}}{\partial x}(t_n,x) - \frac{1}{2}\Delta t^2\frac{\partial}{\partial x}\left(\frac{\partial T^{11}}{\partial t}(t_n,x)\right) + O(\Delta t^3)\,,\\
T^{00}(t_n+\Delta t,x) &= T^{00}(t_n,x) - \Delta t\frac{\partial T^{01}}{\partial x}(t_n,x) + \frac{1}{2}\Delta t^2\frac{\partial}{\partial x}\left(\frac{\partial T^{11}}{\partial x}(t_n,x)\right) + O(\Delta t^3)\,.
\end{aligned}
\tag{4.5.11}
$$

Our main goal is to compare the second order accurate Taylor expansion (4.5.11) with the kinetic scheme (4.5.3) and (4.5.4) after expanding the free-flight phase densities up to $O(\Delta t^3)$. This comparison will give us the terms which are missing in the first order kinetic schemes, the so called anti-diffusive terms. The addition of these terms will leed to the second order accuracy in time of the first order kinetic scheme.

In order to compare the equations (4.5.11) with the kinetic scheme solutions (4.5.3) and (4.5.4), we take a second order accurate Taylor expansion of the reduced free-flight phase densities $\phi(x-\Delta t\xi,\xi)$ and $\psi(x-\Delta t\xi,\xi)$ given in (4.5.2), we get

$$
\begin{aligned}
\phi(x-\Delta t\xi,\xi) &= \phi(t_n,x,\xi) - \xi\Delta t\frac{\partial\phi}{\partial x}(t_n,x,\xi) + \frac{\xi^2\Delta t^2}{2}\frac{\partial^2\phi}{\partial x^2}(t_n,x,\xi) + O(\Delta t^3)\,,\\
\psi(x-\Delta t\xi,\xi) &= \psi(t_n,x,\xi) - \xi\Delta t\frac{\partial\psi}{\partial x}(t_n,x,\xi) + \frac{\xi^2\Delta t^2}{2}\frac{\partial^2\psi}{\partial x^2}(t_n,x,\xi) + O(\Delta t^3)\,.
\end{aligned}
\tag{4.5.12}
$$

Introducing the Taylor expansions (4.5.12) in the one-dimensional kinetic scheme formulae (4.5.3) and (4.5.4), we get for $\phi=\phi(t_n,x,\xi)$ and $\psi=\psi(t_n,x,\xi)$

$$
\begin{aligned}
\int_{-1}^{1}\phi(x-\Delta t\xi,\xi)d\xi &= \int_{-1}^{1}\phi d\xi - \Delta t\frac{\partial}{\partial x}\int_{-1}^{1}\xi\phi d\xi + \frac{1}{2}\Delta t^2\frac{\partial}{\partial x}\left(\frac{\partial}{\partial x}\int_{-1}^{1}\xi^2\phi d\xi\right) + O(\Delta t^3)\,,\\
\int_{-1}^{1}\xi\psi(x-\Delta t\xi,\xi)d\xi &= \int_{-1}^{1}\xi\psi d\xi - \Delta t\frac{\partial}{\partial x}\int_{-1}^{1}\xi^2\psi d\xi + \frac{1}{2}\Delta t^2\frac{\partial}{\partial x}\left(\frac{\partial}{\partial x}\int_{-1}^{1}\xi^3\psi d\xi\right) + O(\Delta t^3)\,,\\
\int_{-1}^{1}\psi(x-\Delta t\xi,\xi)d\xi &= \int_{-1}^{1}\psi d\xi - \Delta t\frac{\partial}{\partial x}\int_{-1}^{1}\xi\psi d\xi + \frac{1}{2}\Delta t^2\frac{\partial^2}{\partial x^2}\int_{-1}^{1}\xi^2\psi d\xi + O(\Delta t^3)\,.
\end{aligned}
\tag{4.5.13}
$$

The reduced equilibrium phase densities (4.5.2) satisfy the following relations

$$
\begin{aligned}
&N^0(t_n,x) = \int_{-1}^{1}\phi(t_n,x,\xi)d\xi\,,\quad T^{01}(t_n,x) = \int_{-1}^{1}\xi\psi(t_n,x,\xi)d\xi\,,\quad T^{00}(t_n,x) = \int_{-1}^{1}\psi(t_n,x,\xi)d\xi\,,\\
&N^1(t_n,x) = \int_{-1}^{1}\xi\phi(t_n,x,\xi)d\xi\,,\quad T^{11}(t_n,x) = \int_{-1}^{1}\xi^2\psi(t_n,x,\xi)d\xi\,.
\end{aligned}
\tag{4.5.14}
$$

Using the relations (4.5.14) in (4.5.13) we finally get

$$\begin{aligned}
\int_{-1}^{1}\phi(x-\Delta t\xi,\xi)d\xi &= N^0(t_n,x)-\Delta t\frac{\partial N^1}{\partial x}(t_n,x)+\frac{1}{2}\Delta t^2\frac{\partial}{\partial x}\left(\frac{\partial}{\partial x}\int_{-1}^{1}\xi^2\phi d\xi\right)+O(\Delta t^3)\,,\\
\int_{-1}^{1}\xi\psi(x-\Delta t\xi,\xi)d\xi &= T^{01}(t_n,x)-\Delta t\frac{\partial T^{11}}{\partial x}(t_n,x)+\frac{1}{2}\Delta t^2\frac{\partial}{\partial x}\left(\frac{\partial}{\partial x}\int_{-1}^{1}\xi^3\psi d\xi\right)+O(\Delta t^3)\,,\\
\int_{-1}^{1}\psi(x-\Delta t\xi,\xi)d\xi &= T^{00}(t_n,x)-\Delta t\frac{\partial T^{01}}{\partial x}(t_n,x)+\frac{1}{2}\Delta t^2\frac{\partial^2 T^{11}}{\partial x^2}(t_n,x)+O(\Delta t^3)\,.
\end{aligned}\tag{4.5.15}$$

The equations (4.5.15) are the solutions coming from the first order kinetic schemes (4.5.3) and (4.5.4) when we expand the free-flight phase density up to $O(\Delta t^3)$.

Now we can rewrite the second order accurate solutions (4.5.11) in the following form by adding and subtracting appropriate order Δt^2 terms that appeared in (4.5.15)

$$\begin{aligned}
N^0(t_n+\Delta t,x) =& N^0(t_n,x)-\Delta t\frac{\partial N^1}{\partial x}(t_n,x)+\frac{1}{2}\Delta t^2\frac{\partial}{\partial x}\left(\frac{\partial}{\partial x}\int_{-1}^{1}\xi^2\phi d\xi\right)\\
&-\frac{1}{2}\Delta t^2\frac{\partial}{\partial x}\left(\frac{\partial N^1}{\partial t}(t_n,x)+\frac{\partial}{\partial x}\int_{-1}^{1}\xi^2\phi d\xi\right)+O(\Delta t^3)\,,\\
T^{01}(t_n+\Delta t,x) =& T^{01}(t_n,x)-\Delta t\frac{\partial T^{11}}{\partial x}(t_n,x)+\frac{1}{2}\Delta t^2\frac{\partial}{\partial x}\left(\frac{\partial}{\partial x}\int_{-1}^{1}\xi^3\psi d\xi\right)\\
&-\frac{1}{2}\Delta t^2\frac{\partial}{\partial x}\left(\frac{\partial T^{11}}{\partial t}(t_n,x)+\frac{\partial}{\partial x}\int_{-1}^{1}\xi^3\psi d\xi\right)+O(\Delta t^3)\,,\\
T^{00}(t_n+\Delta t,x) =& T^{00}(t_n,x)-\Delta t\frac{\partial T^{01}}{\partial x}(t_n,x)+\frac{1}{2}\Delta t^2\frac{\partial^2 T^{11}}{\partial x^2}(t_n,x)+O(\Delta t^3)\,.
\end{aligned}\tag{4.5.16}$$

Now using (4.5.15) in (4.5.16) we finally get

$$\begin{aligned}
N^0(t_n+\Delta t,x) &= \int_{-1}^{1}\phi(x-\Delta t,\xi)d\xi-\frac{1}{2}\Delta t^2\frac{\partial}{\partial x}\left(\frac{\partial N^1}{\partial t}(t_n,x)+\frac{\partial}{\partial x}\int_{-1}^{1}\xi^2\phi d\xi\right)+O(\Delta t^3)\,,\\
T^{01}(t_n+\Delta t,x) &= \int_{-1}^{1}\xi\psi(x-\Delta t,\xi)d\xi-\frac{1}{2}\Delta t^2\frac{\partial}{\partial x}\left(\frac{\partial T^{11}}{\partial t}(t_n,x)+\frac{\partial}{\partial x}\int_{-1}^{1}\xi^3\psi d\xi\right)+O(\Delta t^3)\,,\\
T^{00}(t_n+\Delta t,x) &= \int_{-1}^{1}\psi(x-\Delta t,\xi)d\xi+O(\Delta t^3)\,.
\end{aligned}\tag{4.5.17}$$

Using Section C.1 of Appendix C we can simplify the terms of order Δt^2 in $(4.5.17)_{1,2}$ in order to get

$$
\begin{aligned}
N^0(t_n+\Delta t,x) &= \int_{-1}^{1}\phi(x-\Delta t\xi,\xi)d\xi + \frac{1}{2}\Delta t^2\frac{\partial}{\partial x}g(n,u,p) + O(\Delta t^3)\,,\\
T^{01}(t_n+\Delta t,x) &= \int_{-1}^{1}\xi\psi(x-\Delta t\xi,\xi)d\xi + \frac{1}{2}\Delta t^2\frac{\partial}{\partial x}h(u,p) + O(\Delta t^3)\,,\\
T^{00}(t_n+\Delta t,x) &= \int_{-1}^{1}\psi(x-\Delta t\xi,\xi)d\xi + O(\Delta t^3)\,,
\end{aligned}
\tag{4.5.18}
$$

where

$$
\begin{aligned}
g(n,u,p) &= \left(-\frac{(1+u^2)^{-1/2}}{u^2} + \frac{1}{u^3}\operatorname{arcsinh}(u)\right)\frac{\partial n}{\partial x} - \frac{3n(1+u^2)^{-1/2}}{4p(3+2u^2)}\frac{\partial p}{\partial x}\\
&\quad + \left(\frac{9n\sqrt{1+u^2}}{u^3(3+2u^2)} - \frac{3n}{u^4}\operatorname{arcsinh}(u)\right)\frac{\partial u}{\partial x}\,,\\
h(u,p) &= \left(\frac{9\sqrt{1+u^2}}{u^4(3+2u^2)} + \frac{3\operatorname{arcsinh}(-u)}{u^5}\right)\left(u\frac{\partial p}{\partial x} - 4p\frac{\partial u}{\partial x}\right)\,.
\end{aligned}
\tag{4.5.19}
$$

On the right hand sides of equations $(4.5.18)_{1,2}$ the first terms are from the old kinetic scheme, while the second terms are the antidiffusive terms which must be added to N^0 and T^{01} for the second order accuracy. While the energy density T^{00} is already second order accurate in time. In the non-relativistic case Deshpande [13] observed that the particle density coming from the first order kinetic scheme was already second order accurate in time, but in the first order relativistic kinetic scheme we found that the energy density is second order accurate in time. This is due to the fact that in the non-relativistic Euler equations case the flux of the continuity equation is equal to the conserved momentum variable, while in the relativistic Euler equations case the flux in the total energy equation is equal to the conserved momentum variable.

Second approach: Second order accuracy in time

Since the free-flight phase density is very far from equilibrium, the reduced phase densities $\phi(t,x,\xi)$ and $\psi(t,x,\xi)$ given by (4.5.2) do not satisfy the reduced free-flight transport equation, i.e.,

$$
\frac{\partial\phi}{\partial t} + \xi\frac{\partial\phi}{\partial x} \neq 0\,, \quad \frac{\partial\psi}{\partial t} + \xi\frac{\partial\psi}{\partial x} \neq 0\,. \tag{4.5.20}
$$

In fact from (4.5.2) we have

$$\frac{\partial \phi}{\partial t}+\xi\frac{\partial \phi}{\partial x}=\left(\frac{\partial n}{\partial t}+\xi\frac{\partial n}{\partial x}\right)\frac{\partial \phi}{\partial n}+\left(\frac{\partial u}{\partial t}+\xi\frac{\partial u}{\partial x}\right)\frac{\partial \phi}{\partial u}\,, \tag{4.5.21}$$

$$\frac{\partial \psi}{\partial t}+\xi\frac{\partial \psi}{\partial x}=\left(\frac{\partial p}{\partial t}+\xi\frac{\partial p}{\partial x}\right)\frac{\partial \psi}{\partial p}+\left(\frac{\partial u}{\partial t}+\xi\frac{\partial u}{\partial x}\right)\frac{\partial \psi}{\partial u}\,. \tag{4.5.22}$$

The right hand sides of (4.5.21) and (4.5.22) are very characteristic of the Chapman-Enskog (CE) non-relativistic theory. Using Section C.1 of Appendix C we can replace the time derivatives of n, u and p in equations (4.5.22) and (4.5.22) in terms of the space derivatives. We obtain

$$\frac{\partial \phi}{\partial t}+\xi\frac{\partial \phi}{\partial x}=Q_{CE}\phi \tag{4.5.23}$$

$$\frac{\partial \psi}{\partial t}+\xi\frac{\partial \psi}{\partial x}=M_{CE}\psi, \tag{4.5.24}$$

where Q_{CE} and M_{CE} are polynomials given by

$$Q_{CE}=Q_1\frac{\partial n}{\partial x}+Q_2\frac{\partial p}{\partial x}+Q_3\frac{\partial u}{\partial x}\,, \tag{4.5.25}$$

$$M_{CE}=M_1\frac{\partial p}{\partial x}+M_2\frac{\partial u}{\partial x}\,, \tag{4.5.26}$$

with

$$\begin{aligned} Q_1&=\frac{\xi\sqrt{1+u^2}-u}{n\sqrt{1+u^2}}\,,\quad Q_2=\frac{3\left(4u\sqrt{1+u^2}-4u^2\xi-3\xi\right)}{4p\sqrt{1+u^2}(3+2u^2)(\sqrt{1+u^2}-\xi u)}\,, \\ Q_3&=3\left(\frac{\xi^2\sqrt{1+u^2}(3+2u^2)+2u^2(\sqrt{1+u^2}-\xi u)-\sqrt{1+u^2}(1+2\xi u\sqrt{1+u^2})-2\xi u}{\sqrt{1+u^2}(3+2u^2)(\sqrt{1+u^2}-\xi u)}\right), \end{aligned} \tag{4.5.27}$$

and

$$M_1=\frac{u(1-3\xi^2)+2u^2(2\sqrt{1+u^2}\xi-\xi^2u-u)}{p(3+2u^2)(\sqrt{1+u^2}-\xi u)}\,,\quad M_2=\frac{4}{3}Q_3\,. \tag{4.5.28}$$

The polynomials Q_{CE} and M_{CE} have interesting properties, i.e.,

$$\int_{-1}^{1}Q_{CE}\,\phi\,d\xi=0\,,\quad \int_{-1}^{1}M_{CE}\,\psi\,d\xi=0\,,\quad \int_{-1}^{1}\xi M_{CE}\,\psi\,d\xi=0\,. \tag{4.5.29}$$

These properties can be easily checked by a simple $\xi-$integration in mathematics packages like, Maple or Mathematica. We will see at the end that these properties are also important for the conservativity of the second order order kinetic scheme. We are now ready to construct the second order accurate kinetic scheme which was also obtained in the **first approach**.

Starting with

$$
\begin{aligned}
N^0(t_n+\Delta t,x) &= \int_{-1}^{1}\phi(t_n+\Delta t,x,\xi)d\xi = \int_{-1}^{1}\left(\phi+\Delta t\frac{\partial\phi}{\partial t}+\frac{1}{2}\Delta t^2\frac{\partial^2\phi}{\partial t^2}\right)d\xi+(\Delta t^3)\,,\\
T^{01}(t_n+\Delta t,x) &= \int_{-1}^{1}\xi\psi(t_n+\Delta t,x,\xi)d\xi = \int_{-1}^{1}\xi\left(\psi+\Delta t\frac{\partial\psi}{\partial t}+\frac{1}{2}\Delta t^2\frac{\partial^2\psi}{\partial t^2}\right)d\xi+(\Delta t^3)\,,\\
T^{00}(t_n+\Delta t,x) &= \int_{-1}^{1}\psi(t_n+\Delta t,x,\xi)d\xi = \int_{-1}^{1}\left(\psi+\Delta t\frac{\partial\psi}{\partial t}+\frac{1}{2}\Delta t^2\frac{\partial^2\psi}{\partial t^2}\right)d\xi+(\Delta t^3)\,,
\end{aligned}
\tag{4.5.30}
$$

where $\phi=\phi(t_n,x,\xi)$ and $\psi=\psi(t_n,x,\xi)$. As stated before the equilibrium phase densities ϕ and ψ do not satisfy the free flight equation. But on the other hand they satisfy the moment equations of the free-flight equation which are infect the Euler equations, for example,

$$
\int_{-1}^{1}\frac{\partial\phi}{\partial t}d\xi+\int_{-1}^{1}\xi\frac{\partial\phi}{\partial x}d\xi=0\,,
\tag{4.5.31}
$$

is the continuity equation of the Euler equations (4.5.8). Similarly energy and momentum equations can be obtained from the moment equations of ψ. Therefore, in order to replace the first order time derivatives of ϕ and ψ in above expressions we use (4.5.31) and (4.5.14), we get

$$
\begin{aligned}
N^0(t_n+\Delta t,x) &= \int_{-1}^{1}\left(\phi-\Delta t\xi\frac{\partial\phi}{\partial x}+\frac{1}{2}\Delta t^2\frac{\partial^2\phi}{\partial t^2}\right)d\xi+O(\Delta t^3)\,,\\
T^{01}(t_n+\Delta t,x) &= \int_{-1}^{1}\xi\left(\psi-\Delta t\xi\frac{\partial\psi}{\partial x}+\frac{1}{2}\Delta t^2\frac{\partial^2\psi}{\partial t^2}\right)d\xi+O(\Delta t^3)\,,\\
T^{00}(t_n+\Delta t,x) &= \int_{-1}^{1}\left(\psi-\Delta t\xi\frac{\partial\psi}{\partial x}+\frac{1}{2}\Delta t^2\frac{\partial^2\psi}{\partial t^2}\right)d\xi+O(\Delta t^3)\,.
\end{aligned}
\tag{4.5.32}
$$

Using the relations (4.5.23) and (4.5.24), we obtain

$$
\begin{aligned}
\frac{\partial^2\phi}{\partial t^2} &= -\xi\frac{\partial}{\partial x}\left(\frac{\partial\phi}{\partial t}\right)+\frac{\partial}{\partial t}\left(Q_{CE}\phi\right)\\
&= \xi^2\frac{\partial^2\phi}{\partial x^2}-\xi\frac{\partial}{\partial x}\left(Q_{CE}\phi\right)+\frac{\partial}{\partial t}\left(Q_{CE}\phi\right)\,,\\
\frac{\partial^2\psi}{\partial t^2} &= -\xi\frac{\partial}{\partial x}\left(\frac{\partial\psi}{\partial t}\right)+\frac{\partial}{\partial t}\left(M_{CE}\psi\right)\\
&= \xi^2\frac{\partial^2\psi}{\partial x^2}-\xi\frac{\partial}{\partial x}\left(M_{CE}\psi\right)+\frac{\partial}{\partial t}\left(M_{CE}\psi\right)\,.
\end{aligned}
\tag{4.5.33}
$$

Substituting the above expression for the second order derivatives of ϕ and ψ in (4.5.32) we get after using (4.5.12)

$$N^0(t_n+\Delta t,x) = \int_{-1}^{1} \phi(x-\Delta t\xi,\xi)d\xi - \frac{\Delta t^2}{2}\left(\int_{-1}^{1}\xi\frac{\partial}{\partial x}\left(Q_{CE}\phi\right)d\xi - \frac{\partial}{\partial t}\int_{-1}^{1} Q_{CE}\phi d\xi\right) + (\Delta t^3)\,,$$

$$T^{01}(t_n+\Delta t,x) = \int_{-1}^{1} \xi\psi(x-\Delta t\xi,\xi)d\xi - \frac{\Delta t^2}{2}\left(\int_{-1}^{1}\xi^2\frac{\partial}{\partial x}\left(M_{CE}\psi\right)d\xi - \frac{\partial}{\partial t}\int_{-1}^{1} \xi M_{CE}\psi d\xi\right) + (\Delta t^3)\,,$$

$$T^{00}(t_n+\Delta t,x) = \int_{-1}^{1} \psi(x-\Delta t\xi,\xi)d\xi - \frac{\Delta t^2}{2}\left(\int_{-1}^{1}\xi\frac{\partial}{\partial x}\left(M_{CE}\psi\right)d\xi - \frac{\partial}{\partial t}\int_{-1}^{1} M_{CE}\psi d\xi\right) + (\Delta t^3)\,.$$

The last terms in the $O(\Delta t^2)$ part of the above equations are zero due to the properties (4.5.29) of $Q_{CE}\phi$ and $M_{CE}\psi$. We get

$$N^0(t_n+\Delta t,x) = \int_{-1}^{1} \phi(x-\Delta t\xi,\xi)d\xi - \frac{1}{2}\Delta t^2\int_{-1}^{1}\xi\frac{\partial}{\partial x}\left(Q_{CE}\phi(t_n,x,\xi)\right)d\xi + O(\Delta t^3) \quad (4.5.34)$$

$$T^{01}(t_n+\Delta t,x) = \int_{-1}^{1} \xi\psi(x-\Delta t\xi,\xi)d\xi - \frac{1}{2}\Delta t^2\int_{-1}^{1}\xi^2\frac{\partial}{\partial x}\left(Q_{CE}\phi(t_n,x,\xi)\right)d\xi + O(\Delta t^3)\,,$$

$$T^{00}(t_n+\Delta t,x) = \int_{-1}^{1} \psi(x-\Delta t\xi,\xi)d\xi + O(\Delta t^3)\,, \quad (4.5.35)$$

which shows that in addition to the $\phi(x-\Delta t,\xi)$ and $\psi(x-\Delta t,\xi)$ terms we have one more term in the first two equations containing the polynomials Q_{CE}, M_{CE}. Hence the reduced Jüttner distributions ϕ and ψ alone will not yield a second order accurate kinetic scheme for particle density and momentum, however the total energy T^{00} is already second order accurate in time. Note that if we evaluate the integrals of the second terms in (4.5.34) and $(4.5.35)_1$, we get the same correction terms g and h as given in (4.5.18). In order to obtain (4.5.18) one can simply integrate the coefficients of Δt^2 in above equation using Mathematica or Maple. Let us define

$$\phi_{CE} = \phi\left(1+\frac{\Delta t}{2}Q_{CE}\right)\,, \quad \psi_{CE} = \psi\left(1+\frac{\Delta t}{2}M_{CE}\right)\,. \quad (4.5.36)$$

We can recast (4.5.34) and (4.5.35) as

$$N^0(t_n+\Delta t,x)=\int_{-1}^{1}\phi_{CE}(x-\Delta t\xi,\xi)d\xi+O(\Delta t^3)\,,$$
$$T^{01}(t_n+\Delta t,x)=\int_{-1}^{1}\xi\psi_{CE}(x-\Delta t\xi,\xi)d\xi+O(\Delta t^3)\,, \tag{4.5.37}$$
$$T^{00}(t_n+\Delta t,x)=\int_{-1}^{1}\psi_{CE}(x-\Delta t\xi,\xi)d\xi+O(\Delta t^3)\,.$$

Due to the properties (4.5.29) of $Q_{CE}\phi$ and $M_{CE}\psi$ we can see that the zero quantities N^0, T^{01} and T^{00} are identical within the truncation error, i.e.

$$\int_{-1}^{1}(\phi_{CE}-\phi)\,d\xi=0\,,\quad \int_{-1}^{1}\xi\,(\psi_{CE}-\psi)\,d\xi=0\,,\quad \int_{-1}^{1}(\psi_{CE}-\psi)\,d\xi=0\,.$$

These conditions also can be regarded as conservation conditions, for more details see Deshpande [13] in the non-relativistic case.

Several important features of the above second order accurate in time kinetic scheme are worth noting. Equations (4.5.37), containing different distribution functions, have been obtained from equations (4.5.18) or (4.5.34). As stated before the right-hand sides of equations $(4.5.18)_{1,2}$ and $(4.5.34)_{1,2}$ contain two terms. The first terms, which are moments of the free flight phase densities $\phi(x-\xi\Delta t,\xi)$ and $\phi(x-\xi\Delta t,\xi)$, are upwind in character. The second terms cannot be expressed as moments of $\phi(x-\Delta t\xi,\xi)$ and $\psi(x-\Delta t\xi,\xi)$ and are antidiffusive. The antidiffusive terms may be absorbed in the upwind term only if the distribution function is not the relativistic Maxwellian, i.e., Jüttner distribution. Equations (4.5.37) are an upwind version of a second order accurate solution in which the perturbed relativistic Maxwellian distributions are employed.

Second order accuracy in space: Another important point about equations (4.5.37) is that, $\phi_{CE}(x-\xi\Delta t,\xi)$ and $\phi_{CE}(x-\xi\Delta t,\xi)$ need to be evaluated at various values of ξ. Hence, as noted before, some kind of interpolation scheme is required. This scheme must be second order accurate in space and should not yield non-negative interpolated values, and should satisfy the TVD property. A procedure is given below.

Let ϕ_{CE} and ψ_{CE} be given at mesh points, see Subsection 4.5.1. Also let the mesh point i corresponding to point j be such that

$$x_j-\xi\Delta t=x_i+\eta\Delta x\,,\qquad 0\le\eta\le 1\,.$$

The relation between x_j and x_i and η is given in Figure 4.3. The functions $\phi_{CE}(x_j-\xi\Delta t,\xi)=\phi_{CE}(x_i+\eta\Delta x,\xi)$ and $\psi_{CE}(x_j-\xi\Delta t,\xi)=\psi_{CE}(x_i+\eta\Delta x,\xi)$ then depends on the neighbouring mesh points $i\pm 1$. Therefore the second order interpolation for any function f will be

$$f(x_i+\eta\Delta x,\xi)=f_i+\frac{\eta}{2}(f_{i+1}-f_{i-1})+\frac{\eta^2}{2}(f_{i+1}-2f_i+f_{i-1})\,, \tag{4.5.38}$$

where f_i can be $\phi_{CE}(t_n, x_i, \xi)$ or $\psi_{CE}(t_n, x_i, \xi)$. In order to suppress oscillations in the numerical results we use the min-mod nonlinear limiters [35, 53, 70] on the numerical derivatives appearing in the antidiffusive terms Q_{CE} and M_{CE} given in (4.5.25) and (4.5.26). These min-mod limiters are given by (5.2.16) in Chapter 5.

As pointed out by Deshpande [13], the expression (4.5.38) does not automatically ensure positivity of $f(x_i + \eta\Delta x, \xi)$ even if f_{i-1}, f_i and f_{i+1} are assumed to be positive. This is particularly true for calculations near shocks. With the method of Chakravarthy and Osher [4] limiting the contribution of the second difference, it is possible to devise an interpolation scheme that satisfies the TVD condition given in Subsection 2.3.3. The second order accurate Taylor expansion (4.5.38) can be rewritten as

$$\begin{aligned} f(x_i + \eta\Delta x, \xi) =& f_i + \frac{\eta}{2}\left(f_{i+1} - f_i + f_i - f_{i-1}\right) \\ &+ \frac{\eta^2}{2}\left(f_{i+1} - f_i + f_{i-1} - f_i\right) \\ =& f_i + \frac{\eta(1+\eta)}{2}\left(f_{i+1} - f_i\right) + \frac{\eta(1-\eta)}{2}\left(f_i - f_{i-1}\right) \\ =& f_i + \left(f_{i+1} - f_i\right)\left[\frac{\eta(1+\eta)}{2} + \frac{\eta(1-\eta)}{2} r_D\right], \end{aligned} \tag{4.5.39}$$

where

$$r_D = \frac{\text{Backward difference}}{\text{Forward difference}} = \frac{f_i - f_{i-1}}{f_{i+1} - f_i}.$$

In smooth regions

$$f_{i\pm1} = f_i \pm \Delta x f_i' + \frac{(\Delta x)^2}{2} f_i'' + O(\Delta x^3), \tag{4.5.40}$$

then

$$\begin{aligned} \frac{f_i - f_{i-1}}{\Delta x f_i'} &= 1 - \frac{\Delta x}{2}\frac{f_i''}{f_i'} + O(\Delta x^2), \\ \frac{f_{i+1} - f_i}{\Delta x f_i'} &= 1 + \frac{\Delta x}{2}\frac{f_i''}{f_i'} + O(\Delta x^2). \end{aligned} \tag{4.5.41}$$

This implies

$$\begin{aligned} r_D = \frac{f_i - f_{i-1}}{f_{i+1} - f_i} &= \left(1 - \frac{\Delta x}{2}\frac{f_i''}{f_i'} + O(\Delta x^2)\right)\left(1 + \frac{\Delta x}{2}\frac{f_i''}{f_i'} + O(\Delta x^2)\right)^{-1} \\ &= \left(1 - \frac{\Delta x}{2}\frac{f_i''}{f_i'} + O(\Delta x^2)\right)\left(1 - \frac{\Delta x}{2}\frac{f_i''}{f_i'} + O(\Delta x^2)\right). \end{aligned} \tag{4.5.42}$$

Hence we finally get

$$r_D = 1 - \Delta x \frac{f_i''}{f_i'} + O(\Delta x^2), \tag{4.5.43}$$

and thus r_D remains close to unity. In flow regions near shocks or contact surfaces, r_D can wildly vary and some limiting criterion is required to preserve the TVD condition. The key

to satisfy the TVD condition lies in requiring

$$0 \leq \frac{\eta(1+\eta)}{2} + \frac{\eta(1-\eta)}{2} r_D \leq 1\,. \tag{4.5.44}$$

Two cases arise, namely, $r_D \geq 0$ and $r_D \leq 0$. If we consider the case of $r_D \geq 0$, the condition in equation (4.5.44) is satisfied if

$$r_D \leq 1 + \frac{2}{\eta}\,. \tag{4.5.45}$$

As $0 \leq \eta \leq 1$, the right-hand side of the above inequality has minimum value of 3. One way of satisfying equation (4.5.45) is to limit the value of r_D to 3 when $r_D \geq 0$. For the case when $r_D \leq 0$, the condition in equation (4.5.44) is satisfied if

$$\frac{\eta(1+\eta)}{2} + \frac{\eta(1-\eta)}{2} r_D = \frac{\eta(1+\eta)}{2} - \frac{\eta(1-\eta)}{2} |r_D| \geq 0\,, \tag{4.5.46}$$

or equivalently, if

$$|r_D| \leq \frac{1+\eta}{1-\eta}\,. \tag{4.5.47}$$

Thus, by limiting the relative values of the forward and backward differences and taking $r_D = 1$ outside these limits, we find the interpolation formula in equation (4.5.39) yields not only positive values of $f(x_i + \eta\Delta x, \xi)$ but also satisfies the TVD condition. As mentioned before the basic input to equation (4.5.39) is the set of positive values of f_i at all mesh points.

From the analysis in this section it has become clear that the second-order accurate kinetic scheme requires the use of distribution functions ϕ_{CE} and ψ_{CE} given in equation (4.5.36), as well as second order accurate interpolation scheme. The extension of this kinetic scheme to two-dimensional case is considered in the next section.

Remark: Due to the presence of Q_{CE} and M_{CE}, the distribution functions ϕ_{CE} and ψ_{CE} given in (4.5.36) not only depend on the local values of the field variables but also depend on their neighbouring values as well. The support of ϕ_{CE} and ψ_{CE} is thus more than that of local phase densities ϕ and ψ used in the first order kinetic scheme.

4.6 Kinetic Scheme in Two Space Dimensions

Here we consider solutions which depend on t, $x = x^1$ and $y = x^2$ and satisfy $n = n(t,x,y)$, $\mathbf{u} = (u_1(t,x,y), u_2(t,x,y), 0)$, $p = p(t,x,y)$. In order to calculate the surface integrals (4.3.11) and (4.3.12) we introduce instead of the unit vector $\mathbf{w}$ the new variables $-1 \leq \xi \leq 1$ and $-\pi \leqq \varphi \leqq \pi$ by

$$w^1 = \xi\,, \qquad w^2 = \sqrt{1-\xi^2}\sin\varphi\,, \qquad w^3 = \sqrt{1-\xi^2}\cos\varphi\,, \tag{4.6.1}$$

with the surface element $dS(\mathbf{w}) = d\xi d\varphi$. Therefore the surface integrals for the moments (4.3.11) and (4.3.12) can be rewritten as given below. In the following we use $\tau = \tau_M$, i.e.,

the free-flight is of the order of time step, $t_n + \tau_M = t_{n+1}$. For abbreviation we introduce

$$\phi(\mathbf{y}, w^1, w^2) = \frac{1}{4\pi} \frac{n(\mathbf{y})}{(\sqrt{1 + (u_1^2 + u_2^2)(\mathbf{y})} - u_1(\mathbf{y})\, w^1 - u_2(\mathbf{y})\, w^2)^3}\,,$$
$$\psi(\mathbf{y}, w^1, w^2) = \frac{3}{4\pi} \frac{(nT)(\mathbf{y})}{(\sqrt{1 + (u_1^2 + u_2^2)(\mathbf{y})} - u_1(\mathbf{y})\, w^1 - u_2(\mathbf{y})\, w^2)^4}\,, \tag{4.6.2}$$

then the two-dimensional kinetic scheme is

$$N^k(t_n + \tau_M, x, y) = \int_{-\pi}^{\pi}\int_{-1}^{1} w^k \phi(x - \tau_M w^1, y - \tau_M w^2, w^1, w^2)\, d\xi\, d\varphi\,,$$
$$T^{km}(t_n + \tau_M, x, y) = \int_{-\pi}^{\pi}\int_{-1}^{1} w^k w^m \psi(x - \tau_M w^1, y - \tau_M w^2, w^1, w^2)\, d\xi\, d\varphi\,,$$

where k, $m = 0, 1, 2$ and $w^0 = 1$. Moreover the fields n, u_1, u_2 and T can be found from the same continuity equations (4.3.7)-(4.3.9) except $u_3 = 0$.

The procedure of numerical implementation of the scheme is exactly the same as given in Section 2.4.1 of Chapter 2 for the two-dimensional non-relativistic Euler equations. Therefore we do not explain again the numerical implementation procedure.

4.6.1 Second Order Extension of the Two-Dimensional Kinetic Scheme

Here we aim to extend our two-dimensional kinetic scheme to second order. The procedure of second order time accuracy is analogous to the **second approach** in Subsection 4.5.2 for the one-dimensional case. Therefore we will not go in the details of the derivation.

Since the free-flight phase density is very far from equilibrium, the equilibrium phase densities $\phi(t, x, y, \xi)$ and $\psi(t, x, y, \xi)$ given by (4.6.2) do not satisfy the free-flight transport equation, i.e.,

$$\frac{\partial \phi}{\partial t} + w^1 \frac{\partial \phi}{\partial x} + w^2 \frac{\partial \phi}{\partial y} \neq 0\,, \quad \frac{\partial \psi}{\partial t} + w^1 \frac{\partial \psi}{\partial x} + w^2 \frac{\partial \psi}{\partial y} \neq 0\,, \tag{4.6.3}$$

where $w^1 = \xi$ and $w^2 = \sqrt{1 - \xi^2}\sin\varphi$ as given in (4.6.1). In fact from (4.6.2) we have

$$\frac{\partial \phi}{\partial t} + w^1 \frac{\partial \phi}{\partial x} + w^2 \frac{\partial \phi}{\partial y} = \left(\frac{\partial n}{\partial t} + w^1 \frac{\partial n}{\partial x} + w^2 \frac{\partial n}{\partial y}\right) \frac{\partial \phi}{\partial n} + \left(\frac{\partial u_1}{\partial t} + w^1 \frac{\partial u_1}{\partial x} + w^2 \frac{\partial u_1}{\partial y}\right) \frac{\partial \phi}{\partial u_1}$$
$$+ \left(\frac{\partial u_2}{\partial t} + w^1 \frac{\partial u_2}{\partial x} + w^2 \frac{\partial u_2}{\partial y}\right) \frac{\partial \phi}{\partial u_2}\,, \tag{4.6.4}$$

$$\frac{\partial \psi}{\partial t} + w^1 \frac{\partial \psi}{\partial x} + w^2 \frac{\partial \psi}{\partial y} = \left(\frac{\partial p}{\partial t} + w^1 \frac{\partial p}{\partial x} + w^2 \frac{\partial p}{\partial y}\right) \frac{\partial \psi}{\partial p} + \left(\frac{\partial u_1}{\partial t} + w^1 \frac{\partial u_1}{\partial x} + w^2 \frac{\partial u_1}{\partial y}\right) \frac{\partial \psi}{\partial u_1}$$
$$+ \left(\frac{\partial u_2}{\partial t} + w^1 \frac{\partial u_2}{\partial x} + w^2 \frac{\partial u_2}{\partial y}\right) \frac{\partial \psi}{\partial u_2}\,. \tag{4.6.5}$$

Using Section C.2 of Appendix C we can replace the time derivatives of n, u_1, u_2 and p in the above equations in terms of the space derivatives. Also we calculate the derivatives of the equilibrium phase densities (4.6.2) with respect to the fields. We finally obtain

$$\frac{\partial \phi}{\partial t} + w^1 \frac{\partial \phi}{\partial x} + w^2 \frac{\partial \phi}{\partial y} = Q_{CE}\phi \tag{4.6.6}$$

$$\frac{\partial \psi}{\partial t} + w^1 \frac{\partial \psi}{\partial x} + w^2 \frac{\partial \psi}{\partial y} = M_{CE}\psi, \tag{4.6.7}$$

where Q_{CE} and M_{CE} are polynomials given by

$$\begin{aligned} Q_{CE} =& Q_{nx}\frac{\partial n}{\partial x} + Q_{ny}\frac{\partial n}{\partial y} + Q_{px}\frac{\partial p}{\partial x} + Q_{py}\frac{\partial p}{\partial y} \\ &+ Q_{u1x}\frac{\partial u_1}{\partial x} + Q_{u1y}\frac{\partial u_1}{\partial y} + Q_{u2x}\frac{\partial u_2}{\partial x} + Q_{u2y}\frac{\partial u_2}{\partial y}\,, \\ M_{CE} =& M_{px}\frac{\partial p}{\partial x} + M_{py}\frac{\partial p}{\partial y} + M_{u1x}\frac{\partial u_1}{\partial x} + M_{u1y}\frac{\partial u_1}{\partial y} + M_{u2x}\frac{\partial u_2}{\partial x} + M_{u2y}\frac{\partial u_2}{\partial y}\,, \end{aligned} \tag{4.6.8}$$

where all the coefficients of the derivatives of n, u_1, u_2 and p in above equations are given in the Section C.2 of Appendix C. Now following the same lines of derivation given in Subsection 4.5.2, we finally get the following second order accurate kinetic scheme for the two-dimensional case.

$$N^k(t_n + \Delta t, x, y) = \int_{-\pi}^{\pi}\int_{-1}^{1} w^k \phi_{CE}(x - \Delta w^1, y - \Delta t w^2, w^1, w^2)\, d\xi\, d\varphi + O(\Delta t^3)\,, \tag{4.6.9}$$

$$T^{km}(t_n + \Delta t, x, y) = \int_{-\pi}^{\pi}\int_{-1}^{1} w^k w^m \psi_{CE}(x - \Delta w^1, y - \Delta t w^2, w^1, w^2)\, d\xi\, d\varphi + O(\Delta t^3)\,, \tag{4.6.10}$$

where k, $m = 0, 1, 2$ and $w^0 = 1$. The initial phase densities ϕ_{CE} and ψ_{CE} at time t_n are

$$\begin{aligned} \phi_{CE}(\mathbf{y}, w^1, w^2) &= \phi\left(1 + \frac{\Delta t}{2} Q_{CE}\right)(\mathbf{y}, w^1, w^2)\,, \\ \psi_{CE}(\mathbf{y}, w^1, w^2) &= \psi\left(1 + \frac{\Delta t}{2} M_{CE}\right)(\mathbf{y}, w^1, w^2)\,, \end{aligned}$$

where ϕ and ψ are given in (4.6.2). In order to get second order accuracy in space we need again a second order polynomial to calculate the free flight phase density.

4.7 Numerical Case Studies

In the following we present numerical test cases for the solution of the ultra-relativistic Euler equations. For the comparison we use exact Riemann solution, upwind and central schemes. It was found that kinetic scheme has a comparable accuracy with the upwind and central scheme. The Godunov and central schemes used here are discussed in Chapter 5 and Chapter 7, respectively.

Problem 1: Shock tube problem I

The initial data are

$$(n, u, p) = \begin{cases} (5.0, 0.0, 10.0) & \text{if } x < 0.5\,, \\ (1.0, 0.0, 0.5) & \text{if } x \geq 0.5\,. \end{cases}$$

The spatial domain is taken as $[0, 1]$ with 400 mesh elements and the final time is $t = 0.5$. For the kinetic scheme we consider 100 maximization times. This problem involves the formation of an intermediate state bounded by a shock wave propagating to the right and a transonic rarefaction wave propagating to the left. The fluid in the intermediate state moves at a mildly relativistic speed ($v = 0.58c$) to the right. Flow particles accumulate in a dense shell behind the shock wave compressing the fluid and heating it. The fluid is extremely relativistic from a thermodynamic point of view, but only mildly relativistic dynamically. Figures $(4.4)_{1,2}$ and $(4.5)_{1,2}$ show the particle density n, fluid velocity $v = \frac{u}{\sqrt{1+u^2}}$ and pressure p. Figures $(4.4)_{3,4}$ and $(4.5)_{3,4}$ shows the same results with zooming in order to easily compare the schemes.

Problem 2: Shock tube problem II

The initial data are

$$(n, u, p) = \begin{cases} (1.0, 1.0, 3.0) & \text{if } x < 0.5\,, \\ (1.0, -0.5, 2.0) & \text{if } x \geq 0.5\,. \end{cases}$$

The spatial domain is taken as $[0, 1]$ with 400 mesh elements and the final time is $t = 0.5$. For the kinetic scheme we consider 100 maximization times. The solution consist of left shock, a contact and a right shock. Figure 4.5 represents a plots for the particle density, velocity v and pressure.

Problem 3: Perturbed relativistic shock tube flow

The initial conditions are specified as $(n_L, u_L, p_L) = (1.0, 0.0, 1.0)$ for $0 \leq x \leq 0.5$ and $(n_R, u_R, p_R) = (n_R, 0.0, 0.1)$ for $0.5 \leq x \leq 1.0$. Here the right state is a perturbed density field of sinusoidal wave, $n_R = 0.125 - 0.0875 \sin(50(x - 0.5))$. We run this test for the 400 mesh points. The computed solutions are plotted at $t = 0.5$. The results for particle density n, velocity $v = \frac{u}{\sqrt{1+u^2}}$ and pressure p are shown in Figure 4.6. Since the continuity equation in the Euler equations decouples from the other two equations for the pressure and velocity, therefore we do not see the effect of perturbation in the pressure and velocity.

Problem 4: Single shock solution of the Euler equations

This problem was studied by Yang et al. [94]. In this example we test our kinetic scheme for a single shock problem. We supplied initial data to the program for which we know that a single shock solution results from the Rankine-Hugoniot jump conditions. We select the initial data and the space-time range such that the shock exactly reaches the right lower corner at the time axis. Figure $4.7_{1,2}$ represent the plots of the particle density in the time range $0 \leq t \leq 1.271$ and in the space range $0 \leq x \leq L = 2$. The figures shows that both first order and second order kinetic schemes captures this shock in exactly the same way as

predicted by the Rankine-Hugoniot jump conditions. The Figure 4.7_3 represents the particle density at the fixed time $t = 0.635$ for the same initial data. The Riemann initial data with a jump at $x = L/2 = 1$ are chosen as

$$(n, u, p) = \begin{cases} (1.0, 0.0, 1.0) & \text{if } x < 1.0\,, \\ (2.725, -0.6495, 4.0) & \text{if } x \geq 1.0\,, \end{cases}$$

where 100 maximization times and 1000 mesh points are considered here. In this example we found that our kinetic scheme gives a sharp shock resolution. This is a good test for the kinetic scheme, and its success indicates that the conservation laws for mass, momentum and energy as well as the entropy inequality are satisfied. We have already proved these properties for the solutions of the kinetic scheme.

Problem 5: Two interacting relativistic blast waves We consider here the interaction of two relativistic blast waves. The initial data are

$$(n, u, p) = \begin{cases} (1.0, 0.0, 100.0) & \text{if } 0 < x < 0.1\,, \\ (1.0, 0.0, 0.06) & \text{if } 0.1 < x < 0.9\,, \\ (1.0, 0.0, 10.0) & \text{if } 0.9 < x < 1.0\,. \end{cases}$$

The reflective boundary conditions are applied at both $x = 0.0$ and $x = 1.0$. The results are given in Figure 4.8 for the particle density n, velocity v and pressure p. The number of mesh points are 1000 and the output time is $t = 0.75$.

Problem 6: Experimental order of convergence in one space dimension

Here we check the experimental order of convergence (EOC) of the first and second order kinetic schemes. The initial data are

$$n = \sin(2\pi x) + 2.0, \qquad u = 0.0\,, \qquad p = 1.0\,.$$

The computational domain is $0 \leq x \leq 1$, and the final time for the numerical solution is $t = 1.0$. In a real gas there is a diffusion due to the difference in initial particle density and temperature at the initial contact discontinuity. However, this phenomenon is not described by the Euler equations. In this example the gas is initially at rest therefore the solution is stationary with same data. If $h = \Delta x$ is the cells width then L^1-norm is given by

$$\|W(.,t) - W_h(.,t)\|_{L^1(\mathbb{R})} = ch^\alpha\,, \tag{4.7.1}$$

where α is the order of the L^1-error. Here W denotes the exact solution and W_h the numerical solution. The L^1-error is defined as $\|W(.,t) - W_h(.,t)\|_{L^1} = \Delta x \sum_{i=1}^{N} |W(x_i,t) - W_h(x_i,t)|$, where N is the number of mesh points. Then (4.7.1) gives

$$EOC := \alpha = \ln\left(\frac{\|W(.,t) - W_{\frac{h}{2}}(.,t)\|_{L^1}}{\|W(.,t) - W_h(.,t)\|_{L^1}}\right) \Big/ \ln\left(\frac{1}{2}\right)\,.$$

Table 4.1 give the L^1-error and experimental order of convergence for the first order and second order kinetic schemes. The plots for numerical solution and error difference in the exact and numerical solutions are given in Figure 4.9.

Table 4.1: L^1-error and EOC in the kinetic scheme

	First Order		Second Order	
N	L^1-error	EOC	L^1-error	EOC
50	0.110296		0.012974	
100	0.057260	0.9458	0.003643	1.8324
200	0.029149	0.9741	0.001010	1.8508
400	0.014694	0.9882	0.000272	1.8927
800	0.007369	0.9957	0.000071	1.9377
1600	0.003686	0.9994	0.000018	1.9798
3200	0.001842	1.0008	4.52E-06	1.9936

Problem 7: Experimental order of convergence in two space dimensions

Here we check the experimental order of convergence (EOC) of the two-dimensional kinetic scheme. The initial data are

$$n = \sin(2\pi(x+y)) + 2.0, \qquad u_1 = 0.0\,, \qquad u_2 = 0.0\,, \qquad p = 1.0\,.$$

The computational domain is $[0,1]\times[0,1]$ and the final time is $t = 0.5$. In the two-dimensional kinetic scheme (4.6.3) we have to evaluate the double integrals with respect to $\xi-$ and $\varphi-$integration in each computational cell by using composit trapezoidal rule. This increase the computational time if we use large number of discretization points. Here we have used 25 points for ξ and φ discretizations. Table 4.2 give the L^1-error and EOC.

Table 4.2: L^1-error and EOC in the kinetic scheme

	First Order		Second Order	
N	L^1-error	EOC	L^1-error	EOC
30	0.148764		0.02139021	
60	0.080797	0.8807	0.00699767	1.6120
120	0.043190	0.9036	0.00209437	1.7404
280	0.022538	0.9383	0.00059263	1.8213
480	0.011604	0.9577	0.00016085	1.8667

Problem 8: Cylindrical explosion problem

Consider a square domain $[0,1] \times [0,1]$. The initial data are constant in two regions separated by a circle of radius 0.2 centered at $(0.5, 0.5)$. Inside the circle density is 5.0 and the pressure is 10.0, while outside the density is 1.0 and pressure is equal to 0.5. The velocities are zero everywhere. The solution consists of a circular shock wave propagating outwards from the origin, followed by a circular contact discontinuity propagating in the same direction, and a circular rarefaction wave traveling towards the origin. The results at $y = 0.5$ from the first and second order kinetic schemes, KFVS schemes and central schemes are compared in Figure 4.10. While Figures 4.11 and 4.12 show the contour plots of first and second order kinetic schemes results. We have used 400 mesh points and the final time is $t = 0.2$.

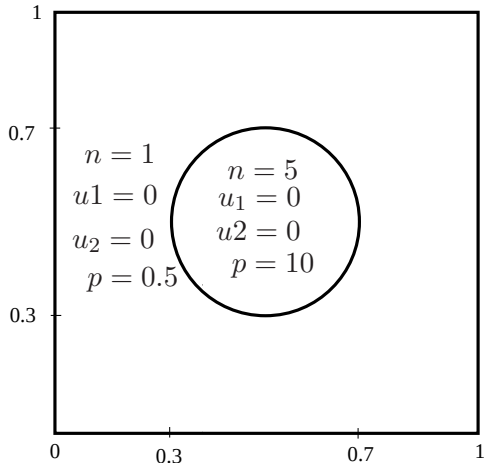

4.8 Summary

In this chapter we have presented the first and second order kinetic schemes for the ultra-relativistic Euler equations. We have numerically implemented the one- and two-dimensional kinetic schemes. The numerical results from the kinetic schemes were compared with the Godunov and central schemes. The programing codes for the kinetic schemes are simple like Godunov and central schemes. As explained before the boundary condition implementations strategy for the kinetic schemes are different compared to the Godunov and central schemes. It was found that kinetic schemes give a better resolution of the contact discontinuity as compared to the Godunov and central schemes, especially in the second order case. We found in Chapter 2 that first order Godunov scheme has better resolution at the contact discontinuity than the first order kinetic scheme, but here we do not see such a difference between the two schemes. The one reason could be that, in the non-relativistic kinetic schemes we have to cut the $\mathbf{c}-$integration limits by using the error function which can produce error in the solution. But in the ultra-relativistic case we do not use any error function due to the finite limits of integration. The kinetic scheme was found to be computationally expensive and is five to six times slower than the other schemes due to the inside loop for the $\mathbf{q}-$integration in each computational cell. However, as discussed in introduction the kinetic schemes have other advantages like, they need no CFL condition and are truly multi-dimensional.

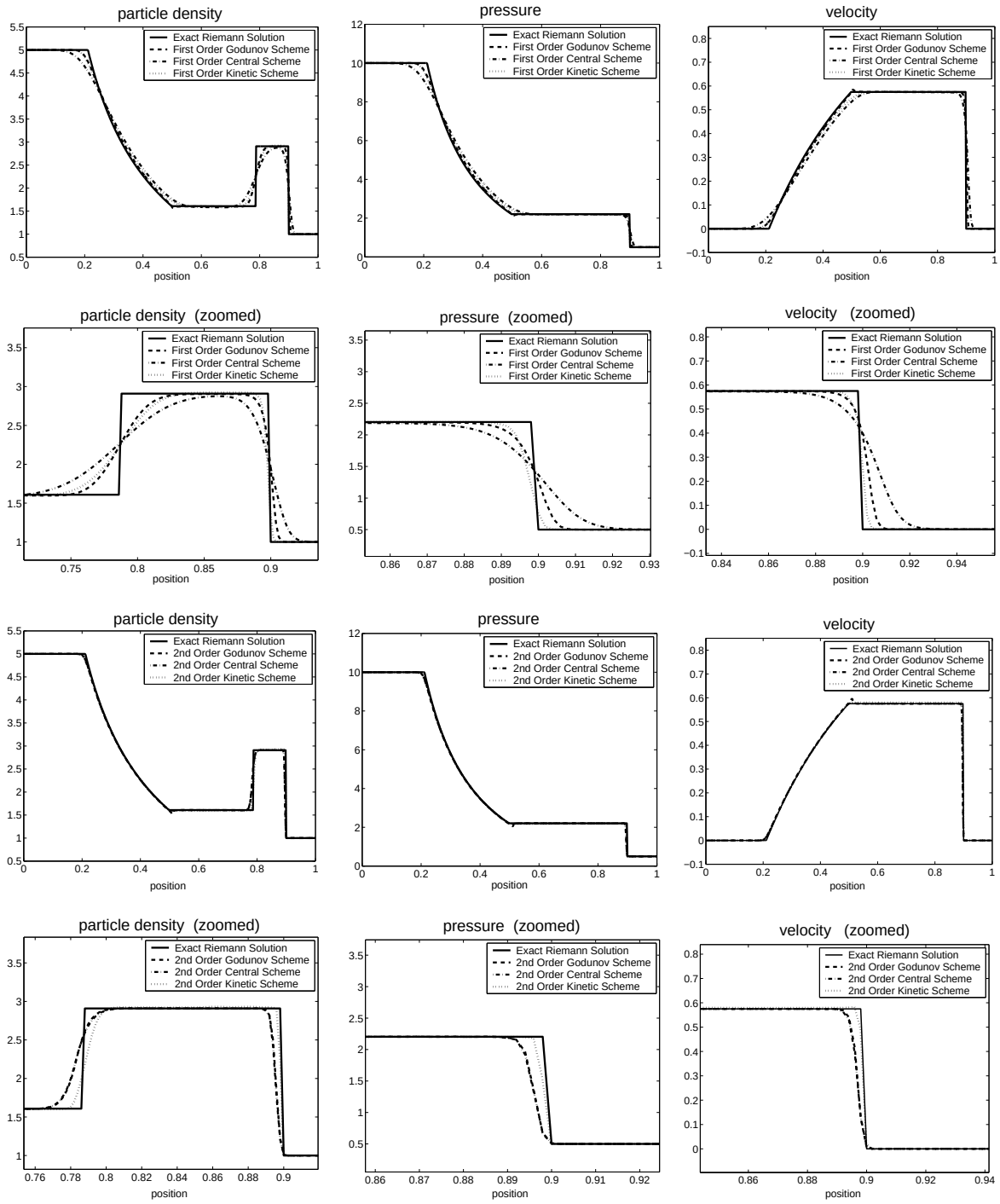

Figure 4.4: Comparison of the results of problem 1 at time $t = 0.5$.

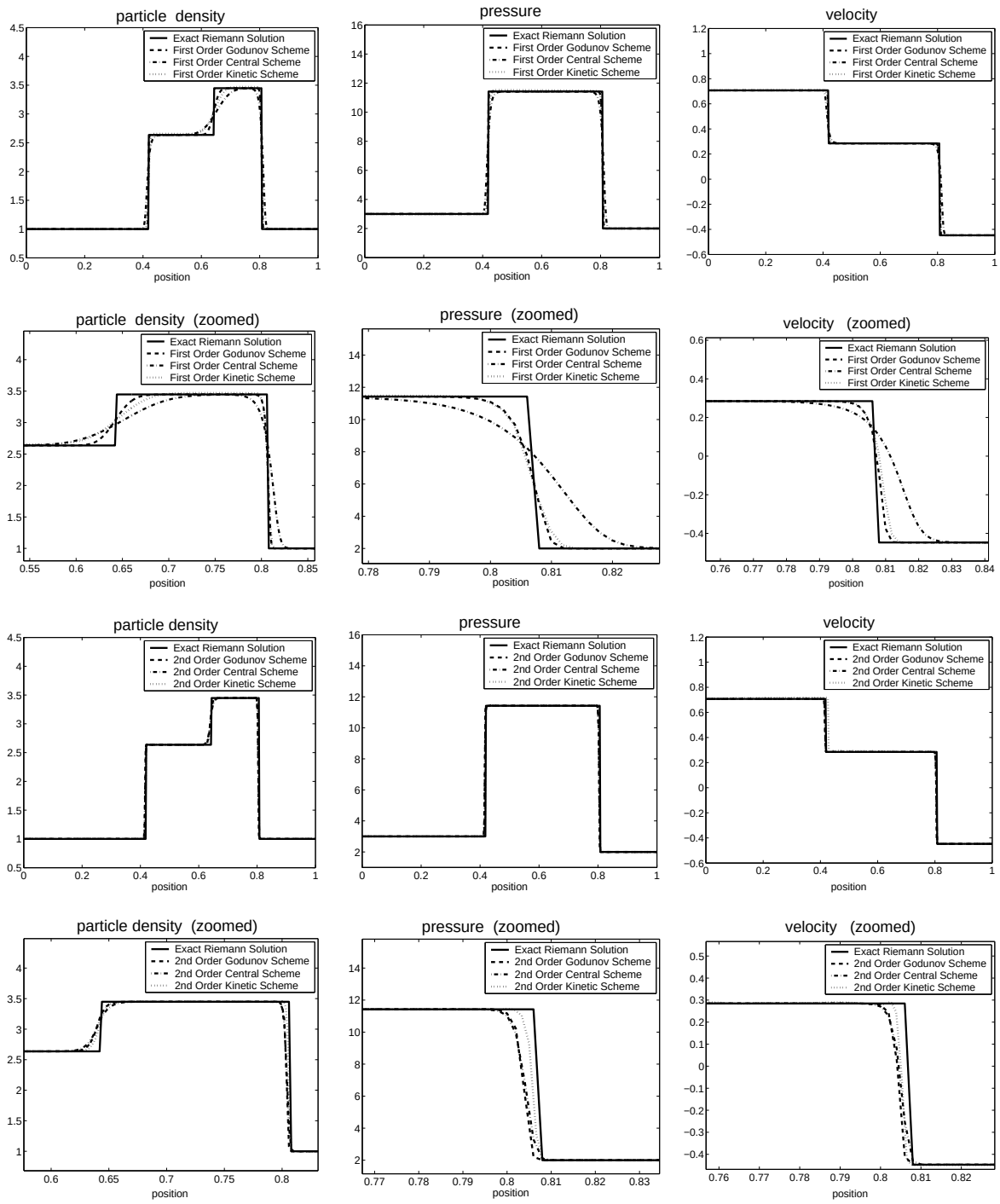

Figure 4.5: Comparison of the results of problem 2 at time $t = 0.5$.

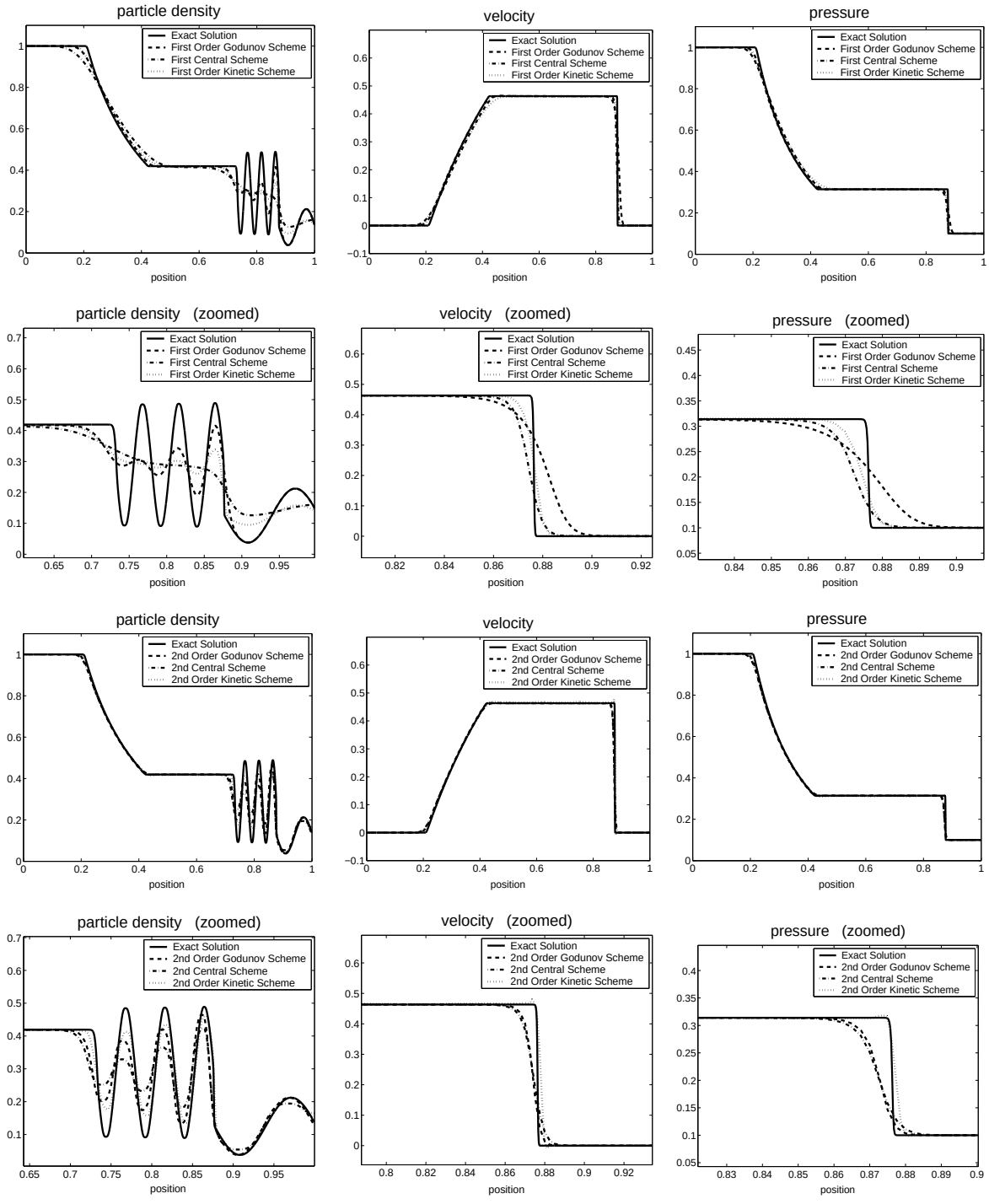

Figure 4.6: Perturbed relativistic shock tube flow at time $t = 0.5$.

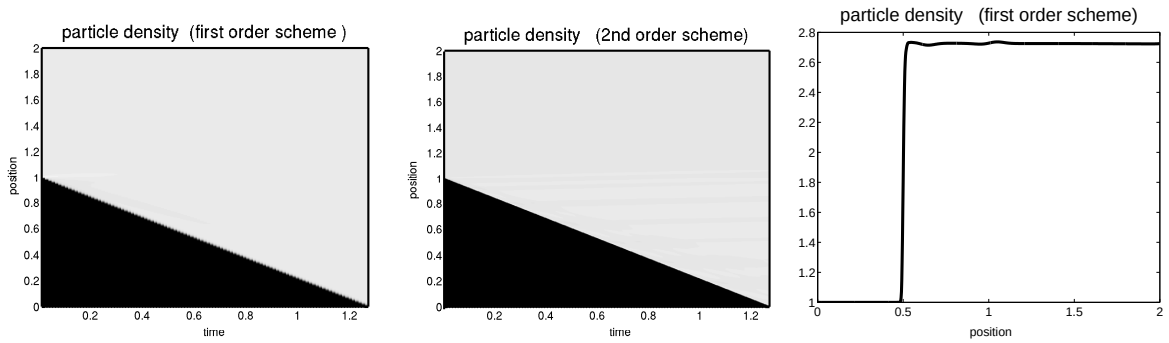

Figure 4.7: A single shock solution using kinetic scheme.

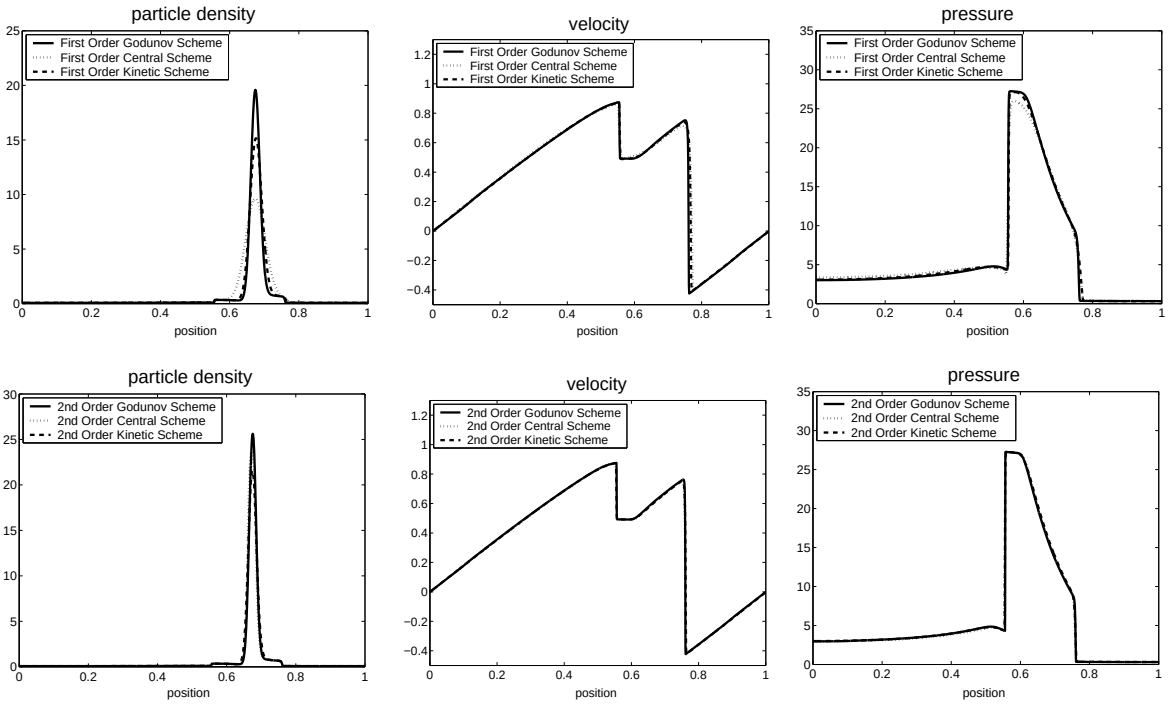

Figure 4.8: Two interacting relativistic blast waves at time $t = 0.75$.

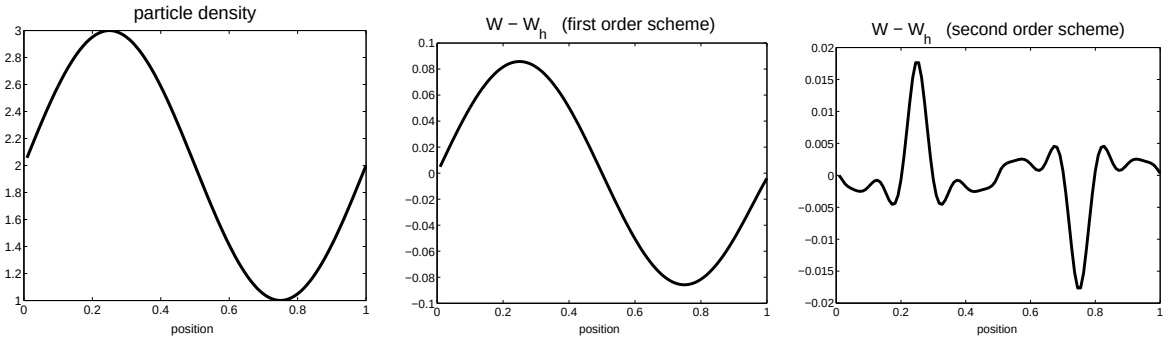

Figure 4.9: Comparison of the results of problem 6 at time $t = 0.5$.

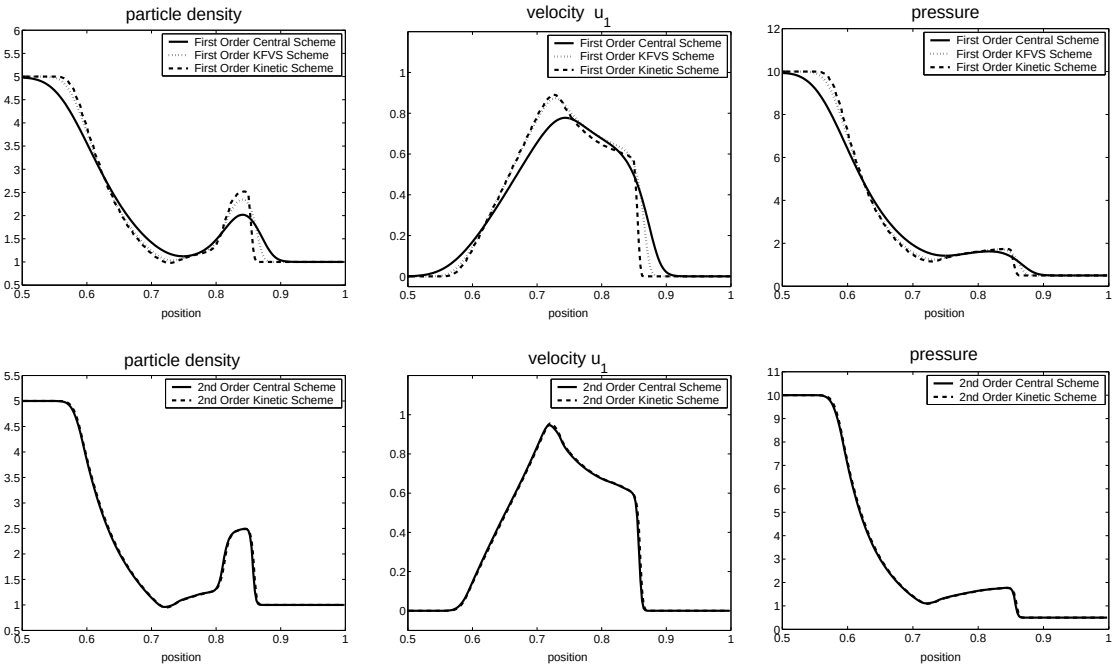

Figure 4.10: Comparison of the schemes applied to cylindrical explosion at $t = 0.2$.

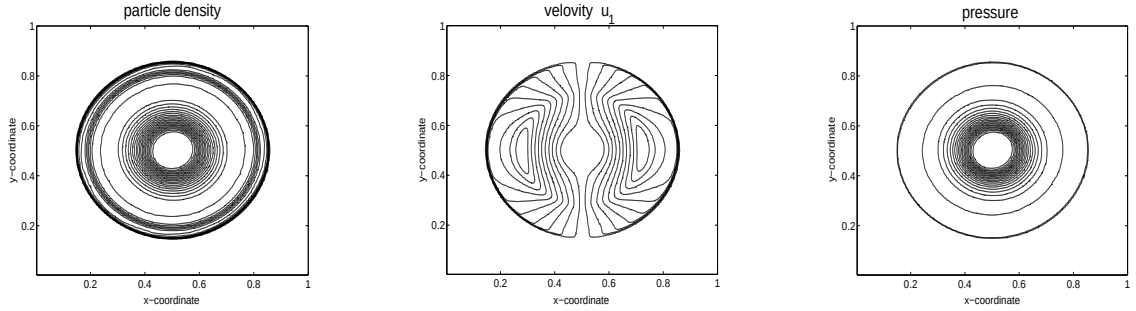

Figure 4.11: First order kinetic scheme at $t = 0.2$.

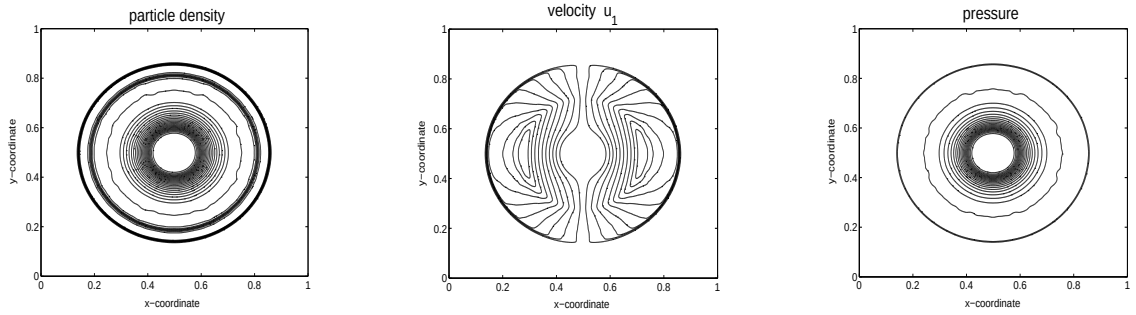

Figure 4.12: Second order kinetic scheme at $t = 0.2$.

Chapter 5

BGK-type KFVS and Godunov Schemes

In this chapter we develop a BGK-type kinetic flux vector splitting (KFVS) schemes for the ultra-relativistic Euler equations. These new scheme are based on the direct splitting of the flux function of the Euler equations with the inclusion of "particle" collisions in the transport process. Consequently, the artificial dissipation in the new schemes are much reduced in comparison with the usual kinetic flux vector splitting (KFVS) schemes which are based on the free particle transport at the cell interfaces in the gas evolution stage. Although in a usual KFVS schemes the free particle transport gives a robust solution, it gives smeared solutions at the contact discontinuities. The new BGK-type KFVS schemes solves this problem and gives a robust and reliable solutions as well as good resolution of the contact discontinuity. We also derive the first order and second order Godunov scheme for the one-dimensional ultra-relativistic Euler equation. We will compare the numerical results of the Godunov, KFVS and BGK-types KFVS schemes.

In the past decades, tremendous progress has been made in the development of numerical methods for compressible flow simulations. Most of them are largely based on upwind concepts, see [34, 36, 65]. There are mainly two kinds of flux functions derived for the inviscid Euler equations. The first group is the flux vector splitting (FVS) schemes. Flux splitting is a technique for achieving upwinding bias in numerical flux functions, which is a natural consequence of regarding fluid motion as a superposition of waves. Since waves can move forward or backward, this automatically splits the fluxes of mass, momentum and energy into forward and backward fluxes through the cell interface, i.e.,

$$F_{i+\frac{1}{2}} = F^{+}(W_i) + F^{-}(W_{i+1}) \,,$$

where W_i represents mass, momentum and energy densities inside a computational cell i. The equivalence between the above splitting mechanism and the collisionless transport equation was first realized by Harten, Lax and van Leer [36]. Numerically it is observed that the explicit flux formulation of the KFVS schemes, by solving collisionless transport equation, are identical to the flux function of van Leer [58]. We will discuss the KFVS schemes for the solution of the ultra-relativistic Euler equations. For more discussion on the KFVS schemes the reader is referred to Xu et al. [90] and Xu [91, 92, 93].

On the other hand, the flux difference splitting (FDS) schemes based on the exact or approximate Riemann solvers, such as the Godunov, Roe and Osher methods [34, 69, 78], account for the wave interactions in the gas evolution process. Especially for the Godunov method, the exact solution of the Euler equations is used. The wave interaction in the FDS schemes can be clearly observed in the Roe average $\overline{W}_{i+\frac{1}{2}}$ between the left W_i and the right state W_{i+1}, see Roe [78]. In the smooth flow region, there is basically no difference among the Godunov, Roe and Osher schemes. For example, the above three schemes can precisely keep a shear layer in the 2D case once the shear layer is aligned with the mesh, see Gressier and Moschetta [31], as well as Quirk [76]. This fact is consistent with the exact solution of the Euler equations. Therefore, the FDS schemes can accurately capture the Navier-Stokes solutions in the resolved dissipative boundary layer, where the numerical dissipation is much smaller than the physical dissipation, see Xu [90] for details. However, this advantage is also accompanied with a disadvantage, the Godunov scheme in strong shock regions produces spurious oscillations such as the carbuncle phenomena and odd-even decoupling in the multi-dimensional case, see Pandolfi and D'ambrosio [71]. FVS schemes do not generate these spurious solutions, since they are intrinsically solving "viscous" equations rather than the inviscid Euler equations. An optimum choice to get a better scheme is to combine both, the FVS and FDS methodology. This is the main aim of this chapter by considering the ultra-relativistic case of the Euler equations.

Even with initial equilibrium states, the collisionless Boltzmann transport equation cannot keep the local equilibrium property dynamically. Physically, the mechanism for bringing the distribution function close to equilibrium state simulates the collisions suffered by the molecules of the gas, the so called collision term in the Boltzmann equation. But the collisionless Boltzmann equation in the free-transport evolution stage totally ignores the dynamical process of particle collisions.

Although the KFVS schemes lacks particle collisions in the free-transport evolution stage, numerically they still can be used in compressible flow calculations, and the numerical solution is different from the free particle stream solutions. The basic reason for this is that an artificial collision term has been implicitly added in the projection stage. For example at the end of each time step, a Maxwellian distribution function f_M inside each cell is re-initiated, which is equivalent to performing particle collisions instantaneously to make the transition from non-equilibrium state, i.e. free-flight f, to equilibrium state f_M inside each cell. The dynamical effect from the two numerical stages, i.e. free-flight and projection, in the KFVS scheme is qualitatively described in the Figure 5.1, where the free transport in the gas evolution stage evolves the system away from the Euler solution, f becomes more and more different from a Maxwellian, the projection stage drives the system towards to the Euler solution, the instantaneous preparation of equilibrium states, see Xu [90]. Kinetic flux splitting schemes (KFVS) have been widely used in solving multi-dimensional non-relativistic Euler equations, see Section 2.5 of Chapter 2.
In this chapter we are interested to derive a new BGK-type KFVS schemes in order to solve one- and two-dimensional ultra-relativistic Euler equations. In these new schemes the particle collisions are added to the free particle transport mechanism in the following convex combination form of the fluxes,

$$F_{i+\frac{1}{2}} = \eta F^f_{i+\frac{1}{2}} + (1-\eta) F^e_{i+\frac{1}{2}} \,,$$

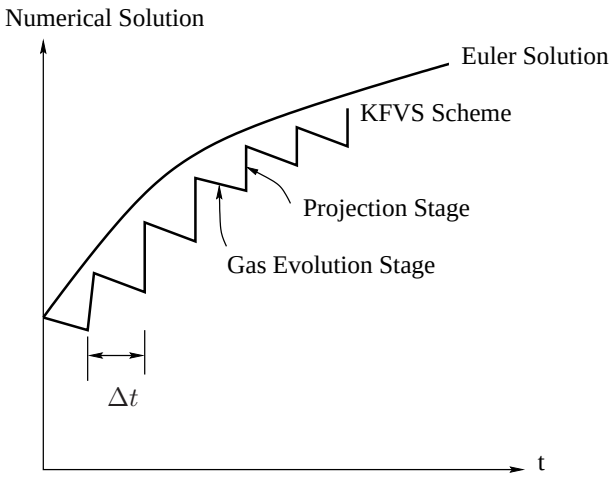

Figure 5.1: KFVS solution vs Euler solution, where Δt is a CFL time step.

where F^f is the flux term from the free-flight phase density and F^e is equilibrium flux obtained from the equilibrium phase density which is relativistic Maxwellian (Jüttner phase density) in our case. Here η is an adjustable parameter and will be analyzed in the coming sections when we derive the scheme. These schemes have been successfully applied to the classical magnetohydrodynamics by Xu [93].

In the BGK-type KFVS schemes we start with a cell averaged initial data of the conservative variables and get back the cell averaged values of the conservative variables at the next time step. In two-dimensional case the flux splitting is done in a usual dimensionally split manner, that is, the formulae for the fluxes can be used along each coordinate direction. In order to get second order accuracy we use a MUSCL-type reconstruction in both one and two-dimensional cases.

5.1 The Ultra-Relativistic Euler Equations

The three-dimensional ultra-relativistic Euler equations (4.1.12)-(4.1.14), can be rewritten as

$$\frac{\partial W}{\partial t} + \sum_{k=1}^{3} \frac{\partial F^k(W)}{\partial x^k} = 0\,, \tag{5.1.1}$$

where

$$W = \begin{pmatrix} N^0 \\ T^{0i} \\ T^{00} \end{pmatrix} = \begin{pmatrix} n\sqrt{1+\mathbf{u}^2} \\ 4pu^i\sqrt{1+\mathbf{u}^2} \\ 3p + 4p\mathbf{u}^2 \end{pmatrix}, \quad F^k(W) = \begin{pmatrix} N^k \\ T^{ik} \\ T^{0k} \end{pmatrix} = \begin{pmatrix} n\,u^k \\ p\,\delta^{ik} + 4pu^iu^k \\ 4pu^k\sqrt{1+\mathbf{u}^2} \end{pmatrix}, \tag{5.1.2}$$

where $i = 1, 2, 3$ and the pressure $p = nT$.

In order to get the primitive variables n, u^k and p from the conserved variables W we use

$$
\begin{aligned}
p(t,\mathbf{x}) &= \frac{1}{3}\left[-T^{00}+\sqrt{4(T^{00})^2-3\sum_{k=1}^{3}(T^{0k})^2}\right], \\
u^k(t,\mathbf{x}) &= \frac{T^{0k}}{\sqrt{4p(t_n^+,\mathbf{x})[p(t,\mathbf{x})+T^{00}]}}, \quad k=1,2,3, \\
n(t,\mathbf{x}) &= \frac{N^0}{\sqrt{1+\sum_{k=1}^{3}[u^k(t_n^+,\mathbf{x})]^2}}.
\end{aligned}
\tag{5.1.3}
$$

5.1.1 One-Dimensional Moment Integrals

Here we rewrite the free-flight moment integrals (4.5.3) and (4.5.4) of the one-dimensional kinetic scheme. As explained there, we only consider the solutions which depend on t and $x = x^1$ and satisfy $n = n(t,x)$, $\mathbf{u} = (u(t,x),0,0)$, $p = p(t,x)$. Here we use Δt as a time step which is equal to the time step $\tau = \tau_M$ used in (4.5.3) and (4.5.4). Therefore we have

$$
W(t_{n+1},x) = \begin{pmatrix} N^0(t_{n+1},x) \\ T^{01}(t_{n+1},x) \\ T^{00}(t_{n+1},x) \end{pmatrix} = \int_{-1}^{1} \begin{pmatrix} \Phi(x-\Delta t\xi,\xi) \\ \xi\,\Psi(x-\Delta t\xi,\xi) \\ \Psi(x-\Delta t\xi,\xi) \end{pmatrix} d\xi, \tag{5.1.4}
$$

$$
F^f(t_{n+1},x) = \begin{pmatrix} N^1(t_{n+1},x) \\ T^{11}(t_{n+1},x) \\ T^{01}(t_{n+1},x) \end{pmatrix} = \int_{-1}^{1} \begin{pmatrix} \xi\,\Phi(x-\Delta t\xi,\xi) \\ \xi^2\,\Psi(x-\Delta t\xi,\xi) \\ \xi\,\Psi(x-\Delta t\xi,\xi) \end{pmatrix} d\xi\,, \tag{5.1.5}
$$

where $t_{n+1} = t_n + \Delta t$ and

$$
\Phi(y,\xi) = \frac{1}{2}\frac{n(y)}{(\sqrt{1+u^2(y)}-\xi u(y))^3}\,, \quad \Psi(y,\xi) = \frac{3}{2}\frac{(nT)(y)}{(\sqrt{1+u^2(y)}-\xi u(y))^4}\,. \tag{5.1.6}
$$

Here we have suppressed for simplicity the fixed time-argument t in the fields, which will not lead to confusions.

5.1.2 Two-Dimensional Moment Integrals

We also rewrite the two-dimensional moment integrals (4.6.3). In this case we consider the solutions which depend on t, $x = x^1$ and $y = x^2$ and satisfy $n = n(t,x,y)$, $\mathbf{u} = (u_1(t,x,y), u_2(t,x,y), 0)$, $p = p(t,x,y)$. Then for

$$
w^1 = \xi\,, \qquad w^2 = \sqrt{1-\xi^2}\sin\varphi\,, \qquad w^3 = \sqrt{1-\xi^2}\cos\varphi\,, \tag{5.1.7}
$$

$$W(t_{n+1},x,y)=\begin{pmatrix} N^0(t_{n+1},x,y)\\ T^{01}(t_{n+1},x,y)\\ T^{02}(t_{n+1},x,y)\\ T^{00}(t_{n+1},x,y)\end{pmatrix}=\int_{-\pi}^{\pi}\int_{-1}^{1}\begin{pmatrix} \Phi(\mathbf{y},w^1,w^2)\\ w^1\,\Psi(\mathbf{y},w^1,w^2)\\ w^2\,\Psi(\mathbf{y},w^1,w^2)\\ \Psi(\mathbf{y},w^1,w^2)\end{pmatrix}d\xi d\varphi\,,$$

$$F^f(t_{n+1},x,y)=\begin{pmatrix} N^1(t_{n+1},x,y)\\ T^{11}(t_{n+1},x,y)\\ T^{12}(t_{n+1},x,y)\\ T^{01}(t_{n+1},x,y)\end{pmatrix}=\int_{-\pi}^{\pi}\int_{-1}^{1}\begin{pmatrix} w^1\,\Phi(\mathbf{y},w^1,w^2)\\ (w^1)^2\,\Psi(\mathbf{y},w^1,w^2)\\ w^1w^2\,\Psi(\mathbf{y},w^1,w^2)\\ w^1\,\Psi(\mathbf{y},w^1,w^2)\end{pmatrix}d\xi d\varphi\,, \tag{5.1.8}$$

$$G^f(t_{n+1},x,y)=\begin{pmatrix} N^2(t_{n+1},x,y)\\ T^{12}(t_{n+1},x,y)\\ T^{22}(t_{n+1},x,y)\\ T^{02}(t_{n+1},x,y)\end{pmatrix}=\int_{-\pi}^{\pi}\int_{-1}^{1}\begin{pmatrix} w^2\,\Phi(\mathbf{y},w^1,w^2)\\ w^1w^2\,\Psi(\mathbf{y},w^1,w^2)\\ (w^2)^2\,\Psi(\mathbf{y},w^1,w^2)\\ w^2\,\Psi(\mathbf{y},w^1,w^2)\end{pmatrix}d\xi d\varphi\,,$$

where $\mathbf{y}=(x-\Delta t\,w^1,y-\Delta t\,w^2)$, $t_{n+1}=t_n+\Delta t$ and

$$\Phi(\mathbf{y},w^1,w^2)=\frac{1}{4\pi}\frac{n(\mathbf{y})}{(\sqrt{1+(u_1^2+u_2^2)(\mathbf{y})}-u_1(\mathbf{y})\,w^1-u_2(\mathbf{y})\,w^2)^3}\,,$$
$$\Psi(\mathbf{y},w^1,w^2)=\frac{3}{4\pi}\frac{(nT)(\mathbf{y})}{(\sqrt{1+(u_1^2+u_2^2)(\mathbf{y})}-u_1(\mathbf{y})\,w^1-u_2(\mathbf{y})\,w^2)^4}\,.$$

The above one- and two-dimensional free-flight moments integrals will be used in order to derive the BGK-type KFVS scheme for the ultra-relativistic Euler equations.

5.2 One-Dimensional BGK-type KFVS Scheme

The equations (5.1.1) in the one-dimensional case gives

$$\frac{\partial W}{\partial t}+\frac{\partial F(W)}{\partial x}=0\,, \tag{5.2.1}$$

where

$$W=\begin{pmatrix} N^0\\ T^{01}\\ T^{00}\end{pmatrix}=\begin{pmatrix} n\sqrt{1+u^2}\\ 4pu\sqrt{1+u^2}\\ 3p+4pu^2\end{pmatrix},\quad F(W)=\begin{pmatrix} N^1\\ T^{11}\\ T^{01}\end{pmatrix}=\begin{pmatrix} n\,u\\ p+4pu^2\\ 4pu\sqrt{1+u^2}\end{pmatrix}. \tag{5.2.2}$$

We start with piecewise constant initial data $\overline{W}_i(t_n)$ over the cells $[x_{i-\frac{1}{2}},x_{i+\frac{1}{2}}]$ of a given mesh size $\Delta x=x_{i+\frac{1}{2}}-x_{i-\frac{1}{2}}$, and we have to compute $\overline{W}_i(t_{n+1})$ over the same cells. We take the natural CFL condition $\Delta t=\frac{\Delta x}{2}$ in order to ensure that neighbouring light-cones will not interact, see Figure 5.2. Note that in the theory of the classical Euler-equations one has to assume a bound for the characteristic speeds which depend on the choice of the initial data in order to obtain a CFL-condition. This is not necessary in our case, since every signal speed is bounded by the velocity of light.

Using again Figure 5.2, the one-dimensional weak form of conservation laws $(4.3.13)_{1,2}$ over the domain $[t_n, t_{n+1}] \times [x_{i-\frac{1}{2}}, x_{i+\frac{1}{2}}]$ gives

$$\oint_{\partial\Omega} W(t,x)\,dx - F(W(t,x))\,dt = 0\,,$$

implying

$$\int_{x_{i-\frac{1}{2}}}^{x_{i+\frac{1}{2}}} [W(t_{n+1},x) - W(t_n,x)]\,dx + \int_{t_n}^{t_{n+1}} \left[F(\tau, x_{i+\frac{1}{2}}) - F(\tau, x_{i-\frac{1}{2}})\right] d\tau = 0\,.$$

Let us define the integral mean values by

$$\overline{W}_i(t) = \frac{1}{\Delta x} \int_{x_{i-\frac{1}{2}}}^{x_{i+\frac{1}{2}}} W(t,x)dx\,.$$

Dividing the above balance equations by Δx, we get the following conservative formula

$$\overline{W}_i(t_{n+1}) = \overline{W}_i(t_n) - \frac{1}{\Delta x} \int_{t_n}^{t_{n+1}} \left[F(\tau, x_{i+\frac{1}{2}}) - F(\tau, x_{i-\frac{1}{2}})\right] d\tau\,, \tag{5.2.3}$$

with

$$F(\tau, x_{i+\frac{1}{2}}) = \eta F^f(\tau, x_{i+\frac{1}{2}}) + (1-\eta)F^e(\tau, x_{i+\frac{1}{2}})\,.$$

Here $F^f(\tau, x_{i+\frac{1}{2}})$ is given by (5.1.5) while we have to derive $F^e(\tau, x_{i+\frac{1}{2}})$. Also we will analyze the parameter η when we complete the derivation of the scheme for the 1D case.

From (5.1.5) we have

$$\int_{t_n}^{t_{n+1}} F^f(\tau, x_{i+\frac{1}{2}})\,d\tau = \int_{t_n}^{t_{n+1}} \int_{-1}^{1} f(x_{i+\frac{1}{2}} - \tau\xi, \xi)\,d\xi\,d\tau\,, \tag{5.2.4}$$

where

$$f(y,\xi) = \begin{pmatrix} \frac{1}{2}\frac{\xi\, n(y)}{(\sqrt{1+u^2(y)}-\xi u(y))^3} \\ \frac{3}{2}\frac{\xi^2\,(nT)(y)}{(\sqrt{1+u^2(y)}-\xi u(y))^4} \\ \frac{3}{2}\frac{\xi\,(nT)(y)}{(\sqrt{1+u^2(y)}-\xi u(y))^4} \end{pmatrix}.$$

The CFL condition states that ξ-integration is limited to ξ such that $|\xi|\tau \le \Delta x$. This means that $x_{i\pm\frac{1}{2}} - \xi\tau$ remains in a neighbour cell to $x_{i\pm\frac{1}{2}}$, see Figure 5.2. This implies that the field

variables n, u, T in the split flux integrals will not depend on the $\xi-$integration, therefore equation (5.2.4) gives

$$F^f_{i+\frac{1}{2}} = \frac{1}{\Delta t}\int_{t_n}^{t_{n+1}} F^f(\tau, x_{i+\frac{1}{2}})\,d\tau = \int_0^1 f(x_i,\xi)\,d\xi + \int_{-1}^0 f(x_{i+1},\xi)\,d\xi$$
$$= F_i^+ + F_{i+1}^-\,, \tag{5.2.5}$$

where for each cell I_i

$$F_i^{\pm} = \begin{pmatrix} \pm\frac{n(x_i)}{4\sqrt{1+u^2(x_i)}}\left(\pm u(x_i)+\sqrt{1+u^2(x_i)}\right)^2 \\ \frac{p(x_i)}{2\sqrt{1+u^2(x_i)}}\left(\pm u(x_i)+\sqrt{1+u^2(x_i)}\right)^3 \\ \frac{p(x_i)}{4}\frac{\left(-u(x_i)\pm 3\sqrt{1+u^2(x_i)}\right)\left(\pm u(x_i)+\sqrt{1+u^2(x_i)}\right)^3}{1+u^2(x_i)} \end{pmatrix}, \tag{5.2.6}$$

where $p = nT$. This is exactly the kinetic flux vector splitting scheme for the ultra-relativistic Euler equations.

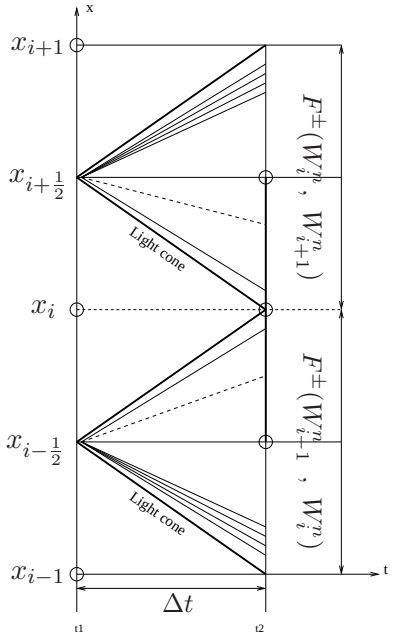

Figure 5.2: Illustration of the conservative kinetic scheme.

Now we are going to derive the equilibrium part of the flux $F^e_{i+\frac{1}{2}}$. As discussed in the introduction all FVS schemes based on positive (negative) particle velocities suffer from the same weakness. The particle free transport across cell interfaces unavoidably introduces a large numerical dissipation, and the viscosity and heat conduction coefficients are proportional to

the CFL time step. In order to reduce the over-diffusivity in flux splitting schemes, particle collisions have to be added in the transport process. Following the idea of Xu [93], the aim is to obtain an equilibrium state $\overline{W}^e_{i+\frac{1}{2}}$ at the cell interface by combining the left and right moving beams. Using this equilibrium state, we get an equilibrium flux function $F^e_{i+\frac{1}{2}}$ through the flux function definition $(5.2.2)_2$.

As a simple particle collisional model, we can imagine that the particles from the left- and right-hand sides of a cell interface collapse totally to form an equilibrium state. In order to define the equilibrium state at the cell interface, we need first to figure out the corresponding macroscopic quantities $\overline{W}^e_{i+\frac{1}{2}}$ there, which are the combination of the total mass, momentum and energy of the left and right moving beams. Now using (5.1.4) we have

$$\overline{W}^e_{i+\frac{1}{2}} = \begin{pmatrix} \overline{N}^0 \\ \overline{T}^{01} \\ \overline{T}^{00} \end{pmatrix}_{i+\frac{1}{2}} = \begin{pmatrix} N^0 \\ T^{01} \\ T^{00} \end{pmatrix}^+_i + \begin{pmatrix} N^0 \\ T^{01} \\ T^{00} \end{pmatrix}^-_{i+1}, \tag{5.2.7}$$

where for each cell I_i

$$\begin{pmatrix} N^0 \\ T^{01} \\ T^{00} \end{pmatrix}^{\pm}_i = \begin{pmatrix} \frac{n(x_i)\left(2\sqrt{1+u^2(x_i)}\mp u(x_i)\right)}{4(1+u^2(x_i))\left(u(x_i)\mp\sqrt{1+u^2(x_i)}\right)^2} \\ \frac{p(x_i)}{4}\frac{\left(-u(x_i)\pm 3\sqrt{1+u^2(x_i)}\right)\left(\pm u(x_i)+\sqrt{1+u^2(x_i)}\right)^3}{1+u^2(x_i)} \\ \frac{p(x_i)\left(3+4u^2(x_i)\mp 3u(x_i)\sqrt{1+u^2(x_i)}\right)}{2\left(1+u^2(x_i)\mp u(x_i)\sqrt{1+u^2(x_i)}\right)^3} \end{pmatrix}. \tag{5.2.8}$$

Now we use the following relation in order to get the averaged values of the primitive variables from the above averaged conservative variables in (5.2.7),

$$p = \frac{1}{3}\left[-\overline{T}^{00} + \sqrt{4(\overline{T}^{00})^2 - 3(\overline{T}^{01})^2}\,\right], \quad u = \frac{\overline{T}^{01}}{\sqrt{4p[p+\overline{T}^{00}]}}, \quad n = \frac{\overline{N}^0}{\sqrt{1+u^2}}. \tag{5.2.9}$$

Then from these "averaged" macroscopic flow quantities in the equation (5.2.9), we can construct the equilibrium flux function

$$F^e_{i+\frac{1}{2}} = \frac{1}{\Delta t}\int_{t_n}^{t_{n+1}} F^e(\tau, x_{i+\frac{1}{2}})\,d\tau = \begin{pmatrix} n\,u \\ p+4pu^2 \\ 4pu\sqrt{1+u^2} \end{pmatrix}_{i+\frac{1}{2}}. \tag{5.2.10}$$

Using (5.2.5) and (5.2.10) in (5.2.3) we finally get the following upwind kinetic scheme

$$\overline{W}_i(t_{n+1}) = \overline{W}_i(t_n) - \frac{\Delta t}{\Delta x}\left[F_{i+\frac{1}{2}} - F_{i-\frac{1}{2}}\right], \tag{5.2.11}$$

with

$$F_{i+\frac{1}{2}} = \eta F^f_{i+\frac{1}{2}} + (1-\eta)F^e_{i+\frac{1}{2}}, \tag{5.2.12}$$

where η is an adaptive parameter. For a first order scheme η can be fixed, such as 0.7 or 0.5, in the numerical calculations. Theoretically, the parameter η should depend on the real flow situations: in the equilibrium and smooth flow regions, the use of $\eta \sim 0$ is physically reasonable, and in discontinuity region, η should be close to 1 in order to have enough numerical dissipation to recover the smooth shock transition. A possible choice for η in high order scheme is to consider it as a function of the pressure difference, such as the switch function in the JST scheme [7]. We follow the MUSCL-type approach to extend the current scheme to high order. For the high-order scheme, the interpolated pressure jump p_l and p_r around a cell interface can naturally be used as a switch function for the parameter η, such as

$$\eta = 1 - \mathrm{Exp}\left(-\frac{|p_l - p_r|}{p_l + p_r}\right), \tag{5.2.13}$$

where α can be some constant, see Xu [93]. In order to get back the primitive variables n, u, T in (5.2.11) we use again (5.2.9).

5.2.1 Second Order Extension of the Scheme in 1D

In order to get the second order accuracy we have the following three steps.

(I): **Data Reconstruction.** Starting with a piecewise-constant solution in time and space, $\sum \overline{W}_i(t_n)\chi_i(x)$, one reconstruct a piecewise linear (MUSCL-type) approximation in space, namely

$$W(t_n, x) = \sum \left[\overline{W}_i(t_n) + W_i^x \frac{(x - x_i)}{\Delta x}\right] \chi_i(x)\,. \tag{5.2.14}$$

Here, $\chi_i(x)$ is the characteristic function of the cell, $I_i := \{\xi \mid |\xi - x_i| \le \frac{\Delta x}{2}\}$, centered around $x_i = i\Delta x$, and W_i^x abbreviates a first order discrete slopes.

The extreme points $x = 0$ and $x = \Delta x$, in local coordinates correspond to the intercell boundaries in general coordinates $x_{i-\frac{1}{2}}$ and $x_{i+\frac{1}{2}}$, respectively, see Figure 5.3. The values W_i at the extreme points are

$$W_i^L = \overline{W}_i(t_n) - \frac{1}{2}W_i^x\,, \quad W_i^R = \overline{W}_i(t_n) + \frac{1}{2}W_i^x\,, \tag{5.2.15}$$

and are usually called *boundary extrapolated values.*

A possible computation of these slopes, which results in an overall non-oscillatory schemes (consult [85]), is given by family of *discrete derivatives* parameterized with $1 \le \theta \le 2$, i.e., for any grid function $\{W_i\}$ we set

$$W_i^x = MM\theta\{W_{i-1}, W_i, W_{i+1}\} = MM\left(\theta\Delta W_{i+\frac{1}{2}}, \frac{\theta}{2}(\Delta W_{i-\frac{1}{2}} + \Delta W_{i+\frac{1}{2}}), \theta\Delta W_{i-\frac{1}{2}}\right).$$

Here, Δ denotes the central differencing, $\Delta W_{i+\frac{1}{2}} = W_{i+1} - W_i$, and MM denotes the min-mod nonlinear limiter

$$MM\{x_1, x_2, ...\} = \begin{cases} \min_i\{x_i\} & \text{if } x_i > 0 \quad \forall i\,, \\ \max_i\{x_i\} & \text{if } x_i < 0 \quad \forall i\,, \\ 0 & \text{otherwise}\,. \end{cases} \tag{5.2.16}$$

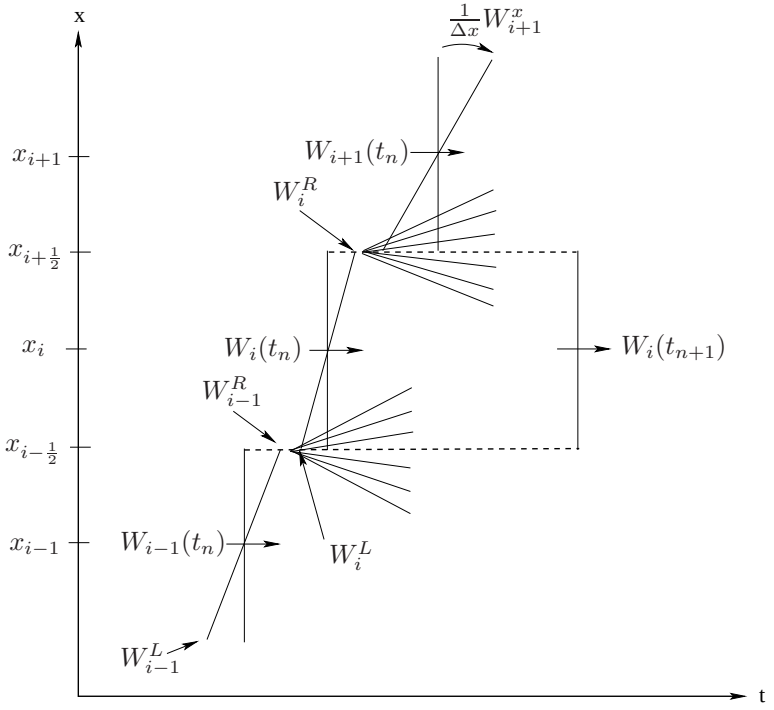

Figure 5.3: Second order reconstruction

This interpolant, (5.2.14), is then evolved exactly in time and projected on the cell-averages at the next time step.

(II): **Evolution.** For each cell I_i, the boundary extrapolated values W_i^L, W_i^R in (5.2.15) are evolved for a time $\frac{1}{2}\Delta t$ by

$$\begin{aligned} \hat{W}_i^L &= W_i^L + \frac{1}{2}\frac{\Delta t}{\Delta x}\left[F(W_i^L) - F(W_i^R)\right] , \\ \hat{W}_i^R &= W_i^R + \frac{1}{2}\frac{\Delta t}{\Delta x}\left[F(W_i^L) - F(W_i^R)\right] , \end{aligned} \tag{5.2.17}$$

where F is the flux term from in the Euler equations $(5.2.2)_2$.

Note that this evolution step is entirely contained in each cell I_i, as the intercell fluxes are evaluated at the boundary extrapolated values of each cell. At each intercell position $i + \frac{1}{2}$ there are two fluxes, namely W_i^R and W_{i+1}^L, which are in general distinct. This does not really affect the *conservative* character of the overall method, as this step is only an intermediate step [85].

(III): Finally we use the conservative formula (5.2.11) in order to get the conservative variables at next time step

$$\overline{W}_i(t_{n+1}) = \overline{W}_i(t_n) - \frac{\Delta t}{\Delta x}\left[F_{i+\frac{1}{2}} - F_{i-\frac{1}{2}}\right] , \tag{5.2.18}$$

with

$$F_{i+\frac{1}{2}} = \eta F^f_{i+\frac{1}{2}} + (1-\eta) F^e_{i+\frac{1}{2}}\,, \tag{5.2.19}$$

where $F^f_{i+\frac{1}{2}} = F^+(\hat{W}^R_i) + F^-(\hat{W}^L_{i+1})$, and $F^\pm$ is given by (5.2.6). Similarly to calculate $F^e_{i+\frac{1}{2}}$, we have

$$\overline{W}^e_{i+\frac{1}{2}} = (\hat{W}^+)^R_i + (\hat{W}^-)^L_{i+1}\,,$$

using (5.2.8) $\hat{W}^\pm_i$ can be calculated from (5.2.17), then

$$F^e_{i+\frac{1}{2}} = F^e(\overline{W}^e_{i+\frac{1}{2}})\,.$$

In order to get back the fields n, u_1, u_2, T we use the relations (5.2.9).

5.3 Two-Dimensional BGK-type KFVS Scheme

Here we want to solve the two-dimensional Euler equations

$$\frac{\partial W}{\partial t} + \frac{\partial F(W)}{\partial x} + \frac{\partial G(W)}{\partial y} = 0\,, \tag{5.3.1}$$

where

$$W = \begin{pmatrix} N^0 \\ T^{01} \\ T^{02} \\ T^{00} \end{pmatrix} = \begin{pmatrix} n\sqrt{1+\mathbf{u}^2} \\ 4p\,u1\sqrt{1+\mathbf{u}^2} \\ 4p\,u2\sqrt{1+\mathbf{u}^2} \\ 3p + 4p\,\mathbf{u}^2 \end{pmatrix},\ F(W) = \begin{pmatrix} N^1 \\ T^{11} \\ T^{12} \\ T^{01} \end{pmatrix} = \begin{pmatrix} n\,u_1 \\ p + 4p\,u_1^2 \\ 4p\,u_1\,u_2 \\ 4p\,u_1\sqrt{1+\mathbf{u}^2} \end{pmatrix},$$

$$G(W) = \begin{pmatrix} N^2 \\ T^{12} \\ T^{22} \\ T^{02} \end{pmatrix} = \begin{pmatrix} n\,u_2 \\ 4p\,u_1\,u_2 \\ p + 4p\,u_2^2 \\ 4p\,u_2\sqrt{1+\mathbf{u}^2} \end{pmatrix}, \tag{5.3.2}$$

where $\mathbf{u} = \sqrt{1+u_1^2+u_2^2}$. We start again with a piecewise constant initial data of the conservative variables $\overline{W}_{i,j}(t_n)$. Using the weak conservation laws $(4.3.13)_{1,2}$ in two-dimensional case over the volume $[t_n, t_{n+1}] \times [x_{i-\frac{1}{2}}, x_{i+\frac{1}{2}}] \times [y_{j-\frac{1}{2}}, y_{j+\frac{1}{2}}]$, we get

$$\overline{W}_{i,j}(t_{n+1}) = \overline{W}_{i,j}(t_n) - \frac{\Delta t}{\Delta x}\left[F_{i+\frac{1}{2},j} - F_{i-\frac{1}{2},j}\right] - \frac{\Delta t}{\Delta y}\left[G_{i,j+\frac{1}{2}} - G_{i,j-\frac{1}{2}}\right], \tag{5.3.3}$$

where

$$\overline{W}_{i,j}(t) = \frac{1}{\Delta x \Delta y} \int_{x_{i-\frac{1}{2}}}^{x_{i+\frac{1}{2}}} \int_{y_{j-\frac{1}{2}}}^{y_{j+\frac{1}{2}}} W(t,x,y)\,dxdy\,,$$

$$F_{i+\frac{1}{2},j} = \eta F^f_{i+\frac{1}{2},j} + (1-\eta) F^e_{i+\frac{1}{2},j}\,,\ \ G_{i,j+\frac{1}{2}} = \eta G^f_{i,j+\frac{1}{2}} + (1-\eta) G^e_{i,j+\frac{1}{2}}\,.$$

Here

$$F^f_{i+\frac{1}{2},j} = \frac{1}{\Delta t}\int_{t_n}^{t_{n+1}} F^f(\tau, x_{i+\frac{1}{2}}, y_j)\, d\tau\,, \quad G^f_{i,j+\frac{1}{2}} = \frac{1}{\Delta t}\int_{t_n}^{t_{n+1}} G^f(\tau, x_i, y_{j+\frac{1}{2}})\, d\tau\,,$$

where the flux moments $F^f(\tau, x_{i+\frac{1}{2}}, y_j)$ and $G^f(\tau, x_i, y_{j+\frac{1}{2}})$ are given in (5.1.8).

If the CFL condition $\Delta t \le \frac{1}{2}\min(\Delta x, \Delta y)$ is satisfied, then we can utilize the kinetic flux vector splitting (KFVS). Since after flux splitting the fields n, u_1, u_2 and T in (5.1.8) are not depending on the integration variables ξ and φ, therefore we can solve analytically these moments integrals for the fluxes. This gives

$$F^f_{i+\frac{1}{2},j} = F^+_{i,j} + F^-_{i+1,j}\,, \qquad G^f_{i,j+\frac{1}{2}} = G^+_{i,j} + F^-_{i,j+1}\,, \tag{5.3.4}$$

where from (5.1.8)

$$F^\pm_{i,j} = \begin{pmatrix} N^1 \\ T^{11} \\ T^{12} \\ T^{01} \end{pmatrix}^\pm_{i,j}, \quad G^\pm = \begin{pmatrix} N^2 \\ T^{12} \\ T^{22} \\ T^{02} \end{pmatrix}^\pm_{i,j}.$$

Here for the fluxes $F^\pm_{i,j}$ we split the integrals with respect to variable ξ and take the integration with respect to variable φ as a whole. While for the fluxes $G^\pm_{i,j}$, we split the integrals with respect to variable φ and integrate the integrals with respect to ξ as a whole. Thus we get the following relations for the fluxes $F^\pm_{i,j}$ and $G^\pm_{i,j}$ for each cell $I_{i,j}$

$$F^\pm_{i,j} = \begin{pmatrix} \frac{nu_1}{2} \pm \frac{n(1+2u_1^2)}{4\sqrt{1+u_1^2}} \\ \frac{p(1+4u_1^2)}{2} \pm \frac{pu_1(3+4u_1^2)}{2\sqrt{1+u_1^2}} \\ 2pu_1u_2 \pm \frac{pu_2(3+12u_1^2+8u_1^4)}{4(1+u_1^2)^{\frac{3}{2}}} \\ p\sqrt{1+\mathbf{u}^2}\left(2u_1 \pm \frac{(3+12u_1^2+8u_1^4)}{4(1+u_1^2)^{\frac{3}{2}}}\right) \end{pmatrix}_{i,j}, \tag{5.3.5}$$

$$G^\pm_{i,j} = \begin{pmatrix} \frac{nu_2}{2} \pm \frac{n(1+2u_2^2)}{4\sqrt{1+u_2^2}} \\ 2pu_1u_2 \pm \frac{pu_2(3+12u_1^2+8u_1^4)}{4(1+u_1^2)^{\frac{3}{2}}} \\ \frac{p(1+4u_2^2)}{2} \pm \frac{pu_2(3+4u_2^2)}{2\sqrt{1+u_2^2}} \\ p\sqrt{1+\mathbf{u}^2}\left(2u_2 \pm \frac{(3+12u_2^2+8u_2^4)}{4(1+u_2^2)^{\frac{3}{2}}}\right) \end{pmatrix}_{i,j}.$$

where $\mathbf{u} = \sqrt{u_1^2+u_2^2}$.

As discussed in the introduction and in the one-dimensional case, all FVS schemes based on positive (negative) particle velocities suffer from the same weakness. The particle free transport across the cell interfaces unavoidably introduces a large numerical dissipation, and the

viscosity and heat conduction coefficients are proportional to the CFL time step. In order to reduce the over-diffusivity in flux splitting schemes, particle collisions have to be added in the transport process.

As a simple particle collisional model, we can imagine that the particles at the cell interface moving in positive and negative $x-$ and $y-$ directions collapse totally to form an equilibrium state. In order to define the equilibrium state at the cell interface, we need first to figure out the corresponding macroscopic quantities $\overline{W}^e_{i+\frac{1}{2},j}$ and $\overline{W}^e_{i,j+\frac{1}{2}}$ there, which are the combination of the total mass, momentum and energy of the moving beams in negative and positive direction of x- and y-axis. Now using $(5.1.8)_1$ we have

$$\overline{W}^e_{i+\frac{1}{2},j} = \begin{pmatrix} \overline{N}^0 \\ \overline{T}^{01} \\ \overline{T}^{02} \\ \overline{T}^{00} \end{pmatrix}_{i+\frac{1}{2},j} = \begin{pmatrix} N^0 \\ T^{01} \\ T^{02} \\ T^{00} \end{pmatrix}^+_{i,j} + \begin{pmatrix} N^0 \\ T^{01} \\ T^{02} \\ T^{00} \end{pmatrix}^-_{i+1,j},$$

where for each cell $I_{i,j}$

$$\begin{pmatrix} N^0 \\ T^{01} \\ T^{02} \\ T^{00} \end{pmatrix}^{\pm}_{i,j} = \begin{pmatrix} \frac{n\sqrt{1+\mathbf{u}^2}}{2}\left(1 \pm \frac{u_1(3+2u_1^2)}{2(1+u_1^2)^{\frac{3}{2}}}\right) \\ p\sqrt{1+\mathbf{u}^2}\left(2u_1 \pm \frac{(3+12u_1^2+8u_1^4)}{4(1+u_1^2)^{\frac{3}{2}}}\right) \\ pu_2\sqrt{1+\mathbf{u}^2}\left(2 \pm \frac{u_1(15+20u_1^2+8u_1^4)}{4(1+u_1^2)^{\frac{5}{2}}}\right) \\ \frac{p\left(3+4\mathbf{u}^2\right)}{2} \pm \frac{pu_1\left(12+15(u_1^2+\mathbf{u}^2)+8u_1^4\mathbf{u}^2+2u_1^2(3u_1^2+10\mathbf{u}^2)\right)}{4(1+u_1^2)^{\frac{5}{2}}} \end{pmatrix}_{i,j}. \tag{5.3.6}$$

Similarly

$$\overline{W}^e_{i,j+\frac{1}{2}} = \begin{pmatrix} \overline{N}^0 \\ \overline{T}^{01} \\ \overline{T}^{02} \\ \overline{T}^{00} \end{pmatrix}_{i,j+\frac{1}{2}} = \begin{pmatrix} N^0 \\ T^{01} \\ T^{02} \\ T^{00} \end{pmatrix}^+_{i,j} + \begin{pmatrix} N^0 \\ T^{01} \\ T^{02} \\ T^{00} \end{pmatrix}^-_{i,j+1},$$

where for each cell $I_{i,j}$ with $\mathbf{u} = \sqrt{u_1^2 + u_2^2}$ we have

$$\begin{pmatrix} N^0 \\ T^{01} \\ T^{02} \\ T^{00} \end{pmatrix}^{\pm}_{i,j} = \begin{pmatrix} \frac{n(x_i)\sqrt{1+\mathbf{u}^2}}{2}\left(1 \pm \frac{u_2(3+2u_2^2)}{2(1+u_2^2)^{\frac{3}{2}}}\right) \\ pu_1\sqrt{1+\mathbf{u}^2}\left(2 \pm \frac{u_2(15+20u_2^2+8u_2^4)}{4(1+u_2^2)^{\frac{5}{2}}}\right) \\ p\sqrt{1+\mathbf{u}^2}\left(2u_2 \pm \frac{(3+12u_2^2+8u_2^4)}{4(1+u_2^2)^{\frac{3}{2}}}\right) \\ \frac{p\left(3+4\mathbf{u}^2\right)}{2} \pm \frac{pu_2\left(12+15(u_2^2+\mathbf{u}^2)+8u_2^4\mathbf{u}^2+2u_2^2(3u_2^2+10\mathbf{u}^2)\right)}{4(1+u_2^2)^{\frac{5}{2}}} \end{pmatrix}_{i,j}. \tag{5.3.7}$$

Now we use the following relation in order to get the averaged values of the primitive variables from the above averaged conservative variables

$$p = \frac{1}{3}\left[-\overline{T}^{00} + \sqrt{4(\overline{T}^{00})^2 - 3\left[(\overline{T}^{01})^2 + (\overline{T}^{02})^2\right]}\right],$$
$$u_1 = \frac{\overline{T}^{01}}{\sqrt{4p[p+\overline{T}^{00}]}}, \quad u_2 = \frac{\overline{T}^{02}}{\sqrt{4p[p+\overline{T}^{00}]}}, \quad n = \frac{\overline{N}^{0}}{\sqrt{1+u_1^2+u_2^2}}. \tag{5.3.8}$$

Then from these "averaged" macroscopic flow quantities in the equation (5.3.8), we can construct the equilibrium flux functions

$$F^e_{i+\frac{1}{2},j} = \frac{1}{\Delta t}\int_{t_n}^{t_n+\Delta t} F^e(\tau, x_{i+\frac{1}{2}}, y_j)\, d\tau = \begin{pmatrix} n\,u_1 \\ p + 4p\,u_1^2 \\ 4p\,u_1\,u_2 \\ 4p\,u_1\sqrt{1+u_1^2+u_2^2} \end{pmatrix}_{i+\frac{1}{2},j}, \tag{5.3.9}$$

$$G^e_{i,j+\frac{1}{2}} = \frac{1}{\Delta t}\int_{t_n}^{t_n+\Delta t} F^e(\tau, x_i, y_{j+\frac{1}{2}})\, d\tau = \begin{pmatrix} n\,u_2 \\ 4p\,u_1\,u_2 \\ p + 4p\,u_2^2 \\ 4p\,u_2\sqrt{1+u_1^2+u_2^2} \end{pmatrix}_{i,j+\frac{1}{2}}. \tag{5.3.10}$$

Using (5.3.4), (5.3.9) and (5.3.10) in (5.3.3) we finally get the following upwind kinetic scheme

$$\overline{W}_{i,j}(t_{n+1}) = \overline{W}_{i,j}(t_n) - \frac{\Delta t}{\Delta x}\left[F_{i+\frac{1}{2},j} - F_{i-\frac{1}{2},j}\right] - \frac{\Delta t}{\Delta y}\left[G_{i,j+\frac{1}{2}} - G_{i,j-\frac{1}{2}}\right], \tag{5.3.11}$$

with

$$F_{i+\frac{1}{2},j} = \eta F^f_{i+\frac{1}{2},j} + (1-\eta)F^e_{i+\frac{1}{2},j}, \; G_{i,j+\frac{1}{2}} = \eta G^f_{i,j+\frac{1}{2}} + (1-\eta)G^e_{i,j+\frac{1}{2}}, \tag{5.3.12}$$

again η is an adaptive parameter and can be taken fixed, for example 0.5 or 0.7. It can also be calculated from the left and right state pressure at the cell interface by using the relation (5.2.13). In order to get back the fields n, u_1, u_2, T from the conservative variable at next time we use the relations (5.3.8).

5.3.1 Second Order Extension of the Scheme in 2D

Here we present the second-order MUSCL-type approach for the two-dimensional case. Keeping in view the MUSCL approach discussed in the previous section for the one-dimensional case, we have again the following three steps.

(I): **Data Reconstruction and Boundary Extrapolated Values.** Starting with a piecewise-constant solution in time and space, $\overline{W}_{i,j}(t_n)$, one reconstruct a piecewise linear (MUSCL-type) approximation independently in x- and y-directions by selecting selecting respective slope vectors (differences) W^x and W^y. Boundary extrapolated values are

$$W^{LX}_{i,j} = \overline{W}_{i,j}(t_n) - \frac{1}{2}W^x_{i,j}, \quad W^{RX}_{i,j} = \overline{W}_{i,j}(t_n) + \frac{1}{2}W^x_{i,j},$$
$$W^{LY}_{i,j} = \overline{W}_{i,j}(t_n) - \frac{1}{2}W^y_{i,j}, \quad W^{RY}_{i,j} = \overline{W}_{i,j}(t_n) + \frac{1}{2}W^y_{i,j}. \tag{5.3.13}$$

A possible computation of these slopes is given by family of *discrete derivatives* parameterized with $1 \le \theta \le 2$, for example

$$W^x_{i,j} = MM\left\{\theta\Delta\overline{W}_{i+\frac{1}{2},j}, \frac{\theta}{2}\left(\Delta\overline{W}_{i+\frac{1}{2},j} + \Delta\overline{W}_{i-\frac{1}{2},j}\right), \theta\Delta\overline{W}_{i-\frac{1}{2},j}\right\},$$
$$W^y_{i,j} = MM\left\{\theta\Delta\overline{W}_{i,j+\frac{1}{2}}, \frac{\theta}{2}\left(\Delta\overline{W}_{i,j+\frac{1}{2}} + \Delta\overline{W}_{i,j-\frac{1}{2}}\right), \theta\Delta\overline{W}_{i,j-\frac{1}{2}}\right\}. \qquad (5.3.14)$$

Here Δ denotes central differencing,

$$\Delta\overline{W}_{i+\frac{1}{2},j} = \overline{W}_{i+1,j} - \overline{W}_{i,j}\,, \qquad \Delta\overline{W}_{i,j+\frac{1}{2}} = \overline{W}_{i,j+1} - \overline{W}_{i,j}\,,$$

and MM denotes the min-mod nonlinear limiter given in (5.2.16).

(II): **Evolution of Boundary Extrapolated Values.** The boundary extrapolated values are evolved at a time $\frac{\Delta t}{2}$ by using

$$\hat{W}^l_{i,j} = W^l_{i,j} + \frac{1}{2}\frac{\Delta t}{\Delta x}\left[F(W^{LX}_{i,j}) - F(W^{RX}_{i,j})\right] + \frac{1}{2}\frac{\Delta t}{\Delta y}\left[G(W^{LY}_{i,j}) - G(W^{RY}_{i,j})\right], \quad (5.3.15)$$

for $l = LX, RX, LY, RY$. Here the values of F and G are obtained from the Euler equations $(5.3.2)_{2,3}$.

(III): **Solution at the Next Time Step.** At each intercell position one solves

$$\overline{W}_{i,j}(t_{n+1}) = \overline{W}_{i,j}(t_n) - \frac{\Delta t}{\Delta x}\left[F_{i+\frac{1}{2},j} - F_{i+\frac{1}{2},j}\right] - \frac{\Delta t}{\Delta y}\left[G_{i,j+\frac{1}{2}} - G_{i,j+\frac{1}{2}}\right],$$

with

$$F_{i+\frac{1}{2},j} = \eta F^f_{i+\frac{1}{2},j} + (1-\eta)F^e_{i+\frac{1}{2},j}\,,\ G_{i,j+\frac{1}{2}} = \eta G^f_{i,j+\frac{1}{2}} + (1-\eta)G^e_{i,j+\frac{1}{2}}\,, \qquad (5.3.16)$$

where

$$F^f_{i+\frac{1}{2},j} = F^+(\hat{w}^{RX}_{i,j}) + F^-(\hat{w}^{LX}_{i+1,j})\,,\ G^f_{i,j+\frac{1}{2}} = G^+(\hat{w}^{RY}_{i,j}) + G^-(\hat{w}^{LY}_{i,j+1})\,,$$

where $F^\pm$ and $G^\pm$ are given by (5.3.5). Similarly to calculate $F^e_{i+\frac{1}{2},j}$ and $G^e_{i,j+\frac{1}{2}}$, we have

$$\overline{W}^e_{i+\frac{1}{2},j} = (\hat{W}^+)^{RX}_{i,j} + (\hat{W}^-)^{LX}_{i+1,j}\,, \quad \overline{W}^e_{i,j+\frac{1}{2}} = (\hat{W}^+)^{RY}_{i,j} + (\hat{W}^-)^{LY}_{i,j+1}\,,$$

using (5.3.15) $\hat{W}^\pm$ can be obtained from (5.3.6) for $\overline{W}_{i+\frac{1}{2},j}$ and by (5.3.7) for $\overline{W}_{i,j+\frac{1}{2}}$, then we have

$$F^e_{i+\frac{1}{2},j} = F^e(\overline{W}^e_{i+\frac{1}{2},j})\,, \quad G^e_{i,j+\frac{1}{2}} = G^e(\overline{W}^e_{i,j+\frac{1}{2}})\,.$$

In order to get back the fields n, u_1, u_2, T we use the relations (5.3.8).

5.4 Godunov Upwind Scheme

The evolution of an initial discontinuity separating two constant initial states (*Riemann problem*) has played a very important role in the development of numerical fluid dynamics codes in classical (Newtonian) fluid dynamics after the pioneering work of Godunov in 1959. Nowadays, most modern high-resolution shock-capturing methods, LeVeque [55], are based on the exact or approximate solution of Riemann problems between adjacent numerical cells and the development of efficient Riemann solvers has become a research field in numerical analysis in its own, Toro [85]. Godunov [34] produced a conservative extension of the first order upwind scheme of Courant, Isaacson and Rees [10] to non-linear systems of hyperbolic conservation laws. The essential ingredient of the scheme is the solution of the Riemann problem, which may be the exact solution or some suitable approximation to it. Here we will present the scheme in terms of the exact Riemann solution which we have developed in Chapter 4 for the ultra-relativistic Euler equations. We apply the MUSCL approach to extend the first order Godunov upwind scheme to second order. Here we present the Godunov scheme by taking under consideration the ultra-relativistic Euler equations.

Given general initial data in terms of the conserved variables $W(t_n, x)$ at time $t = t_n$, the Godunov method first assumes a piecewise constant distribution of the data which is obtained by defining the cell averages

$$\overline{W}_i(t_n) = \frac{1}{\Delta x} \int\limits_{x_{i-\frac{1}{2}}}^{x_{i+\frac{1}{2}}} W(t_n, \xi) d\xi \,, \tag{5.4.1}$$

which produces the desired piecewise constant distribution in each cell $I_i = [x_{i-\frac{1}{2}}, x_{i+\frac{1}{2}}]$. This averaging is illustrated in Figure 5.4. Using the following balance law over the control volume $\left[x_{i-\frac{1}{2}}, x_{i+\frac{1}{2}}\right] \times [t_n, t_{n+1}]$

$$\oint\limits_{\partial\Omega} W dx - F(W) dt = 0 \,,$$

we get

$$\int\limits_{t_n}^{t_{n+1}} F[W(t, x_{i+\frac{1}{2}})] dt + \int\limits_{x_{i-\frac{1}{2}}}^{x_{i+\frac{1}{2}}} W(t_{n+1}, \xi) d\xi - \int\limits_{t_n}^{t_{n+1}} F[W(t, x_{i-\frac{1}{2}})] dt - \int\limits_{x_{i-\frac{1}{2}}}^{x_{i+\frac{1}{2}}} W(t_n, \xi) d\xi = 0 \,.$$

Since in ultra-relativistic case the maximum speed of the waves is $s_{max} = \pm 1$, therefore to avoid the interaction of waves, we take $\Delta t \leq \frac{\Delta x}{2}$. A consequence of this restriction is that only two Riemann solutions affect the cell I_i, namely the right traveling waves of $W_{i-\frac{1}{2}}(\bar{x}/\bar{t})$ and the left traveling waves of $W_{i+\frac{1}{2}}(\bar{x}/\bar{t})$, where $(\bar{t}, \bar{x})$ are the local coordinates for the local Riemann problem. Figure 5.4 shows typical wave patterns emerging from intercell boundaries $x_{i-\frac{1}{2}}$ and $x_{i+\frac{1}{2}}$ when solving two Riemann problems $RP\left(W^n_{i-1}, W^n_i\right)$ and $RP\left(W^n_i, W^n_{i+1}\right)$. For a time step Δt one can define a global solution $W(t, x)$ in the strip $0 \leq x \leq L$, $t_n \leq t \leq t_{n+1}$ in terms of the local coordinates as follows

$$W(t, x) = W_{i+\frac{1}{2}}\left(\bar{x}/\bar{t}\right) \,, \quad x \in [x_i, x_{i+1}] \,, \tag{5.4.2}$$

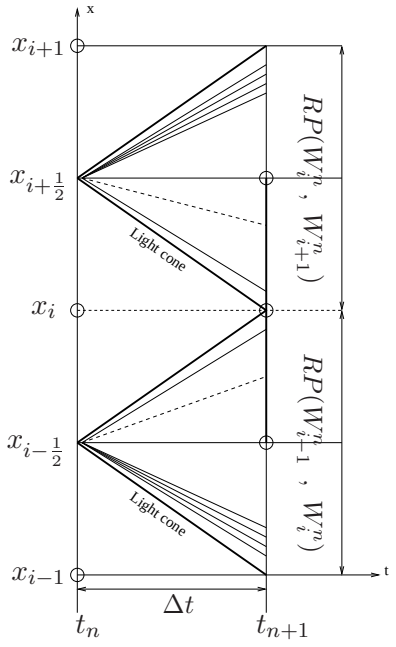

Figure 5.4: Illustration of Godunov scheme for the relativistic Euler equations.

where the correspondence between the global (t, x) and local $(\bar{t}, \bar{x})$ coordinates is given by

$$\begin{aligned} &\bar{x} = x - x_{i+\frac{1}{2}}\,, \qquad \bar{t} = t - t_n\,, \\ &x \in [x_i, x_{i+1}]\,, \qquad t \in [t_n, t_{n+1}]\ , \\ &\bar{x} \in [-\frac{\Delta x}{2}, \frac{\Delta x}{2}]\,, \quad t \in [0, \Delta t]\ . \end{aligned}$$

Having found a solution $W(t, x)$ in terms of solutions $W_{i+\frac{1}{2}}\,(\bar{x}/\bar{t})$ to local Riemann problems, the Godunov method advances the solution to a time $t_{n+1} = t_n + \Delta t$ by defining a new set of average values $\overline{W}_i(t_{n+1})$ as follow

$$\overline{W}_i(t_{n+1}) = \frac{1}{\Delta x} \int\limits_{x_{i-\frac{1}{2}}}^{x_{i+\frac{1}{2}}} W(t_{n+1}, \xi) d\xi\,, \tag{5.4.3}$$

within each cell $I_i = [x_{i-\frac{1}{2}}, x_{i+\frac{1}{2}}]$. Now dividing the above balance equation by Δx and using (5.4.1) and (5.4.3) we get the following Godunov upwind scheme in conservative form

$$W_i(t_{n+1}) = W_i(t_n) + \frac{\Delta t}{\Delta x}\left[F_{i-\frac{1}{2}} - F_{i+\frac{1}{2}}\right]\,, \tag{5.4.4}$$

with intercell fluxes is given by

$$F_{i-\frac{1}{2}} = F\left(W_{i-\frac{1}{2}}(0)\right)\,, \quad F_{i+\frac{1}{2}} = F\left(W_{i+\frac{1}{2}}(0)\right)\,, \tag{5.4.5}$$

where $W_{i-\frac{1}{2}}(0)$ is the solution of the Riemann problem $RP(W_{i-1}(t_n), W_i(t_n))$ along the ray $x/t = 0$, which is t-axis in local frame. Similarly $W_{i+\frac{1}{2}}(0)$ is the solution of the Riemann

problem $RP(W_i(t_n), W_{i+1}(t_n))$ along the t-axis. We use exact Riemann solver to calculate the intercell fluxes. Lastly we use the relations (5.2.9) in order to get the solution in term of the primitive variables n, u, p. For the details about Godunov schemes the reader is referred to the book of Toro [85].

Remark: The procedure for the second order accuracy in Godunov scheme is exactly the same as given in Subsection 5.2.1 for KFVS scheme. The only difference is the way to calculate the fluxes in step (III). In the Godunov scheme we use the exact Riemann solver in order to calculate fluxes.

5.4.1 Boundary Conditions in Godunov Scheme

For a domain $[0, L]$ discretized into M computational cells of lenght Δx we need boundary conditions at the boundaries x=0 and x=L as given in Figure 5.5.

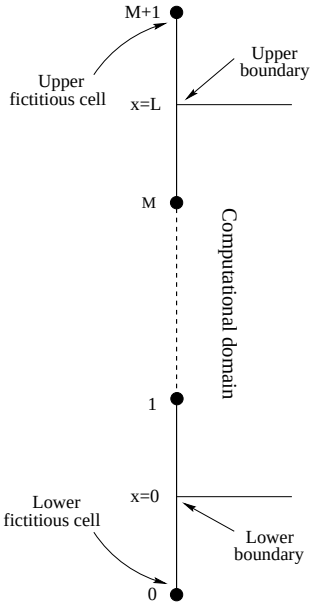

Figure 5.5: Boundary conditions. Fictitious cells outside the computational domain are created

Reflective boundary conditions: Consider the lower boundary at $x = 0$ and suppose it physically consist of a fixed, reflective wall. Then the physical situation is correctly modeled by creating a fictitious state $\mathbf{U}_0(t_n)$ on the left side of the boundary and defining the boundary Riemann problem $RP(\mathbf{U}_0(t_n), \mathbf{U}_1(t_n))$. The fictitious state $\mathbf{U}_0(t_n)$ is defined from the known state $\mathbf{U}_1(t_n)$ inside the computational domain, namely

$$n_0(t_n) = n_1(t_n)\,, \quad u_0(t_n) = -u_1(t_n)\,, \quad p_0(t_n) = p_1(t_n)\,. \tag{5.4.6}$$

The exact solution of this boundary Riemann problem consists of either (i) two shocks if $u_1 > 0$ or two rarefaction waves if $u_1 \leq 0$. In both cases $u_* = 0$ along the boundary, which is the desired condition. In a similar way we can define the reflective boundary conditions for

the upper boundary $x = L$.

Transmissive boundary conditions: Transmissive or transparent boundary conditions arise from the need to define finite, or sufficiently small, computational domains. The corresponding boundary conditions are a numerical attempt to produce boundaries that allow the passage of waves without any effect on them. For this case we have the following boundary conditions, see Toro [85].

$$n_0(t_n) = n_1(t_n)\,, \quad u_0(t_n) = u_1(t_n)\,, \quad p_0(t_n) = p_1(t_n)\,. \tag{5.4.7}$$

Remark: The procedure for the boundary conditions in KFVS schemes is exactly the same as for the Godunov Schemes.

5.5 Numerical Test Cases

Here we compare the results of the BGK-type KFVS schemes with the exact solution, KFVS, central and Godunov schemes. We found that KFVS and BGK-type KFVS schemes give comparable solutions to the central and Godunov schemes. The central schemes are discussed in Chapter 7.

Problem 1: In this test problem we consider the time evolution of an initial discontinuous state of a fluid moving in opposite directions. The initial data are

$$(n, u, p) = \begin{cases} (1.0, 1.0, 3.0) & \text{if } x < 0.5\,, \\ (1.0, -0.5, 2.0) & \text{if } x \geq 0.5\,, \end{cases}$$

where $0 \leq x \leq 1$. This problem consist of a left shock, a contact and a right shock. Figures 5.6 and 5.7 show the particle density n, velocity $v = \frac{u}{\sqrt{1+u^2}}$ and pressure p at time $t = 0.5$. Figures $(5.6)_{3,4}$ and $(5.7)_{3,4}$ show the zoomed solutions for better comparison of the schemes. We have used 400 mesh points in the spatial domain.

Problem 2: In this test problem we consider the time evolution of an initial discontinuous state of a fluid at rest. The initial data are

$$(n, u, p) = \begin{cases} (5.0, 0.0, 10.0) & \text{if } x < 0.5\,, \\ (1.0, 0.0, 0.5) & \text{if } x \geq 0.5\,, \end{cases}$$

where $0 \leq x \leq 1$. Figures $(5.8)_{1,2}$ and $(6.6)_{1,2}$ shows the particle density, velocity v and pressure at time $t = 0.5$. Figures $(5.8)_{3,4}$ and $(6.6)_{3,4}$ shows the same results with zooming in order to easily compare the schemes. We have used 400 mesh points in the spatial domain.

Problem 3: The initial data are

$$(n, u, p) = \begin{cases} (1.0, -0.5, 2.0) & \text{if } x < 0.5\,, \\ (1.0, 0.5, 2.0) & \text{if } x \geq 0.5\,, \end{cases}$$

where $0 \leq x \leq 1$. This problem has a solution consisting of two strong rarefactions and a trivial stationary contact discontinuity, Figures 5.10 and 5.11 shows the solution profiles for the particle density, velocity v and pressure at time $t = 0.5$. Figures $(5.10)_{3,4}$ and $(5.10)_{3,4}$ are

zoomed solutions. Here we can see a downward peak in the Godunov solution. These types of instabilities usually happens in the Godunov schemes. We have used 400 mesh points in the spatial domain.

Problem 4: Perturbed relativistic shock tube flow

The initial conditions are specified as $(n_L, u_L, p_L) = (1.0, 0.0, 1.0)$ for $0 \leq x \leq 0.5$ and $(n_R, u_R, p_R) = (n_R, 0.0, 0.1)$ for $0.5 \leq x \leq 1.0$. Here the right state is a perturbed density field of sinusoidal wave, $n_R = 0.125 - 0.0875\ \sin(50(x - 0.5))$. We run this test for the 400 mesh points. The computed solutions are plotted at $t = 0.5$. The results are shown in Figure 5.12. Since the continuity equation in the Euler equations decouples from the other two equations for the pressure and velocity, therefore we do not see the effect of perturbation in the pressure.

Problem 5: Two interacting relativistic blast waves

We consider here the interaction of two relativistic blast waves. The initial data are

$$(n, u, p) = \begin{cases} (1.0, 0.0, 100.0) & \text{if } 0 < x < 0.1\,, \\ (1.0, 0.0, 0.06) & \text{if } 0.1 < x < 0.9\,, \\ (1.0, 0.0, 10.0) & \text{if } 0.9 < x < 1.0\,. \end{cases}$$

The reflective boundary conditions are applied at both $x = 0.0$ and $x = 1.0$. The results are given in Figure 5.13 for the particle density n, velocity $v = \frac{u}{\sqrt{1+u^2}}$ and pressure p. The number of mesh points are 700 and the output time is $t = 0.75$.

Problem 6: Experimental order of convergence in the one-dimensional case

Here we check the experimental order of convergence (EOC) of the first and second order KFVS and BGK-type KFVS schemes. The initial data are

$$n = \sin(2\pi x) + 2.0, \qquad u = 0.0\,, \qquad p = 1.0\,.$$

The computational domain is $0 \leq x \leq 1$, and the final time for the numerical solution is $t = 1.0$. The solution is stationary with same data. Tables 5.1 and 5.2 give the L^1-error and EOC for the first order and second order KFVS and BGK-type KFVS schemes.

Table 5.1: L^1-error and EOC in the first order schemes

	KFVS scheme		BGK-type KFVS scheme	
N	L^1-error	EOC	L^1-error	EOC
50	0.114860		0.117429	
100	0.060002	0.9368	0.060046	0.9676
200	0.030687	0.9674	0.030704	0.9837
400	0.015522	0.9833	0.015526	0.9917
800	0.007807	0.9915	0.007808	0.9959
1600	0.003915	0.9958	0.003915	0.9974
3200	0.001961	0.9974	0.000981	0.9993

Table 5.2: L^1-error and EOC in the second order schemes

	KFVS scheme		BGK-type KFVS scheme	
N	L^1-error	EOC	L^1-error	EOC
50	0.015537		0.007861	
100	0.004374	1.8287	0.002187	1.8458
200	0.001197	1.8695	0.000594	1.8804
400	0.000325	1.8809	0.000160	1.8924
800	0.000086	1.9180	0.000042	1.9296
1600	0.000022	1.9668	0.000011	1.9329
3200	5.53E-06	1.9922	2.85E-06	1.9485

Problem 7: Experimental order of convergence in the two-dimensional case

The initial data are

$$n = \sin(2\pi x) + 2.0, \qquad u_1 = 0.0\,, \qquad u_2 = 0.0\,, \qquad p = 1.0\,.$$

The computation domain is $0 \leq x, y \leq 1$, and the final time for the numerical solution is $t = 0.5$. Table 5.3 and Table 5.4 give the L^1-error and EOC for the first order and second order KFVS and BGK-type KFVS schemes.

Table 5.3: L^1-error and EOC in the first order schemes

	KFVS scheme		BGK-type KFVS scheme	
N	L^1-error	EOC	L^1-error	EOC
30	0.156645		0.088754	
60	0.086700	0.8516	0.046886	0.9207
120	0.046256	0.9064	0.024285	0.9491
240	0.024108	0.9401	0.012430	0.9662
480	0.012382	0.9613	0.006314	0.9772

Table 5.4: L^1-error and EOC in the second order schemes

	KFVS scheme		BGK-type KFVS scheme	
N	L^1-error	EOC	L^1-error	EOC
30	0.032213		0.017540	
60	0.010356	1.6372	0.005378	1.7055
120	0.003003	1.7860	0.001513	1.8297
240	0.000826	1.8622	0.000414	1.8697
480	0.000225	1.8762	0.000111	1.8991

Problem 8: Simulation of ultra-relativistic jets

As a 2D application we have simulated the evolution of a fluid injected supersonically into the computational domain through a small nozzle. This simple initial setup allows for the study of morphology and dynamics of relativistic jets encountered in some astrophysical scenarios.

A similar studies for the phenomenological relativistic Euler equations have been done by Martí and Müller [61] and references therin.

Test Case 1: Here we use a slab which is 18 units long and 7 units wide. The domain is covered by a numerical grid consisting of 700×400 zones. The beam fluid is injected in to the grid parallel to the x-axis through a nozzle located at the middle of the left boundary (i.e. along y-axis) at $x = 0$, which is one unit wide. Outflow boundary conditions are used at all boundaries except at the symmetry axis (x=0 boundary) where reflected boundary conditions are imposed, and at the nozzle, where fixed inflow beam conditions are used. The initial data are

$$(n_b, v_b, p_b) = (0.01, 0.999, 10.0)\,, \quad (n_m, v_m, p_m) = (1.0, 0.0, 10.0)\,,$$

where "b" correspond to the beam and "m" correspond to the medium. The Mach number of the flow for $\Gamma = \frac{1}{\sqrt{1-v^2}}$ is due to Königl [43]

$$M_b = \frac{v_b}{c_s}\frac{\Gamma_b}{\Gamma_s} = 31\,.$$

The results are shown in Figure 5.14 and 5.15 .

Test Case 2: Here we use a slab which is 14 units long and 7 units wide. The domain is covered by a numerical grid consisting of 500×300 zones. The initial data are

$$(n_b, v_b, p_b) = (0.01, 0.99, 10.0)\,, \quad (n_m, v_m, p_m) = (1.0, 0.0, 10.0)\,.$$

The flow Mach number is 31. The results are shown in Figure 5.16 and 5.17.

Test Case 3: Here we use a slab which is 16 units long and 7 units wide. The domain is covered by a numerical grid consisting of 700×400 zones. The initial data are

$$(n_b, v_b, p_b) = (1.0, 0.999, 10.0)\,, \quad (n_m, v_m, p_m) = (0.001, 0.0, 10.0)\,.$$

The flow Mach number is 10. The results are shown in Figure 5.18 and 5.19 .

Problem 9: Explosion in a box

In this example we consider a two-dimensional Riemann problem inside a square box of sides length 2, with reflecting walls. Initially the velocities are zero. The pressure is 10 and density is 4 inside a small square box of sides length 0.5 in the center of the large box, while pressure and density are unity elsewhere. The results are shown at $t = 3.0$ in Figures 5.20, 5.21, while at $t = 12.0$ in Figures 5.22 and 5.23. In all the results we have used 400×400 mesh points.

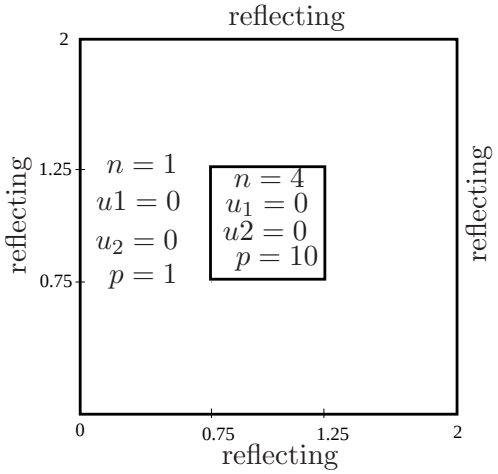

Problem 10: Cylindrical explosion problem

Consider a square domain $[0,1] \times [0,1]$. The initial data are constant in two regions separated by a circle of radius 0.2 centered at $(0.5, 0.5)$. Inside the circle density is 5.0 and the pressure is 10.0, while outside the density is 1.0 and pressure is equal to 0.5. The velocities are zero everywhere. The solution consists of a circular shock wave propagating outwards from the origin, followed by a circular contact discontinuity propagating in the same direction, and a circular rarefaction wave traveling towards the origin. The results are shown in Figure 5.24 and Figures 5.25,5.26 for 400 mesh points at $t = 0.2$.

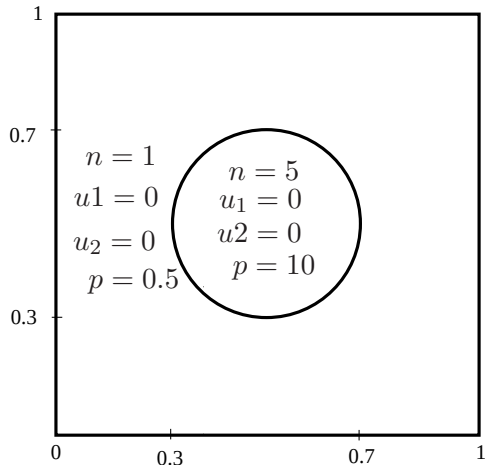

5.6 Summary

In this chapter we have presented the first and second order KFVS, BGK-type KFVS and Godunov schemes for the ultra-relativistic Euler equations. We have numerically implemented the one- and two-dimensional KFVS and BGK-type KFVS schemes. While the Godunov scheme is implemented only for the one space dimension. The numerical results from both KFVS and BGK-type KFVS schemes were compared with the Godunov and central schemes. Like in the non-relativistic case, here again the programing code for the KFVS, BGK-type KFVS and central schemes are compact and simpler as compared to the Godunov scheme. The boundary conditions implementation for the KFVS and BGK-type schemes are analogous to the Godunov scheme. It was found that BGK-type KFVS schemes give a better resolution of the contact discontinuity as compared to the KFVS and central schemes. However the Godunov scheme gives slightly better resolution than all the other three schemes. The computational time for the KFVS and BGK-type KFVS scheme is comparable to both central and Godunov schemes. The main advantage of the KFVS and BGK-type schemes over Godunov schemes is that we do not need Riemann solvers to calculate the fluxes. This advantage is especially important in the multi-dimensional case. Although we do not need the Riemann solvers in KFVS and BGK-type KFVS schemes we are still able to utilize all the properties of upwinding methods. Furthermore, KFVS and BGK-type KFVS schemes resolve the contact discontinuity much better than the central schemes. The advantage of KFVS schemes over the kinetic schemes in Chapter 4 is computational efficiency and compactness. However, the KFVS schemes need a CFL condition and has more smearing at the contact discontinuity as compared to kinetic schemes (continuous in space).

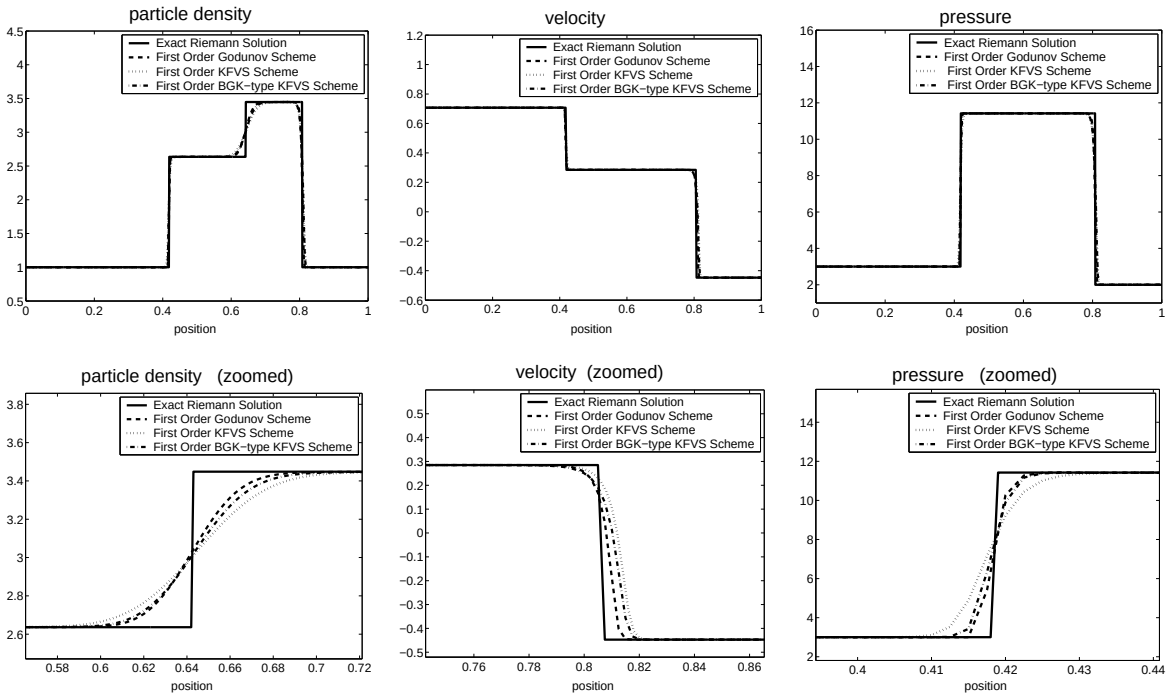

Figure 5.6: Comparison of the first order schemes at $t = 0.5$.

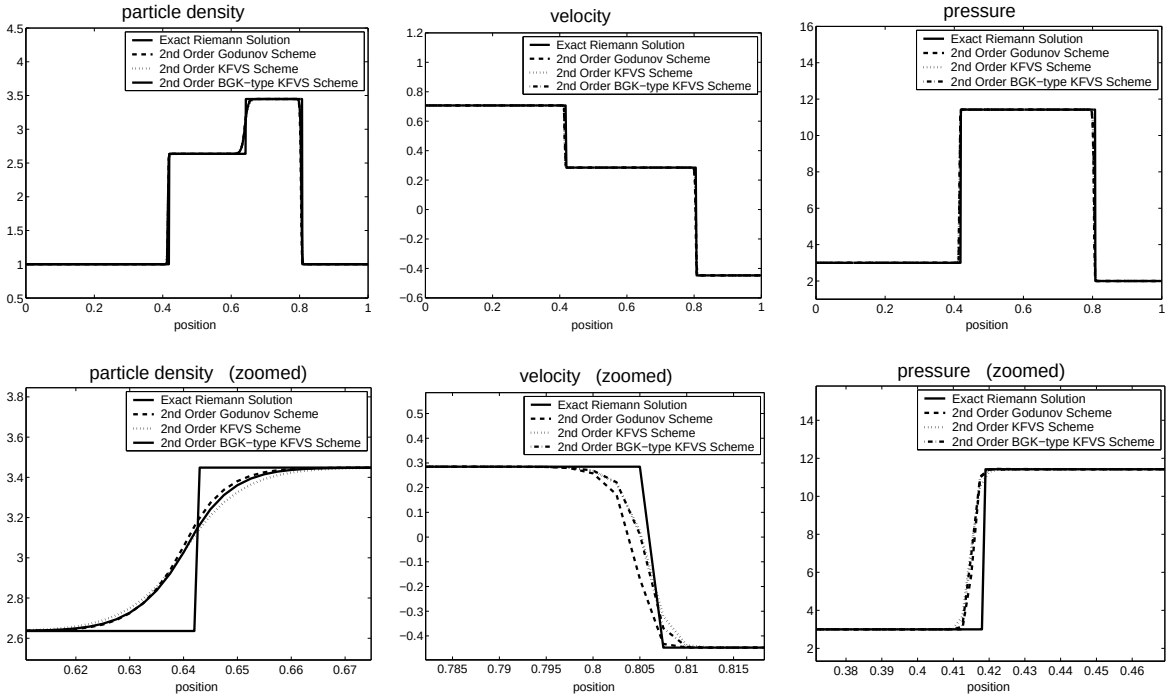

Figure 5.7: Comparison of the 2nd order schemes at $t = 0.5$.

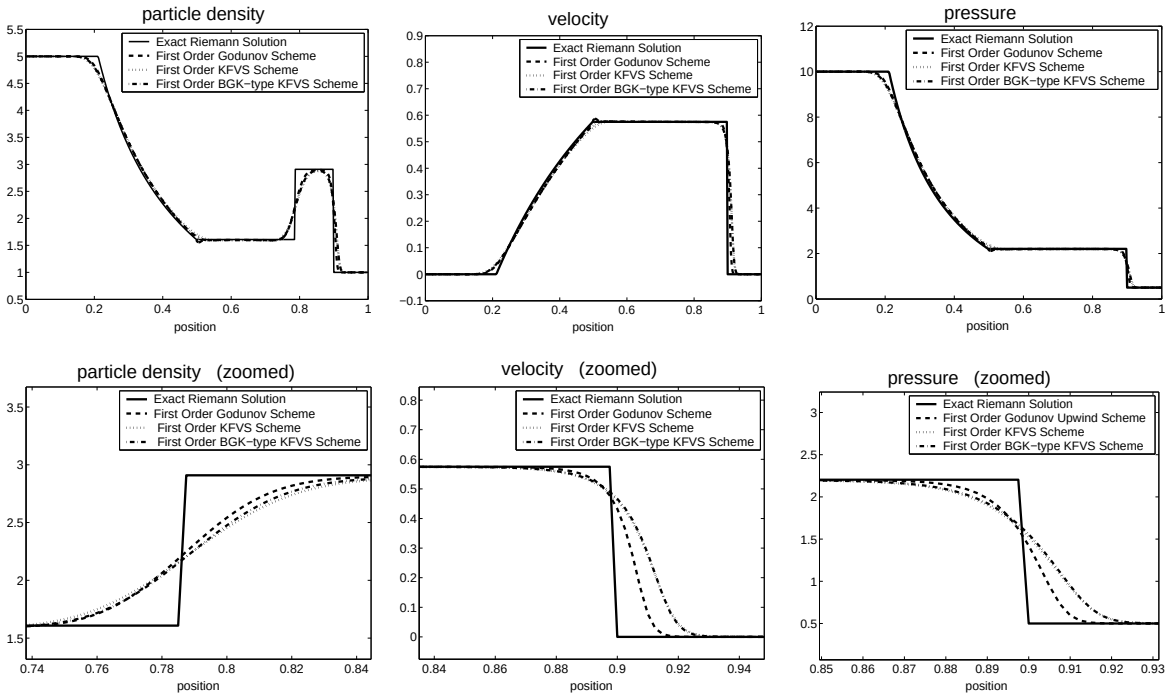

Figure 5.8: Comparison of the first order schemes at $t = 0.5$.

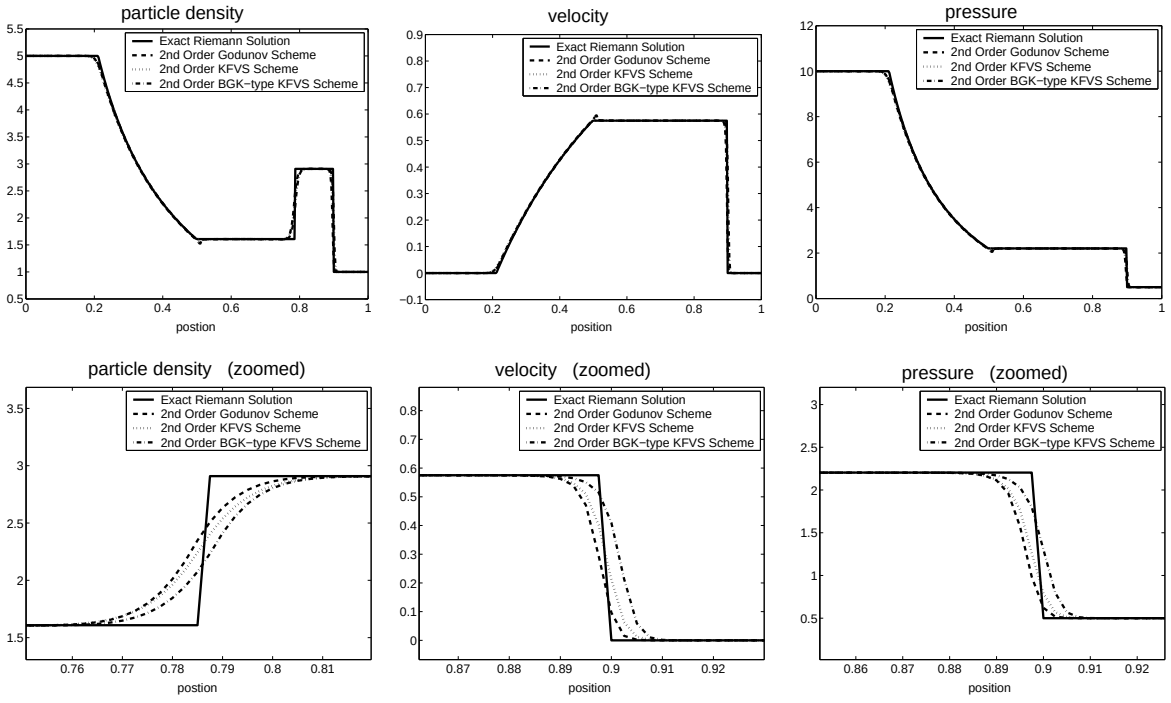

Figure 5.9: Comparison of the 2nd order schemes at $t = 0.5$.

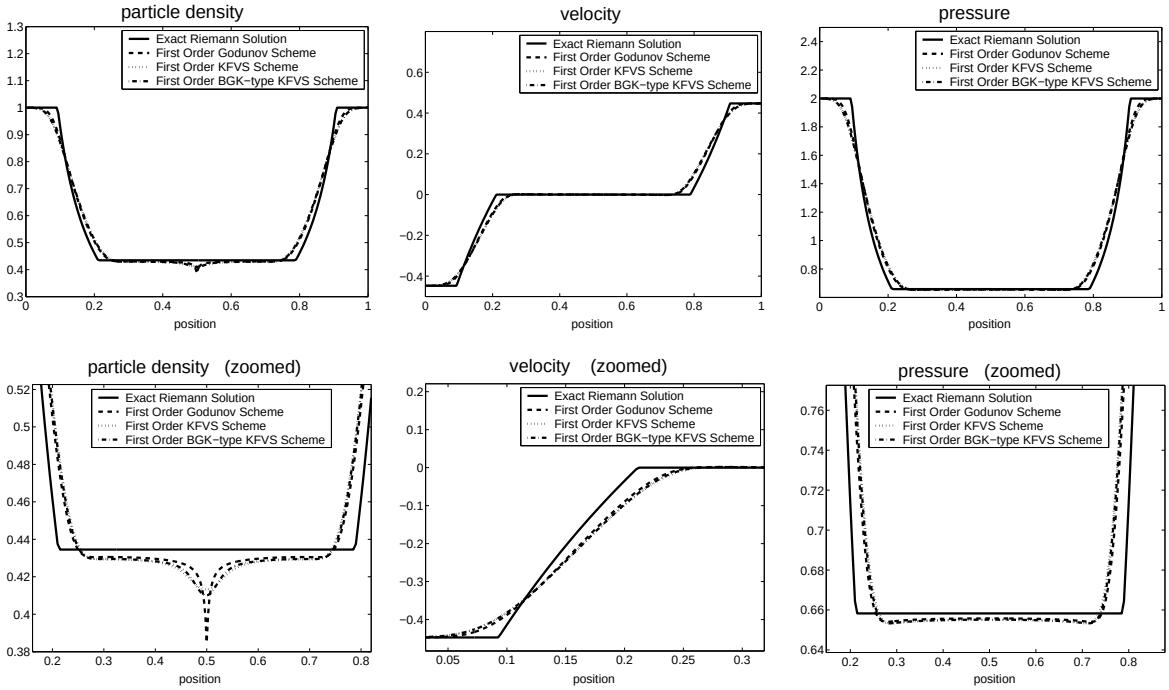

Figure 5.10: Comparison of the first order schemes at $t = 0.5$.

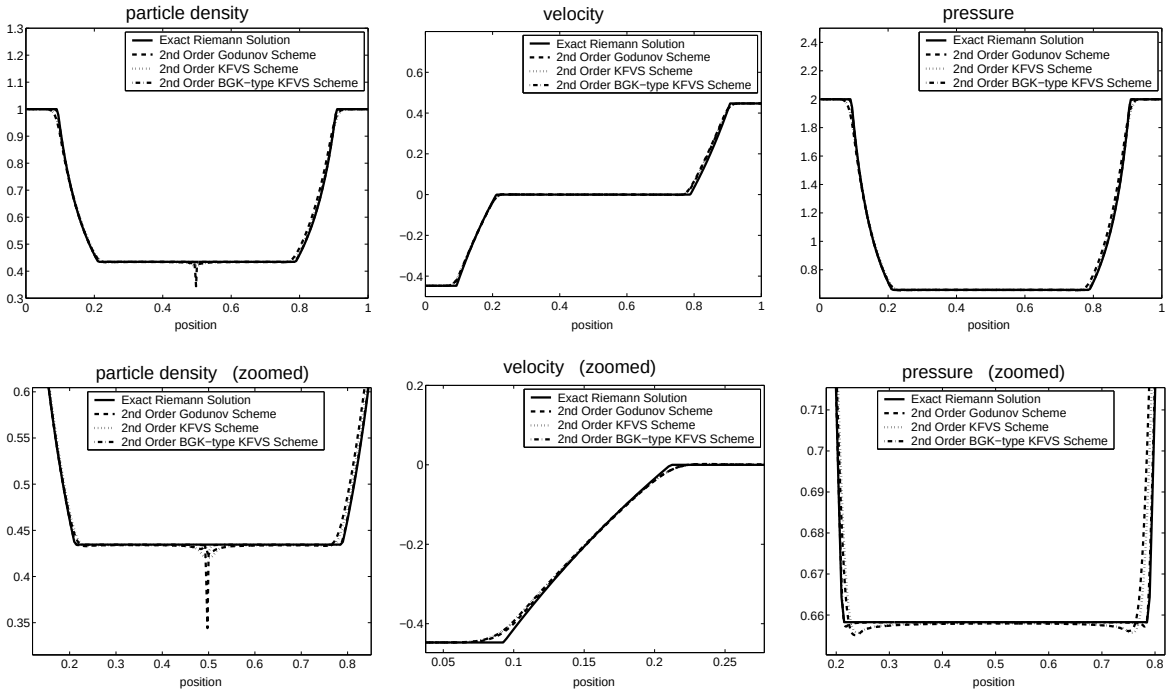

Figure 5.11: Comparison of the 2nd order schemes at $t = 0.5$.

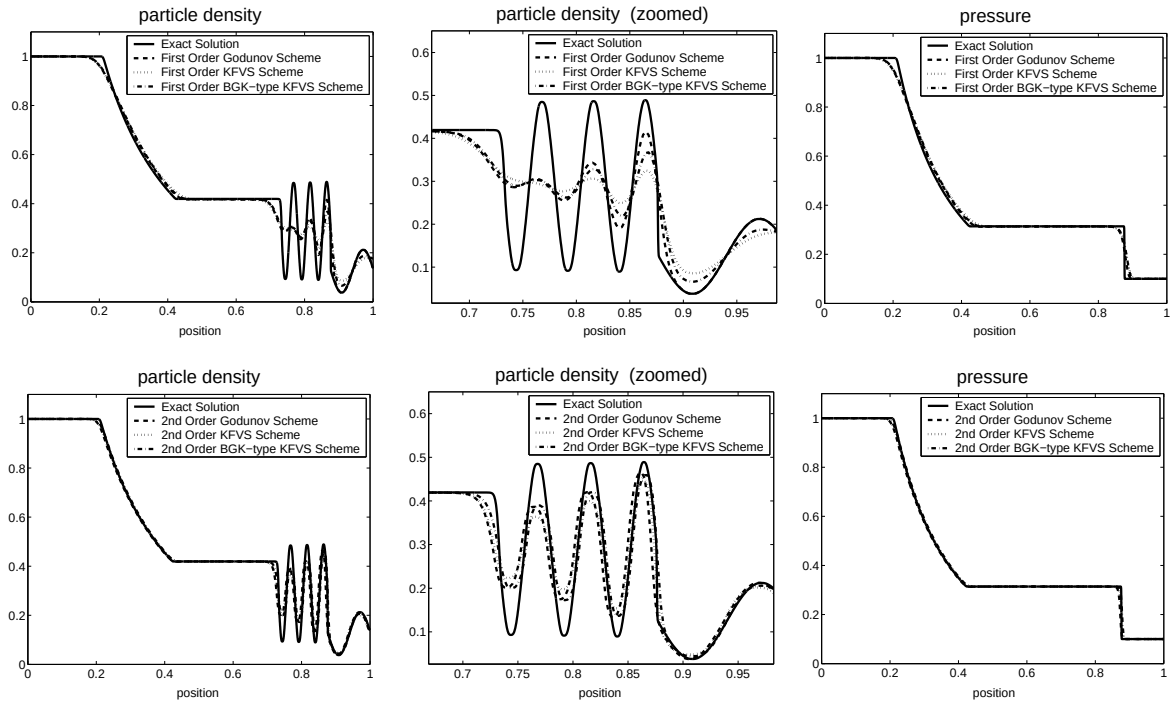

Figure 5.12: Perturbed relativistic shock tube flow at time $t = 0.5$.

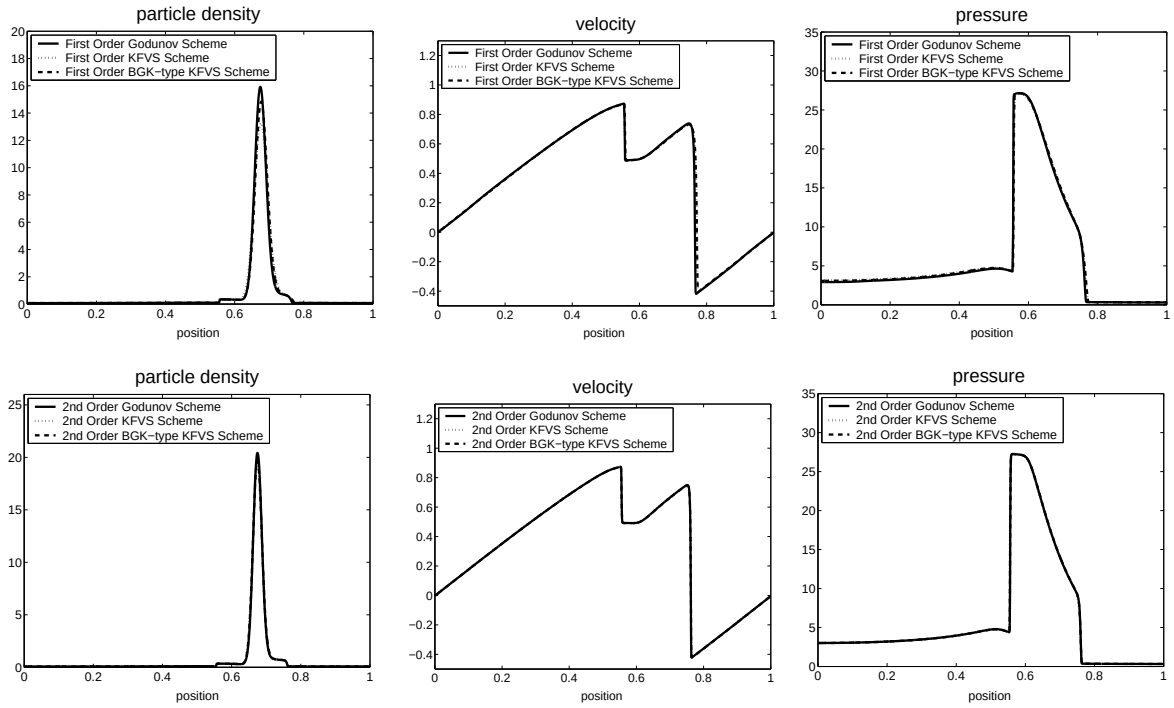

Figure 5.13: Two interacting relativistic blast waves at time $t = 0.75$.

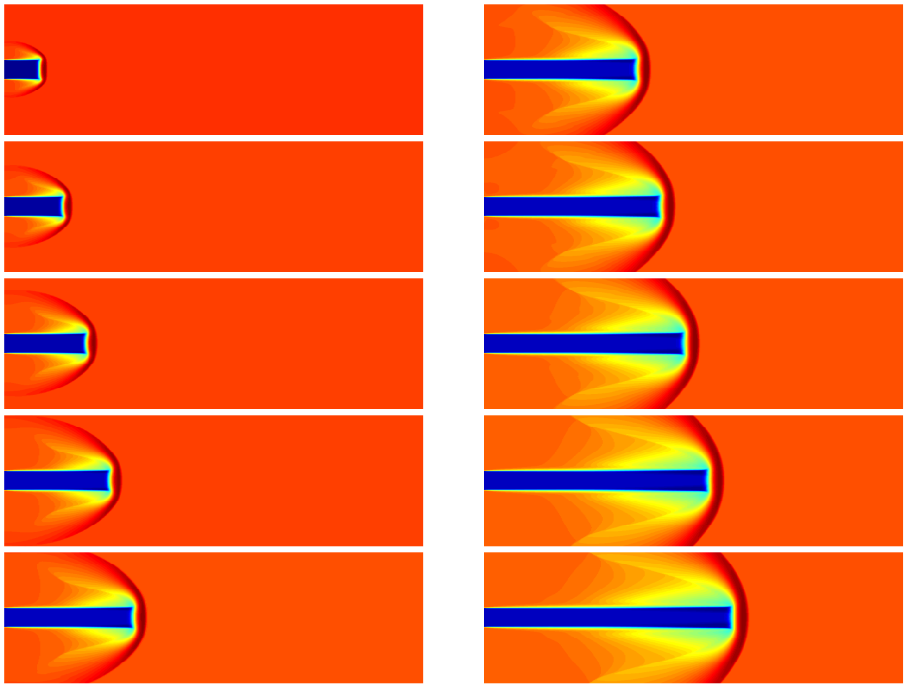

Figure 5.14: Ultra-relativistic jet problem at $v = 0.999$.

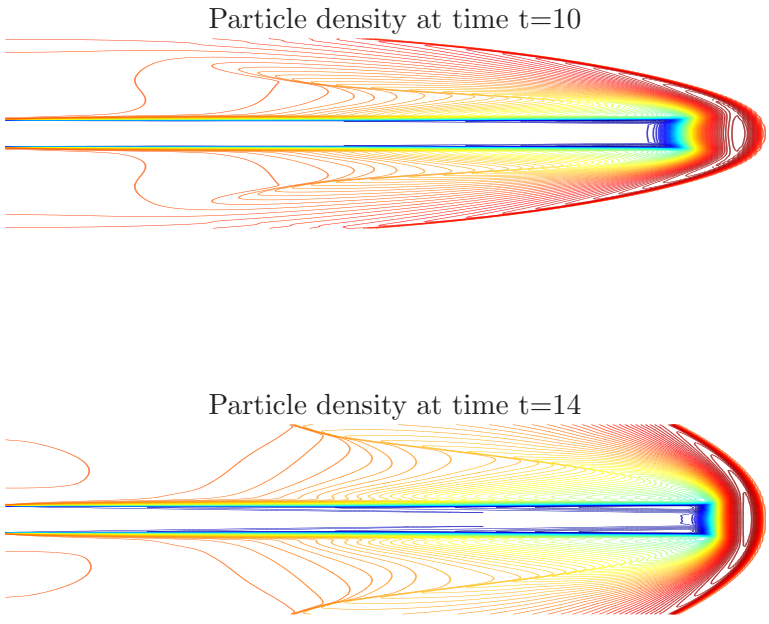

Figure 5.15: Contour plots of ultra-relativistic jet at $v = 0.999$.

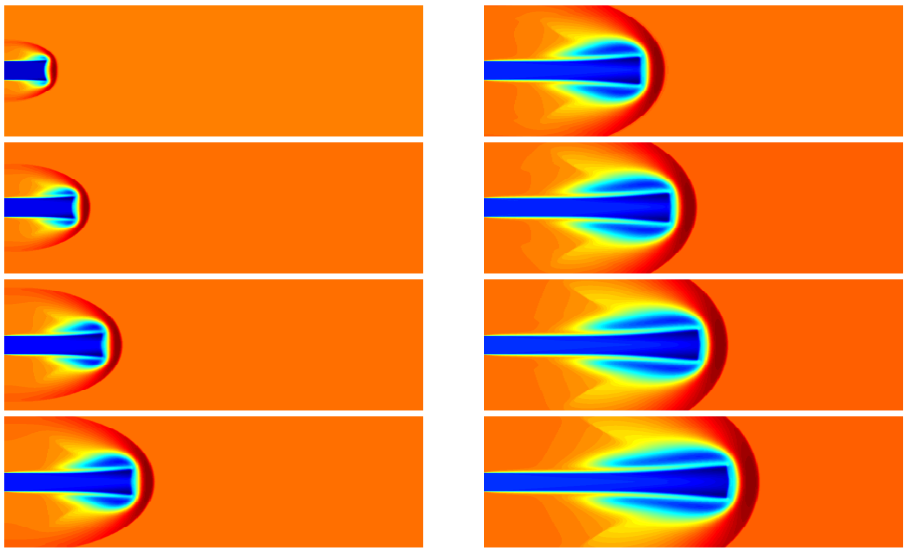

Figure 5.16: Ultra-relativistic jet problem at $v = 0.99$.

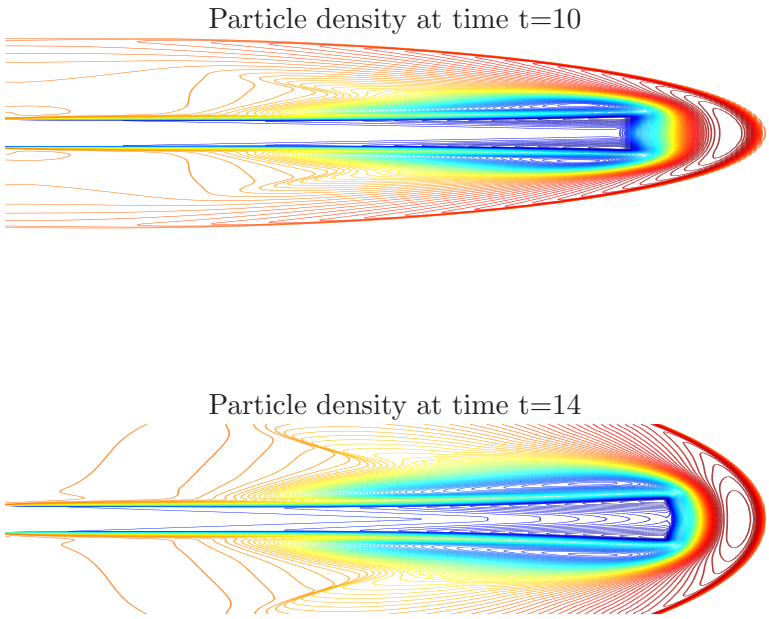

Figure 5.17: Contour plots of ultra-relativistic jet at $v = 0.99$.

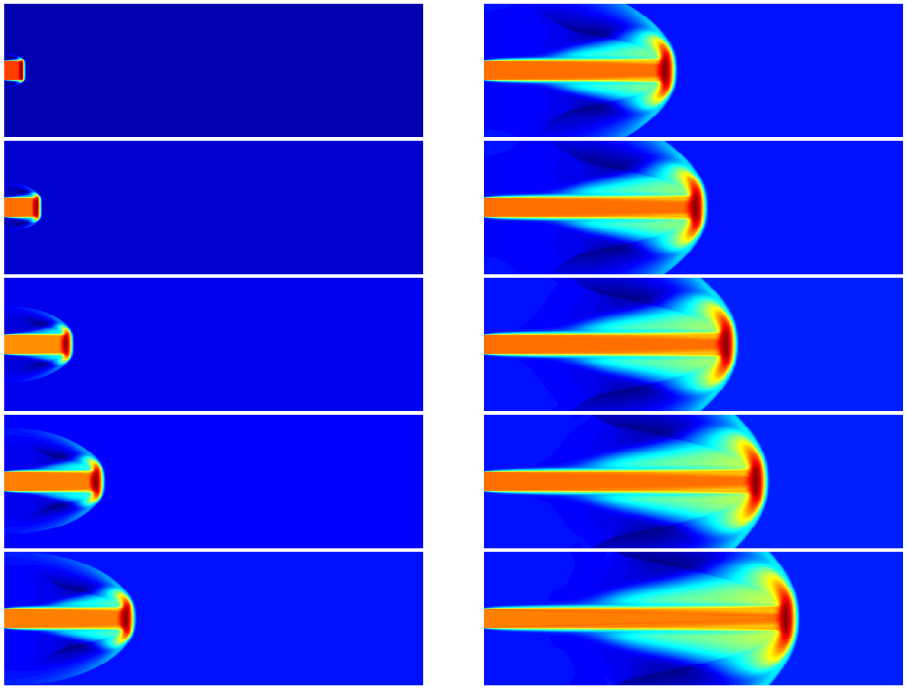

Figure 5.18: Ultra-relativistic jet problem at $v = 0.999$.

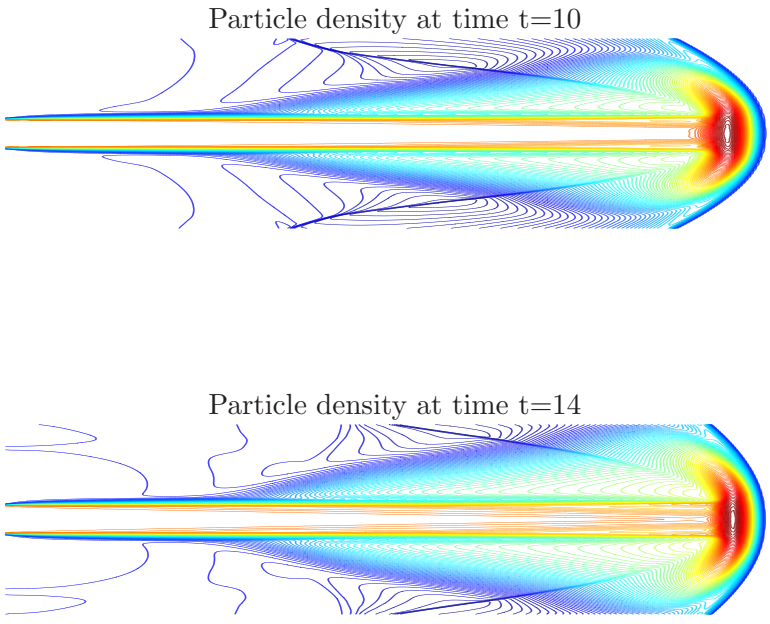

Figure 5.19: Contour plots of ultra-relativistic jet at $v = 0.999$.

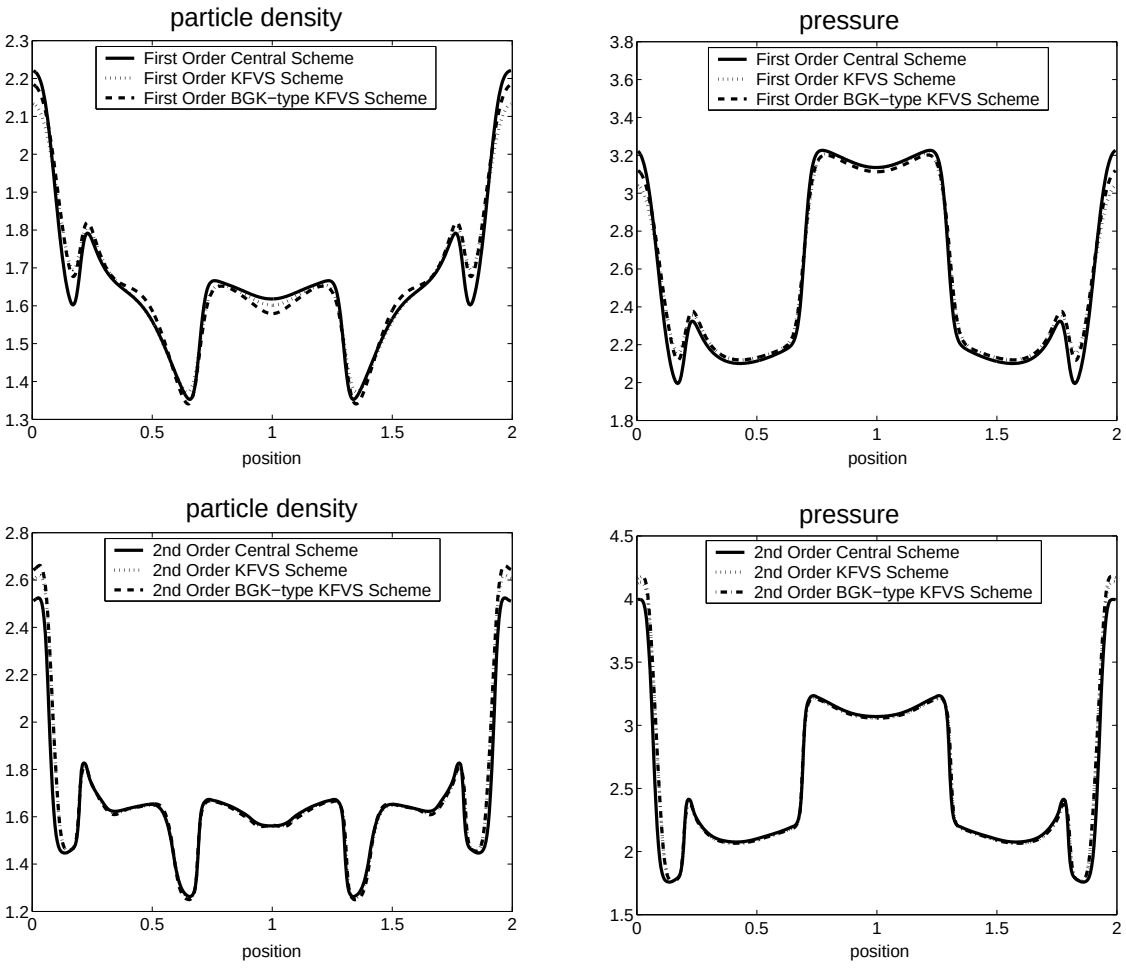

Figure 5.20: First and second order schemes for the explosion in a box at $t = 3.0$.

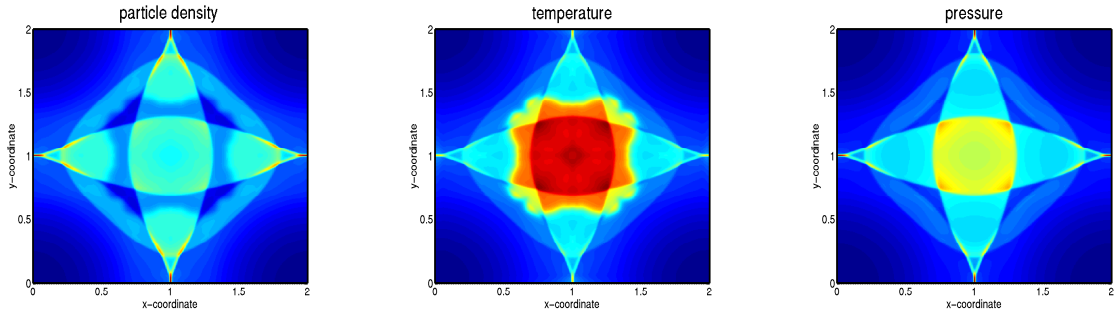

Figure 5.21: BGK-type KFVS scheme applied to explosion in a box at $t = 3.0$.

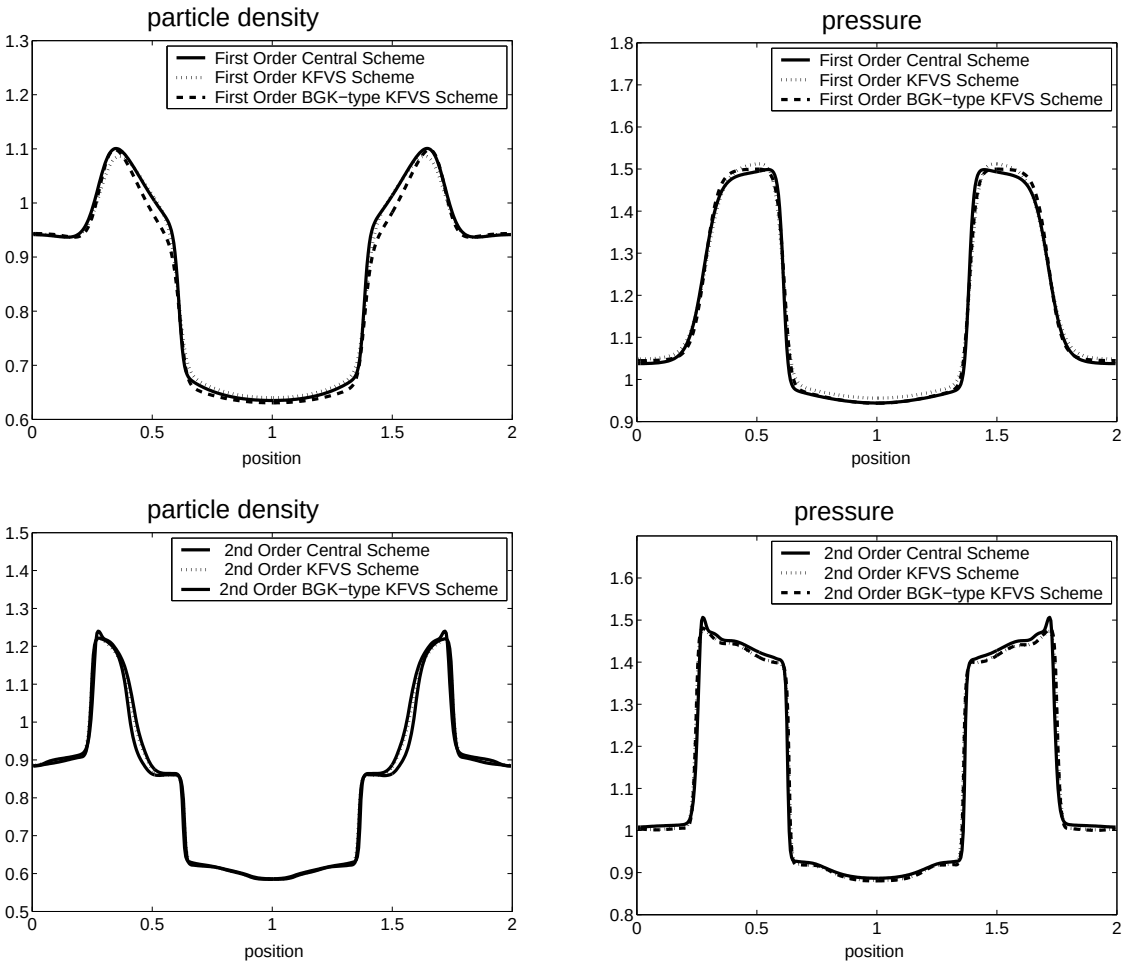

Figure 5.22: First and second order schemes for the explosion in a box at $t = 12.0$.

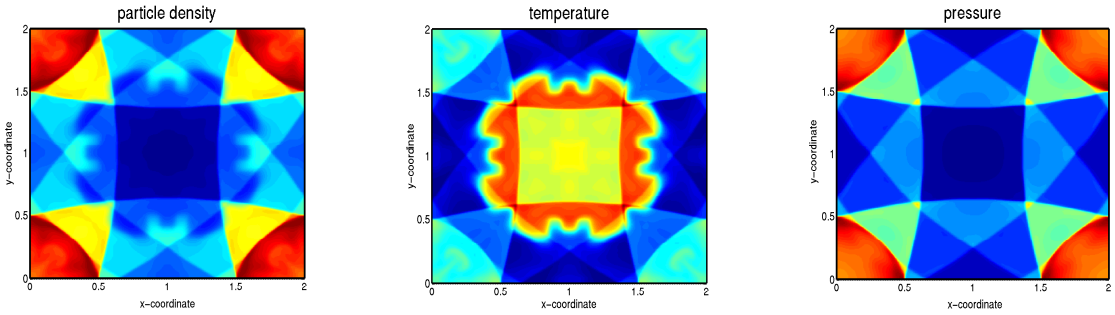

Figure 5.23: BGK-type KFVS scheme for the explosion in a box at $t = 12.0$.

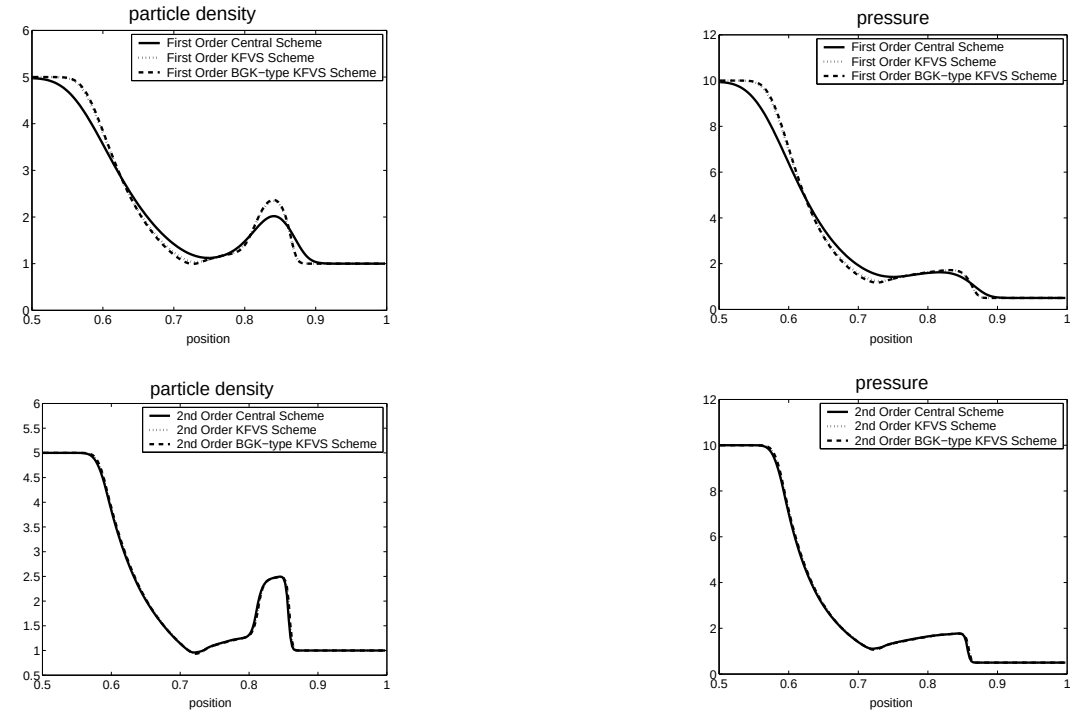

Figure 5.24: Comparison of the schemes applied to cylindrical explosion at $t = 0.2$.

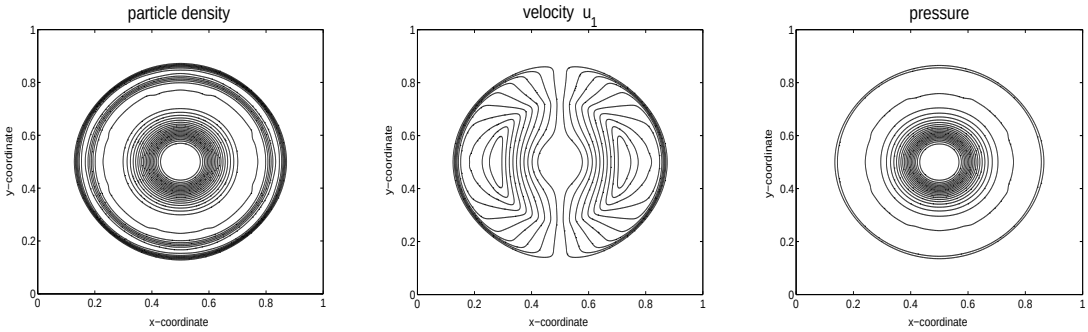

Figure 5.25: First order BGK-type KFVS scheme at $t = 0.2$.

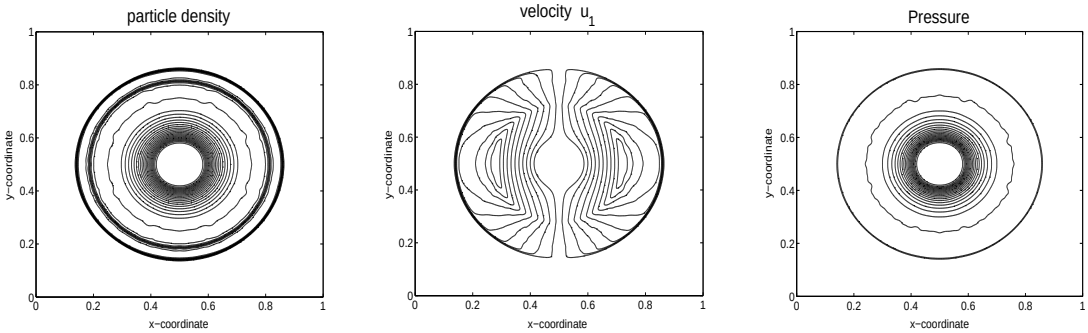

Figure 5.26: Second order BGK-type KFVS scheme at $t = 0.2$.

Chapter 6

General Form of Special Relativistic Euler Equations

In this chapter we deal with the general form of relativistic Euler equations which includes the modified Bessel functions of second kind. These Euler equations cover the whole range from the non-relativistic to ultra-relativistic limits. The limiting equations for the Bessel functions are given in Chapter 3. These inequalities give us the non-relativistic and the ultra-relativistic limits of the special relativistic kinetic theory of gases.

We prove the Maximum Entropy Principle for these Euler equations. Jüttner [41, 42] has also given such a proof, but we use a different approach and obtain the full entropy inequality. We utilize the modern Lorentz invariant properties which were not available at that time. At the end of the proof, we have the same result as obtained by Jüttner. We also give the Rankine-Hugoniot jump conditions for these Euler equations. Instead of using the pressure as jump parameter, here we use the inverse of temperature as a jump parameter. This gives us the explicit Rankine conditions which are not possible if we consider the pressure as jump parameter.

We develop the unconditionally stable kinetic schemes (continuous in space) for these special relativistic Euler equations. We also prove the positivity and L_1-stability of the schemes. The proofs of conservation laws and entropy inequality are similar to that in ultra-relativistic case. Therefore we omit these proofs.

Finally we introduce the phenomenological form of the relativistic Euler equations. These are the relativistic Euler equation which can be obtained by using the classical constitutive relation for the internal energy density and the $gamma-$gas law. Since these equations are in Lorentz invariant form, they are still relativistic Euler equations. The disadvantage is, it seems that there is no consistent kinetic phase density which can recover all the constitutive relations for these Euler equations. Several numerical methods for solving these relativistic Euler equations have been reported, see Martí and Müller [61] and references therein. All these methods are mostly developed out of the existing reliable methods for solving the Euler equations of non-relativistic or Newtonian gas dynamics. Here we will use the second order central scheme to solve these Euler equations in one space dimension. These second order central schemes are presented in Chapter 7. We will also compare the numerical results of the central schemes with the exact Riemann solutions obtained in [61].

6.1 Constitutive Relations

Using the relativistic Jüttner distribution (3.5.1), the relations (3.5.5) and (3.5.7), we calculate the moments (3.6.1), (3.6.2) and (3.6.3). In the global rest frame, where u^μ has components $(1,0,0,0)^T$, we obtain

$$\begin{aligned} e &= -n\frac{M'(\beta)}{M(\beta)} = n\Psi(\beta)\,, \\ p &= -\frac{n}{3M(\beta)}(M'(\beta)+\eta(\beta)) = nT = \frac{n}{\beta}\,, \\ \sigma &= -n\ln\left(\frac{n\beta}{K_2(\beta)}\right) + \beta n\Psi(\beta) + \eta n\,. \end{aligned} \tag{6.1.1}$$

Where $\Psi(\beta)$ is given by (3.5.9). Here the choice of the entropy constant η is not so important in general. Since e, p and σ are Lorentz invariant, we see that (6.1.1) is already true in any other Lorentz-frame, without the restriction that $u^\mu = (1,0,0,0)^T$.

Starting with the rest frame and then applying the inverse of the Lorentz boost given by (3.4.13), we get the following relations for the general frame, where $\mathbf{u}$ may or may not be zero,

$$N^\mu = n\,u^\mu\,, \qquad T^{\mu\nu} = -p\,g^{\mu\nu} + (e+p)u^\mu u^\nu\,, \qquad S^\mu = \sigma u^\mu\,. \tag{6.1.2}$$

Moreover one can see by similar calculations given in Lemma 4.1 that σ in $(6.1.1)_3$ obeys the Gibbs equation

$$T d\left(\frac{\sigma}{n}\right) = p\,d\left(\frac{1}{n}\right) + d\left(\frac{e}{n}\right). \tag{6.1.3}$$

Since the relativistic moments (6.1.2) are valid in a special Lorentz frame and since these equations are written in tensor invariant form, they are generally valid in every Lorentz frame. This can also be seen directly without making use of the Lorentz-boosts.

6.2 Maximum Entropy Principle

The Jüttner distribution f_J (3.5.1) has some important properties. First of all it generalizes the non-relativistic Maxwellian of a gas in equilibrium to the relativistic case, and secondly f_J satisfies the so called Maximum Entropy Principle in equilibrium, which will be formulated and proved below. For this purpose we need the following lemmas.

Lemma 6.1: *let be* $\mathbf{u}$, $\mathbf{q} \in \mathbb{R}^3$ *and* $u^\mu = (\sqrt{1+\mathbf{u}^2}, \mathbf{u})^T$, $q^\mu = (\sqrt{1+\mathbf{q}^2}, \mathbf{q})^T$. *Then the scalar product* $q^\mu u_\mu$ *satisfies the inequality* $q^\mu u_\mu \geq 1$, *where* $q^\mu u_\mu = 1$ *if and only if* $\mathbf{u} = \mathbf{q}$.

Proof: We consider

$$\begin{aligned} q^\mu u_\mu - 1 &= \sqrt{1+\mathbf{q}^2}\sqrt{1+\mathbf{u}^2} - \mathbf{q}\cdot\mathbf{u} - 1 \\ &= \frac{(\sqrt{1+\mathbf{q}^2}\sqrt{1+\mathbf{u}^2} - \mathbf{q}\cdot\mathbf{u} - 1)\cdot(\sqrt{1+\mathbf{q}^2}\sqrt{1+\mathbf{u}^2} + \mathbf{q}\cdot\mathbf{u} + 1)}{\sqrt{1+\mathbf{q}^2}\sqrt{1+\mathbf{u}^2} + \mathbf{q}\cdot\mathbf{u} + 1} \\ &= \frac{(\mathbf{q}-\mathbf{u})^2 + \mathbf{q}^2\mathbf{u}^2 - (\mathbf{q}\cdot\mathbf{u})^2}{\sqrt{1+\mathbf{q}^2}\sqrt{1+\mathbf{u}^2} + \mathbf{q}\cdot\mathbf{u} + 1}\,. \end{aligned} \tag{6.2.1}$$

Due to the Cauchy-Schwarz inequality we know that

$$(\mathbf{q}\cdot\mathbf{u})^2 \le \mathbf{q}^2\mathbf{u}^2, \text{ i.e. } \mathbf{q}^2\mathbf{u}^2 - (\mathbf{q}\cdot\mathbf{u})^2 \ge 0. \tag{6.2.2}$$

If $\mathbf{q} \neq \mathbf{u}$ then from (6.2.1) we have

$$(\mathbf{q}-\mathbf{u})^2 + \mathbf{q}^2\mathbf{u}^2 - (\mathbf{q}\cdot\mathbf{u})^2 > 0\,, \tag{6.2.3}$$

and this implies again from (6.2.1) that $q^\mu u_\mu - 1 > 0$ or $q^\mu u_\mu > 1$.

Lemma 6.2: *The derivative $\Psi' : \mathbb{R}^+ \to \mathbb{R}$ has the representation*

$$\Psi'(\beta) = \frac{d}{d\beta}\left(\frac{3}{\beta} + \frac{K_1(\beta)}{K_2(\beta)}\right) = -\frac{3}{\beta^2} + \frac{3}{\beta}\cdot\frac{K_1(\beta)}{K_2(\beta)} + \left(\frac{K_1(\beta)}{K_2(\beta)}\right)^2 - 1\,, \tag{6.2.4}$$

and is negative for any $\beta > 0$. Moreover $\Psi(\beta)$ satisfies the inequality

$$\Psi(\beta) > 1\,, \tag{6.2.5}$$

which indicates that the specific energy is larger than the rest mass energy of a single atom.

Proof: We divide the proof of this lemma in two cases as follow.

Case 1 when $0 < \beta < 1$: From the definition of the modified Bessel functions we have $0 < K_1(\beta) < K_2(\beta)$. So we can write due to (6.2.4)

$$\begin{aligned} \Psi'(\beta) &= -\frac{3}{\beta^2} + \frac{3}{\beta}\cdot\frac{K_1(\beta)}{K_2(\beta)} + \left(\frac{K_1(\beta)}{K_2(\beta)}\right)^2 - 1 \\ &< -\frac{3}{\beta^2} + \frac{3}{\beta} + 1 - 1 = \frac{3}{\beta^2}(\beta - 1) < 0. \end{aligned} \tag{6.2.6}$$

Thus we have proved for $0 < \beta < 1$ that $\Psi'(\beta) < 0$.

Case 2 when $\beta \ge 1$: Recall the integral definition (3.5.4) for the modified Bessel functions $K_m(\beta)$. We also know that $\cosh(s) = 1 + 2\sinh^2(\frac{s}{2})$ and make the substitution $\alpha = \sinh(\frac{s}{2})$ with $ds = \frac{2d\alpha}{\sqrt{1+\alpha^2}}$ in (3.5.4) in order to get

$$\frac{1}{4}\exp\left(\frac{\beta}{4}\right)K_0\left(\frac{\beta}{4}\right) = \frac{1}{2}\int_0^\infty \frac{\exp\left(\frac{-\beta\alpha^2}{2}\right)}{\sqrt{1+\alpha^2}}d\alpha\,, \tag{6.2.7}$$

$$\frac{1}{4}\exp\left(\frac{\beta}{4}\right)\left[K_0\left(\frac{\beta}{4}\right) + K_1\left(\frac{\beta}{4}\right)\right] = \int_0^\infty \sqrt{1+\alpha^2}\exp\left(\frac{-\beta\alpha^2}{2}\right)d\alpha\,. \tag{6.2.8}$$

Also we have the following estimates

$$\frac{1}{\sqrt{1+\alpha^2}} \geq 1 - \frac{\alpha^2}{2}\,, \qquad \sqrt{1+\alpha^2} \leq 1 + \frac{\alpha^2}{2}\,. \tag{6.2.9}$$

Keeping in view (6.2.7) and (6.2.8), we obtain from (6.2.9)

$$\frac{1}{4}\exp\left(\frac{\beta}{4}\right) K_0\left(\frac{\beta}{4}\right) \geq \frac{1}{2}\sqrt{\frac{\pi}{2\beta}}\left(1 - \frac{1}{2\beta}\right)\,, \tag{6.2.10}$$

$$\frac{1}{4}\exp\left(\frac{\beta}{4}\right)\left[K_0\left(\frac{\beta}{4}\right) + K_1\left(\frac{\beta}{4}\right)\right] \leq \sqrt{\frac{\pi}{2\beta}}\left(1 + \frac{1}{2\beta}\right)\,. \tag{6.2.11}$$

Note that also the right hand side of (6.2.10) is positive due to $\beta \geq 1$. We take the inverse of (6.2.10) and multiply with (6.2.11) in order to get

$$1 + \frac{K_1\left(\frac{\beta}{4}\right)}{K_0\left(\frac{\beta}{4}\right)} \leq 2\left(1 + \frac{1}{2\beta}\right)\cdot\left(1 - \frac{1}{2\beta}\right)^{-1}\,. \tag{6.2.12}$$

Using the recursion relation (3.5.6) for $m = 1$ and replacing β by $\frac{\beta}{4}$ we get

$$\frac{K_2\left(\frac{\beta}{4}\right)}{K_1\left(\frac{\beta}{4}\right)} - \frac{K_0\left(\frac{\beta}{4}\right)}{K_1\left(\frac{\beta}{4}\right)} = \frac{8}{\beta}\,. \tag{6.2.13}$$

Now using (6.2.12) and (6.2.13) we get the following inequality after some manipulations and replacing $\frac{\beta}{4}$ by β

$$\frac{K_1(\beta)}{K_2(\beta)} \leq \frac{1 + \frac{3}{8\beta}}{1 + \frac{15}{8\beta} + \frac{3}{4\beta^2}}\,. \tag{6.2.14}$$

Substituting (6.2.14) in (6.2.4) for $\frac{K_1(\beta)}{K_2(\beta)}$, we finally get after simplification

$$\Psi'(\beta) \leq -\frac{9}{64\beta^6}\cdot\frac{12 + 60\beta + 105\beta^2 + 69\beta^3 + 8\beta^4}{\left(1 + \frac{15}{8\beta} + \frac{3}{4\beta^2}\right)^2} < 0\,. \tag{6.2.15}$$

It follows that $\Psi'(\beta) < 0$ for any $\beta > 0$.

Hence we have proved that $\Psi(\beta)$ is a strictly monotonically decreasing function which satisfies due to $(3.5.15)_3$ the asymptotic relation

$$\lim_{\beta\to\infty} \Psi(\beta) = 1\,. \tag{6.2.16}$$

Thus we conclude that $\Psi(\beta)$ is strictly bounded below by one.

Lemma 6.3:

(i) Let be $f = f(\mathbf{q}) \geq 0$ for $\mathbf{q} \in \mathbb{R}^3$ any phase density which does not vanish almost everywhere and for which the moments N^μ, $T^{\mu\nu}$ exist. Let be n and e the corresponding particle density and energy density, respectively. Then there holds the inequality chain $0 < n < e$.

(ii) Let be $0 < n < e$ and $\mathbf{u} \in \mathbb{R}^3$ given parameters, corresponding to the particle density, energy density and the spatial part of the macroscopic four-velocity. Then there exists exactly one temperature $T > 0$ such that the Jüttner phase density $f_J(n, T, \mathbf{u}, \mathbf{q})$ gives the prescribed energy density $e > n$.

Proof: In order to prove (i) we use from Lemma 6.1 that $q^\mu u_\mu > 1$ for $\mathbf{q} \neq \mathbf{u}$. Therefore we can write

$$(q^\mu u_\mu)(q^\nu u_\nu) > q^\mu u_\mu \,. \tag{6.2.17}$$

This implies that

$$\int_{\mathbb{R}^3} (q^\mu u_\mu)(q^\nu u_\nu) f \, \frac{d^3q}{q^0} > \int_{\mathbb{R}^3} q^\mu u_\mu f \, \frac{d^3q}{q^0} \,. \tag{6.2.18}$$

Using the definitions (3.6.4), (3.6.5) for N^μ and $T^{\mu\nu}$, respectively, we can write (6.2.18) in the following form

$$u_\mu u_\nu T^{\mu\nu} > u_\mu N^\mu \,. \tag{6.2.19}$$

Also using the definitions (3.4.7) and (3.4.8) for n and e we finally conclude that $e > n$.

Now we prove the part (ii). We know from the part (i) of this lemma that the restriction $e > n > 0$ is necessary. Moreover we know from Lemma 6.2 that $\frac{e}{n} = \Psi(\beta) > 1$ has exactly one solution for $\beta > 0$. Let be $T = \frac{1}{\beta} > 0$ the corresponding temperature. Then we know from $(6.1.1)_1$ that the Jüttner phase density $f_J(n, T, \mathbf{u}, \mathbf{q})$ leads to the prescribed energy density e.

Remark: The restriction $e > n$ is also natural from the physical point of view since it states that the energy density is always larger then the rest-mass energy.

Now we are able to prove Maximum Entropy Principle using the above lemmas.

Proposition 6.4 (Maximum Entropy Principle):

Let $f(\mathbf{q}) \geq 0$ be any phase density which does not vanish everywhere and for which the moments N^μ and $T^{\mu\nu}$ exist. Let n, $\mathbf{u}$, e be the values resulting from f for the particle density, the spatial part of the velocity four-vector and the energy density, respectively. Then there is exactly one temperature $T > 0$ for which the Jüttner phase density $f_J(n, T, \mathbf{u}, \mathbf{q})$ leads to the prescribed energy density e. Let be σ and σ_J the entropy densities corresponding to f and f_J, respectively. Then there holds the Maximum Entropy Inequality $\sigma_J \geq \sigma$.

Proof: Due to Lemma 6.3 we have exactly one temperature $T > 0$ for which the Jüttner phase density $f_J(n, T, \mathbf{u}, \mathbf{q})$ gives the prescribed energy density $e > n$ coming from the general phase

density $f(\mathbf{q})$. In the following proof we will fix this temperature T and the corresponding phase density $f_J(n, T, \mathbf{u}, \mathbf{q})$. Using the definition (3.6.6) and (3.4.10) we have due to the constraint on $\mathbf{u}$

$$\begin{aligned}\sigma_J - \sigma &= S_J^\mu u_\mu - S^\mu u_\mu \\ &= -u_\mu \int_{\mathbb{R}^3} q^\mu \left(f_J(n,T,\mathbf{u},\mathbf{q}) \ln f_J(n,T,\mathbf{u},\mathbf{q}) - f(\mathbf{q}) \ln f(\mathbf{q})\right) \frac{d^3q}{q^0}\,. \end{aligned} \tag{6.2.20}$$

In the following we omit the arguments of f and f_J for the sake of simplicity, which will not lead to confusion here. We use Lemma 2.4 for $u = f_J$, $v = f$ and get

$$f \ln f - f_J \ln f_J = (\ln f_J + 1)(f - f_J) + R(f_J, f). \tag{6.2.21}$$

Using equation (6.2.21) in (6.2.20) we have

$$\begin{aligned}\sigma_J - \sigma =& u_\mu \int_{\mathbb{R}^3} q^\mu \ln f_J \,(f - f_J) \frac{d^3q}{q^0} + u_\mu \int_{\mathbb{R}^3} q^\mu \,(f - f_J) \frac{d^3q}{q^0} \\ &+ u_\mu \int_{\mathbb{R}^3} q^\mu \, R(f_J, f) \frac{d^3q}{q^0}\,. \end{aligned} \tag{6.2.22}$$

The second integral in (6.2.22) is zero due to the constraints on n and $\mathbf{u}$,

$$u_\mu N^\mu - u_\mu N_J^\mu = n - n = 0\,, \tag{6.2.23}$$

so we are left with

$$\sigma_J - \sigma = u_\mu \int_{\mathbb{R}^3} q^\mu \ln f_J \,(f - f_J) \frac{d^3q}{q^0} + u_\mu \int_{\mathbb{R}^3} q^\mu \, R(f_J, f) \frac{d^3q}{q^0}\,. \tag{6.2.24}$$

From Jüttner's phase density (3.5.1) we have

$$\begin{aligned}\ln f_J &= \ln\left(\frac{n}{M(\beta)} \exp\left(-\frac{1}{T} u_\nu q^\nu\right)\right) \\ &= \ln\left(\frac{n}{M(\beta)}\right) - \frac{1}{T} u_\nu q^\nu\,. \end{aligned} \tag{6.2.25}$$

Using (6.2.25) in (6.2.24) and the fact that n and T are independent of the integration variable $\mathbf{q}$ we get

$$\begin{aligned}\sigma_J - \sigma =& \ln\left(\frac{n}{M(\beta)}\right) u_\mu \int_{\mathbb{R}^3} q^\mu \,(f - f_J) \frac{d^3q}{q^0} - \frac{1}{T}\, u_\mu u_\nu \int_{\mathbb{R}^3} q^\mu q^\nu \,(f - f_J) \frac{d^3q}{q^0} \\ &+ u_\mu \int_{\mathbb{R}^3} q^\mu \, R(f_J, f) \frac{d^3q}{q^0}\,. \end{aligned} \tag{6.2.26}$$

Here the first integral is zero due to (6.2.23). Also we know from (3.4.8) and our constraints on the velocity and energy density that

$$e = u_\mu u_\nu T^{\mu\nu} = e_J = u_\mu u_\nu T_J^{\mu\nu}\,, \tag{6.2.27}$$

where $T^{\mu\nu}$ and $T_J^{\mu\nu}$ are the energy momentum tensors for f and f_J, respectively. Thus equation (6.2.26) finally reduces to

$$\sigma_J - \sigma = \int_{\mathbb{R}^3} u_\mu q^\mu \, R(f_J, f) \, \frac{d^3q}{q^0} \geq 0. \tag{6.2.28}$$

The integral in (6.2.28) is positive because $u_\mu q^\mu$ is the scalar product of time-like vectors which is positive due to Lemma 6.1 and $R(f_J, f)$ is positive due to Lemma 2.3. Hence we have proved that Jüttner's phase density satisfies the Maximum Entropy Principle, i.e. $\sigma_J \geq \sigma$.

6.3 Constitutive Relations in Limiting Cases

In order to get the non-relativistic values of the energy density, pressure and entropy density, we substitute the asymptotic relations (3.5.15) for $K_2(\beta)$ and $\Psi(\beta)$ into the constitutive relations (6.1.1). We get the following expressions for the non-relativistic limit, where $\beta \to \infty$,

$$e = n + \frac{3}{2} nT \,, \qquad p = nT \,, \qquad \sigma = n \ln \frac{p^{\frac{3}{2}}}{n^{\frac{5}{2}}} + \eta n \,. \tag{6.3.1}$$

Which is the same result as in Chapter 2 for the ratio specific heat $\gamma = \frac{5}{3}$. In Chapter 2 the particle density n is represented by the mass density ρ and entropy density σ is denoted by h. The term n in $(6.3.1)_1$ is the energy density of the rest mass.

In order to get ultra-relativistic limit where $\beta \to 0$, we substitute the asymptotic relations (3.5.19) into the constitutive relations (6.1.1) and (6.1.2), we get the relations (4.1.1) and (4.1.2).

6.4 Relativistic Euler Equations

Now we use the moments (6.1.2) and the conservation laws (3.4.15) in order to get the three-dimensional Euler equations at regular points in differential form. For this purpose we introduce the abbreviation

$$\chi(\beta) = \Psi(\beta) + \frac{1}{\beta} \,, \tag{6.4.1}$$

and obtain

$$\frac{\partial}{\partial t} \left(n \sqrt{1 + \mathbf{u}^2} \right) + \sum_{k=1}^{3} \frac{\partial (n u^k)}{\partial x^k} = 0 \,, \tag{6.4.2}$$

$$\frac{\partial}{\partial t} \left(n \chi(\beta) u^i \sqrt{1 + \mathbf{u}^2} \right) + \sum_{k=1}^{3} \frac{\partial}{\partial x^k} \left(\frac{n}{\beta} \delta^{ik} + n \chi(\beta) u^i u^k \right) = 0 \,, \tag{6.4.3}$$

$$\frac{\partial}{\partial t} \left(-\frac{n}{\beta} + n \chi(\beta) (1 + \mathbf{u}^2) \right) + \sum_{k=1}^{3} \frac{\partial}{\partial x^k} \left(n \chi(\beta) u^k \sqrt{1 + \mathbf{u}^2} \right) = 0 \,. \tag{6.4.4}$$

Remarks:

(i) These equations constitutes a closed system in terms of the unknown fields n, $\mathbf{u}$, and β. Also note that $\beta = \frac{1}{T}$.

(ii) The classical Euler equations result with (3.5.15) in the following way: From (6.4.2) we obtain the classical continuity equation by neglecting the second order terms in $\mathbf{u}$, whereas the classical momentum equations are obtained from (6.4.3) by setting $\chi(\beta)$ equal to one and neglecting the third order terms in $\mathbf{u}$. Finally, the classical energy equation results if we subtract (6.4.2) from (6.4.4) and then neglect the fourth order terms in $\mathbf{u}$ and terms which contain $p\mathbf{u}^2$ as a factor.

(iii) The ultra-relativistic Euler equations result directly from (3.5.19).

6.4.1 Rankine Hugoniot Jump Conditions

Now we are looking for a spatially one-dimensional solutions of the three-dimensional Euler equations, which will not depend on x^2, x^3 but only on $x = x^1$. Moreover we restrict to a one-dimensional flow field $\mathbf{u} = (u(t,x), 0, 0)^T$

$$\begin{aligned} (n\sqrt{1+u^2})_t + (nu)_x &= 0\,, \\ (n\chi(\beta)u\sqrt{1+u^2})_t + (\tfrac{n}{\beta} + n\chi(\beta)u^2)_x &= 0\,, \\ (-\tfrac{n}{\beta} + n\chi(\beta)(1+u^2))_t + (n\chi(\beta)u\sqrt{1+u^2})_x &= 0\,. \end{aligned} \tag{6.4.5}$$

Note that these differential equations constitute a strictly hyperbolic system with the sound speed

$$\lambda_* = \left[\frac{1 - 1/(\beta^2\Psi'(\beta))}{1+\beta\Psi(\beta)}\right]^{\frac{1}{2}}\,, \tag{6.4.6}$$

and the characteristic velocities

$$\lambda_1 = \frac{-\lambda_*\sqrt{1+u^2}+u}{\sqrt{1+u^2}-\lambda_* u}\,,\ \lambda_2 = \frac{u}{\sqrt{1+u^2}}\,,\ \lambda_3 = \frac{\lambda_*\sqrt{1+u^2}+u}{\sqrt{1+u^2}+\lambda_* u}\,. \tag{6.4.7}$$

Note that $\Psi'(\beta) < 0$ was proved in Lemma 6.2.

These eigenvalues may first be obtained in the Lorentz zero rest frame where u=0. Then using the additivity law for the velocities (3.3.1) in the general Lorentz frame we can easily obtain (6.4.7).

Note that by using the asymptotic relations (3.5.15) and (3.5.19) one can easily get from (6.4.7), the classical eigenvalues (2.1.5) and ultra-relativistic eigenvalues (4.1.16).

The differential equations (6.4.5) are not sufficient if we take shock discontinuities into account. Therefore we need a weak integral formulation of the one-dimensional hyperbolic system for the three unknown fields n, u and β, which is given by

$$\begin{aligned} \oint_{\partial\Omega} n\sqrt{1+u^2}dx - nudt &= 0\,, \\ \oint_{\partial\Omega} (n\chi(\beta)u\sqrt{1+u^2})dx - (\tfrac{n}{\beta} + n\chi(\beta)u^2)dt &= 0\,, \\ \oint_{\partial\Omega} (-\tfrac{n}{\beta} + n\chi(\beta)(1+u^2))dx - (n\chi(\beta)u\sqrt{1+u^2})dt &= 0\,. \end{aligned} \tag{6.4.8}$$

Here $\Omega \subset \mathbb{R} \times \mathbb{R}_0^+$ is a normal region in space-time with piecewise smooth, positive oriented boundary. Note that this weak formulation takes discontinuities into account, since there are no longer derivatives of the fields. If we apply the Gauss Divergence Theorem in regular space-time regions to the weak formulation (6.4.8) we come back to the differential form of Euler's equation (6.4.5).

Furthermore we require that the weak solution (6.4.8) must also satisfy the one-dimensional *entropy-inequality*

$$\oint_{\partial\Omega} S^0 dx - S^1 dt \geq 0\,, \tag{6.4.9}$$

where

$$\begin{aligned} S^0 &= -n\sqrt{1+u^2}\left(\ln\tfrac{n\beta}{K_2(\beta)} + \beta\Psi(\beta)\right)\,, \\ S^1 &= -nu\left(\ln\tfrac{n\beta}{K_2(\beta)} + \beta\Psi(\beta)\right)\,. \end{aligned} \tag{6.4.10}$$

Now we consider bounded and integrable *initial data* for a positive particle density n, transformed velocity u and absolute temperature T, which may have jumps

$$n(0,x) = n_0(x) > 0, \qquad u(0,x) = u_0(x), \qquad T(0,x) = T_0(x) > 0. \tag{6.4.11}$$

If $x = x(t)$ is a shock-discontinuity of the weak solution (6.4.8) with speed $v_s = \dot{x}(t)$, $W_- = (n_-, u_-, p_-)$ the state left to the shock and $W_+ = (n_+, u_+, p_+)$ the state to the right, then (6.4.8) leads to the Rankine-Hugoniot jump conditions

$$\begin{aligned} v_s(N_+^0 - N_-^0) &= N_+^1 - N_-^1\,, \\ v_s(T_+^{01} - T_-^{01}) &= T_+^{11} - T_-^{11}\,, \\ v_s(T_+^{00} - T_-^{00}) &= T_+^{01} - T_-^{01}\,, \end{aligned} \tag{6.4.12}$$

where

$$\begin{aligned} &N_\pm^0 = n_\pm\sqrt{1+u_\pm^2}\,, \qquad N_\pm^1 = n_\pm u_\pm\,, \qquad T_\pm^{01} = n_\pm\chi(\beta_\pm)u_\pm\sqrt{1+u_\pm^2}\,, \\ &T_\pm^{11} = p_\pm + n_\pm\chi(\beta_\pm)u_\pm^2\,, \qquad T_\pm^{00} = -p_\pm + n_\pm\chi(\beta_\pm)(1+u_\pm^2)\,. \end{aligned}$$

Also in singular points the local form of (6.4.9) reads

$$-v_s(S_+^0 - S_-^0) + (S_+^1 - S_-^1) \geq 0, \tag{6.4.13}$$

which must be satisfied at each shock curve of (6.4.8). The shock that satisfies (6.4.12) and (6.4.13) is called *entropy shock*.

Now we give parameter representations for the single entropy shocks. For this purpose we choose the initial data as follows:

Let be $(n_*, u_*, \beta_*) \in \mathbb{R}^+ \times \mathbb{R} \times \mathbb{R}^+$ and define $p_* = n_* T_* = \frac{n_*}{\beta_*}$. We use the inverse temperature β as a shock-parameter and impose the restriction $\beta < \beta_*$ in order to obtain from (6.4.12)

and (6.4.13) the following parametrization of the particle density and the pressure

$$\begin{aligned}
\gamma(\beta) &= \Psi(\beta_*)\,\chi(\beta_*) - \Psi(\beta)\,\chi(\beta)\,,\\
n(\beta) &= \frac{n_*\beta}{2\chi(\beta_*)}\left[\sqrt{\gamma(\beta)^2 + 4\frac{\chi(\beta_*)\chi(\beta)}{\beta_*\beta}} - \gamma(\beta)\right]\,,\\
p(\beta) &= \frac{n(\beta)}{\beta}\,.
\end{aligned} \tag{6.4.14}$$

For the parametrization of the velocities we have

$$\begin{aligned}
\hat{u}(\beta) &= \left(\frac{(p(\beta)-p_*)\cdot(n(\beta)\,\Psi(\beta) - n_*\Psi(\beta_*))}{n(\beta)\,n_*\chi(\beta)\chi(\beta_*)}\right)^{\frac{1}{2}}\,,\\
u(\beta) &= u_*\sqrt{1+\hat{u}(\beta)^2} \pm \hat{u}(\beta)\sqrt{1+u_*^2}\,,\\
\hat{u}_s(\beta) &= \left[\frac{(p(\beta)-p_*)\,(p_* + n(\beta)\Psi(\beta))}{n_*\,\chi(\beta_*)\left[n(\beta)\,(\Psi(\beta)-\frac{1}{\beta}) - n_*(\Psi(\beta_*)-\frac{1}{\beta_*})\right]}\right]^{\frac{1}{2}}\,,\\
u_s(\beta) &= u_*\sqrt{1+\hat{u}_s(\beta)^2} \pm \hat{u}_s(\beta)\sqrt{1+{u_*}^2}\,,\\
v_s &= \frac{u_s}{\sqrt{1+u_s^2}}\,,\ v = \frac{u}{\sqrt{1+u^2}}\,,\ v_* = \frac{u_*}{\sqrt{1+u_*^2}}\,.
\end{aligned} \tag{6.4.15}$$

Remarks: The restriction $\beta < \beta_*$ guarantees that all the expressions under the square roots in (6.4.14) and (6.4.15) are positive because

(i) $\gamma(\beta)$ is negative since $\Psi(\beta) > 0$ and $\chi(\beta) > 0$ are strictly monotonically decreasing functions due to Lemma 6.2,

(ii) $n(\beta)$ is a strictly monotonically decreasing and positive function,

(iii) $\Psi(\beta) - \frac{1}{\beta}$ is also a strictly monotonically decreasing and positive function, the same with $p(\beta) > p_*$.

Now there results the following parametrization for the different kind of shock waves:

- The "+" sign in (6.4.15) and $\beta < \beta_*$ gives the so called *3-shocks* with the constant state (n_*, u_*, β_*) on the right

  $$(n_-, u_-, \beta_-) = (n(\beta), u(\beta), \beta), \quad (n_+, u_+, \beta_+) = (n_*, u_*, \beta_*).$$

  These 3-shocks satisfy both the Rankine-Hugoniot conditions (6.4.12) as well as the entropy condition (6.4.13).

- The "-" sign in (6.4.15) and $\beta < \beta_*$ gives the so called *1-shocks* with the constant state (n_*, u_*, β_*) on the left:

  $$(n_-, u_-, \beta_-) = (n_*, u_*, \beta_*), \quad (n_+, u_+, \beta_+) = (n(\beta), u(\beta), \beta).$$

  These 1-shocks satisfy both the Rankine-Hugoniot conditions (6.4.12) as well as the entropy condition (6.4.13).

Now we define the *2-contacts*, that turn out to be contact-discontinuities without entropy-production. Only for these we choose $n > 0$ instead of β as a wave parameter and set

$$(n_-, u_-, \beta_-) = (n_*, u_*, \beta_*), \quad (n_+, u_+, \beta_+) = \left(n, u_*, \frac{n\beta_*}{n_*}\right).$$

These waves satisfy the Rankine-Hugoniot and entropy conditions. Note that velocity and pressure are constant across a 2-contact. Here the wave-speed is $v_s = v_* = \frac{u_*}{\sqrt{1+u_*^2}}$.

Remark. One can prove that the only discontinuities satisfying (6.4.12) and (6.4.13) are 1- and 3-shocks as well as 2-contact, see Courant and Friedrichs [9].

6.5 Formulation of the Kinetic Scheme

We first formulate the scheme for the three-dimensional Euler equations. After that we solve the one-dimensional Euler equations, using a special integration technique. Recalling the relativistic Jüttner phase density (3.5.1), we start with the given initial data $n_I(\mathbf{x}) = n(0, \mathbf{x})$, $T_I(\mathbf{x}) = T(0, \mathbf{x})$, $\mathbf{u}_I(\mathbf{x}) = \mathbf{u}(0, \mathbf{x})$. We prescribe a time step $\tau_M > 0$ and let $t_n = n\,\tau_M$, $n = 0, 1, 2, 3....$ Then we define the moments and the entropy four-vector in the free-flight for $0 < \tau < \tau_M$ as

$$\begin{aligned} N^\mu(t_n + \tau, \mathbf{x}) &= \int_{\mathbb{R}^3} q^\mu\, f_n(\mathbf{x} - \tau\frac{\mathbf{q}}{q^0}, \mathbf{q})\frac{d^3q}{q^0}\,, \\ T^{\mu\nu}(t_n + \tau, \mathbf{x}) &= \int_{\mathbb{R}^3} q^\mu q^\nu\, f_n(\mathbf{x} - \tau\frac{\mathbf{q}}{q^0}, \mathbf{q})\frac{d^3q}{q^0}\,, \end{aligned} \tag{6.5.1}$$

$$S^\mu(t_n + \tau, \mathbf{x}) = -\int_{\mathbb{R}^3} q^\mu\,(f_n \ln f_n)(\mathbf{x} - \tau\frac{\mathbf{q}}{q^0}, \mathbf{q})\frac{d^3q}{q^0}\,, \tag{6.5.2}$$

with the relativistic initial phase density (3.5.1) at the maximization time t_n

$$f_n(\mathbf{y}, \mathbf{q}) = f_J(n(t_n, \mathbf{y}), T(t_n, \mathbf{y}), \mathbf{u}(t_n, \mathbf{y}), \mathbf{q})\,. \tag{6.5.3}$$

Moreover n, T, u^μ are calculated from N^μ and $T^{\mu\nu}$ for the next time step from the following generally valid definitions

$$n = \sqrt{N^\mu N_\mu}, \qquad u^\mu = \frac{1}{n}N^\mu\,, \qquad T = \frac{1}{3n}(u_\mu u_\nu - g_{\mu\nu})\,T^{\mu\nu}\,. \tag{6.5.4}$$

In order to initialize the kinetic scheme for the next time step, we first require the following continuity conditions for the zero-components of the moments across the maximization time t_n, $n \geq 1$

$$\begin{aligned} N^0(t_n^+, \mathbf{x}) &= N^0(t_n^-, \mathbf{x})\,, \\ T^{0k}(t_n^+, \mathbf{x}) &= T^{0k}(t_n^-, \mathbf{x}),\ k = 1, 2, 3\,, \\ T^{00}(t_n^+, \mathbf{x}) &= T^{00}(t_n^-, \mathbf{x})\,. \end{aligned} \tag{6.5.5}$$

Here we have used the following abbreviations for the one-sided limits across the maximization time t_n, $n \geq 1$, where ε is a positive real number

$$N^\mu(t_n^\pm, \mathbf{x}) = \lim_{\varepsilon \to 0} N^\mu(t_n \pm \varepsilon, \mathbf{x})\,,$$
$$T^{\mu\nu}(t_n^\pm, \mathbf{x}) = \lim_{\varepsilon \to 0} T^{\mu\nu}(t_n \pm \varepsilon, \mathbf{x})\,.$$

These conditions are necessary in order to guarantee the conservation laws for mass, momentum and energy across the maximization time t_n. Moreover we start again with a relativistic Jüttner distribution for the next time step. Then we obtain, using the constitutive relations (6.1.2) for the three-dimensional Euler equations which are valid for the t_n^+ side of the maximization time

$$\begin{aligned} N^0(t_n^+, \mathbf{x}) &= n(t_n^+, \mathbf{x})\sqrt{1 + \mathbf{u}^2(t_n^+, \mathbf{x})}\,, \\ T^{0k}(t_n^+, \mathbf{x}) &= n(t_n^+, \mathbf{x})\chi(\beta(t_n^+, \mathbf{x}))u^k(t_n^+, \mathbf{x})\sqrt{1 + \mathbf{u}^2(t_n^+, \mathbf{x})}\,, \\ T^{00}(t_n^+, \mathbf{x}) &= -p(t_n^+, \mathbf{x}) + n(t_n^+, \mathbf{x})\chi(\beta(t_n^+, \mathbf{x}))(1 + \mathbf{u}^2(t_n^+, \mathbf{x}))\,. \end{aligned} \tag{6.5.6}$$

Here $k = 1, 2, 3$ again denote a spatial index. Since these components of the moments are continuous across the maximization time t_n, we can replace them by the free-flight moments for t_n^- and solve the equations (6.5.6) for $p, \mathbf{u}, n$ in order to initialize the kinetic scheme for the next time step. Using for positive γ the definitions

$$\gamma^2 = \frac{\sum_{k=1}^{3} (T^{0k})^2}{(N^0)^2}\,, \qquad F(\beta) = \frac{T^{00}}{N^0}\sqrt{1 + \frac{\gamma^2}{\chi(\beta)^2}} - \frac{\gamma^2}{\chi(\beta)} - \psi(\beta)\,, \tag{6.5.7}$$

we will find the following relations for the fields at the next time step

$$F(\beta(t_n^+, \mathbf{x})) = 0\,, \tag{6.5.8}$$
$$u^k(t_n^+, \mathbf{x}) = \frac{T^{0k}}{N^0\,\chi(\beta(t_n^+, \mathbf{x}))}\,, \tag{6.5.9}$$
$$n(t_n^+, \mathbf{x}) = \frac{N^0}{\sqrt{1 + \frac{\gamma^2}{\chi(\beta(t_n^+, \mathbf{x}))^2}}}\,. \tag{6.5.10}$$

In the formulae (6.5.7)-(6.5.10), N^0, T^{00} and T^{0k} are abbreviations for the free-flight moments $N^0(t_n^-, \mathbf{x})$, $T^{00}(t_n^-, \mathbf{x})$ and $T^{0k}(t_n^-, \mathbf{x})$, respectively.

We first solve the implicit equation $F(\beta(t_n^+, \mathbf{x})) = 0$ by using Newton's method. We have checked that for sufficiently small value of β the function $F(\beta)$ is negative, while $F(\beta)$ has a positive limit for $\beta \to \infty$. So we conclude from the mean-value theorem that $F(\beta)$ has at least one real root. Unfortunately it is very difficult to prove that $F(\beta)$ is a monotonically increasing function, which could only be checked numerically in several cases. Once we get the value of $\beta(t_n^+, \mathbf{x})$, the other quantities $u^k(t_n^+, \mathbf{x})$ and $n(t_n^+, \mathbf{x})$ can be easily calculated in the prescribed order from the free-flight moments N^0, T^{00} and T^{0k}. Since the continuity conditions initialize the scheme for the next time step they conclude the formulation of the kinetic scheme.

Proposition 6.5: *Let $\Omega \subset \mathbb{R}_0^+ \times \mathbb{R}^3$ be any bounded convex region in space and time. By do_ν we denote the positive oriented boundary element of $\partial\Omega$. Let $\tau_M > 0$ be a fixed time step. The moment representations* (6.5.1) *and* (6.5.2) *calculated by the iterated scheme have the following properties:*

(i) *There hold the conservation laws for the particle number, the momentum and energy:*

$$\oint_{\partial\Omega} N^\nu do_\nu = 0, \quad \oint_{\partial\Omega} T^{\mu\nu} do_\nu = 0. \tag{6.5.11}$$

(ii) *The following entropy inequality is satisfied:*

$$\oint_{\partial\Omega} S^\nu do_\nu \geq 0. \tag{6.5.12}$$

Here the covariant vector do_ν is a positive oriented surface element to the boundary $\partial\Omega$. It can be written in covariant form as

$$do_\kappa = \varepsilon_{\kappa\lambda\mu\nu} \sum_{i,j,m=1}^{3} \frac{\partial x^\lambda}{\partial u^i} \frac{\partial x^\mu}{\partial u^j} \frac{\partial x^\nu}{\partial u^m} du^i\, du^j\, du^m\,,$$

where $x^\alpha = x^\alpha(u^1, u^2, u^3)$ is a positive oriented parametrization of the boundary $\partial\Omega$.

Remark. Note that these weak formulations are the weak representations of the differential forms

$$\frac{\partial N^\nu}{\partial x^\nu}(t_n + \tau, \mathbf{x}) = 0, \quad \frac{\partial T^{\mu\nu}}{\partial x^\nu}(t_n + \tau, \mathbf{x}) = 0, \quad \frac{\partial S^\nu}{\partial x^\nu}(t_n + \tau, \mathbf{x}) = 0. \tag{6.5.13}$$

The proof of this proposition runs along the same lines as was carried out in Chapter 4 for the ultra-relativistic Euler equations, and may therefore be omitted.

6.5.1 Positivity and L^1-Stability of the Kinetic Scheme

Here we show that our kinetic scheme preserve positivity of the density and pressure. This also implies that the scheme is L^1-stable. A similar theorem has been proved in Chapter 4 for ultra-relativistic kinetic scheme.

Theorem 6.6: *Assume that the initial distribution function $f_n(\mathbf{y}, \mathbf{q}) \geq 0$, additionally $f_n(\mathbf{y}, \mathbf{q})$ does not vanish almost everywhere for all microscopic velocities $\mathbf{q}$, macroscopic velocities $\mathbf{u}$ and positive desnsity and pressure. Then the numerical solution obtained by the resulting kinetic scheme has the following property: Its density, pressure and total energy remain positive for all times.*

$$n(t_n + \tau, \mathbf{x}) > 0\,, \quad p(t_n + \tau, \mathbf{x}) > 0\,, \quad T^{00}(t_n + \tau, \mathbf{x}) > 0\,. \tag{6.5.14}$$

This also mean that the numerical scheme defined by (6.5.1) *and* (6.5.2) *is stable in L^1.*

Proof: Since the particle density is defined as $n = \sqrt{N^\mu N_\mu}$, Therefore we have to prove that

$$N^\mu\, N_\mu(t_n+\tau,\mathbf{x}) = \left((N^0)^2-(N^1)^2-(N^2)^2-(N^3)^2\right)(t_n+\tau,\mathbf{x}) > 0. \tag{6.5.15}$$

From the moments (6.5.1), we have

$$N^0(t_n+\tau,\mathbf{x}) = \int_{\mathbb{R}^3} f_n(\mathbf{x}-\tau\frac{\mathbf{q}}{q^0},\mathbf{q})\, d^3q > 0\,. \tag{6.5.16}$$

Using the free-flight moments (6.5.1) and Cauchy Schwarz inequality (4.3.35), we have

$$\begin{aligned}
(N^1)^2(t_n+\tau,\mathbf{x}) &= \left(\int_{\mathbb{R}^3} q^1\, f_n(\mathbf{x}-\tau\frac{\mathbf{q}}{q^0},\mathbf{q})\,\frac{d^3q}{q^0}\right)^2 \\
&= \left(\int_{\mathbb{R}^3}\left(\left(\frac{q^1}{q^0}\sqrt{f_n}\right)\cdot\left(\sqrt{f_n}\right)\right)(\mathbf{x}-\tau\frac{\mathbf{q}}{q^0},\mathbf{q})\, d^3q\right)^2 \\
&< \left(\int_{\mathbb{R}^3}\left(\frac{q^1}{q^0}\sqrt{f_n}\right)^2(\mathbf{x}-\tau\frac{\mathbf{q}}{q^0},\mathbf{q})\, d^3q\right)\cdot\left(\int_{\mathbb{R}^3}\left(\sqrt{f_n}\right)^2(\mathbf{x}-\tau\frac{\mathbf{q}}{q^0},\mathbf{q})\, d^3q\right) \\
&= N^0(t_n+\tau,\mathbf{x})\left(\int_{\mathbb{R}^3}\left(\frac{q^1}{q^0}\right)^2 f_n(\mathbf{x}-\tau\frac{\mathbf{q}}{q^0},\mathbf{q})\, d^3q\right).
\end{aligned} \tag{6.5.17}$$

Where in Cauchy-Schwarz inequality we have not taken the equality sign, because the functions $\frac{q^1}{q^0}\sqrt{f_n(\mathbf{y},\mathbf{q})}$ and $\sqrt{f_n(\mathbf{y},\mathbf{q})}$ are linearly independent. Similarly

$$\begin{aligned}
(N^2)^2(t_n+\tau,\mathbf{x}) &< N^0(t_n+\tau,\mathbf{x})\left(\int_{\mathbb{R}^3}\left(\frac{q^2}{q^0}\right)^2 f_n(\mathbf{x}-\tau\frac{\mathbf{q}}{q^0},\mathbf{q})\, d^3q\right), \\
(N^3)^2(t_n+\tau,\mathbf{x}) &< N^0(t_n+\tau,\mathbf{x})\left(\int_{\mathbb{R}^3}\left(\frac{q^3}{q^0}\right)^2 f_n(\mathbf{x}-\tau\frac{\mathbf{q}}{q^0},\mathbf{q})\, d^3q\right).
\end{aligned} \tag{6.5.18}$$

Now we use (6.5.17) and (6.5.18) in (6.5.15). Also, since

$$q^0 = \sqrt{1+\sum_{k=1}^{3}(q^k)^2}\,,$$

we finally get

$$\begin{aligned}
N^\mu\, N_\mu(t_n+\tau,\mathbf{x}) &= \left((N^0)^2-(N^1)^2-(N^2)^2-(N^3)^2\right)(t_n+\tau,\mathbf{x}) \\
&> N^0(t_n+\tau,\mathbf{x})\left(N^0(t_n+\tau,\mathbf{x}) - \int_{\mathbb{R}^3}\frac{\sum_{k=1}^{3}(q^k)^2}{(q^0)^2} f_n(\mathbf{x}-\tau\frac{\mathbf{q}}{q^0},\mathbf{q})\, d^3q\right) \\
&> N^0(t_n+\tau,\mathbf{x})\left[N^0(t_n+\tau,\mathbf{x}) - \int_{\mathbb{R}^3} f_n(\mathbf{x}-\tau\frac{\mathbf{q}}{q^0},\mathbf{q})\, d^3q\right]. \\
&= 0\,.
\end{aligned}$$

Thus we have proved that $n(t_n+\tau,\mathbf{x}) = \sqrt{N^\mu\, N_\mu(t_n+\tau,\mathbf{x})} > 0$.

Also from (3.4.9) the pressure is given by

$$p(t_n+\tau,\mathbf{x}) = \frac{1}{3}\left(u_\mu u_\nu - g_{\mu\nu}\right) T^{\mu\nu}(t_n+\tau,\mathbf{x})\,. \tag{6.5.19}$$

Using the free-flight moments (6.5.1) in (6.5.19), we get after simplification

$$p(t_n+\tau,\mathbf{x}) = \frac{1}{3}\int_{\mathbb{R}^3}\left((q^\mu u_\mu)^2 - 1\right)\, f_n(\mathbf{x}-\tau\frac{\mathbf{q}}{q^0},\mathbf{q})\frac{d^3q}{q^0}\,. \tag{6.5.20}$$

We also know from Lemma 6.1 that $q^\mu u_\mu > 1$, this implies

$$(q^\mu u_\mu)^2 > q^\mu u_\mu > 1\,. \tag{6.5.21}$$

Therefore (6.5.20) and (6.5.21) implies $p(t_n+\tau,\mathbf{x}) > 0$. Also we know from (6.5.1) that

$$T^{00}(t_n+\tau,\mathbf{x}) = \int_{\mathbb{R}^3} q^0 f_n(\mathbf{x}-\tau\frac{\mathbf{q}}{q^0},\mathbf{q})\, d^3q > 0\,. \tag{6.5.22}$$

Now since our scheme is conservative, using (6.5.16), (6.5.22), we have

$$\begin{aligned}
||N^0(t_n+\tau,.)||_{L^1(R)} &= \int_{\mathbb{R}^3} |N^0(t_n+\tau,\mathbf{x})| d^3\mathbf{x} = \int_{\mathbb{R}^3} N^0(t_n+\tau,\mathbf{x}) d^3\mathbf{x} \\
&= \int_{\mathbb{R}^3} N^0(t_n,\mathbf{x}) d^3\mathbf{x} = \int_{\mathbb{R}^3} |N^0(t_n,\mathbf{x})| d^3\mathbf{x} \\
&= ||N^0(t_n,.)||_{L^1(R)}\,.
\end{aligned}$$

Similarly $||T^{00}(t_n+\tau,.)||_{L^1(R)} = \|T^{00}(t_n,.)\|_{L^1(R)}$. Now using (6.5.1) with $\mathbf{y} = \mathbf{x} - \tau\frac{\mathbf{q}}{q^0}$ and Cauchy-schwarz inequality (4.3.35) we get

$$\begin{aligned}
||T^{0k}(t_n+\tau,.)||_{L^1(R)} &= \int_{\mathbb{R}^3}\left|\int_{\mathbb{R}^3} q^k f_n(\mathbf{y},\mathbf{q})\,\frac{d^3q}{q^0}\right| d^3\mathbf{x} \\
&= \int_{\mathbb{R}^3}\left|\int_{\mathbb{R}^3}\left(\sqrt{f_n}\right)\left(q^k\sqrt{f_n}\right)(\mathbf{y},\mathbf{q})\frac{d^3q}{q^0}\right| d^3\mathbf{x} \\
&< \left[\int_{\mathbb{R}^3}\left|\int_{\mathbb{R}^3} f_n(\mathbf{y},\mathbf{q})\frac{d^3q}{q^0}\right| d^3\mathbf{x}\cdot\int_{\mathbb{R}^3}\left|\int_{\mathbb{R}^3}\left(q^0\right)^2 f_n(\mathbf{y},\mathbf{q})\frac{d^3q}{q^0}\right| d^3\mathbf{x}\right]^{\frac{1}{2}} \\
&= \left(||n(t_n,.)||_{L^1(R)}\,||T^{00}(t_n,.)||_{L^1(R)}\right)^{\frac{1}{2}}.
\end{aligned}$$

This proves the L^1 stability of the scheme. ∎

6.5.2 A Kinetic Scheme for the One-Dimensional Case

In the following we are looking for the spatially one-dimensional solutions, which are nevertheless solutions to the full three dimensional equations. In order to initialize the scheme, we consider the initial data

$$n_I(\mathbf{x}) = n(0,x^1),\ \mathbf{u}_I(\mathbf{x}) = (u(0,x^1),0,0)^T,\ p_I(\mathbf{x}) = p(0,x^1). \tag{6.5.23}$$

This special form of the initial data will lead to a kinetic solution of the same form for all later times $t > 0$ and $x = x^1$, namely

$$n = n(t,x),\ \mathbf{u} = (u(t,x),0,0),\ p = p(t,x). \tag{6.5.24}$$

Thus we have got a one-dimensional solution from the three-dimensional kinetic scheme. We will use the (generally valid) equation $p = nT = \frac{n}{\beta}$ and start with the full three-dimensional scheme.

In order to formulate the scheme we first consider the rest frame where $u^0 = 1$ and $u = 0$. Then we will apply a Lorentz-transformation in order to come back to a general frame where u may or may not be zero. In the rest frame the spatial part of the dimensionless microscopic four-vector is denoted by $\mathbf{q}' = (q'^1, q'^2, q'^3) \in \mathbb{R}^3$. For the integration variable $\mathbf{q}'$ we will apply the substitution

$$q'^1 = \vartheta\xi\,, \qquad q'^2 = \vartheta\sqrt{1-\xi^2}\sin\varphi\,, \qquad q'^3 = \vartheta\sqrt{1-\xi^2}\cos\varphi\,, \tag{6.5.25}$$

with $|\mathbf{q}'| = \vartheta$, where the domains of the new variables are given by $0 \le \vartheta < \infty$, $-1 \le \xi \le 1$ and $0 \le \varphi \le 2\pi$. In order to avoid the unnecessary integration over the whole range of ϑ, we wish to find a finite domain for ϑ which only contributes to the solution, and remove the rest range which has only a very small contribution to the integral. The Jüttner phase density (3.5.1) in the rest frame can be written as

$$f_J(n,T,\mathbf{0},\mathbf{q}') = \frac{n}{M(\beta)\exp(\beta)}\,\exp\left(-\beta(\sqrt{1+\mathbf{q}'^2}-1)\right)\,. \tag{6.5.26}$$

So we want to have $\exp\left(-\beta(\sqrt{1+\mathbf{q}'^2}-1)\right) \le \varepsilon$ for sufficiently small value of ε. This gives

$$|\mathbf{q}'| \le R(T,\varepsilon) := \sqrt{\left(1+T\,\ln\frac{1}{\varepsilon}\right)^2 - 1}\,. \tag{6.5.27}$$

From the above equation it is clear that we have a sphere of center zero and radius $R(T,\varepsilon)$ in the rest frame. Also it is important to note that this value of $R(T,\varepsilon)$ covers the whole range from non-relativistic to ultra-relativistic limit. Here ε is a constant value, for example $\varepsilon = 10^{-4}$. Now we transform to a general frame where the initial speed u may or may not be zero, using the inverse of the Lorentz boost given in (3.4.13)

$$q^\mu = \Lambda^\mu{}_\nu(-\hat{u},0,0)q'^\nu\,, \qquad \mu = 0,1,2,3\,. \tag{6.5.28}$$

Here $\hat{u} \in \mathbb{R}$ is a fixed one-dimensional velocity parameter, which will be given later for the formulation of the kinetic scheme. Using the equations (6.5.25) and (6.5.28), we get the values for q^μ, namely

$$q^1 = \hat{u}\sqrt{1+\vartheta^2} + \vartheta\xi\sqrt{1+\hat{u}^2}\,, \tag{6.5.29}$$

$$q^2 = \vartheta\sqrt{1-\xi^2}\sin\varphi\,, \tag{6.5.30}$$

$$q^3 = \vartheta\sqrt{1-\xi^2}\cos\varphi\,, \tag{6.5.31}$$

$$q^0 = \sqrt{1+(q^1)^2+(q^2)^2+(q^3)^2}\,. \tag{6.5.32}$$

Also the Jacobian of integration is given by

$$J(\hat{u},\xi,\vartheta) = \frac{\hat{u}\vartheta^3\xi}{\sqrt{1+\vartheta^2}} + \vartheta^2\sqrt{1+\hat{u}^2}\,. \tag{6.5.33}$$

Here the parameter $\hat{u}$ is not depending on ϑ, ξ and φ. Recall that the spatial initial data (6.5.23) lead to the restrictions (6.5.24) for the fields at all later times. Due to (6.5.24) the fields n, T and u in the free-flight phase density f_n are not depending on the variable φ. This fact enables us to do the integration with respect to φ directly. Thus we have the following reduced integrals in this case

$$\begin{aligned} N^0(t_n+\tau,\mathbf{x}) &= 2\pi \int_0^R \int_{-1}^1 J\,\hat{f}_n(x-\tau\tfrac{q^1}{q^0},\mathbf{q})d\xi\,d\vartheta\,,\\ N^1(t_n+\tau,\mathbf{x}) &= 2\pi \int_0^R \int_{-1}^1 J\,\tfrac{q^1}{q^0}\hat{f}_n(x-\tau\tfrac{q^1}{q^0},\mathbf{q})d\xi\,d\vartheta\,, \end{aligned} \tag{6.5.34}$$

$$\begin{aligned} T^{00}(t_n+\tau,x) &= 2\pi \int_0^R \int_{-1}^1 J\,q^0\hat{f}_n(x-\tau\tfrac{q^1}{q^0},\mathbf{q})d\xi\,d\vartheta\,,\\ T^{01}(t_n+\tau,x) &= 2\pi \int_0^R \int_{-1}^1 J\,q^1\hat{f}_n(x-\tau\tfrac{q^1}{q^0},\mathbf{q})d\xi\,d\vartheta\,,\\ T^{11}(t_n+\tau,x) &= 2\pi \int_0^R \int_{-1}^1 J\,\tfrac{(q^1)^2}{q^0}\hat{f}_n(x-\tau\tfrac{q^1}{q^0},\mathbf{q})d\xi\,d\vartheta\,,\\ T^{22}(t_n+\tau,x) &= 2\pi \int_0^R \int_{-1}^1 J\,\tfrac{(q^2)^2}{q^0}\hat{f}_n(x-\tau\tfrac{q^1}{q^0},\mathbf{q})d\xi\,d\vartheta\,, \end{aligned} \tag{6.5.35}$$

where

$$\hat{f}_n(y,\mathbf{q}) := f_n(y,0,0,\mathbf{q})\,,\quad y\in\mathbb{R}\,,\,\mathbf{q}=(q^1,q^2,q^3)^T\in\mathbb{R}^3\,, \tag{6.5.36}$$

with the function $f_n(\mathbf{y},\mathbf{q})$ given by (3.5.1), the Jacobian $J := J(u(t_n,x),\xi,\vartheta)$ for $\hat{u}=u(t_n,x)$ and with the radius $R := R(T,\varepsilon)$ for the temperature $T = \max\{T(t_n,y)\,|\,x-\tau\le y\le x+\tau\}$. Moreover we obtain

$$\begin{aligned} N^2(t_n+\tau,x) &= N^3(t_n+\tau,x) = 0\,,\\ T^{10}(t_n+\tau,x) &= T^{01}(t_n+\tau,x)\,,\\ T^{22}(t_n+\tau,x) &= T^{33}(t_n+\tau,x)\,, \end{aligned}$$

where all the other components of $T^{\mu\nu}$ are zero. So in the one-dimensional case n,u and T can be obtained from the generally valid relations in equation (6.5.4) as follows:

$$n(t,x) = \sqrt{(N^0(t,x))^2-(N^1(t,x))^2}\,, \tag{6.5.37}$$

$$u(t,x) = \frac{1}{n}N^1(t,x)\,, \tag{6.5.38}$$

$$\begin{aligned} p(t,x) =& \frac{1}{3}[u^2(t,x)T^{00}(t,x) - 2u\sqrt{1+u^2(t,x)}\,T^{01}(t,x)\\ &+ (1+u^2(t,x))T^{11}(t,x) + 2T^{22}(t,x)]\,. \end{aligned} \tag{6.5.39}$$

Note that we still need the resolved continuity conditions (6.5.7)-(6.5.10) in order to initialize the scheme for the next time step. Since only the zero-components N^0, $T^{0\mu}$ are continuous across the maximization times t_n, we have to distinguish between the left- and right-handed limits $n(t_n^{\pm},x)$, $u(t_n^{\pm},x)$ and $p(t_n^{\pm},x)$ at the maximization times t_n in (6.5.37)- (6.5.39).

6.5.3 From the Kinetic Scheme to the Eulerian Limit ($\tau_M \to 0$)

In the previous sections we have calculated the solution of the kinetic scheme in the three- and one-dimensional case, respectively. This was done for the prescribed initial data of n, u and p for a given free-flight time step $\tau_M > 0$. If we calculate these solutions for $\tau_M \to 0$ then we get the Eulerian limit

$$N^\mu \to n\,u^\mu\,, \qquad T^{\mu\nu} \to -pg^{\mu\nu} + (e+p)u^\mu u^\nu\,, \qquad S^\mu \to \sigma\,u^\mu\,, \tag{6.5.40}$$

where p, e and σ are given by (6.1.1). First we pass to the Eulerian limit (6.5.40) at the points of smoothness in the following way using (3.4.16)

$$\begin{aligned}
\lim_{\tau\to 0}\frac{\partial}{\partial\tau}N^0(t_n+\tau,\mathbf{x}) &= \lim_{\tau\to 0}\frac{\partial}{\partial\tau}(n(t_n+\tau,\mathbf{x})\sqrt{1+u^2(t_n+\tau,\mathbf{x})}\,)\\
&= \lim_{\tau\to 0}\frac{\partial}{\partial\tau}\int_{\mathbb{R}^3} q^0 f_n(\mathbf{x}-\tau\frac{\mathbf{q}}{q^0},\mathbf{q})\frac{d^3q}{q^0}\\
&= -\lim_{\tau\to 0}\int_{\mathbb{R}^3} q^0\sum_{k=1}^3\frac{q^k}{q^0}\frac{\partial}{\partial x^k}f_n(\mathbf{x}-\tau\frac{\mathbf{q}}{q^0},\mathbf{q})\frac{d^3q}{q^0}\\
&= -\int_{\mathbb{R}^3}\sum_{k=1}^3 q^k\frac{\partial}{\partial x^k}f_n(\mathbf{x},\mathbf{q})\frac{d^3q}{q^0}\\
&= -\sum_{k=1}^3\frac{\partial}{\partial x^k}(u^k(t_n^+,\mathbf{x})n(t_n^+,\mathbf{x}))\\
&= -\nabla\cdot(\mathbf{u}(t_n^+,\mathbf{x})n(t_n^+,\mathbf{x}))\,,
\end{aligned}$$

$$\Rightarrow \frac{\partial}{\partial t}(n(t_n^+,\mathbf{x})\sqrt{1+u^2(t_n^+,\mathbf{x})}\,) + \nabla\cdot(\mathbf{u}(t_n^+,\mathbf{x})n(t_n^+,\mathbf{x})) = 0\,, \tag{6.5.41}$$

which is a first Euler equation (6.4.2). Similarly we get the other two Euler equations (6.4.3) and (6.4.4) if we differentiate $T^{00}(t_n+\tau,\mathbf{x})$ and $T^{0k}(t_n+\tau,\mathbf{x})$ with respect to τ and pass to the limit $\tau \to 0$.

Secondly on the left hand side of (6.5.40) there are the moments N^μ, $T^{\mu\nu}$ and S^μ as calculated by the kinetic scheme, see (6.5.1) and (6.5.2). Since the solution of the kinetic scheme satisfies the conservation laws and the entropy inequality as stated in Proposition 6.5, we conclude from (6.5.40) that these also result for the weak entropy solution in the Eulerian limit $\tau_M \to 0$. The weak entropy solution in the Eulerian limit in one space dimension is given by (6.4.8), (6.4.9) and (6.4.10).

6.6 Phenomenological Relativistic Euler Equations

Let us consider the Euler equations which can be obtained from the general form of special relativistic Euler equations (6.4.2)-(6.4.4) by taking the non-relativistic limit of internal energy given by (3.5.15), i.e,

$$e = n\Psi(\beta) = n + \frac{p}{\gamma-1}\,, \qquad p = (\gamma-1)(e-n)\,, \tag{6.6.1}$$

where γ is the ratio of specific heats, $1 \leq \gamma \leq \frac{5}{3}$. For $\gamma = \frac{5}{3}$ we get the same classical limit of $\Psi(\beta)$ as given in $(3.5.15)_3$. Since this constitutive relation for the energy density cannot be recovered from the relativistic phase density and there is no limiting phase density for these Euler equations. We call these equations the phenomenological form of the relativistic Euler equations. On the other hand we have shown in Chapter 3 that the phase densities for the classical and ultra-relativistic Euler equations can be automatically obtained from the the general form of the relativistic phase density by using classical and relativistic limits, respectively. We cannot formulate a kinetic scheme for these phenomenological relativistic Euler equations which is fully consistent with kinetic theory and can satisfy the conservation laws. However these Euler equations satisfy the Lorentz transformation rules and hence are relativistic Euler equations. The Rankine-Hugoniot jump conditions for these Euler equations can be obtained from those of the general form of the relativistic equations by just using the relation $(6.6.1)_1$ for $\Psi(\beta)$. A good introduction about these equations can be found in the review article of Martí and Müller [61] and references therein. Several numerical methods for solving these relativistic Euler equations have been reported. All these methods are mostly developed out of the existing reliable methods for solving the Euler equations of non-relativistic or Newtonian gas dynamics, see [61]. We will use the central scheme in order to to solve these equations. We will compare the central schemes results with exact Riemann solutions which were obtained in [61]. Using $(6.6.1)_1$ equations (6.4.2)-(6.4.4) gives

$$\frac{\partial}{\partial t}\left(n\sqrt{1+\mathbf{u}^2}\right) + \sum_{k=1}^{3} \frac{\partial (nu^k)}{\partial x^k} = 0\,, \tag{6.6.2}$$

$$\frac{\partial}{\partial t}\left((e+p)u^i\sqrt{1+\mathbf{u}^2}\right) + \sum_{k=1}^{3} \frac{\partial}{\partial x^k}\left(p\delta^{ik} + (e+p)u^iu^k\right) = 0\,, \tag{6.6.3}$$

$$\frac{\partial}{\partial t}\left(-p + (e+p)(1+\mathbf{u}^2)\right) + \sum_{k=1}^{3} \frac{\partial}{\partial x^k}\left((e+p)u^k\sqrt{1+\mathbf{u}^2}\right) = 0\,, \tag{6.6.4}$$

for $i = 1, 2, 3$. These are five equations with five unknowns. We can rewrite the above equations in the following conservative form

$$\frac{\partial W}{\partial t} + \sum_{k=1}^{3} \frac{\partial F^k(W)}{\partial x^k} = 0\,, \tag{6.6.5}$$

with the conserved variables W and fluxes F^i

$$W = \begin{pmatrix} N^0 \\ T^{0i} \\ T^{00} \end{pmatrix}, \qquad F^i = \begin{pmatrix} N^1 \\ T^{ik} \\ T^{0k} \end{pmatrix}, \tag{6.6.6}$$

where

$$\begin{aligned} &N^0 = n\sqrt{1+\mathbf{u}^2} \quad N^k = nu^k\,, \quad T^{0i} = (e+p)u^i\sqrt{1+\mathbf{u}^2}\,, \\ &T^{ik} = p\delta^{ik} + (e+p)u^iu^k\,, \quad T^{00} = -p + (e+p)(1+\mathbf{u}^2)\,, \quad i = 1, 2, 3. \end{aligned} \tag{6.6.7}$$

In order to get primitive variables from the conserved variables, we have the equation for finding n,

$$h(n) = (N^0)^2 \left(1 - \frac{\sum_{k=1}^{3} \left(T^{0k}\right)^2}{\left(T^{00} + p(n)\right)^2} \right) - n^2 = 0\,, \tag{6.6.8}$$

where

$$p = p(e,n) = p\left(T^{00} - \sqrt{\sum_{k=1}^{3} \left(T^{0k}\right)^2 \left(1 - n^2/(N^0)^2\right)}\,,\, n \right). \tag{6.6.9}$$

A Newton-Raphson procedure can be applied to solve for n. Once the value of n has been obtained, the energy density, and pressure, and velocity are obtained via

$$\begin{aligned} e &= T^{00} - \sqrt{\sum_{k=1}^{3} \left(T^{0k}\right)^2 \left(1 - n^2/(N^0)^2\right)}\,, \\ p &= (\gamma - 1)(e - n)\,, \quad u^k = \frac{n\,T^{0k}}{N^0\,(e+p)}\,, \quad v^k = \frac{u^k}{\sqrt{1+\mathbf{u}^2}}\,. \end{aligned} \tag{6.6.10}$$

6.6.1 One-Dimensional Phenomenological Euler equations

Here we are looking for spatially one-dimensional solutions of the phenomenological relativistic Euler equations. We only consider the solutions which depend on t and $x = x^1$ and satisfy $\rho = \rho(t,x)$, $v = (v(t,x), 0, 0)$ and $p = p(t,x)$. The three-dimensional Euler equations (6.6.5) then reduce to

$$\frac{\partial W}{\partial t} + \frac{\partial F(W)}{\partial x} = 0\,, \tag{6.6.11}$$

with the conserved variables W and fluxes F given as

$$W = \begin{pmatrix} N^0 \\ T^{01} \\ T^{00} \end{pmatrix}\,, \qquad F = \begin{pmatrix} N^1 \\ T^{11} \\ T^{01} \end{pmatrix}\,, \tag{6.6.12}$$

where

$$\begin{aligned} N^0 &= n\sqrt{1+u^2}\,, \quad N^1 = nu\,, \\ T^{01} &= (e+p)u\sqrt{1+u^2}\,, \quad T^{00} = -p + (e+p)(1+u^2)\,. \end{aligned} \tag{6.6.13}$$

In order to get primitive variables from the conserved variables, we have the equation for finding n,

$$h(n) = (N^0)^2 \left(1 - \frac{\left(T^{01}\right)^2}{\left(T^{00} + p(n)\right)^2} \right) - n^2 = 0\,, \tag{6.6.14}$$

where

$$p = p(e, n) = p\left(T^{00} - \sqrt{(T^{01})^2\,(1 - n^2/(N^0)^2)}, n\right). \tag{6.6.15}$$

Once the value of n have been obtained, the energy density, and pressure, and velocity are obtained via

$$\begin{aligned} e &= T^{00} - \sqrt{(T^{01})^2\,(1 - n^2/(N^0)^2)}\,, \\ p &= (\gamma - 1)(e - n)\,, \quad u = \frac{n\,T^{01}}{N^0\,(e + p)}\,, \quad v = \frac{u}{\sqrt{1 + u^2}}\,. \end{aligned} \tag{6.6.16}$$

6.7 Numerical Case Studies

Here we present the numerical results for both general form and phenomenological form of the special relativistic Euler equations.

6.7.1 General Form of Special Relativistic Euler Equations

Here we compare the results of our kinetic scheme with central schemes results.

Problem 1: Relativistic shock tube flow

We consider gas flow in a shock tube at relativistic velocity. In this problem a diaphragm, which is located at $x = 0.5$, separates two regions, each in a constant equilibrium state at $t = 0$. The initial conditions are specified as $(n_L, u_L, p_L) = (1.0, 0.0, 1.0)$ for $0 \le x \le 0.5$ and $(n_R, u_R, p_R) = (0.125, 0.0, 0.1)$ for $0.5 \le x \le 1.0$. This is a mildly relativistic case and the wave structures are quite similar to the nonrelativistic case, namely shock wave, contact surface, and rarefaction fan. We use 500 mesh points in the spatial domain, while we use 100 maximization times in the kinetic scheme. The exact solution is obtained by using the second order central scheme on very fine mesh. The results are given in Figure 6.2 at $t = 0.5$.

Problem 2: Relativistic shock tube flow with shock heating

This case includes shock heating of a cold fluid. The initial conditions are $(n_L, u_L, p_L) = (5.0, 0.0, 3.8)$ for $0 \le x \le 0.5$ and $(n_R, u_R, p_R) = (1.0, 0.0, 0.0.027)$ for $0.5 \le x \le 1.0$. The fluid flow velocity is about 0.7 and relativistic effects are more pronounced than the previous case. We use 500 mesh points in the spatial domain. The exact solution is obtained by using the second order central scheme on very fine mesh. The results are given in Figure 6.3 at time $t = 0.52$.

Problem 3: A quadratic pulse

The initial data are

$$(n, u, p) = \begin{cases} (1.0, 0.0, 1.0) & \text{if } 0 < x < 0.4\,, \\ (4.0, 0.0, 4.0) & \text{if } 0.4 < x < 0.6\,, \\ (1.0, 0.0, 1.0) & \text{if } 0.6 < x < 1.0\,. \end{cases}$$

We use 1000 mesh points in the spatial domain with 100 maximization times in the kinetic scheme. The exact solution is obtained by using the second order central scheme on very fine mesh. The results are given in Figure 6.4 at time $t = 0.25$.

Problem 4: Perturbed relativistic shock tube flow

The initial conditions are specified as $(n_L, u_L, p_L) = (1.0, 0.0, 1.0)$ for $0 \leq x \leq 0.5$ and $(n_R, u_R, p_R) = (n_R, 0.0, 0.1)$ for $0.5 \leq x \leq 1.0$. Here the right state is a perturbed density field of sinusoidal wave, $n_R = 0.125 - 0.0875 \sin(50(x - 0.5))$. We run this test on 1000 mesh points. The computed solutions are plotted at $t = 0.5$. The results of first order central and kinetic schemes are shown in Figure 6.5. Again the exact solution is obtained by using second order central scheme on very fine mesh.

Problem 5: A single shock reflection

In this section we test our spatially one-dimensional kinetic scheme for a single shock problem. We introduce an adiabatic wall at $x = 0$. This single shock data can be obtained from the shock parametrizations given in Subsection 6.4.1 for the relativistic Euler equations. We start with a 1-shock running to the lower adiabatic wall. After the reflection there results an outcoming 3-shock. Figure 6.1 shows a sketch of this single shock reflection.

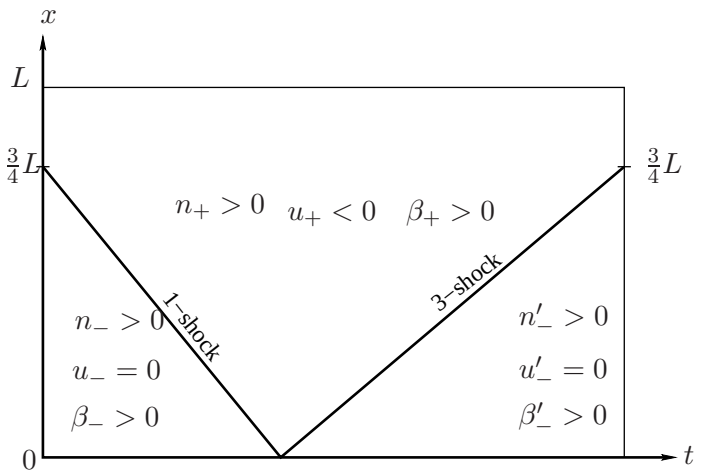

Figure 6.1: Sketch of a single shock reflection.

The initial and boundary value problem for the relativistic Euler equations is defined for $t \geq 0$ and $x \geq 0$, where $x = 0$ is the boundary for the lower adiabatic wall. The initial data for n, u and β are prescribed for $x > 0$, whereas for $t \geq 0$ we prescribe the boundary data $u(t, 0) = 0$. Following the idea presented in Chapters 2 and 4, we can use the one-dimensional scheme presented in Subsection 6.5.2 with the following two modifications:

(i) In (6.5.34) and (6.5.35) we have to replace the phase density $\hat{f}_n(x - \tau \frac{q^1}{q^0}, \mathbf{q})$ by the new

one $\hat{f}_n(|x-\tau\frac{q^1}{q^0}|,\mathbf{q}^*)$, where $\mathbf{q}^*$ is given by

$$q^{*1} = \mathrm{sgn}(x-\tau\frac{q^1}{q^0})\,(\hat{u}\sqrt{1+\vartheta^2}+\vartheta\xi\sqrt{1+\hat{u}^2})\,, \tag{6.7.1}$$

$$q^{*2} = \vartheta\sqrt{1-\xi^2}\sin\varphi\,, \tag{6.7.2}$$

$$q^{*3} = \vartheta\sqrt{1-\xi^2}\cos\varphi\,, \tag{6.7.3}$$

$$q^{*0} = \sqrt{1+(q^{*1})^2+(q^{*2})^2+(q^{*3})^2}\,. \tag{6.7.4}$$

Recall that the function $\hat{f}_n(y,\mathbf{q})$ is defined in (6.5.36).

(ii) In (6.5.34) and (6.5.35) we have to replace the temperature T for the integration radius $R = R(T,\varepsilon)$, see (6.5.27), by the new one

$$T := \max\{T(t_n,y)\,|\,y\geq 0\ \&\ x-\tau\leq y\leq x+\tau\}\,. \tag{6.7.5}$$

Figure 6.6, which is computed from the kinetic scheme, represents a plot for the particle density n, the velocity u and the temperature T in the time range $0\leq t\leq 2.63125$ and in the space range $0\leq x\leq L=1$. We have calculated the final time in such a way that the outcoming 3-shock finally arrives at the same position $x=\frac{3}{4}L$ where the original 1-shock has initially started. The Riemann initial data for the 1-shock with the jump at $x=\frac{3}{4}L$ are chosen according to the Rankine-Hugoniot jump conditions given in Subsection 6.4.1. The initial data are

$$\begin{gathered} n_- = 1.0 \quad u_- = 0.0 \quad \beta_- = 0.5 \quad p_- = 2.0\,, \\ n_+ = 1.35396 \quad u_+ = -0.175227 \quad \beta_+ = 0.45 \quad p_+ = 3.0088\,, \end{gathered}$$

where 200 maximization times are considered here, so that $\tau_M = 0.0131563$.

Moreover we obtained the constant states left and right to the reflected 3-shock analytically from the Rankine-Hugoniot shock parametrizations (6.4.14), (6.4.15) as well as numerically from the kinetic scheme. Both are compared below, where we use the notations from Figure 6.1.

The 3-shock data from the Rankine-Hugoniot jump conditions are
$n'_- = 1.83235 \quad u'_- = 0.0 \quad \beta'_- = 0.405264 \quad p'_- = 4.52136\,,$
$n_+ = 1.35396 \quad u_+ = -0.175227 \quad \beta_+ = 0.45 \quad p_+ = 3.0088\,.$

The 3-shock data from the kinetic scheme are
$n'_- = 1.83200 \quad u'_- = 0.0 \quad \beta'_- = 0.40852 \quad p'_- = 4.48448\,,$
$n_+ = 1.35394 \quad u_+ = -0.175236 \quad \beta_+ = 0.450024 \quad p_+ = 3.0086\,.$

We see a very good agreement between the analytical and numerical results.

6.7.2 Phenomenological Relativistic Euler Equations

Here we compare the second order central schemes results with the exact Riemann solutions.

Problem 6: Relativistic shock tube I

The initial data are

$$\begin{aligned} W_l = (\rho_l, u_l, p_l) &= (10.0, 0.0, 13.33) && \text{if } x < 0.5\,, \\ W_r = (\rho_r, u_r, p_r) &= (1.0, 0.0, 0.66 \times 10^{-6}) && \text{if } x \geq 0.5\,, \end{aligned}$$

where we take $\gamma = \frac{5}{3}$. The computational domain is $0 \leq x \leq 1$. This test problem has been considered by several authors, for example, Hawley, Smarr and Wilson [37], Schneider et al. [80], Martí and Müller [60, 61] etc. It involves the formation of an intermediate state bounded by a shock wave propagating to the right and transonic rarefaction wave propagating to the left. The fluid in the intermediate state moves at a mildly relativistic speed ($v = 0.72c$) to the right. Flow particles accumulate in a dense shell behind the shock wave compressing the fluid by a factor of 5 and heating it up to values of internal energy much larger than the rest-mass energy. Hence the fluid is extremely relativistic in thermodynamical point of view, but mildly relativistic dynamically. The results are shown in Figure 6.7 for 500 mesh points at time $t = 0.43$.

Problem 7: Relativistic shock tube II

The initial data are

$$\begin{aligned} W_l = (\rho_l, u_L, p_l) &= (1.0, 0.0, 1000.0) && \text{if } x < 0.5\,, \\ W_r = (\rho_r, u_R, p_r) &= (1.0, 0.0, 0.01) && \text{if } x \geq 0.5\,, \end{aligned}$$

where we take $\gamma = \frac{5}{3}$. The computational domain is $0 \leq x \leq 1$. This problem was first considered by Norman and Winkler [67]. The flow pattern is similar to that of the above problem, but more extreme. The relativistic effects reduce the post-shock state to a thin dense shell with a width of only about 1% of the grid length at t=0.4. The fluid in the shell moves with $v_{\text{shell}} = 0.96$, while the jump in density in the shell reaches a value of 10.6. The results are shown in Figure 6.8 for 500 mesh points at time $t = 0.43$.

Problem 8: Collision of two relativistic blast waves

$$\begin{aligned} W_l = (\rho_l, u_L, p_l) &= (1.0, 0.0, 1000.0) && \text{if } x <= 0.1\,, \\ W_m = (\rho_m, u_m, p_m) &= (1.0, 0.0, 0.01) && \text{if } 0.1 < x < 0.9\,, \\ W_r = (\rho_r, u_R, p_r) &= (1.0, 0.0, 100.0) && \text{if } x \geq 0.9\,, \end{aligned}$$

where the computational domain is $0 \leq x \leq 1$. The collision of two strong blast waves was used by Woodward and Colella [88] to compare the performance of several numerical methods in classical hydrodynamics. In the relativistic case, Yang et al. [94] considered this problem to test the high-order extensions of their relativistic beam scheme, whereas Martí and Müller [60] used it to evaluate the performance of their relativistic PPM [88] code. In this last case, the original boundary conditions were changed from reflecting to out flow to avoid the reflection and subsequent interaction of rarefaction waves allowing for a comparison with an analytical solution. We will also consider the out flow boundary conditions in this example.

The initial data consist of three constant states with large pressure jumps at the interfaces which are located at $x = 0.1$ and $x = 0.9$. The propagation velocity of the two blast waves is slower than in the Newtonian case, but close to the speed of light, i.e., 0.9567 and -0.8830 for the shock wave propagating to the right and left, respectively. Hence the shock interaction occurs much later (at t=0.43) than in the Newtonian problem (at about t=0.028). The collision give rise to a narrow region of very high density bounded by two shocks. The results are shown in Figure 6.9 for 500 mesh points at time $t = 0.43$.

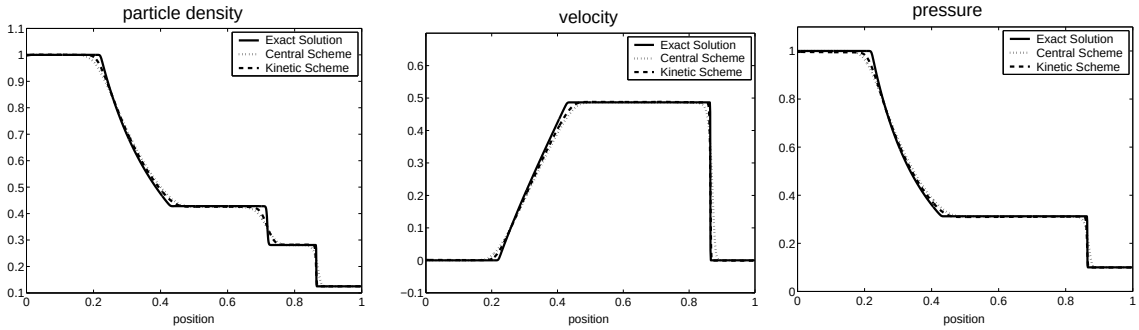

Figure 6.2: Relativistic shock tube at time $t = 0.5$.

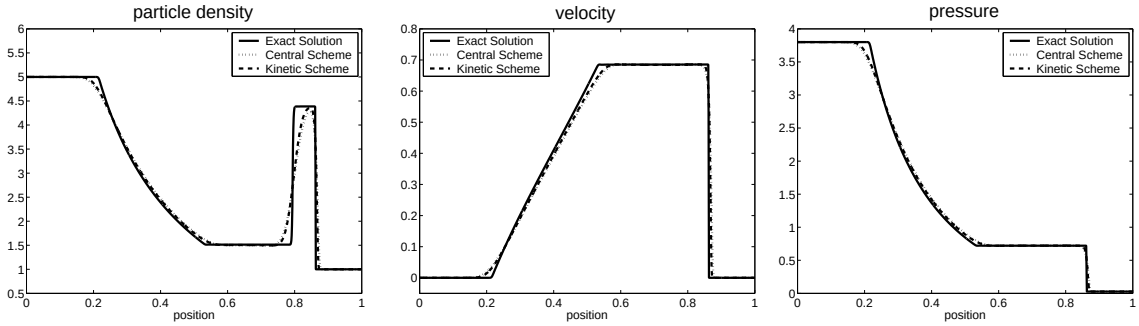

Figure 6.3: Relativistic shock tube with shock heating at time $t = 0.52$.

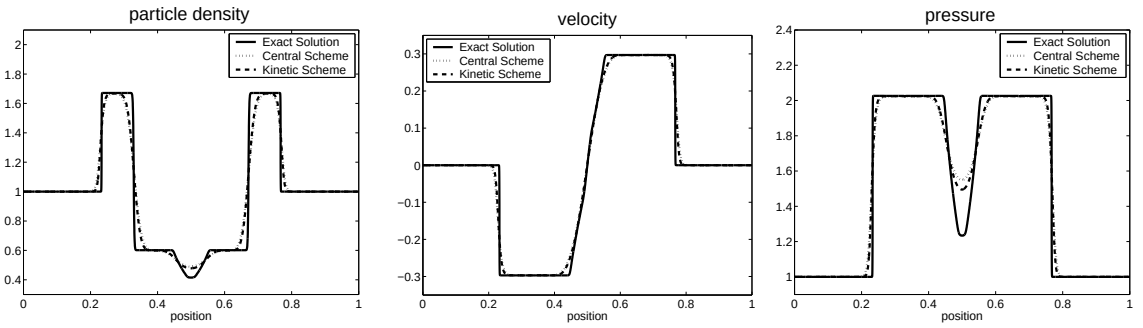

Figure 6.4: Quadratic pulse at time $t = 0.25$.

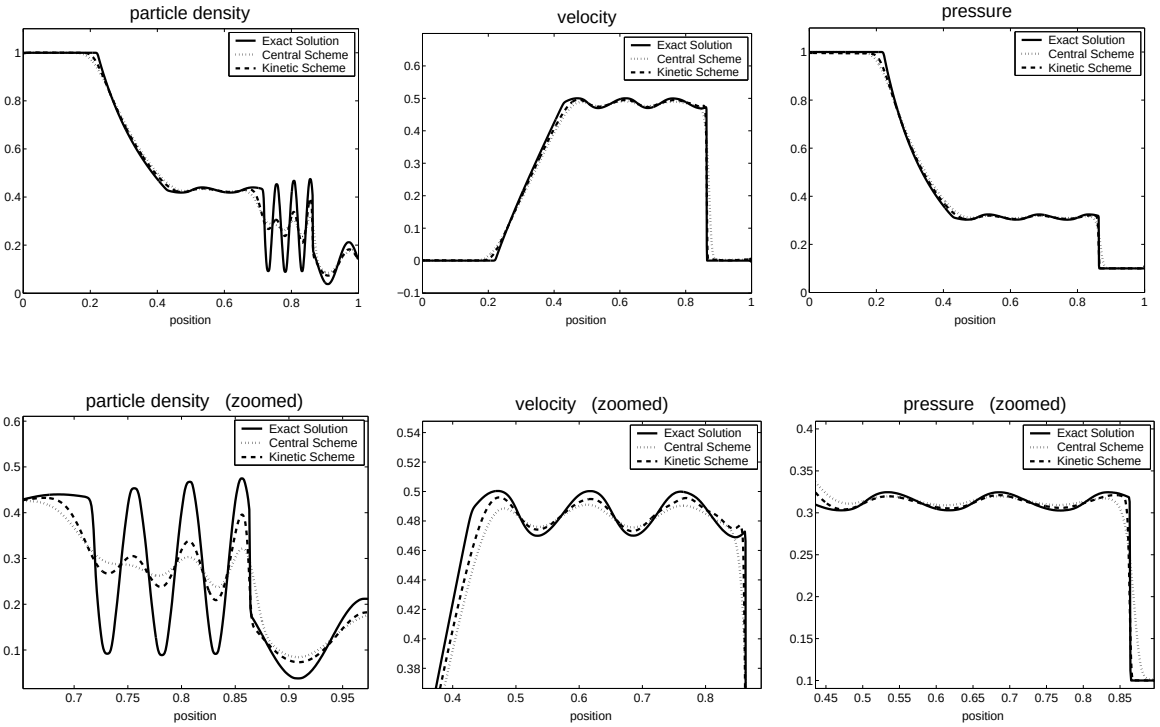

Figure 6.5: Perturbed relativistic shock tube problem at time $t = 0.5$.

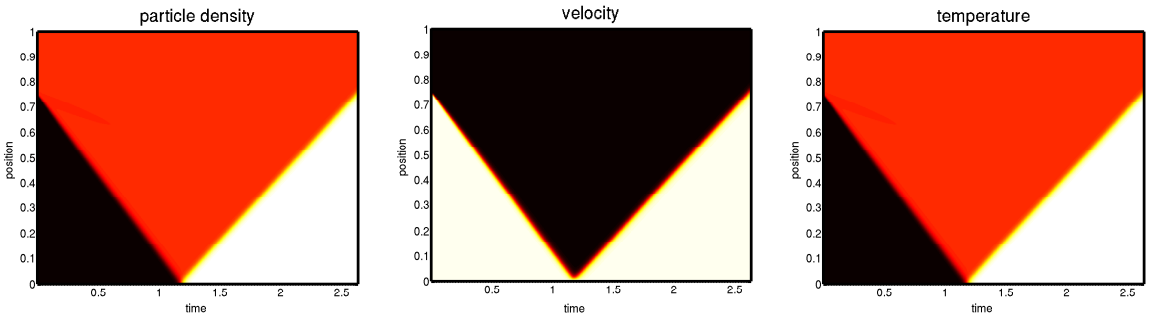

Figure 6.6: A single shock reflection.

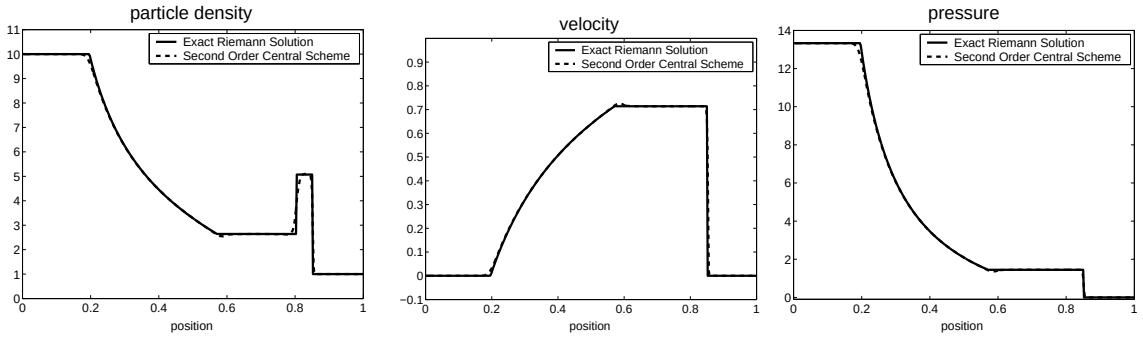

Figure 6.7: Relativistic shock tube I at $t = 0.43$.

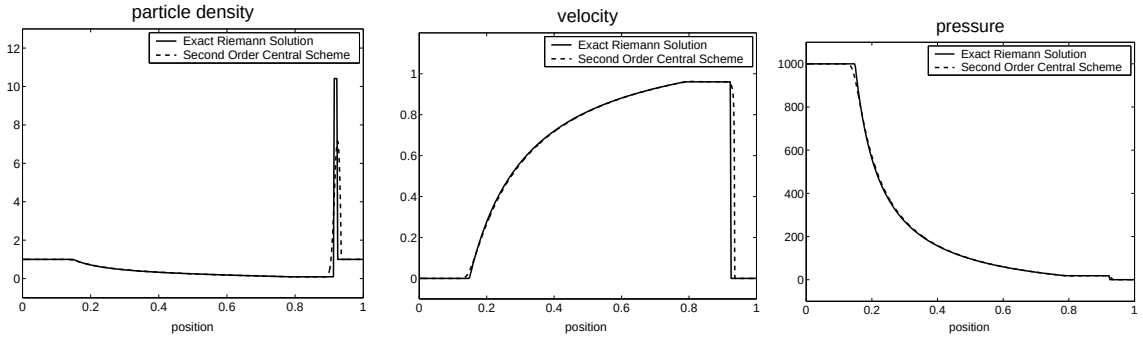

Figure 6.8: Relativistic shock tube II at $t = 0.43$.

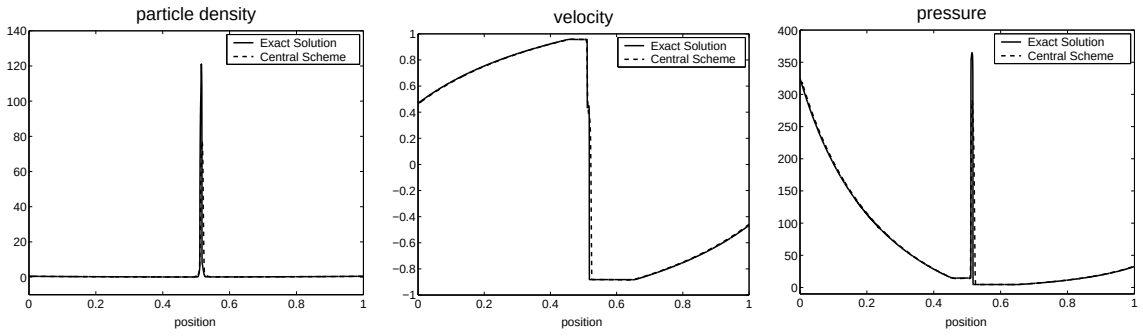

Figure 6.9: Collision of two relativistic blast waves at $t = 0.43$.

Chapter 7

Central Schemes

In recent years, central schemes for approximating solutions of hyperbolic conservations laws received a lot of attention. A family of high-resolution, non-oscillatory, central schemes, was developed to handle such problems. As compared to the "classical" *upwind* schemes, these central schemes have shown to be both simple to implement and stable for many problems ranging from one-dimensional scalar problems to multi-dimensional systems of conservation laws. They were successfully implemented for a variety of problems, such as, e.g., the incompressible and compressible Euler equations [56, 39, 64], the magnetohydrodynamics equations [89], hyperbolic systems with relaxation [2], non-linear optics [79] and multi-component flows by Qamar and Warnecke [75].

In Chapters $2-6$, we have used the central schemes in order to solve non-relativistic and relativistic Euler equations. The schemes are predictor-corrector methods which consist of two steps: starting with given cell averages, we first predict point values which are based on non-oscillatory piecewise-linear reconstructions from the cell averages; at the second corrector step, we use staggered averaging, together with the predicted mid-values, to realize the evolution of these averages. This results in a second-order, non-oscillatory central schemes, see [39, 64].

These second order schemes are based on a MUSCL-type reconstruction. Like upwind schemes, the reconstructed piecewise-polynomials used by the central schemes also make use of non-linear limiters which guarantee the overall non-oscillatory nature of the approximate solution. But unlike the upwind schemes, central schemes do not require the intricate and time-consuming (approximate) Riemann solvers which are essential for the high-resolution upwind schemes. This advantage is especially important in the multi-dimensional case where there is no exact Riemann solver. Moreover, the central schemes are "genuinely multi-dimensional" in the sense that they do not need dimensional splitting, see [39, 64] .

The central schemes are also very important in the relativistic case especially for the general form of the special relativistic Euler equations, see (6.4.2)-(6.4.4). Due to the presence of Bessel functions it is looking not possible to derive the parametrization of rarefaction waves for these Euler equations, and hence we cannot develop an exact Riemann solver for these equations. With the central schemes we can easily solve these equations without any difficulty, see Chapter 6.

Let us begin by introducing the well-known first order Lax-Friedrichs (LxF) scheme for one-dimensional conservation laws. This first order scheme is then extended to a second order central scheme. Next we study the first order LxF scheme for the two dimensional conservation laws and then extend it to the second order non-oscillatory central scheme, see [39, 64].

7.1 One-Dimensional Central Schemes

Here we want to solve the one-dimensional hyperbolic system of conservation laws

$$\frac{\partial W}{\partial t} + \frac{\partial F}{\partial x} = 0\,, \tag{7.1.1}$$

where $W(t,x)$ is a vector of conserved variables and $F(t,x)$ is the corresponding vector of fluxes.

7.1.1 One-Dimensional First Order LxF Scheme

Let us denote by $\overline{W}_i^n$, the approximate cell-average at time $t = t_n$, associated with the cell I_i, centered around $x_i = i\Delta x$, i.e.,

$$I_i = \left\{ \xi \;\middle|\; |\xi - x_i| \le \frac{\Delta x}{2} \right\}.$$

We take $\chi_i(x)$ to be the characteristic function of the cell I_i, $\chi_i(x) = 1$ for $x \in I_i$, $\chi_i(x) = 0$ for $x \in \mathbb{R}\backslash I_i$. To approximate (7.1.1), we start with a piecewise constant solution of the form $\sum \overline{W}_i^n \chi_i(x)$. Integrating (7.1.1) over the rectangle $[x_i, x_{i+1}] \times [t_n, t_{n+1}]$, we get

$$\oint_{\partial\Omega} W dx - F(W)dt = 0 \Leftrightarrow$$

$$-\int_{t_n}^{t_{n+1}} F\left(W(t,x_i)\right) dt + \int_{x_i}^{x_{i+1}} W(t_{n+1},\xi)d\xi + \int_{t_n}^{t_{n+1}} F\left(W(t,x_{i+1})\right) dt - \int_{x_i}^{x_{i+1}} W(t_n,\xi)d\xi = 0\,.$$

Note that our cells I_i are staggered with respect to the interval $[x_i, x_{i+1}]$ of integration. This leads to the LxF scheme as given below

$$\overline{W}_{i+\frac{1}{2}}^{n+1} = \frac{1}{2}(\overline{W}_i^n + \overline{W}_{i+1}^n) + \lambda\left(f(W_i^n) - f(W_{i+1}^n)\right)\,, \quad W_i^n := W(t_n, x_i) = \overline{W}_i^n\,, \tag{7.1.2}$$

where $\lambda = \frac{\Delta t}{\Delta x}$. The piecewise constant cells in each step are staggered with respect to those in the previous step.

7.1.2 A Second-Order Extension of the One-Dimensional Scheme

Starting with a piecewise-constant solution in time and space, $\sum \overline{W}_i^n \chi_i(x)$, one reconstruct a piecewise linear (MUSCL-type) approximation in space, namely

$$W(t_n, x) = \sum \left(\overline{W}_i^n + W_i^x \frac{(x - x_i)}{\Delta x} \right) \chi_i(x)\,, \tag{7.1.3}$$

where the discrete slopes W_i^x, see Figure 5.3, are calculated by using the min-mod limiters (5.2.16). The interpolant (7.1.3) is then evolved exactly in time and projected on to the staggered cell-averages on the next time step, t_{n+1}. Consider the balance law over the control volume $\Omega = [x_i, x_{i+1}] \times [t_n, t_{n+1}]$. We have

$$\begin{aligned} 0 &= \oint_{\partial\Omega} W dx - F(W) dt \Leftrightarrow \\ &= -\int_{t_n}^{t_{n+1}} F(W_i(t)) dt + \int_{x_i}^{x_{i+1}} W(t_{n+1}, \xi) d\xi + \int_{t_n}^{t_{n+1}} F(W_{i+1}(t)) dt - \int_{x_i}^{x_{i+1}} W(t_n, \xi) d\xi \,. \end{aligned}$$

This yields

$$\overline{W}_{i+\frac{1}{2}}^{n+1} = \overline{W}_{i+\frac{1}{2}}^{n} + \lambda \left(\frac{1}{\Delta t} \int_{t_n}^{t_{n+1}} F(W_i(t)) dt - \frac{1}{\Delta t} \int_{t_n}^{t_{n+1}} F(W_{i+1}(t)) dt \right) . \tag{7.1.4}$$

Where $\lambda = \frac{\Delta t}{\Delta x}$. The averaging of the linear data (7.1.3) at $t = t_n$, yields

$$\begin{aligned} \overline{W}_{i+\frac{1}{2}}^{n} &= \frac{1}{\Delta x} \int_{x_i}^{x_{i+1}} W(t_n, \xi) d\xi \\ &= \frac{1}{\Delta x} \left(\int_{x_i}^{x_{i+\frac{1}{2}}} W_i(t_n, \xi) d\xi + \int_{x_{i+\frac{1}{2}}}^{x_{i+1}} W_{i+1}(t_n, \xi) d\xi \right) , \\ &= \frac{1}{2}(W_i^n + W_{i+1}^n) + \frac{1}{8}(W_i^x - W_{i+1}^x) \,. \end{aligned} \tag{7.1.5}$$

So far every thing is *exact*. Moreover the Courant-Friedrichs-Levy (CFL) condition guarantees that $F(W_i(t))$ and $F(W_{i+1}(t))$, are smooth functions of t; hence they can be integrated approximately by the mid point rule at the expense of an $O(\Delta t^3)$ local truncation error. Thus we can write

$$\frac{1}{\Delta t} \int_{t_n}^{t_{n+1}} F(W_{i+1}(t)) dt \sim F(W_i^{n+\frac{1}{2}}) + O(\Delta t^3) \,. \tag{7.1.6}$$

Putting (7.1.5) and (7.1.6) in (7.1.4) we finally get

$$\overline{W}_{i+\frac{1}{2}}^{n+1} = \frac{1}{2}(W_i^n + W_{i+1}^n) + \frac{1}{8}(W_i^x - W_{i+1}^x) + \lambda \left[F(W_i(t_{n+\frac{1}{2}})) - F(W_{i+1}(t_{n+\frac{1}{2}})) \right] . \tag{7.1.7}$$

By Taylor expansion and the conservation laws (5.2.3), we have

$$W_i^{n+\frac{1}{2}} = \overline{W}_i^n + \frac{\Delta t}{2} \frac{\partial}{\partial t} W(t, x_i) + O(\Delta t)^2 = \overline{W}_i^n - \frac{\lambda}{2} F^x(W_i) + O(\Delta t)^2 \,. \tag{7.1.8}$$

This may serve as our approximate midvalues $W_i^{n+\frac{1}{2}}$ within the permissible second-order accuracy requirement. Here, $\frac{1}{\Delta x}F^x(W_i)$ stands for an approximate numerical derivatives of the flux $F(W(t, x = x_i))$,

$$\frac{1}{\Delta x}F^x(W_i) = \frac{\partial}{\partial x}F(W(t, x = x_i) + O(\Delta x)$$

The fluxes $F^x(W_i)$ are computed by applying the min-mod limiter to each of the components of F, i.e.,

$$\begin{aligned} F^x(W_i) &= MM\theta\{F(W_{i-1}), F(W_i), F(W_{i+1})\} \\ &= MM\left(\theta\Delta F(W_{i+\frac{1}{2}}), \frac{\theta}{2}\left(\Delta F(W_{i-\frac{1}{2}}) + \Delta F(W_{i+\frac{1}{2}})\right), \theta\Delta F(W_{i-\frac{1}{2}})\right). \end{aligned}$$

Here, Δ denotes the central differencing, $\Delta F(W_{i+\frac{1}{2}}) = F(W_{i+1}) - F(W_i)$, and MM denotes the min-mod nonlinear limiter given by (5.2.16) .

This component wise approach is one of the main advantages offered by central schemes over corresponding characteristic decompositions required by upwind schemes, see [39] and [64]. It is important to emphasize that while using the central type LxF solver, we integrate over the entire Riemann fan, which consists of both the left and right going waves. On the one hand, this enables us to ignore the detailed knowledge about the exact (or approximate) generalized Riemann solver. On the other hand, this enables us to accurately compute the numerical flux $\int_{t_n}^{t_{n+1}} F(w(\tau, x))d\tau$, whose values are extracted from the smooth interface of two non-interacting Riemann problems.

In summary, this family of central differencing scheme takes the easily implemented predictor-corrector form,

$$W_i^{n+\frac{1}{2}} = \overline{W}_i^n - \frac{\lambda}{2}F^x(W_i)\,, \tag{7.1.9}$$

$$\overline{W}_{i+\frac{1}{2}}^{n+1} = \frac{1}{2}(\overline{W}_i^n + \overline{W}_{i+1}^n) + \frac{1}{8}(W_i^x - W_{i+1}^x) + \lambda\left[F(W_i^{n+\frac{1}{2}}) - F(W_{i+1}^{n+\frac{1}{2}})\right]. \tag{7.1.10}$$

7.2 Two-Dimensional Central Schemes

Here we want to solve the one-dimensional hyperbolic system of conservation laws

$$\frac{\partial W}{\partial t} + \frac{\partial F}{\partial x} + \frac{\partial G}{\partial y} = 0\,, \tag{7.2.1}$$

where $W(t, x, y)$ is a vector of conserved variables and $F(t, x, y)$ and $G(t, x, y)$ are the corresponding vectors of fluxes.

We again start with a first order Lax-Friedrichs scheme for the two-dimensional conservation laws. This first order scheme is then extended to second order, see [39]. The procedure is similar to that of one-dimensional central scheme presented above.

7.2.1 The First Order LxF Scheme in 2D.

To approximate (7.2.1), we begin with a piecewise constant solution of the form $\sum \overline{W}^n_{i,j}\chi_{i,j}(x,y)$. We denote by $\overline{W}^n_{i,j}$, the approximate cell-average at time $t = t_n$, associated with the cell $C_{i,j} = I_i \times J_j$, centered around $(x_i = i\Delta x,\ y_j = j\Delta y)$, and $\chi_{i,j}(x,y)$ is the characteristic function of the cell $C_{i,j}$.

The arguments applied to the one-dimensional case can be easily extended to the higher dimensions. In the following we will abbreviate $\fint_B = \frac{1}{|B|}\int_B$ to denote the normalized integral, i.e., normalized over its length, area, etc. Also let $\lambda = \frac{\Delta t}{\Delta x}$ and $\mu = \frac{\Delta t}{\Delta y}$ denote the fixed mesh-ratio in the x- and y-directions, respectively. Let

$$\overline{W}_{i+\frac{1}{2},j+\frac{1}{2}}(t) = \fint_{C_{i+\frac{1}{2},j+\frac{1}{2}}} W(t,x,y)dxdy\,,$$

denote the staggered averages. Integrating (7.2.1) over the volume $[x_i, x_{i+1}] \times [y_j, y_{j+1}] \times [t_n, t_{n+1}]$, we get,

$$\begin{aligned}\overline{W}^{n+1}_{i+\frac{1}{2},j+\frac{1}{2}} =& \fint_{C_{i+\frac{1}{2},j+\frac{1}{2}}} W(t_n,x,y)dxdy \\ &- \lambda\left\{\fint_{t_n}^{t_{n+1}}\int_{y_j}^{y_{j+1}} \left[F(W(t,x_{i+1},y)) - F(W(t,x_i,y))\right]dydt\right\} \\ &- \mu\left\{\fint_{t_n}^{t_{n+1}}\int_{x_i}^{x_{i+1}} \left[G(W(t,x,y_{j+1})) - G(W(t,x,y_j))\right]dxdt\right\}.\end{aligned}$$

As given in Figure 7.1, the first integral has contribution from the four cells $C_{i,j}$, $C_{i+1,j}C_{i+1,j+1}$, and $C_{i,j+1}$. Simplifying the above balance law we finally get the following LxF scheme,

$$\begin{aligned}\overline{W}^{n+1}_{i+\frac{1}{2},j+\frac{1}{2}} =& \frac{1}{4}(\overline{W}^n_{i,j} + \overline{W}^n_{i+1,j} + \overline{W}^n_{i,j+1} + \overline{W}^n_{i+1,j+1}) \\ &- \frac{\lambda}{2}\left(F(W^n_{i+1,j}) - F(W^n_{i,j}) + F(W^n_{i+1,j+1}) - F(W^n_{i,j+1})\right) \\ &- \frac{\mu}{2}\left(G(W^n_{i,j+1}) - G(W^n_{i,j}) + G(W^n_{i+1,j+1}) - G(W^n_{i+1,j})\right).\end{aligned} \tag{7.2.2}$$

7.2.2 A Second-Order Extension of the Two-Dimensional Scheme

A two-dimensional extension of the second order central scheme was introduced in [39]. Like in the one-dimensional case, this staggered scheme can be viewed as an extension to the first order LxF Scheme. A piecewise-linear interpolant is reconstructed from the calculated cell-averages at time t_n,

$$W(t_n,x,y) = \sum\left(\overline{W}^n_{i,j} + W^x_{i,j}\left(\frac{x-x_i}{\Delta x}\right) + W^y_{i,j}\left(\frac{y-y_j}{\Delta y}\right)\right)\chi_{i,j}(x,y)\,. \tag{7.2.3}$$

Here $W^x_{i,j}$ and $W^y_{i,j}$ are discrete slopes in the $x-$ and $y-$directions, respectively, which are reconstructed from the given cell averages. To guarantee second-order accuracy, these slopes

should approximate the corresponding derivatives,

$$W^x_{i,j} \sim \Delta x \frac{\partial}{\partial x} W(t_n, x_i, y_j) + O(\Delta x)^2\,, \qquad W^y_{i,j} \sim \Delta y \frac{\partial}{\partial x} W(t_n, x_i, y_j) + O(\Delta y)^2\,. \tag{7.2.4}$$

A possible computation of these slopes, which results in an overall non-oscillatory schemes is given by (5.2.16) and (5.3.14). This guarantees that the corresponding piecewise-linear reconstruction of $W(t_n, x, y)$ in (7.2.3) is co-monotone with the underlying piecewise-constant approximation, $\sum \overline{W}^n_{i,j}\chi_{i,j}(x, y)$.

Similar to one-dimensional case, the construction of the central scheme proceeds with a second step of an exact evolution. The integration of (7.2.1) over volume $[x_i, x_{i+1}] \times [y_j, y_{j+1}] \times [t_n, t_{n+1}]$ yields

$$\begin{aligned}\overline{W}^{n+1}_{i+\frac{1}{2},j+\frac{1}{2}} = &\fint_{C_{i+\frac{1}{2},j+\frac{1}{2}}} w(t_n, x, y)dxdy \\ &- \lambda\left\{\fint_{t_n}^{t_{n+1}}\int_{y_j}^{y_{j+1}} [F(W(t, x_{i+1}, y)) - F(W(t, x_i, y))]dydt\right\} \\ &- \mu\left\{\fint_{t_n}^{t_{n+1}}\int_{x_i}^{x_{i+1}} [G(W(t, x, y_{j+1})) - G(W(t, x, y_j))]dxdt\right\}.\end{aligned} \tag{7.2.5}$$

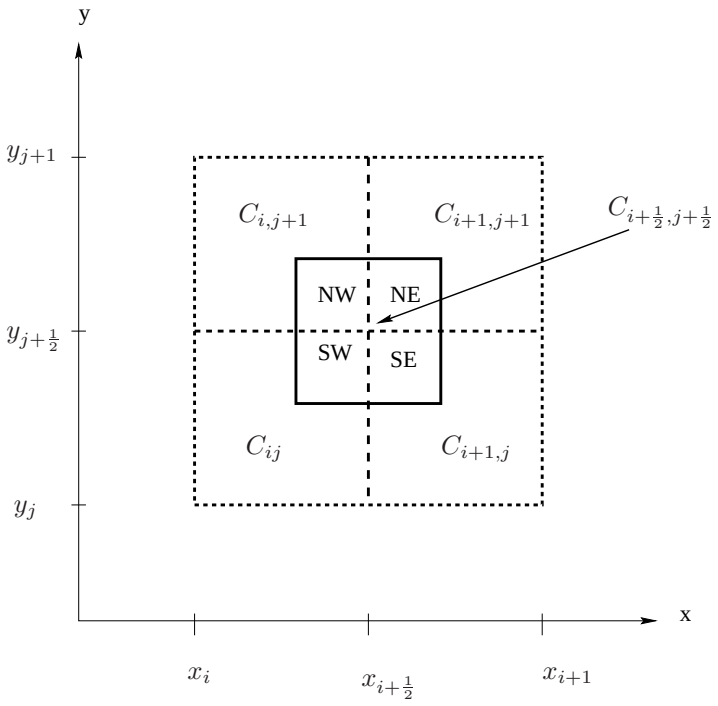

Figure 7.1: Floor plane of the staggered grid.

We begin by evaluating the cell average $\fint_{C_{i+\frac{1}{2},j+\frac{1}{2}}} W(t_n, x, y)dxdy$. As before it has contribution from the four intersecting cells, $C_{i,j}$, $C_{i+1,j}$, $C_{i+1,j+1}$, and $C_{i,j+1}$. Starting with the

intersecting cell $C_{i,j}$ at the corner (see Figure 7.1), $C^{SW}_{i+\frac{1}{2},j+\frac{1}{2}} = C_{i+\frac{1}{2},j+\frac{1}{2}} \cap C_{i,j}$, we find the average of the reconstructed polynomial in (7.2.3),

$$\begin{aligned}\fint_{C^{SW}_{i+\frac{1}{2},j+\frac{1}{2}}} W(t_n,x,y)dxdy &= \int_{x_i}^{x_{i+\frac{1}{2}}}\int_{y_j}^{y_{j+\frac{1}{2}}} \left(\overline{W}^n_{i,j} + W^x_{i,j}\left(\frac{x-x_i}{\Delta x}\right) + W^y_{i,j}\left(\frac{y-y_i}{\Delta y}\right)\right) dxdy \\ &= \frac{1}{4}\overline{W}^n_{i,j} + \frac{1}{16}(W^x_{i,j} + W^y_{i,j})\,. \end{aligned} \tag{7.2.6}$$

Continuing in a counter clockwise direction, we have

$$\fint_{C^{SE}_{i+\frac{1}{2},j+\frac{1}{2}}} W(t_n,x,y)dxdy = \frac{1}{4}\overline{W}^n_{i+1,j} + \frac{1}{16}(-W^x_{i+1,j} + W^y_{i+1,j})\,, \tag{7.2.7}$$

$$\fint_{C^{NE}_{i+\frac{1}{2},j+\frac{1}{2}}} W(t_n,x,y)dxdy = \frac{1}{4}\overline{W}^n_{i+1,j+1} - \frac{1}{16}(W^x_{i+1,j+1} + W^y_{i+1,j+1})\,, \tag{7.2.8}$$

$$\fint_{C^{NW}_{i+\frac{1}{2},j+\frac{1}{2}}} W(t_n,x,y)dxdy = \frac{1}{4}\overline{W}^n_{i,j+1} + \frac{1}{16}(W^x_{i,j+1} - W^y_{i,j+1})\,. \tag{7.2.9}$$

By adding the last four integrals we find that the exact staggered averages of the reconstructed solution at $t = t_n$ are

$$\begin{aligned}\overline{W}^n_{i+\frac{1}{2},j+\frac{1}{2}} =& \fint_{C_{i+\frac{1}{2},j+\frac{1}{2}}} W(t_n,x,y)dxdy \\ =& \frac{1}{4}\left(\overline{W}^n_{i,j} + \overline{W}^n_{i+1,j} + \overline{W}^n_{i,j+1} + \overline{W}^n_{i+1,j+1}\right) \\ &+ \frac{1}{16}\{(W^x_{i,j} - W^x_{i+1,j}) + (W^x_{i,j+1} - W^x_{i+1,j+1}) \\ &+ (W^y_{i,j} - W^y_{i,j+1}) + (W^y_{i+1,j} - W^y_{i+1,j+1})\}\,. \end{aligned} \tag{7.2.10}$$

So far everything is *exact*. We now turn to *approximating* the four fluxes on the right hand side of (7.2.5), starting with the one along the east face (consult Figure 7.2), i.e.

$$\fint_{t_n}^{t_{n+1}} \fint_{y\in J_{j+\frac{1}{2}}} F(W(t,x_{i+1},y))dydt.$$

We use midpoint quadrature rule for second-order approximation of the temporal integral

$$\fint_{y\in J_{j+\frac{1}{2}}} F(W(t_{n+\frac{1}{2}},x_{i+1},y))dy\,,$$

and, for the reasons to be clarified below, we use the second-order trapezium rule for the spatial integration across the y-axis, yielding

$$\fint_{t_n}^{t_{n+1}} \fint_{y\in J_{j+\frac{1}{2}}} F(W(t,x_{i+1},y))dydt \sim \frac{1}{2}\left(F(W^{n+\frac{1}{2}}_{i+1,j}) + F(W^{n+\frac{1}{2}}_{i+1,j+1})\right)\,. \tag{7.2.11}$$

In similar manner we approximate the remaining fluxes,

$$\fint_{t_n}^{t_{n+1}} \int_{x\in I_{i+\frac{1}{2}}} G(W(t,x,y_{j+1}))dxdt \sim \frac{1}{2}\left(G(W_{i,j+1}^{n+\frac{1}{2}}) + G(W_{i+1,j+1}^{n+\frac{1}{2}})\right), \tag{7.2.12}$$

$$\fint_{t_n}^{t_{n+1}} \int_{y\in J_{j+\frac{1}{2}}} F(W(t,x_i,y))dydt \sim \frac{1}{2}\left(F(W_{i,j}^{n+\frac{1}{2}}) + F(W_{i,j+1}^{n+\frac{1}{2}})\right), \tag{7.2.13}$$

$$\fint_{t_n}^{t_{n+1}} \int_{x\in I_{i+\frac{1}{2}}} G(W(t,x,y_j))dxdt \sim \frac{1}{2}\left(G(W_{i,j}^{n+\frac{1}{2}}) + G(W_{i+1,j}^{n+\frac{1}{2}})\right). \tag{7.2.14}$$

The fluxes in (7.2.11)-(7.2.14) use the midpoint values, $W_{i,j}^{n+\frac{1}{2}} = W(t_{n+\frac{1}{2}}, x_i, y_j)$, and it is

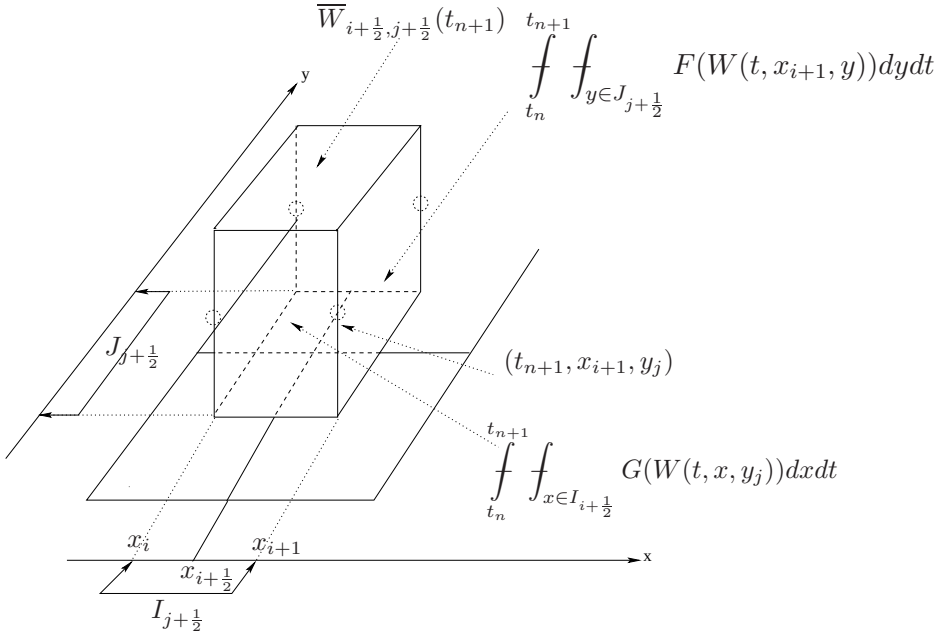

Figure 7.2: The central, staggered stencil.

here that we take advantage of utilizing these midvalues for the spatial integration by the rectangle rule. Namely, since these midvalues are secured at the smooth center of the cells $C_{i,j}$ bounded away from the jump discontinuities along the edges, we may use local Taylor expansion,

$$W(t_{n+\frac{1}{2}}, x_i, y_j) = \overline{W}_{i,j}^n + \frac{\Delta t}{2} W_t(t_n, x_i, y_j) + O(\Delta t)^2 .$$

Finally, we use the differential form of conservation laws (7.2.1) to express the time derivative, W_t, in terms of the spatial derivatives $F(W)_x$ and $G(W)_y$,

$$\begin{aligned} W_{i,j}^{n+\frac{1}{2}} &= \overline{W}_{i,j}^n - \frac{\Delta t}{2}\frac{\partial}{\partial x}F(W_{i,j}) - \frac{\Delta t}{2}\frac{\partial}{\partial y}G(W_{i,j}) + O(\Delta t)^2 \\ &= \overline{W}_{i,j}^n - \frac{\lambda}{2}F^x(W_{i,j}) - \frac{\mu}{2}G^y(W_{i,j}) + O(\Delta t)^2 . \end{aligned} \tag{7.2.15}$$

Here

$$F^x(W_{i,j}) \sim \Delta x \frac{\partial}{\partial x}F(W(t_n,x_i,y_j)) + O(\Delta x)^2, \quad G^y(W_{i,j}) \sim \Delta y \frac{\partial}{\partial y}G(W(t_n,x_i,y_j)) + O(\Delta y)^2 ,$$

are one-dimensional discrete slopes of the fluxes in the x- and y-directions, of the type reconstructed in (7.2.4). We find these slopes in the same way as done for the conservative field variables using the min-mod limiter (5.2.16). Inserting these values, together with the staggered averages computed in (7.2.10), into (7.2.5), we conclude with new staggered averages at $t = t_{n+1}$, given by

$$\begin{aligned}
\overline{W}^{n+1}_{i+\frac{1}{2},j+\frac{1}{2}} =& \frac{1}{4}(\overline{W}^{n}_{i,j} + \overline{W}^{n}_{i+1,j} + \overline{W}^{n}_{i,j+1} + \overline{W}^{n}_{i+1,j+1}) \\
&+ \frac{1}{16}(W^{x}_{i,j} - W^{x}_{i+1,j}) - \frac{\lambda}{2}\left(F(W^{n+\frac{1}{2}}_{i+1,j}) - F(W^{n+\frac{1}{2}}_{i,j})\right) \\
&+ \frac{1}{16}(W^{x}_{i,j+1} - W^{x}_{i+1,j+1}) - \frac{\lambda}{2}\left(F(W^{n+\frac{1}{2}}_{i+1,j+1}) - F(W^{n+\frac{1}{2}}_{i,j+1})\right) \\
&+ \frac{1}{16}(W^{y}_{i,j} - W^{y}_{i,j+1}) - \frac{\mu}{2}\left(G(W^{n+\frac{1}{2}}_{i,j+1}) - G(W^{n+\frac{1}{2}}_{i,j})\right) \\
&+ \frac{1}{16}(W^{y}_{i+1,j} - W^{y}_{i+1,j+1}) - \frac{\mu}{2}\left(G(W^{n+\frac{1}{2}}_{i+1,j+1}) - G(W^{n+\frac{1}{2}}_{i+1,j})\right) . \qquad (7.2.16)
\end{aligned}$$

In summary, we end up with a simple two-step predictor-corrector scheme (7.2.15)-(7.2.16). Starting with the cell averages, $\overline{W}^{n}_{i,j}$, we use the first order predictor (7.2.15) for the evolution of the midpoint values, $\overline{W}^{n+\frac{1}{2}}_{i,j}$, which is followed by the second-order corrector (7.2.16) for computation of the new cell averages, $\overline{W}^{n+1}_{i,j}$. This results in a second-order accurate non-oscillatory central schemes. As in the one-dimensional case no exact (approximate) Riemann solvers are involved. The non-oscillatory behaviour of the scheme hinges on the reconstructed discrete slopes, W^x,W^y, $F^x(W)$, and $G^y(W)$.

7.3 Applications of the Central Schemes

We have applied the central schemes to the relativistic and non-relativistic Euler equations. In Chapter 2 we have used the central schemes in order compare their results with the first order Godunov, kinetic and KFVS schemes. In Chapter 4 we have used the central schemes to compare their results with with the first and second order kinetic and Godunov schemes for the ultra-relativistic Euler equations. In Chapter 5 we have also compared the central schemes to the first and second order KFVS and BGK-type KFVS schemes for the ultra-relativistic Euler equations. In Chapter 6 we have applied the central schemes to the general and phenomenological form of special relativistic Euler equations.

We found that the computer implementation of the central schemes is very simple and the computer codes for them are very compact. The schemes are found to be at least two times faster than the Godunov schemes. The first order central schemes give smeared solutions at the contact discontinuities as compared to the Godunov, kinetic and KFVS schemes. However the second order central schemes resolve the contact discontinuity quite well. The main advantage of the schemes is that they do not need any exact or approximate Riemann solver. In these schemes the cells in each step are staggered with respect to those in the previous step.

Appendix A

Weak Form of the One-Dimensional Transport Equation

Here we consider a one-dimensional spatial flow such that the fields n, u, T are only depending on the space x and time t. Let $\Omega \subset \mathbb{R}^+ \times \mathbb{R}$ be a normal region in space-time with piecewise smooth positively oriented boundary. The one-dimensional differential form the transport equation is given by

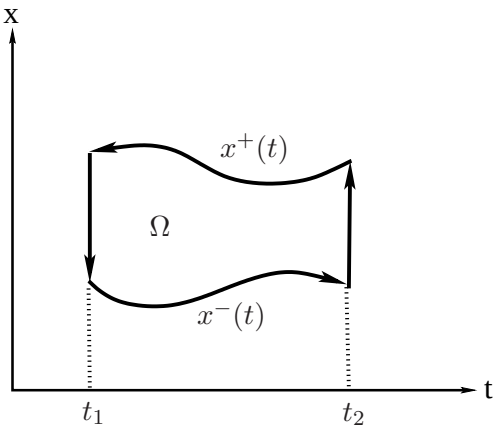

Normal region Ω in space-time

$$q^0 \frac{\partial f}{\partial t} + q^1 \frac{\partial f}{\partial x} = 0\,. \tag{A.0.1}$$

The differential equation (A.0.1) is not sufficient if we take discontinuities into account. Therefore we need a weak integral formulation of the above differential form of the transport equation. If we apply the Gaussian divergence theorem to (A.0.1), we get the following weak formulation due to Oleinik [68] of the transport equation

$$\oint_{\partial\Omega} q^0 f dx - q^1 f dt = 0\,. \tag{A.0.2}$$

In following we prove that this weak form of the transport equation is zero over the closed domain as shown in the figure above. Let us define for abbreviation

$$A = A(t,x) = q^0 f(t,x,\mathbf{q})\,, \quad B(t,x,\mathbf{q}) = q^1 f(t,x,\mathbf{q})\,,$$

then the weak form (A.0.2) becomes

$$\oint_{\partial\Omega} A dx - B dt = 0\,. \tag{A.0.3}$$

Now evaluating the curve integrals we get

$$\oint\limits_{\partial\Omega} A dx - B dt = \int\limits_{t_1}^{t_2} \left[A(t, x^-(t))\dot{x}^-(t) - B(t, x^-(t))\right] dt + \int\limits_{x^-(t_2)}^{x^+(t_2)} A(t_2, x) dx$$
$$+ \int\limits_{t_2}^{t_1} \left[A(t, x^+(t))\dot{x}^+(t) - B(t, x^+(t))\right] dt + \int\limits_{x^+(t_1)}^{x^-(t_1)} A(t_1, x) dx\,. \tag{A.0.4}$$

Let $f_*(y, \mathbf{q}),\ y \in \mathbb{R},\ \mathbf{q} \in \mathbb{R}^3$, not necessarily differentiable, be the initial phase density. Then the solution of the linear transport equation (A.0.1) is

$$f(t, x, \mathbf{q}) = f_*(x - t\frac{q^1}{q^0}, \mathbf{q})\,. \tag{A.0.5}$$

Let us define

$$J_1 := \int\limits_{t_1}^{t_2} f_* \left(x^-(t) - \frac{q^1}{q^0}\right) \left(q^0\dot{x}^-(t) - q^1\right) dt\,, \tag{A.0.6}$$

$$J_2 := q^0 \int\limits_{x^-(t_2)}^{x^+(t_2)} f_* \left(x^-(t) - \frac{q^1}{q^0}\right) dx\,, \tag{A.0.7}$$

$$J_3 := \int\limits_{t_1}^{t_2} f_* \left(x^+(t) - \frac{q^1}{q^0}\right) \left(q^0\dot{x}^+(t) - q^1\right) dt\,, \tag{A.0.8}$$

$$J_4 := q^0 \int\limits_{x^-(t_1)}^{x^+(t_1)} f_* \left(x^-(t) - \frac{q^1}{q^0}\right) dx\,. \tag{A.0.9}$$

Therefore equation (A.0.4) becomes

$$\oint\limits_{\partial\Omega} A dx - B dt = J_1 + J_2 + J_3 + J_4\,. \tag{A.0.10}$$

Our aim is to show that $J_1 + J_2 + J_3 + J_4 = 0$. Let us define for abbreviation

$$y^-(t) = x^-(t) - \frac{q^1}{q^0}\,, \quad y^+(t) = x^+(t) - \frac{q^1}{q^0}\,, \tag{A.0.11}$$

then we can calculate J_1, J_2, J_3, J_4 as follows

$$J_1 = q^0 \int\limits_{t_1}^{t_2} f_* \left(y^-(t), \mathbf{q}\right) \dot{y}^-(t) dt$$
$$= q^0 \int\limits_{t_1}^{t_2} \frac{d}{dt} \left(\int\limits_{y^-(t_1)}^{y^-(t)} f_* \left(y, \mathbf{q}\right) dy \right) dt = q^0 \int\limits_{y^-(t_1)}^{y^-(t_2)} f_* \left(y, \mathbf{q}\right) dy\,. \tag{A.0.12}$$

By a similar calculations we can obtain

$$J_3 = q^0 \int_{y^+(t_2)}^{y^+(t_1)} f_* (y, \mathbf{q})\, dy\,. \tag{A.0.13}$$

In order to calculate J_2 and J_4 we use the substitution $y := x - \frac{q^1}{q^0}$. We obtain

$$J_2 = q^0 \int_{y^-(t_2)}^{y^+(t_2)} f_* (y, \mathbf{q})\, dy \quad J_4 = q^0 \int_{y^+(t_1)}^{y^-(t_1)} f_* (y, \mathbf{q})\, dy\,. \tag{A.0.14}$$

This implies

$$\begin{aligned}
\oint_{\partial\Omega} A dx - B dt =& J_1 + J_2 + J_3 + J_4 \\
=& q^0 \left(\int_{y^-(t_1)}^{y^-(t_2)} f_* dy + \int_{y^-(t_2)}^{y^+(t_2)} f_* dy + \int_{y^+(t_2)}^{y^+(t_1)} f_* dy + \int_{y^+(t_1)}^{y^-(t_1)} f_* dy \right) \\
=& q^0 \left(\int_{y^-(t_1)}^{y^+(t_2)} f_* dy + \int_{y^+(t_2)}^{y^-(t_1)} f_* dy \right) \\
=& 0\,.
\end{aligned}$$

Appendix B

The Lorentz Invariance of $\frac{d^3q}{q^0}$

Let $\Re$ be any arbitrary Lorentz frame, with respect to which we want to study a gas particles. Let $\Re'$ be any other reference frame which moves with velocity $\mathbf{v}$ with respect to $\Re$. For the reasons of simplicity we choose $\mathbf{v}$ parallel to $\mathbf{q}$, the momentum of the particle within the volume element $d^3x d^3q$ on which we are focusing our attention. Furthermore, we choose the $x-axes$ of $\Re$ and $\Re'$ both parallel to $\mathbf{v}$.

Because changes occur only in the $x-$direction, the $y-$ and $z-$components of position $\mathbf{x}$ and momentum $\mathbf{q}$ variables remain unchanged under the Lorentz-transformations relating the reference systems $\Re$ and $\Re'$. If we suppose, for a moment, that q^0, on the one hand, and q^1, q^2, q^3 on the other hand, are independent variables, we have:

$$\begin{aligned} q'^0 &= \gamma(v)\left(q^0 - c^{-1}vq^1\right), \\ q'^1 &= \gamma(v)\left(q^1 - c^{-1}vq^0\right), \\ q'^2 &= q^2, \quad q'^3 = q^3, \end{aligned} \tag{B.0.1}$$

where $\gamma(v) = \frac{1}{\sqrt{1-\mathbf{v}^2/c^2}}$. The inverse transformation of (B.0.1) can be written as

$$\begin{aligned} q^0 &= \gamma(v)\left(q'^0 + c^{-1}vq'^1\right), \\ q^1 &= \gamma(v)\left(q'^1 + c^{-1}vq'^0\right), \\ q^2 &= q'^3, \quad q^3 = q'^3. \end{aligned} \tag{B.0.2}$$

However, q^0 and $\mathbf{q}$ are not independent. From the normalization of the four-momentum $q^\mu q_\mu = m^2c^2$ we find:

$$\begin{aligned} q^0 &= \sqrt{m^2c^2 + (q^1)^2 + (q^2)^2 + (q^3)^2}, \\ q'^0 &= \sqrt{m^2c^2 + \left(q'^1\right)^2 + \left(q'^2\right)^2 + \left(q'^3\right)^2}. \end{aligned} \tag{B.0.3}$$

Since d^3q is a volume element, according to the transformation of coordinates rule

$$d^3q = \left|\frac{\partial(q^1, q^2, q^3)}{\partial(q'^1, q'^2, q'^3)}\right| d^3q', \tag{B.0.4}$$

where $J = \left|\frac{\partial(q^1,\, q^2,\, q^3)}{\partial(q'^1,\, q'^2,\, q'^3)}\right|$ is the Jacobian determinant. Now using (B.0.2) we get

$$\frac{\partial q^1}{\partial q'^1} = \gamma(v)\left(1 + c^{-1}v\frac{q'^1}{q'^0}\right) = \frac{\gamma(v)}{q'^0}\left(q'^0 + c^{-1}vq'^1\right) = \frac{q^0}{q'^0}\,,$$
$$\frac{\partial q^1}{\partial q'^2} = \gamma(v)\left(c^{-1}v\frac{q'^2}{q'^0}\right), \quad \frac{\partial q^1}{\partial q'^3} = \gamma(v)\left(c^{-1}v\frac{q'^3}{q'^0}\right),$$
$$\frac{\partial q^2}{\partial q'^1} = 0\,, \quad \frac{\partial q^2}{\partial q'^2} = 1, \quad \frac{\partial q^2}{\partial q'^3} = 0\,, \qquad \frac{\partial q^3}{\partial q'^1} = 0\,, \quad \frac{\partial q^3}{\partial q'^2} = 0, \quad \frac{\partial q^3}{\partial q'^3} = 1\,.$$

Thus

$$J = \begin{vmatrix} \frac{q^0}{q'^0} & \gamma(v)\frac{vq'^2}{cq'^0} & \gamma(v)\frac{vq'^3}{cq'^0} \\ 0 & 1 & 0 \\ 0 & 0 & 1 \end{vmatrix} = \frac{q^0}{q'^0}\,. \tag{B.0.5}$$

Then (B.0.4) implies the well-known result

$$\frac{d^3q'}{q'^0} = \frac{d^3q}{q^0}\,. \tag{B.0.6}$$

Appendix C

Euler Equations and Second Order Kinetic Schemes

In the following we explain the derivation of some equations used in Sections 4.5.2 and 4.6.1 in order to get second order accuracy in the one- and two-dimensional kinetic schemes for the ultra-relativistic Euler equations.

C.1 One-Dimensional Case

In order to write the time derivatives of the fields n, u and p in term of the spatial derivatives, we use the Euler equations (4.5.8). These Euler equations after expanding the time and spatial derivatives gives

$$\begin{aligned}
\sqrt{1+u^2}\frac{\partial n}{\partial t} + \frac{nu}{\sqrt{1+u^2}}\frac{\partial u}{\partial t} &= -u\frac{\partial n}{\partial x} - n\frac{\partial u}{\partial x}\,, \\
4u\sqrt{1+u^2}\frac{\partial p}{\partial t} + 4p\frac{(1+2u^2)}{\sqrt{1+u^2}}\frac{\partial u}{\partial t} &= -(1+4u^2)\frac{\partial p}{\partial x} - 8pu\frac{\partial u}{\partial x}\,, \\
(3+4u^2)\frac{\partial p}{\partial t} + 8pu\frac{\partial u}{\partial t} &= -4u\sqrt{1+u^2}\frac{\partial p}{\partial x} - 4p\frac{(1+2u^2)}{\sqrt{1+u^2}}\frac{\partial u}{\partial x}\,.
\end{aligned} \tag{C.1.1}$$

These are three equations for three unknowns $\frac{\partial n}{\partial t}$, $\frac{\partial u}{\partial t}$ and $\frac{\partial p}{\partial t}$. After solving these equations we get

$$\begin{aligned}
\frac{\partial u}{\partial t} &= \frac{-3\sqrt{1+u^2}}{4p(3+2u^2)}\frac{\partial p}{\partial x} - \frac{-2u\sqrt{1+u^2}}{3+2u^2}\frac{\partial u}{\partial x}\,, \\
\frac{\partial p}{\partial t} &= \frac{-2u\sqrt{1+u^2}}{3+2u^2}\frac{\partial p}{\partial x} - \frac{4p}{(3+2u^2)\sqrt{1+u^2}}\frac{\partial u}{\partial x}\,, \\
\frac{\partial n}{\partial t} &= \frac{3n}{(3+2u^2)\sqrt{1+u^2}}\left(\frac{u}{4p}\frac{\partial p}{\partial x} - \frac{\partial u}{\partial x}\right) - \frac{u}{\sqrt{1+u^2}}\frac{\partial n}{\partial x}\,.
\end{aligned} \tag{C.1.2}$$

Using the equations (4.5.9) we can write

$$\begin{aligned}\frac{\partial N^1}{\partial t} &= \frac{\partial}{\partial t}(nu) = u\frac{\partial n}{\partial t} + n\frac{\partial u}{\partial t}\,,\\ \frac{\partial T^{11}}{\partial t} &= \frac{\partial}{\partial t}\left(p(1+4u^2)\right) = (1+4u^2)\frac{\partial p}{\partial t} + 8pu\frac{\partial u}{\partial t}\,.\end{aligned} \tag{C.1.3}$$

Now using (C.1.2) in (C.1.3) we finally get after simplifications

$$\begin{aligned}\frac{\partial N^1}{\partial t} &= -\frac{3n}{4p\sqrt{1+u^2}(3+2u^2)}\frac{\partial p}{\partial x} - \frac{(5nu+2nu^3)}{\sqrt{1+u^2}(3+2u^2)}\frac{\partial u}{\partial x} - \frac{u^2}{\sqrt{1+u^2}}\frac{\partial n}{\partial x}\,,\\ \frac{\partial T^{11}}{\partial t} &= -\frac{8u(1+u^2)^{3/2}}{3+2u^2}\frac{\partial p}{\partial x} - \frac{4p(1+8u^2+4u^4)}{\sqrt{1+u^2}(3+2u^2)}\frac{\partial u}{\partial x}\,.\end{aligned} \tag{C.1.4}$$

Next we want to calculate the second terms of order Δt^2 appearing on the right hand sides of (4.5.17). For this purpose we use the definitions (4.5.14) and reduced equilibrium phase densities (4.5.2), we get

$$\begin{aligned}\int_{-1}^{1}\xi^2\phi(x,\xi)d\xi &= n\sqrt{1+u^2}\,\frac{(u^2-1)}{u^2} + \frac{n}{u^3}\,\mathrm{arcsinh}(u)\,,\\ \int_{-1}^{1}\xi^3\psi(x,\xi)d\xi &= \frac{p\sqrt{1+u^2}}{u^3}\left(4u^4-2u^2+3\right) + \frac{3p}{u^4}\,\mathrm{arcsinh}(-u)\,,\end{aligned} \tag{C.1.5}$$

which on differentiating with respect to x gives

$$\begin{aligned}\frac{\partial}{\partial x}\int_{-1}^{1}\xi^2\phi(x,\xi)d\xi &= \left[\frac{(u^2-1)}{u^2}\sqrt{1+u^2} + \frac{1}{u^3}\,\mathrm{arcsinh}(u)\right]\frac{\partial n}{\partial x}\\ &\quad + n\left[\frac{u^4+u^2+3}{u^3\sqrt{1+u^2}} - \frac{3}{u^4}\,\mathrm{arcsinh}(u)\right]\frac{\partial u}{\partial x}\,,\end{aligned} \tag{C.1.6}$$

$$\begin{aligned}\frac{\partial}{\partial x}\int_{-1}^{1}\xi^3\psi(x,\xi)d\xi &= \left[\frac{(4u^4-2u^2+3)}{u^3}\sqrt{1+u^2} + \frac{3}{u^4}\,\mathrm{arcsinh}(-u)\right]\frac{\partial p}{\partial x}\\ &\quad + p\left[\frac{8u^6+4u^4-4u^2-12}{u^4\sqrt{1+u^2}} - \frac{12}{u^5}\,\mathrm{arcsinh}(-u)\right]\frac{\partial u}{\partial x}\,.\end{aligned} \tag{C.1.7}$$

By using the relations (C.1.4), (C.1.6) and (C.1.7), we obtain after simplification

$$\begin{aligned} g(n,u,p) =& \frac{\partial N^1}{\partial t}(t_n,x) + \frac{\partial}{\partial x}\int_{-1}^{1}\xi^2\phi d\xi \\ =& \left(-\frac{(1+u^2)^{-1/2}}{u^2} + \frac{1}{u^3}\operatorname{arcsinh}(u)\right)\frac{\partial n}{\partial x} - \frac{3n(1+u^2)^{-1/2}}{4p(3+2u^2)}\frac{\partial p}{\partial x} \\ &+ \left(\frac{9n\sqrt{1+u^2}}{u^3(3+2u^2)} - \frac{3n}{u^4}\operatorname{arcsinh}(u)\right)\frac{\partial u}{\partial x}, \end{aligned} \tag{C.1.8}$$

$$\begin{aligned} h(u,p) =& \frac{\partial T^{11}}{\partial t}(t_n,x) + \frac{\partial}{\partial x}\int_{-1}^{1}\xi^3\psi d\xi \\ =& \left(\frac{9\sqrt{1+u^2}}{u^4(3+2u^2)} + \frac{3\operatorname{arcsinh}(-u)}{u^5}\right)\left(u\frac{\partial p}{\partial x} - 4p\frac{\partial u}{\partial x}\right). \end{aligned} \tag{C.1.9}$$

The equations (C.1.8) and (C.1.9) are appearing in the order Δt^2 terms of $(4.5.17)_{1,2}$.

C.2 Two-Dimensional Case

Like in the one-dimensional case, here we also need the time derivatives of the fields n, u_1, u_2 and p in terms of the spatial derivatives. For this purpose we use the two-dimensional ultra-relativistic Euler equations (5.3.1). Let us define for abbreviation $\mathbf{u}^2 = (u_1^2 + u_2^2)$. We obtain

$$\begin{aligned} \frac{\partial u_1}{\partial t} =& -\frac{3+3u_1^2+2u_2^2}{4p\sqrt{1+\mathbf{u}^2}(3+2\mathbf{u}^2)}\frac{\partial p}{\partial x} - \frac{u_1u_2}{4p\sqrt{1+\mathbf{u}^2}(3+2\mathbf{u}^2)}\frac{\partial p}{\partial y} \\ &- \frac{u_1(2+2u_1^2+u_2^2)}{\sqrt{1+\mathbf{u}^2}(3+2\mathbf{u}^2)}\frac{\partial u_1}{\partial x} + \frac{u_1(1+u_1^2)}{\sqrt{1+\mathbf{u}^2}(3+2\mathbf{u}^2)}\frac{\partial u_2}{\partial y} \\ &- \frac{u_2(3+3u_1^2+2u_2^2)}{\sqrt{1+\mathbf{u}^2}(3+2\mathbf{u}^2)}\frac{\partial u_1}{\partial y} - \frac{u_1^2u_2}{\sqrt{1+\mathbf{u}^2}(3+2\mathbf{u}^2)}\frac{\partial u_2}{\partial x}, \end{aligned} \tag{C.2.1}$$

$$\begin{aligned} \frac{\partial u_2}{\partial t} =& -\frac{u_1u_2}{4p\sqrt{1+\mathbf{u}^2}(3+2\mathbf{u}^2)}\frac{\partial p}{\partial x} - \frac{3+2u_1^2+3u_2^2}{4p\sqrt{1+\mathbf{u}^2}(3+2\mathbf{u}^2)}\frac{\partial p}{\partial y} \\ &+ \frac{u_2(1+u_2^2)}{\sqrt{1+\mathbf{u}^2}(3+2\mathbf{u}^2)}\frac{\partial u_1}{\partial x} - \frac{u_2(2+u_1^2+2u_2^2)}{\sqrt{1+\mathbf{u}^2}(3+2\mathbf{u}^2)}\frac{\partial u_2}{\partial y} \\ &- \frac{u_1u_2^2}{\sqrt{1+\mathbf{u}^2}(3+2\mathbf{u}^2)}\frac{\partial u_1}{\partial y} - \frac{u_1(3+2u_1^2+3u_2^2)}{\sqrt{1+\mathbf{u}^2}(3+2\mathbf{u}^2)}\frac{\partial u_2}{\partial x}, \end{aligned} \tag{C.2.2}$$

$$\frac{\partial p}{\partial t} = -\frac{2\sqrt{1+\mathbf{u}^2}}{3+2\mathbf{u}^2}\left(u_1\frac{\partial p}{\partial x}+u_2\frac{\partial p}{\partial y}\right)-\frac{4p}{\sqrt{1+\mathbf{u}^2}(3+2\mathbf{u}^2)}\left((1+u_2^2)\frac{\partial u_1}{\partial x}+(1+u_1^2)\frac{\partial u_2}{\partial y}\right)$$
$$+\frac{4pu_1u_2}{\sqrt{1+\mathbf{u}^2}(3+2\mathbf{u}^2)}\left(\frac{\partial u_1}{\partial y}+\frac{\partial u_2}{\partial x}\right), \tag{C.2.3}$$

$$\frac{\partial n}{\partial t} = -\frac{1}{\sqrt{1+\mathbf{u}^2}}\left(u_1\frac{\partial n}{\partial x}+u_2\frac{\partial n}{\partial y}\right)+\frac{3nu_1u_2}{\sqrt{1+\mathbf{u}^2}(3+2\mathbf{u}^2)}\left(\frac{\partial u_1}{\partial y}+\frac{\partial u_2}{\partial x}\right) \tag{C.2.4}$$
$$+\frac{3n}{\sqrt{1+\mathbf{u}^2}(3+2\mathbf{u}^2)}\left[\frac{1}{4p}\left(u_1\frac{\partial p}{\partial x}+u_2\frac{\partial p}{\partial y}\right)-\left((1+u_2^2)\frac{\partial u_1}{\partial x}+(1+u_1^2)\frac{\partial u_2}{\partial y}\right)\right].$$

The coefficients on the right hand side of the equations (4.6.8) are

$$Q_{nx}=\frac{w^1\sqrt{1+\mathbf{u}^2}-u_1}{n\sqrt{1+\mathbf{u}^2}}, \quad Q_{ny}=\frac{w^2\sqrt{1+\mathbf{u}^2}-u_2}{n\sqrt{1+\mathbf{u}^2}}, \tag{C.2.5}$$

$$Q_{px}=\frac{-3(3+3u_1^2+2u_2^2)(w^1\sqrt{1+\mathbf{u}^2}-u_1)-3u_1u_2(w^2\sqrt{1+u^2}-u_2)}{4p(3+2\mathbf{u}^2)(1+\mathbf{u}^2)(\sqrt{1+\mathbf{u}^2}-w^1u_1-w^2u_2)}$$
$$+\frac{3u_1}{4p\sqrt{1+\mathbf{u}^2}(3+2\mathbf{u}^2)}, \tag{C.2.6}$$

$$Q_{py}=\frac{-3(3+2u_1^2+3u_2^2)(w^2\sqrt{1+\mathbf{u}^2}-u_2)-3u_1u_2(w^1\sqrt{1+u^2}-u_1)}{4p(3+2\mathbf{u}^2)(1+\mathbf{u}^2)(\sqrt{1+\mathbf{u}^2}-w^1u_1-w^2u_2)}$$
$$+\frac{3u_2}{4p\sqrt{1+\mathbf{u}^2}(3+2\mathbf{u}^2)}, \tag{C.2.7}$$

$$Q_{u1x}=\frac{-3(1+u_2^2)}{\sqrt{1+\mathbf{u}^2}(3+2\mathbf{u}^2)}+3\frac{(w^1\sqrt{1+\mathbf{u}^2}(3+2\mathbf{u}^2)-u_1(2+2u_1^2+u_2^2))(w^1\sqrt{1+\mathbf{u}^2}-u_1)}{(3+2\mathbf{u}^2)(1+\mathbf{u}^2)(\sqrt{1+\mathbf{u}^2}-w^1u_1-w^2u_2)}$$
$$+\frac{3u_2(1+u_2^2)(w^2\sqrt{1+\mathbf{u}^2}-u_2)}{(3+2\mathbf{u}^2)(1+\mathbf{u}^2)(\sqrt{1+\mathbf{u}^2}-w^1u_1-w^2u_2)}, \tag{C.2.8}$$

$$Q_{u1y}=Q_{u2x}=\frac{12u_1u_2}{\sqrt{1+\mathbf{u}^2}(3+2\mathbf{u}^2)}+\frac{3w^1w^2}{(\sqrt{1+\mathbf{u}^2}-w^1u_1-w^2u_2)}$$
$$-\frac{3(w^1u_2(3+2u_2^2)+w^2u_1(3+2u_1^2))}{\sqrt{1+\mathbf{u}^2}(3+2\mathbf{u}^2)(\sqrt{1+\mathbf{u}^2}-w^1u_1-w^2u_2)}, \tag{C.2.9}$$

$$Q_{u2y}=\frac{-3(1+u_1^2)}{\sqrt{1+\mathbf{u}^2}(3+2\mathbf{u}^2)}+3\frac{(w^2\sqrt{1+\mathbf{u}^2}(3+2\mathbf{u}^2)-u_2(2+u_1^2+2u_2^2))(w^2\sqrt{1+\mathbf{u}^2}-u_2)}{(3+2\mathbf{u}^2)(1+\mathbf{u}^2)(\sqrt{1+\mathbf{u}^2}-w^1u_1-w^2u_2)}$$
$$+\frac{3u_1(1+u_1^2)(w^1\sqrt{1+\mathbf{u}^2}-u_1)}{(3+2\mathbf{u}^2)(1+\mathbf{u}^2)(\sqrt{1+\mathbf{u}^2}-w^1u_1-w^2u_2)}, \tag{C.2.10}$$

$$M_{px} = \frac{-(3+3u_1^2+2u_2^2)(w^1\sqrt{1+\mathbf{u}^2}-u_1) - u_1u_2(w^2\sqrt{1+\mathbf{u}^2}-u_2)}{p(1+\mathbf{u}^2)(3+2\mathbf{u}^2)(\sqrt{1+\mathbf{u}^2}-w^1u_1-w^2u_2)} + \frac{w^1(3+2\mathbf{u}^2)-2u_1\sqrt{1+\mathbf{u}^2}}{p(3+2\mathbf{u}^2)}\,, \tag{C.2.11}$$

$$M_{py} = \frac{-(3+2u_1^2+3u_2^2)(w^2\sqrt{1+\mathbf{u}^2}-u_2) - u_1u_2(w^1\sqrt{1+\mathbf{u}^2}-u_1)}{p(1+\mathbf{u}^2)(3+2\mathbf{u}^2)(\sqrt{1+\mathbf{u}^2}-w^1u_1-w^2u_2)} + \frac{w^2(3+2\mathbf{u}^2)-2u_2\sqrt{1+\mathbf{u}^2}}{p(3+2\mathbf{u}^2)}\,, \tag{C.2.12}$$

$$M_{u1x} = \frac{4}{3}Q_{u1x}\,, \quad M_{u2y} = \frac{4}{3}Q_{u2y}\,, \quad M_{u2x} = \frac{4}{3}Q_{u2x}\,, \quad M_{u1y} = \frac{4}{3}Q_{u1y}\,. \tag{C.2.13}$$

Bibliography

[1] M.A. Aloy, J.M^{a} Ibáñez, J.M^{a} Martí, E. Müller, "GENESIS: A high-resolution code for 3D relativistic hydrodynamics", *Astrophysics. J.* **122**, (1999), pp. 151-166.

[2] F. Bereux, L. Sainsaulieu, "A Roe-type Riemann solver for hyperbolic systems with relaxation based on time-dependent wave decomposition", *Numer. Math* **77**, (1997), pp. 143-185.

[3] P.L. Bhatnagar, E.P. Gross, M. Krook, "A model for collision processes in gases. I. Small amplitude processes in charged and neutral one-component systems", *Phys. Rev.* **94**, (1954), pp. 511-525.

[4] Chakravarthy, R. Sukumar, Osher, "High resolution applications of the Osher upwind scheme for the Euler equations", *Sixth AIAA computational fluid Dynamics conference-collection of technical papers*, (1983), pp. 363-372.

[5] C. Cercignani, "The Boltzmann equation and its applications", *Applied Mathematical Sciences* **67**, Springer Verlag, New York (1988).

[6] C. Cercignani, R. Illner, M. Pulvirenti, "Mathematical theory of dilute gases", *Applied Mathematical Sciences* **106**, Springer Verlag, New York (1994).

[7] N.A. Chernikov, "Equilibrium distribution of the relativistic gas" *Acta Phys. Pol.* **26**, (1964), pp. 1069-1092.

[8] N.A. Chernikov, "Microscopic foundation of relativistic hydrodynamics", *Acta Phys. Pol.* **27**, (1964), pp. 465-489.

[9] R. Courant, K.V. Friedrichs, "Supersonic flow and shock waves", Wiley -Intersciences, New York, (1948).

[10] R. Courant, E. Isaacson, and M. Rees, "On the solution of nonlinear hyperbolic differential equations by finite differences", *Comm. Pure. Appl. Math.* **5**, (1952), pp. 243-255.

[11] C.M. Dafermos, "Entropy and the stability of classical solutions of hyperbolic systems of conservation laws", *Recent Mathematical Methods in Nonlinear Wave Propagation,* Montecatini terme, editor T. Ruggeri, (1994), pp. 48-69.

[12] S. M. Deshpande, R. Raul, "Kinetic theory based fluid-in-cell method for Eulerian fluid dynamics", Rep. 82 FM 14, Department of Aerospace Engineering, Indian Institute of Science (Bangalore, India), (1982).

[13] S. M. Deshpande, "A second order accurate, kinetic-theory based, method for inviscid compressible flows", NASA Langley Tech. paper No. 2613, (1986).

[14] S. M. Deshpande, S. Sekar, S. Nagaratinam, M. Krishnamurthy, R. Sinha and P.S. Kulkarni, "A 3-dimensional upwind Euler solver using kinetic flux vector splitting method", *In the 3rd International Conference on Numerical Methods in Fluid Dynamics*, Lecture Notes in Physics, Springer-Verlag **414**, (1992), pp. 105-109.

[15] S. M. Deshpande, "Kinetic flux splitting schemes", *In Computational Fluid Dynamics Review 1995, (Edited by M. Hafez and K. Oshima)*, John Wiley & Sons, (1995).

[16] S. M. Deshpande and P.S. Kulkarni, "New developments in kinetic schemes", *Computer math. Applic.* **35**, (1998), pp. 75-93.

[17] W. Dreyer, M. Kunik, K. Sabelfeld, N. Simonov, K. Wilmański, "Iterative procedure for multidimensional Euler equations", *Monte Carlo Methods and Appl.* **4**, (1998), pp. 253-271.

[18] W. Dreyer and M. Kunik, "The maximum entropy principle revisited", *Cont. Mech. Thermodyn.* **10**, (1998), pp. 331-347.

[19] W. Dreyer and M. Kunik, "Reflections of Eulerian shock waves at moving adiabatic boundaries", *Monte Carlo Methods and Appl.* **4**, (1998), pp. 231-252.

[20] W. Dreyer and M. Kunik, "Initial and boundary value problems of hyperbolic heat conduction", *Cont. Mech. Thermodyn.* **11**.**4**, (1999), pp. 227-245.

[21] W. Dreyer, M. Herrmann and M. Kunik, "Kinetic schemes and initial boundary value problems for the Euler system", *WIAS-Preprint* No. **607**, Berlin (2000).

[22] W. Dreyer, M. Junk and M. Kunik, "On the approximation of the Fokker-Planck equation by moment systems", *Nonlinearity* **14**, (2001), pp. 881-906.

[23] C. Eckart, "The thermodynamics of irreversible process I: The simple fluid", *Phys. Rev.* **58**, (1940), pp. 267-269.

[24] C. Eckart, "The thermodynamics of irreversible process II: Fluid mixtures", *Phys. Rev.* **58**, (1940), pp. 269-275.

[25] C. Eckart, "The thermodynamics of irreversible process III: Relativistic theory of the simple fluid", *Phys. Rev.* **58**, (1940), pp. 919-928.

[26] B. Einfeldt, "On Godunov-type methods for gas dynamics", *SIAM J. Numer.Anal* **25**, (1988), pp. 294-318.

[27] M. Fey, "Multidimensional upwinding part I: The method of transport for solving the Euler equations", *J. Comp. Phys.* **143**, (1998), pp. 159-180.

[28] M. Fey, "Multidimensional upwinding part II: Decomposition of the Euler equations into advection equations", *J. Comp. Phys.* **143**, (1998), pp. 181-199.

[29] K.O. Friedrichs and P.D. Lax, "Systems of conservation equations with a convex extension", *Proc. Acad. Sci. USA* **68**, (1971), pp. 16-86.

[30] J. Glimm, "Solution in the large for nonlinear hyperbolic systems of equations", *Comm. Pure. Appl. Math.* **18**, (1965), pp. 697-715.

[31] J. Gressier and J.M. Moschetta, "On the pathological behaviour of upwind schemes", AIAA 98-0110, (1998).

[32] S.R. deGroot, W.A. van Leeuven and Ch.G. van Weert, "Relativistic kinetic theory. Principles and applications", North Holland, Amsterdam (1980).

[33] E. Godlewski, P.A. Raviart, "Numerical approximation of hyperbolic systems of conservation laws", *Applied Mathematical Sciences* **118**, Springer-Verlag, New York (1996).

[34] S.K. Godunov, "A finite difference method for the computation of discontinuous solutions of the equations of fluid dynamics", *Mat. Sb.* **47**, (1959), pp. 357-393.

[35] A. Harten, "High resolution schemes for hyperbolic conservation laws", *J. Comput. Phys.* **49**, (1983), pp. 357-393.

[36] A. Harten, P.D. Lax, and B. Van Leer, "On upstream differencing and Godunov-type schemes for hyperbolic conservation laws", *SIAM Review* **25**, (1983), pp. 35-62.

[37] J.F. Hawley, L.L. Smarr, J.R. Wilson, "A numerical study of nonspherical balck hole accretion. I. Equations and test problems", *The Astrophysical Journal* **277**, (1984), pp. 296-311.

[38] W. Israel, "Nonstationary irreversible thermodynamics: a causal relativistic theory", *Ann. Phys.* (N.Y.) **100**, (1976), pp. 310-331.

[39] G.-S. Jiang , E. Tadmor, "non-oscillatory central schemes for multidimensional hyperbolic conservation laws", *SIAM J. Sci. Comput.* **19**, (1998), pp. 1892-1917.

[40] A. Jeffrey, "Hand book of mathematical formulas and integrals", Academic Press, (1995).

[41] F. Jüttner, "Das Maxwellsche gesetz der geschwindigkeitsverteilung in der relativtheorie", *Ann. Phys.* (Leipzig), **34**, (1911), pp. 856-882.

[42] F. Jüttner, "Die Relativistische quantentheorie des idealen gases", *Z. Phys.* **47**, (1928) pp. 542-566.

[43] A. Königl, "Relativistic gasdynamics in two dimensions", Physics of Fluids **23**, (1980), pp. 1083-1090.

[44] T. Kröger, S. Noelle and S. Zimmermann, "On the connection between some Riemann-solver free approaches to the approximation of multi-dimensional systems of hyperbolic conservation laws", *Conservation Laws Preprint Server*, preprint Nr. 060, (2003).

[45] M. Kunik, S. Qamar and G. Warnecke, "Kinetic schemes for the ultra-relativistic Euler equations", Preprint Nr. **21**, Otto-von-Guericke University, (2001), accepted in *Journal of Computational Physics*.

[46] M. Kunik, S. Qamar and G. Warnecke, "Kinetic schemes for the relativistic gas dynamics", Preprint Nr. **21**, Otto-von-Guericke University, (2002).

[47] M. Kunik, S. Qamar and G. Warnecke, "A BGK-type kinetic flux-vector splitting schemes for the ultra-relativistic relativistic gas dynamics", Preprint Nr. **4**, Otto-von-Guericke University, (2003).

[48] M. Kunik, S. Qamar and G. Warnecke, "A reduction of the Boltzmann-Peierls equation", Preprint Nr. **6**, Otto-von-Guericke University, (2003).

[49] O. Langseth, "On an implementation of a front tracking method for hyperbolic conservation laws", *Advances in Engineering Software* **26**, (1996), pp. 43-63.

[50] J.O. Langseth, R.J. LeVeque, "A wave propagation method for three-dimensional hyperbolic conservation Laws ", *J. Comput. Phys.* **165**, (2000), pp. 126-166.

[51] B. van Leer, "Towards the ultimate conservative difference scheme III. Upstream-centered finite difference scheme for ideal compressible flow", *J. Comput. Phys.* **23**, (1977), pp. 263-275.

[52] B. van Leer, "Towards the ultimate conservative difference scheme IV. A new approach to numerical convection", *J. Comput. Phys.* **23**, (1977), pp. 276-299.

[53] B. van Leer, "Towards the ultimate conservative difference scheme V. A second order sequel to Godunov's method", *J. Comput. Phys.* **32**, (1979), pp. 101-136.

[54] B. van Leer, "Flux vector splitting for the Euler equations", ICASE Report No. 82-30 (1982).

[55] R.J. LeVeque, "Numerical methods for conservation laws", Second Edition, Birkhäuser, (1992).

[56] D. Levy, E. Tadmor, "Non-oscillatory central schemes for the incompressible 2-D Euler equations", *Math. Res. Let.* **4**, (1997), pp. 321-340.

[57] S. Lui and K. Xu, "Entropy analysis of kinetic flux vector splitting scheme for the compressible Euler equations", NASA/CR-1999-208981, ICASE Report No. 99-5, (1999).

[58] J.C. Mandal and S.M. Deshpande, "Kinetic flux -vector splitting for Euler equations", *Computer & Fluids* **23**(**2**), (1994), pp. 447-478.

[59] J.M$^{\underline{a}}$ Martí, E. Müller, J.A. Font, J.M$^{\underline{a}}$ Ibáñez, "Morphology and dynamics of highly supersonic relativistic jets", *Astrophysics. J.* **448**, (1995), 105-108.

[60] J.M$^{\underline{a}}$ Martí, E. Müller, "Extension of the piecewise parabolic method to one-dimensional relativistic hydrodynamics", *J. Comp. Phys.* **123**, (1996), pp. 1-14.

[61] J.M$^{\underline{a}}$ Martí, E. Müller, "Numerical hydrodynamics in special relativity", *Living Reviews in Relativity* **2**, (1999), p. 1-101.

[62] J. Maurer, "An efficient advection solver for the method of transport on unstructured grid", Research Report ETH Zürich, (2000).

[63] I. Müller, "Speeds of propagation in classical and relativistic extended thermodynamics", Published by the *Max Planck Institute for Gravitational Physics,* Albert Einstein Institute, Germany, (1999).

[64] H. Nessyahu, E. Tadmor, "Non-oscillatory central differencing fo hyperbolic conservation Laws",*SIAM J. Comput. Phys.* **87**, (1990), pp. 408-448.

[65] J.V. Neumann and R.D Richtmyer, "A method for the numerical calculations of hydrodynamic shock", *Appl. Phys.* **21**, (1950), pp. 232-237.

[66] S. Noelle, "The MoT-ICE: A new high-resolution wave-propagation algorithm for multidimensional systems of conservation laws based on Fey's method of transport", *J. Comput. Phys.* **164**, (2000), pp. 283-334 .

[67] M.L. Norman, K.-H.A. Winkler, "Why ultra-relativistic hydrodynamics is difficult", *Astrophysical Radiation Hydrodynamics,* eds. M.L. Norman and K,-H.A. Winkler, Reidel, Dordrecht, (1986), pp. 449-476.

[68] O.A. Oleinik, "Discontinuous solutions of nonlinear differential equations", *Amer. Math. Soc. Trans. Serv.* **26**, (1957), pp. 95-172.

[69] S. Osher and F. Solomon, "Upwind difference schemes for hyperbolic systems of conservation laws", *Math. Comput.* **38**, (1982), pp. 339-374.

[70] S. Osher and E. Tadmor, "On the convergence of difference approximations to scalar conservation laws", *Math. Comput.* **50**, (1988), pp. 19-51.

[71] M. Pandolfi, D. D'ambrosio, "Upwind methods and carbuncle phenomenon", *J. Comput. Phys.* **98**, (1998), pp. 339-374.

[72] B. Perthame, "Global existence of solutions to the BGK model of Boltzmann equation", *J. Diff. Equ.* **82** (1989) pp. 191-205.

[73] B. Perthame, "Boltzmann type schemes for gas dynamics and the entropy property", *SIAM J.Numer.Anal.* **27.6** (1990) pp. 1405-1421.

[74] B. Perthame, "Second-order Boltzmann scheme for compressible Euler equations in one and two Space dimensions", *SIAM J.Numer.Anal.* **29**, (1992), pp. 1-19.

[75] S. Qamar and G. Warnecke, "Simulation of multi-component flows using high order central schemes",
http://www.mathpreprints.com/math/Preprint/qamarshamsul/20021215/2, (2002).

[76] J. Quirk, "A contribution to the great Riemann solver debate", *Int. J. Num. Met. in Fluids* **18**, (1994), pp. 445-483.

[77] R.D. Reitz, "One-dimensional compressible gas dynamics calculations using the Boltzmann equation", *J. Comput. Phys.* **42**, (1981), pp. 108-123.

[78] P.L. Roe, "Approximate Riemann solvers, parameter vectors and difference scheme", *J. Comput. Phys.* **43**, (1981), pp. 357-372.

[79] O. Runborg, "Multiphase computations in geometrical optics", *J. Comput. Appl. Math.* **74**, (1996), pp. 175-192.

[80] V. Schneider, U. Katscher, D. H. Rischke, B. Waldhauser, J.A. Maruhn, C.-D. Munz, "New algorithms for ultra-relativistic numerical hydrodynamics", *J. Comp. Phys.* **105**, (1993), pp. 92-107.

[81] C.W. Schulz-Rinne, J. P. Collins, and H. M. Glaz, "Numerical solution of the Riemann problem for two-dimensional gas dynamics", *SIAM J. Sci. Compute* **14**, (1993), pp. 1394-1414.

[82] G. A. Sod, "A survey of several finite difference methods for systems of nonlinear hyperbolic conservation Laws", *J. Comp. Phys.* **27**, (1978), pp. 1-31.

[83] T. Tang and K. Xu, "Gas-kinetic schemes for the compressible Euler equations: Positivity-preserving analysis", *Z. angew. Math. Phys.* **50**, (1999), pp. 258-281.

[84] E.F. Toro, "On Glimm-related schemes for conservation laws", technical report MMu-9602, department of mathematics and physics, Manchester Metropolotan University, UK, (1996).

[85] E.F. Toro, "Riemann solvers and numerical method for fluid dynamics", Second Edition, Springer-Verlag, (1999).

[86] N.P. Weatherill, J.S. Mathur and M.J. Marchant, "An upwind kinetic flux vector splitting method on general mesh topologies", *International Journal for Numerical Methods in Engineering*, **37**(**2**), (1994), pp. 623-643.

[87] S. Weinberg, "Gravitation and cosmology", Wiley, New York,(1972).

[88] P. Woodward, P. Colella, "The numerical simulation of two-dimensional fluid flow with strong shocks", *J. Comput. Phys.* **54**, (1988), pp. 115-173.

[89] C.C. Wu, T. Chang, "Further study of the dynamics of two-dimensional MHD coherent structures – a large-scale simulation", Journal of Atmospheric and Solar-Terrestrial Physics **63**, (2001), 1447-1453.

[90] K. Xu, L. Martinelli and A. Jameson, "Gas-kinetic finite volume methods, flux-vector splitting and artificial diffusion", *J. Compute. Phys.* **120**, (1995), pp. 48-65.

[91] K. Xu, "Gas kinetic schemes for unsteady compressible flow simulations", 29th CFD, Lecture Series (1998).

[92] K. Xu, "Gas-kinetic theory based flux splitting method for ideal magnetohydrodynamics", *J. Compute. Phys.* **153**, (1999), pp. 334-352.

[93] K. Xu, "Gas evolution dynamics in Godunov-type schemes and analysis of numerical shock instability", ICASE Report No. Tr. 99-6, (1998).

[94] J. Y. Yang, M. H. Chen, I. N. Tsai, and J. W. Chang, "A kinetic beam scheme for relativistic gas dynamics", *J. Comput. Phys.* **136**, (1997), pp. 19-40.

[95] S. A. Zimmermann, "Properties of the method of transport for the Euler equations", Ph.D. Thesis, Diss, ETH NO. 13957, Swiss Federal Institute of Technology , Switzerland, (2001).